Analysis and Enhancement of Human Cognitive Control using Noninvasive Brain-Computer Interfaces

A Dissertation Presented for the
Doctor of Philosophy
Degree
The University of Tennessee, Knoxville

Soheil Borhani
December 2020

Copyright © Soheil Borhani 2020
All rights reserved.

To my lovely wife, Sara, my fabulous sister Setareh and my incredible mom and dad, Nora & Ali

ACKNOWLEDGEMENTS

I would like to thank everyone who have supported me throughout my doctoral program. First and foremost, I would like to express my sincere gratitude to my academic advisor, Professor Xiaopeng Zhao for his constant support and knowledge. I would have not been able to carry out this body of work without his invaluable assistance, supervision, and advice. I am also grateful to Dr. Yang Jiang at the University of Kentucky for having her constant support and her precious insights and knowledge to the topics. Also, I would like to thank my other committee members, Dr. Jeffrey A. Reinbolt and Dr. Subhadeep Chakraborty for their insightful comments.

Since the studies in this dissertation were involved with real-time platforms and human subject participants, the completion of works would not have been possible without the support of many people. I would like to acknowledge my former labmate, Dr. Reza Abiri, who collaborated with me on multiple projects. Additionally, I would also like to thank undergraduate research assistants, Justin Kilmarx, James Cate, Jinxiao Yu, Michael O'Neil, Joshua Dunkley, and Taylor Berger who worked me in setting up the platforms and run the experiments.

ABSTRACT

Cognitive control including attention and working memory are crucial to human daily life. Whether a civilian who walks across a street or a military service member who is responsible for navigating a mission, cognitive control is involved, entirely. This ability is subject to impairment. People with attention disorder are easily disposed to distraction and lacks the ability to maintain the focus to a task. Multiple treatment strategies have been suggested which most of them has been pharmaceutical. Evidently, the medical treatment has side effects for long-term use. Moreover, it has a risk of drug misuse. Another line of treatment is psychological therapy which is safe but not always effective. There is an emerging evidence that signifies the role of cognitive stimulating activities to improve neuroplasticity and treat neurodegenerative diseases. An alternative strategy to improve neuroplasticity is using Brain-Computer Interfaces (BCIs). A BCI, sometimes called a Brain-Machine Interface (BMI) refers to a unidirectional or bidirectional communication pathway between the brain and an external machine. BMIs utilizes mathematical and machine learning methods to tap into the central nervous system (CNS). The aim of present dissertation is to investigate the possibility of using noninvasive mobile BCI to evaluate and enhance cognitive control while offering appropriate solutions and major contributions to these fields of work. Electroencephalography (EEG) signals as a convenient brain imaging technology is employed to capture real-time activities of the CNS. I investigated cognitive control and motor learning during imagined body movement. Also, I examined the neural pattern associated with visual selective attention in occlusion-free and occluded conditions. Further, working memory as an instrumental brain mechanism has been investigated and, a novel real-time EEG-based short-term memory evaluation and enhancement platform based on neurofeedback is developed and discussed.

Table of Contents

1 Chapter One: Introduction 1
1.1 Overview of the dissertation 1
1.2 Problem Statement 2
1.3 Originality of Proposed Research 6
1.4 Fundamental Contributions 7
2 Chapter Two: Literature Review 9
2.1 What is BCI? 9
2.2 Brain Imaging Techniques for BCI Systems 15
2.3 Closed-Loop BCI 18
2.4 Noninvasive EEG-based BCI paradigms 19
2.4.1 Endogenous Paradigms Based on Motor Imagery Paradigms 19
2.4.2 Exogenous Paradigms Based on External Stimulation Paradigms 23
2.4.3 Hybrid Paradigms 26
3 Chapter Three: Modeling the Imagined Body Kinematics and Optimizing Model Prediction 29
3.1 Introduction 29
3.2 Methods 30
3.2.1 Data 30
3.2.2 Training Protocols 31
3.2.3 Multivariate Regression of Cursor Velocity 31
3.2.4 Classification of Cursor Movement Direction 34
3.3 Results 35
3.3.1 Multiple Linear Regression 35
3.3.2 Channel-Wise Regression 37
3.3.3 Classification 39
3.4 Discussion 39
3.5 Conclusion 43
4 Chapter Four: Brain Connectivity Evaluation during Selective Attention Using EEG-based Brain-Computer Interface 48
4.1 Introduction 48
4.2 Materials and methods 48
4.2.1 Participants 48

4.2.2 EEG recording 49
4.2.3 Phase 1: Image recognition 49
4.2.4 Phase 2: Attention evaluation 50
4.2.5 Statistical analysis of the behavioral responses 50
4.2.6 Signal preprocessing 53
4.2.7 Independent component analysis 53
4.2.8 Equivalent current dipole extraction 54
4.2.9 Calculation of ERSP 54
4.2.10 Group level analysis 56
4.2.11 Causal connectivity analysis 56
4.2.12 Connectivity model validation 58
4.3 Results 58
4.3.1 Behavioral response 58
4.3.2 Time-Frequency EEG response 59
4.3.3 Connectivity Analysis using time-frequency distribution 59
4.4 Discussion 60
4.5 An Application of Selective Attention Combined with Motor Imagery: A BCI Car Racing Game 63
4.6 Significance 63
4.7 Training paradigm 66
4.8 Results 67
5 Chapter Five: Gauging Working Memory Using Resting-State and Task-Related Brainwaves in Healthy Older Adults 74
5.1 Memory and different models of short-term and long-term memory 74
5.2 Brain areas associated with short-term memory 75
5.3 Processes associated with short-term memory 77
5.4 Significance of the resting-state brainwaves 78
5.5 Significance of task-related brainwaves 78
5.6 Identification of task-related EEG surrogates for “efficient” short-term memory using machine learning 79
5.7 Findings on the resting-state brainwaves correlates of cognitive control 83
5.8 Findings on the task-related brainwaves correlates of working memory 86
5.9 Materials and methods 87

5.9.1 Human Participants 87
5.9.2 Wireless EEG signal acquisition and the experimental procedure 88
5.9.3 Experimental design 90
5.9.4 Data analysis 90
5.10 Results 93
5.10.1 Memory performance 93
5.11 Discussions 105
5.11.1 Summary of the findings 105
5.11.2 Reaction times and Delta / Theta band powers 105
5.11.3 Selective neural communications within working memory network via frequency oscillations and coherence 110
5.11.4 Significance, limitation, and future potential 111
6 Chapter Six: Portable Neurofeedback Intervention for Cognitive Control 113
6.1 Operant conditioning 113
6.2 Neurofeedback 113
6.3 How BCI can help Neurofeedback 115
6.4 Neurofeedback training for improving memory performance 116
6.5 Neurofeedback software architecture 120
6.5.1 GUI 120
6.5.2 Signal acquisition module 120
6.5.3 Visualizer module 120
6.5.4 Recorder module 123
6.5.5 Experimental design 123
7 Chapter Seven: Conclusions and future works 124
7.1 Noninvasive assistive BCI 124
7.2 Investigating brainwave biomarkers for cognitive decline 124
7.3 Closed-loop neurotechnologies for targeted treatments 124
7.4 Embodied cognition: Applying multisensory BCI to human-robot interaction 125
Bibliography 127
Appendix 150
7.5 Neurofeedback GUI code 150
7.6 Neurofeedback epoch visualizer code (visualizer module) 150
7.7 Neurofeedback signal acquisition module 153

7.8 Neurofeedback recorder module 155
Vita.. 156

List of Tables

Table 3.1. Model comparisons for horizontal and vertical trials 38
Table 3.2. Prediction accuracy for various channel combinations 40
Table 3.3. Previous BCI studies on EEG-based object control. ERS/ERD: event-related synchronization/desynchronization. LMS: least square method. SVM: support vector machine. PSD: power spectral density. LDA: linear discriminant analysis. KPLS: kernel partial least squares classification. MLD: Mahalanobis linear distance. RBF: radial basis function. GA: genetic algorithm. 46
Table 4.1. The subcategories of images to which a participant should pay attention during each block and the expected behavioral responses from the participant. 51
Table 5.1. Correlations between eyes-closed resting-state EEG and mean accuracy score. 102

List of Figures

Figure 1.1. Differences in cognitive functioning by age based on different cognitive tests, Midlife in the United States, N = 4,268. The use of Z-scores, shown on the vertical axis, allows data from different tests to be shown on the same scale [17]. 3
Figure 1.2 Proportions of people age 65 and older with moderate or severe memory impairment versus no or mild memory impairment, Health and Retirement Study, United States, 2002 [17]. 3
Figure 2.1 The schematic of action production in a) a natural CNS and b) BCI-mediated output. Borrowed from [26]. 12
Figure 2.2. A schematic of design and operation of brain-computer interface. modified from Wolpaw et al. [27]. 13
Figure 2.3. The location of different electrophysiological systems. Borrowed from [28]. 16
Figure 2.4. Comparison of spatial and temporal resolution of different brain imaging techniques. 16
Figure 2.5. MEG scanner with a patient. Borrowed from [29]. 17
Figure 2.6. A schematic of closed-loop BCI. 20
Figure 2.7. An example of a change in frequency spectra for EEG recorded from C3 and C4. The top row (a, b) shows spectral power changes in C3 and C4 electrodes while performing imagined movement of right hand versus left hand. The middle row (c, d) shows spectral power change in C3 and C4 electrodes while performing imagined movement of both hands versus rest. The bottom row (e, f) shows spectral power change in C3 and C4 electrodes for imagined movement of right hand versus rest and left hand versus rest, respectively (Figure copied from [56] with permission of a Creative Commons Attribution (CC BY) license). 22
Figure 2.8. ERP components after the onset of a visual stimulus (figure copied from [62] with permission). 24
Figure 2.9. Flow diagram of taxonomy for BCIs. 28
Figure 3.1. Schematic of the EEG-based BCI platform in cursor control task. 32
Figure 3.2. Training protocol and model generation for horizontal and vertical trials. ... 32
Figure 3.3. Regression results of one subject across two horizontal (top) and vertical (bottom) trials. Predicted velocity (orange) and target velocity (blue) with goodness of fit score above plot. 36
Figure 3.4. Predicted velocities plotted over the target for least squares, Ridge, and Theil-Sen regression for one sample subject and one sample horizontal trial. 38
Figure 3.5. Average goodness of fit of each channel for a) horizontal trials and b) vertical trials (bottom). 38
Figure 3.6. Heat map for channel-wise prediction in a) horizontal and b) vertical trials. 40
Figure 3.7. Emotiv EPOC channel locations. 40
Figure 3.8. Boxplots of the classification accuracies using four different feature sets. (1) All channels and all features; (2) all channels and mean of the 4 frequency bands independently; (3) six channels (AF3, AF4, F3, F4, F7, and F8) and all features; (4) six channels (AF3, AF4, F3, F4, F7, and F8) and all features; (4) six channels (AF3, AF4, F3, F4, F7, and F8) and mean of the 4 frequency bands independently. 44

Figure 3.9. Estimated independent components of a) neural activity, b) vertical eye movement, and c) horizontal eye movement from a sample participant..... 44
Figure 3.10. Violin plot of Goodness of Fit (%) for horizontal cursor velocity showing the contribution of different components 45
Figure 3.11. Violin plot of Goodness of Fit (%) for vertical cursor velocity showing the contribution of different components 45
Figure 4.1. A schematic of sample blocks of trials of phase 1: image recognition phase. 51
Figure 4.2. A schematic of sample phase 2: attention evaluation phase using superimposed images. 52
Figure 4.3. Data processing pipeline using EEGLAB. 55
Figure 4.4. Estimated current dipoles of each participant's independent component in the FFA cluster for the trials during a) "image recognition" and b) "attention evaluation" phases. The picture from left to right constitutes sagittal, coronal, and axial slices..... 55
Figure 4.5. Violin plot of the mean RT in the a) "Image recognition" and b) "Attention evaluation" phases. The red dotted line shows the mean correct response time (RT) over all participants. 61
Figure 4.6. Violin plot of mean correct responses in both "Image recognition" and "Attention evaluation" phases. The red dotted line shows the average over all participants. The mean[std] behavioral performance was 95.7 [2.7] % for "Image recognition" and 88.1 [5. 4] % for "Attention evaluation" phases. 61
Figure 4.7. ERSP response for a representative participant over all a) face and b) scene stimuli in image recognition phase. An enhanced response was found in [25-40] Hz in scenes vs. faces..... 62
Figure 4.8. ERSP response for a representative participant over all a) face and b) scene stimuli in attention evaluation phase. Stronger early response was found during high attention demand, in faces vs. scenes in [15-30] Hz. 62
Figure 4.9. Time-frequency distribution of Granger causality from left occipital (OccL), right occipital (OccR), left supplementary motor area (SmaL), and right supplementary motor area (SmaR) as source on the columns to the same areas on the rows as sink for (a) Face trials and (b) Scene trials in the image recognition phase. The red dotted lines show the average behavioral response time for each condition. Non-zero connectivity with the significance level of $p\_value < 0.05$ is illustrated with warm regions (Red)..... 64
Figure 4.10. Time-frequency distribution of Granger causality from left occipital (OccL), right occipital (OccR), left supplementary motor area (SmaL), and right supplementary motor area (SmaR) as source on the columns to the same areas on the rows as sink for (a) Face trials and (b) Scene trials in the attention evaluation phase. The red dotted lines show the average behavioral response time for each condition. Non-zero connectivity with the significance level of $p\_value = 0.05$ is illustrated with warmer regions (Red). 65
Figure 4.11. A schematic of a) supervised and b) unsupervised learning 68
Figure 4.12. A schematic of the hybrid BCI game and the data decoding pipeline 68
Figure 4.13. A schematic of the hybrid MI/SSVEP training experimental setup 69

Figure 4.14. Event-related spectral perturbation (ERSP) averaged over EEG signals of central lobe over all subjects for a) Resting and b) Pushing states 70
Figure 4.15. Estimated current dipoles from each participating independent component (blue) and their centroid (red). The rendered maps are coronal (bottom right), sagittal (top right), and axial (bottom left) slices of the Montreal Neurological Institute (MNI) template. 70
Figure 4.16. Power spectral density (PSD) averaged over EEG signals of occipital cortex over all subjects for a) Left flicker, b) Right flicker, c) Top flicker, and d) Bottom flicker 71
Figure 4.17. An evaluation of CCA decoding accuracy on the Congruent vs. Incongruent flicker frequency with respect to varied sliding window size 73
Figure 5.1. Three subdivisions of the memory system. The figure shows information flows for both information retention and information retrieval according to Atkinson and Shiffrin model [214]. 76
Figure 5.2. A schematic of information flow according to Baddeley and Hitch model [220]. 76
Figure 5.3. The ERP response generated as the grand average EEG waveform deflection over all participants of A) Normal healthy control group, B) the amnestic mild cognitive impairment group, and C) the Alzheimer's disease group over the correct behavioral response for target match and target non-match visual stimuli, borrowed from [225]. 80
Figure 5.4. The spatial distribution of the neural activity by subtracting the ERP response of target match and target non-match visual stimuli for normal healthy control group, the amnestic mild cognitive impairment group, and the Alzheimer's disease group, borrowed from [225]. 81
Figure 5.5. A schematic of the resting EEG (rEEG) and Bluegrass short-term memory in a right-hand dominate human participant. The participants' (age 60 and over) eyes-opened resting-state, followed by eyes-closed resting-state EEG followed by a memory task (a modified delayed match-to-sample paradigm) where a subject encoded two targets in mind, then responded with the right index to indicate the memory target match (pressing L key on the key board) and left index finger for non-target in a 5-min task; During the second 5-min testing block, the participant was asked to indicate memory target match by using the left index finger (pressing A key on the key board). 89
Figure 5.6. Schematic representation of task-related EEG data epoching and analysis. 92
Figure 5.7. Bar plot showing group mean and standard deviation of the mean accuracy of retrieval of target and non-target stimuli. 95
Figure 5.8. Bar plot showing the group mean and standard deviation of the reaction time to target and non-target stimuli. 95
Figure 5.9. The distribution of a) mean accuracy score and b) mean reaction time (RT) across age for both male and female groups. 96
Figure 5.10. A flattened histogram distribution of all participants' reaction time. Warmer colors show a higher concentration of reaction time. 96

Figure 5.11. Bar plot showing the distribution of individualized “fast” and “slow” correct reaction to target and non-target stimuli during the memory task..... 97
Figure 5.12. Bar plot showing the group average and standard deviation of the the Alpha band power occipital and parietal sites (O1 and O2 electrodes) during eyes-open and eyes-closed. 97
Figure 5.13. Average power spectral density over occipital sites (O1, O2), the corresponding dorsal view topographic distribution of the alpha wave (8–13 Hz), and the point by point confidence level shown by p-value during resting state eyes-close and eyes-open over all participants. The black color curves show the average over all participants and the blue curves show individuals’ power spectral density. 99
Figure 5.14. Topographical plot of Pearson correlations between EEG relative frequency band power recorded during resting-state eyes-closed before the task and mean reaction time during the working memory task. The distribution of the correlation between rEEG and mean reaction time follows a trend, meaning that increased mean reaction time corresponds to the higher activity in higher frequency bands (Beta and Gamma) over frontal sites and decreased mean reaction time corresponds to the higher activity in the lower frequency bands (Delta and Theta) over left temporal and left frontocentral areas. 100
Figure 5.15. Topographical plot of Pearson correlations between EEG relative frequency band power recorded during resting-state eyes-closed before the task and accuracy score (% correct response) during working memory task. 100
Figure 5.16. Brain connectivity graphs showing the significant correlations between paired EEG channels’ magnitude-squared coherence during the eye-closed resting-state and mean reaction time in a) Delta, b) Theta, c) Alpha, d) Beta, and e) Gamma bands. The color designates the level of correlation between all paired coherence and the corresponding measure where the observed correlation was significant $(p < 0.05)$. 102
Figure 5.17. Brain connectivity graphs showing the significant correlations between paired EEG channels’ magnitude-squared coherence during the eye-closed resting-state and mean accuracy score in a) Delta, b) Theta, c) Alpha, d) Beta, and e) Gamma bands. The color designates the level of correlation between all paired coherence and the corresponding measure where the observed correlation was significant $(p < 0.05)$. 103
Figure 5.18. Event-related potentials of the average individualized “fast” and “slow” correct memory retrieval in all EEG electrodes 104
Figure 5.19. Dorsal view topographical illustration of a) “fast” and b) “slow ERP responses..... 106
Figure 5.20. a) A point-by-point confidence level of Wilcoxon rank sum test and b) the dorsal view topographical distribution of the confidence level of Wilcoxon rank sum test 107
Figure 5.21. ERP response of “fast” versus “slow” in F3 EEG electrode..... 108
Figure 5.22. Event-related spectral perturbation (ERSP) response of a) “fast”, b) “slow” brain responses, and c) point-by-point time-frequency statistical significance between

ERSP responses of “fast” and “slow” evoked responses with bootstrap and adjusted p-value using false discovery rate (FDR)..... 109
Figure 6.1. The behavioral model of learning based on operant conditioning. 114
Figure 6.2. a) The intensity of Midline Frontal Theta of cognitively young and old adults and b) the correlation between the Theta power intensity and the reaction time in short term memory task, borrowed from [341]..... 119
Figure 6.3. A sample short-term memory neurofeedback trial. The feedback signal will be designed based on the average neural response of the last 3 consecutive responses..... 119
Figure 6.4. A schematic of the experimental setup. 121
Figure 6.5. A high-level diagram of the designed neurofeedback software and the associated modules..... 122
Figure 6.6. A snapshot of the designed GUI 122

1 Chapter One: Introduction

This chapter will cover the introduction of this dissertation. In the following an overview to the chapters that presented in this dissertation is provided. Then, a brief description for the targeted problems is expressed, explicitly. Following that, the originality of research works is discussed. Finally, the major and minor contributions are stated in detail at the end of this chapter.

1.1 Overview of the dissertation

Cognitive control including attention and working memory are crucial to human daily life. Whether a civilian who walks across a street or a military service member who is responsible for navigating a mission, cognitive control is involved, entirely. This ability is subject to impairment. People with attention disorder are easily disposed to distraction and lacks the ability to maintain the focus to a task. Multiple treatment strategies have been suggested which most of them has been pharmaceutical. Evidently, the medical treatment has side effects for long-term use. Moreover, it has a risk of drug misuse. Another line of treatment is psychological therapy which is safe but not always effective. Studies indicates efficacy of 30% for this method.

There is an emerging evidence that signifies the role of cognitive stimulating activities to improve neuroplasticity and treat neurodegenerative diseases [1, 2]. An alternative strategy to improve neuroplasticity is using Brain-Computer Interfaces (BCIs). A BCI, sometimes called a Brain-Machine Interface (BMI) refers to a unidirectional or bidirectional communication pathway between the brain and an external machine [3-5]. BMIs utilizes mathematical and machine learning methods to tap into the central nervous system (CNS).

The aim of present dissertation is to investigate the possibility of using noninvasive mobile BCI to evaluate and enhance cognitive control while offering appropriate solutions and major contributions to these fields of work. Electroencephalography (EEG) signals as a convenient brain imaging technology will be used to capture real-time activities of the CNS. Specifically, I am interested to use wireless EEG headset to record brain activities because of its convenience and the potential to become portable to use in community settings and remote areas.

The dissertation is organized as follows. Chapter 2 covers the literature survey with a general overview of different brain imaging technologies with a focus on noninvasive EEG-based BCI paradigms. Chapter 3 covers a study of EEG-based 2D cursor control. The chapter discusses the design and implementation of the BCI for the cursor control, the outcome measures of the experiment, how imagination of body movement can be distinguished and extracted from noninvasive EEG signals, and how motor learning takes place over multiple session of the experiment. I also focus on the collected neural data in the 2D cursor control task to optimize the predictability of the neural decoder. Chapter 4 covers a study of selective visual attention to image categories, disturbed-

free and disturbed images. Both behavioral and neural responses of the participants are analyzed. I also investigate the time-frequency representation of disturbance-free and disturbed images to evaluate the neural processing resources under these two conditions. Moreover, I explore the brain connectivity in the sense of Granger causality under those conditions. Chapter 5 is focused on short-term memory, different models of short-term memory, and a study to evaluate behavioral and neural data to identify "optimal" pattern of short-term memory. The data collection setup is designed to be open-source, universal to the EEG headset, and freely available so that people can use to evaluate the cognitive states in a mobile and convenient setup. Finally, chapter 6 discuss a design and development of a novel closed-loop neurofeedback BCI for cognitive control. The proposed mobile and closed-loop open-source setup is designed to identify the "optimal" behavioral and neural states of the user and provide real-time feedback of the cognitive state to the user using reinforcement mechanism. The neurofeedback paradigm in this chapter is customized to enhance reaction time during working memory retrieval.

1.2 Problem Statement

The statistics has been shown that there will be over 1 billion aging population in less than 10 years and about 2 billion in 2050, a 22% of the world population [6]. The aging population is prone to functional decline. Cognitive deficits are at the core of many functional declines among aging adults. Figure 1.1 demonstrates the performance of different cognitive systems such as category fluency, attention switch, and backward counting negatively correlated with age. Figure 1.2 shows that 10 to 30% of the entire US population above 65 years old is diagnosed with mild or severe cognitive impairment. It also shows that the impairment is more prevalent in men compared to women, and the cognitive decline has positive correlation with aging.

The main contributor to the deficits is found to be the loss of synchrony and the progressive loss of brain structural and functional neuroplasticity [7, 8]. The cognitive deficit targets executive function including working memory (WM) and sustained attention (SA) [9-11]. This may lead to compromised cognitive abilities to effectively act in daily life goal-directed activities. Currently available pharmaceutical interventions are usually expensive, may not be effective [12] or may have side effects, and may exacerbate other diseases [13-15]. Besides, the available pharmaceutical therapies primarily target co-occurring symptoms rather than treating the core impairments, resulted in inefficacy of the therapies [16]. Thus, it has been suggested to combine pharmacological therapies with other types of treatments.

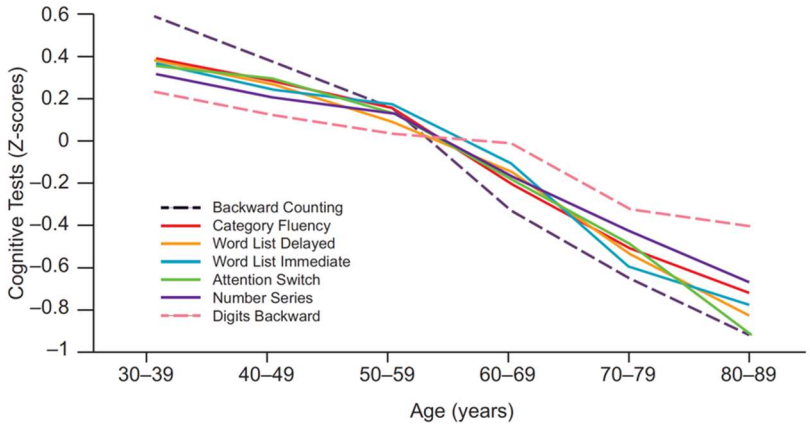


Figure 1.1. Differences in cognitive functioning by age based on different cognitive tests, Midlife in the United States, N = 4,268. The use of Z-scores, shown on the vertical axis, allows data from different tests to be shown on the same scale [17].

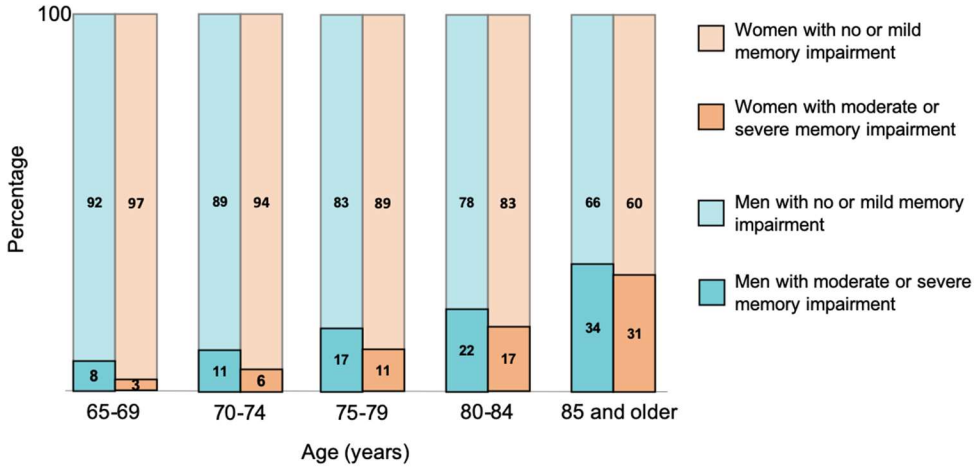


Figure 1.2 Proportions of people age 65 and older with moderate or severe memory impairment versus no or mild memory impairment, Health and Retirement Study, United States, 2002 [17].

A newly emerging field of research focuses on applying BCIs techniques to enhance motor within neurorehabilitation setups. BCIs have conventionally been more concerned with providing additional output to CNS as a mean to restore or repair lost functions in people with severe motor disabilities allowing them to control prosthetic or robotic devices, or to communicate which has been proven feasible with a remarkable accuracy.

BCIs can interpret the cortical neuronal activities in real-time and translate them into a goal-directed actions using different external outputs. Usually, designing a BCI comprises two phases: 1) A training phase in which the neural decoder learns to associate the instantaneous neural activity with the actual variable of interest and 2) testing phase in which the implemented neural decoder in the training phase is given the real-time neural activity and the decoder maps it into the most probable range or value of the variable of interest. Decoding accuracy above the chance-level indicates that the recorded brain activity carries reliable information about the variable of interest. The mapping between the brain activity and the variable of interest depends on the user's interpretation. For instance, identifying the neural code to the corresponding arm movement or face stimuli allows users to map a given endogenous neural pattern to the congruent output. Neuroplasticity allows human and non-human primates learn even more complex associations relying on positive and negative dopaminergic and GABAergic mechanisms known as reinforcement learning. In such complex designs, users learn how to project neural activities that best control the phenomena of interest. Because of sensory feedback (vision, audio, somatosensory, etc.), users can evaluate their controllability over the external phenomena.

An emerging parallel effort is now going on to use BCIs controlled by cognitive activity. Although this approach defines more challenges, it opens new dimensions and new line of treatments for different cognitive disorders. Now, we are able to identify user's motivation [18] and attention orientation in a single trial basis to operate a cognitive BCI [19]. Instead of translating movement-related cortical activity, these cognitive BCIs pursue to access the content of cognitive processes.

One of the principal long-term goals has been to develop therapeutic tools for the treatment of cognitive disorders. Motor cortical activities can be represented and synchronized to overt body movement. In comparison, cognitive control mechanisms such as decision making, holding information in short-term memory and attention orientation are fundamentally endogenous phenomena. Their content is covert and the objective method of inferring the content has been indirectly through their effects on other overt measures such as response time, questionnaires, accuracy of selection, etc. From the perspective of neurophysiological signals, our knowledge and understanding on the neural basis of cognitive control mechanisms is increasing. We now know about some of our cognitive systems and the underlying cognitive processes that we did not know 30 years ago. However, unlike motor cortical processes, the cognitive processes

cannot be precisely time-locked to an evident external output. Moreover, they are often combined and intertwined with sensory, motor and other cognitive signals. As a result, cognitive BCIs is considered as more challenging than conventional pure motor related BCIs.

Van Gerven and Jensen [20] has been the first attempt to identify attention orientation at a single trial level. Participants were covertly attending to one item among four possible spatially divided items while the cortical activities were collected using Magnetoencephalography (MEG). The offline analysis of the recorded signal, particularly the cortical activity on alpha band (8-14) Hz over the parietal and occipital lobe showed an average performance of 69% accuracy in discriminating between two spatial locations. They witnessed higher decoding performances at discriminating left/right locations (78%) than up/down locations (58%). They additionally report an average decoding performance of 41% when discriminating between four possible spatial locations (chance being at 25%). The study has been an evidence that covert spatial attention can be monitored in real-time. Another EEG study with a similar experimental design [21] showed an average accuracy of 75% to discriminate attention orientation. Using near-infrared spectroscopy (NIRS) to capture neural activity, Morioka et al. [22] could get slightly higher accuracy (79%). Indeed, it is not clear if this improved performance results caused by using different brain modality or is due to the fact that an exogenous cue was used instead of an endogenous cue in the experiment. With functional magnetic resonance imaging (fMRI), decoding real-time attention orientation take one step forward. Anderson et al. [23] could determine attention orientation with Blood-oxygen-level-dependent (BOLD) signal with 85% accuracy. In comparison to the EEG study, the fMRI study shows a slightly better performance at discriminating attention orientation between up/down (82%) than between left/right attention (77%). The work established a promising future in the field of cognitive BCI.

Among the brain imaging techniques for recording brain signals, still EEG has shown the most promising brain imagining method that could become portable and affordable for many patients. Improvement and contribution in the BCIs using EEG technology could make a great impact in the real-world applications and could be a revolutionary tool for patients who are in need and for insurance companies in cutting the incurred health insurance costs.

Although many BCI systems have been developed so far, there are still many limitations concerning the cost, adaptability, durability and flexibility of these systems. For example, there are expensive invasive-BCI systems that not all the disabled people can afford and meanwhile some other patients will not accept these methods due to invasiveness and surgical operations. In this work, my focus is to study the learning representation in cortical activity and analyze noninvasive EEG signals collected under visual selective attention. Moreover, a therapeutic EEG-based neurofeedback for enhancing cognitive control based upon operant conditioning is proposed. The

proposed idea is revolved around mobile EEG as hardware and open-source software to offer a flexible, portable, and cost-effective therapeutic BCI while incorporating advanced machine learning techniques to further enhance our understanding of the associated neural activity and increase the performance of the BCI as a learner agent. Later for clinical validation, the developed setups will be evaluated by the real patients in Sanders-Brown Center on Aging and in UK-ADC Lab at the University of Kentucky, Lexington. If successful, the research may have significant impact to bring affordable and convenient therapy mostly for people with various aging conditions including Alzheimer's disease (AD), Mild Cognitive Impairment (MCI), and Traumatic Brain Injury (TBI).

1.3 Originality of Proposed Research

This dissertation investigates cognitive control mechanisms. The study begins with analysis of the neural pattern during a well-known and well-established BCI paradigm, brain-controlled computer cursor control with a new perspective. A number of participants are asked to learn imagining moving a computer cursor with their dominant hand in a natural pace and trajectory. Once they learn the task, they are asked to move the same cursor to hit targets on the four corners of the screen. The learning pattern through multiple sessions of the training are followed and different machine learning models are optimized for decoding neural signals collected during the task. The study tries to augment our understanding on the modeling and decoding of imagined kinematics from noninvasive EEG signals using machine learning techniques. The study focuses on the difference between decoding of horizontal and vertical cursor movement. I study different machine learning methods to increase the accuracy of horizontal and vertical decoding with EEG signals. A novel paradigm is used to learn and associate cortical activity under natural body pace and a multiple linear regression is applied to extract the cursor velocity. A portable EEG headset with only 14 electrodes is used for the entire experiment. The study tries make a bridge between motor and cognitive BCI.

In another experiment with relatively large population, cortical patterns of selective visual attention under disturbance-free and disturbed images are studied. The behavioral and neural response of the population are collected and reaction time as a proxy and a basis for understanding of attention and cognition are analyzed. In addition, time-frequency representation as the average of single-trial experiment under towards the attended image categories in both disturbance-free and disturbed images are extracted and analyzed. Also, the brain connectivity between parieto-occipital and supplementary motor areas under the assumption of Granger causality is analyzed. The study serves as a foundation for the cognitive control enhancement paradigm which uses neurofeedback mechanism to stimulate and modulate enhanced attention if applied for multiple sessions of training.

In a new study on short-term memory, an open source, universal, and easily portable, platform is designed to evaluate short-term memory in a delayed-match-to-sample task. The study tries to enumerate “optimal” and “suboptimal” patterns of short-term memory and correlate the neural pattern with the behavioral response and the performance of user in the task. Response time as a measure of sustained attention and performance as a proxy for short-term memory capacity is included in the behavioral response. In addition, machine learning techniques is incorporated to refine our understanding of neural patterns under “optimal” and “suboptimal” patterns of working memory. The study is an indispensable constituent of the machine learning-behavioral and neural based neurofeedback study to enhance cognitive control. The proposed open-source setup has already been introduced in a recent meeting of National Institute of Aging Digital Biomarkers Workshop in April 2019 and has been acquired by different research labs. In the final study a design and development of a novel closed-loop neurofeedback BCI for cognitive control is discussed. The detected lapse of attention and working memory using the enumerated “optimal” and suboptimal” patterns is used to utilize in an operant conditioning paradigm. Reinforcement learning mechanism embedded in operant conditioning is used as a key neural component to reward subjects for their “optimal” patterns and penalize them for their “suboptimal” patterns of cognition. The time and cost of running a clinical trial may exceed our current budget to evaluate efficacy within the scope of this dissertation. However, the open-source and freely available feature of the proposed setup may provide a convenient testbed for other researcher to gauge the efficacy of the paradigm in a large population in a clinical setup.

1.4 Fundamental Contributions

The present work intends to add knowledge to the current literature of assistive and cognitive BCIs. The following are the itemized expected contribution of the dissertation:

- A novel strategy to train a learner agent for decoding imagery body kinematics from noninvasive EEG signals.
- A novel scheme to compartmentalize training of a 2D cursor control and map cortical activity into a continuous 2D cursor control.
- Development of an open-source BCI platform to evaluate selective visual attention.
- Development of an open-source BCI platform to evaluate short-term working memory and extract “optimal” and “suboptimal” cognitive patterns using behavioral and neural data, combined.
- Identify noninvasive EEG surrogates of “fast” and “efficient” short-term memory retrieval.
- Identify resting-state correlates of working memory performance.
- Study task-specific and resting-state task non-specific brainwave pattern and perform correlative evaluation with visual working memory.

- Development of a novel machine learning scheme to extract features of attentional states and classify patterns of cortical activity under two stimuli categories.
- Investigation of a novel neurofeedback regiments for enhancing cognitive control using open-source software and portable mobile EEG.

2 Chapter Two: Literature Review

2.1 What is BCI?

Advances in brain science and computer technology in the past decade have led to exciting developments in Brain-Computer Interfaces (BCIs), thereby making BCI a top research area in applied science. The renaissance of BCI opens new methods of neurorehabilitation for people with various types of physical and mental deficits (e.g., people with Alzheimer's disease, dementia, or motor neuron disease (MND). Recent technological advances such as the capability of wireless recording, training mathematical and machine learning models on high-performance computer machines, and access to real-time high-resolution temporal data samples have increased interest in electroencephalographic (EEG) based BCI approaches. Human central nervous system (CNS) responds to exogenous (outside) events as well as endogenous (inside) events by generating inhibitory/excitatory/leak reactions. These outputs can be projected in different brain modalities.

CNS can be classified into separate subsystems. The subsystems are Basal Ganglia, Cerebellum, Limbic system, Brain stem, Spinal cord, and Cortex.

Basal Ganglia. The subsystem is located deep inside the brain. It involves in control movement and motor planning. Any harm to the basal ganglia can cause lack of control and tremor and may result in Parkinson's disease. After receiving information from sensory input, the subsystem gauges the course of action by sending signals to the motor cortex. The dopaminergic and rewarding effect of this area steer the output of the area.

Cerebellum. The system is located below the midbrain. It has role in controlling the balance, coordinating body movements and learn motor skills. Also, the area involves in spatial and executive abilities. The area has role in the regulation of heartbeat, breathing, and other autonomous vital functions. Damage to the system may cause unawareness, unresponsiveness, and no sign of reflex which means brain death.

Limbic system. This is the emotional center of the brain and processes information about our internal states including vital signs. The area also plays a significant role in memory and motivation. The system consists of four subsystems including Thalamus, Hypothalamus, Amygdala, and Hippocampus. Thalamus functions as a sensory relay. The information from sensory input is processed first in this area and then travels towards cortex. Hypothalamus regulates our emotions, hunger, thirst, sexual behavior, and our body temperature. It works as a thermostat of our body. Amygdala regulates arousal, fear, and excitement. Our reflex in scary situations conditions and regulates by Amygdala. Hippocampus processes the spatial memory, especially the information during our planning to move from one place to another. Damage to this area may cause problem in short-term working memory.

Brain stem. The area is located inside the cortex and involves in some the basic functions of body. It acts as a relay between cortex and the rest of the CNS. Damage to this area may cause coma.
Spinal cord. It is an extension of our brain and connects our central nervous system to peripheral nervous system which connects to the rest of our body. It is a bidirectional pathway that carries sensory information from our body to the brain and carries commands from the brain to the body through motor neurons.
Cortex. It is the outermost and is the most highly developed part of the brain. The system helps us to analyze sensory information. The area includes four different regions (lobes) each linked to different functions.

1) *Frontal lobe.* The lobe is located to the forward of the cortex. The lobe involves in language, memory, mood, personality, self-awareness, and movement. Decision making and planning are also other functions of the lobe which called executive function. The lobe exerts a top-level governance over other cortex areas. Motor cortex is also part of frontal lobe which is responsible for motor activity. Prefrontal cortex is also part of the area that involves in planning and language. Broca area which plays an essential role in language production is also located in prefrontal cortex.
2) *Parietal lobe.* The lobe is found on the upper middle part of the cortex, behind the frontal lobe. Somatosensory cortex, which is sensitive to temperature and touch, is located in parietal lobe. The lobe pass through vision and touch sensory input to the motor cortex once we pinpoint an object for reaching or grasping.
3) *Temporal lobe.* This part of cortex is essential to hearing and language understanding. Auditory cortex is part of the lobe which includes Wernicke area (language center). Wernicke for right-handed persons is located almost behind the left ear and for left-handed persons behind the right ear. The area is the language production center of the brain. Moreover, the lower part of the temporal lobe is responsible for memory storage.
4) *Occipital lobe.* In human brain, occipital lobe is a large portion of the cortex that located at the back of the brain. Visual cortex is located in this lobe. Dedication of such a large part of our cortex to visual cortex make human as a visual primate which means that we rely strongly to our vision compared to other sensory inputs.

A BCI provides CNS an alternative communication channel as an output as it is shown in Figure 2.1. The new output is beneficial to restore, augment, or to use as an auxiliary to enhance deficits of the CNS system. The activity of CNS system consists of neurochemical, electrical, and metabolic reactions. This includes action potential in neurons and synaptic potentials which constantly occur on our CNS system. The reactions can be quantified and captured directly by measuring the corresponding

electrical activity, magnetic field perturbations, or indirectly by measuring the hemoglobin oxygenation/deoxygenation as a result of the process. A BCI system monitors these brain signals using sensors within the brain, on the surface of cortex, or on the surface of scalp, compute specific measures or features and transform them into outputs. The outputs can act on the outside world or on the user's body. Figure 2.2 demonstrates a schematic of design and operation of BCIs. As illustrated in Figure 2.2, BCI can help through five types of applications.

BCIs can be used for replacing lost capabilities. While most adults can speak, write, and walk, there are millions of people in the US alone that have trouble speaking, writing, or using their motor function to walk or moving their hands caused by injury, disease, or other causes. BCI can be used to replace these functions. BCI speller is an example of lost function replacement. People can type words or convert typed words into speech using speech synthesizer. Also, BCI can replace lost functions by assisting individuals by control devices such as wheelchair or prosthetic arm.

BCI might be utilized for restoring lost functions. Damage to the brain or spinal cord may cause inability of using intact arms or legs, i.e., a function that were once easy for people with spinal cord injury. If the brain areas that generate the muscle movement, or the spinal cord that send the information are damaged, it is not possible to control movement of muscles in different body parts; i.e., the muscle control that activated by electrical current generated from the brain.

The muscle control can be restored with a device called functional electric stimulator (FES). Similar to our CNS system, the device sends a weak electrical current to control muscles. FES pads can be placed over the corresponding muscles to for instance cause the leg or the hand to flex at knee or at wrist, respectively. BCI can be utilized to directly read movement intention-related brain activity. It can be inferred and predicted from brainwaves collected from motor areas in response to motor execution or motor imagery tasks. The decoded movement intention subsequently can trigger FES device to generate electrical stimulating signal to control relevant muscles. The scheme make use of BCI to restore different body movements including walking, grasping, or even bladder and bowel control. A BCI can be used to improve the CNS system output.

There are millions of people with various neurological problems including problems in memory, attention, and movement. Brain injury, stroke, dementia, and several neurodegenerative diseases such as Alzheimer's disease and Parkinson's disease are some of the possible causes. Applying BCI on those population may be beneficial to counteract the deficit and potentially improve the output of the neurological function. For example, physiotherapy is a suggested therapy to help people with stroke re-train their brain to work appropriately. Mirror therapy [24, 25] is a well-accepted therapeutic method for stroke rehabilitation. Paretic upper limb is a common and undesirable consequence of stroke that cause body movement limitation.

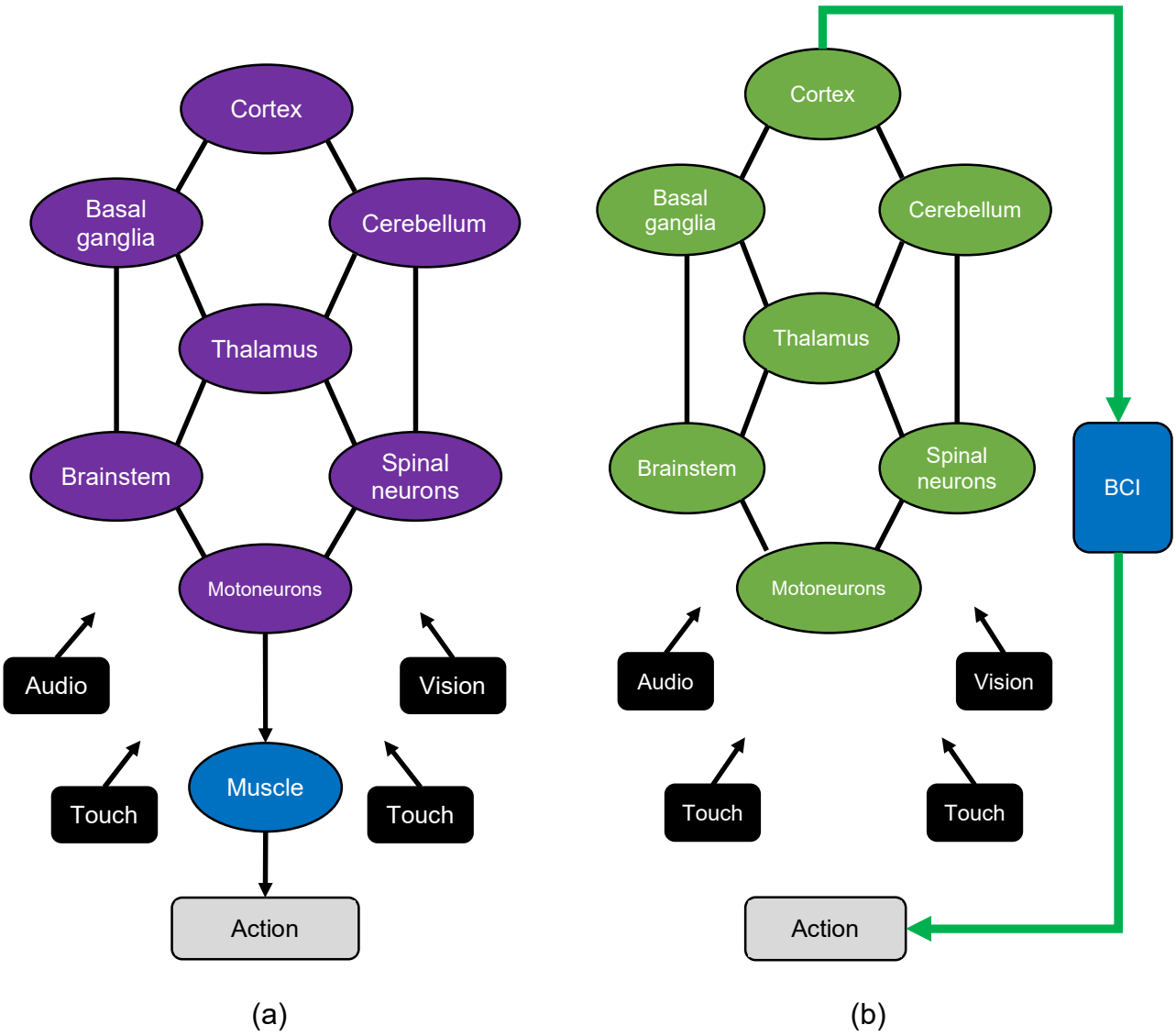


Figure 2.1 The schematic of action production in a) a natural CNS and b) BCI-mediated output. Borrowed from [26].

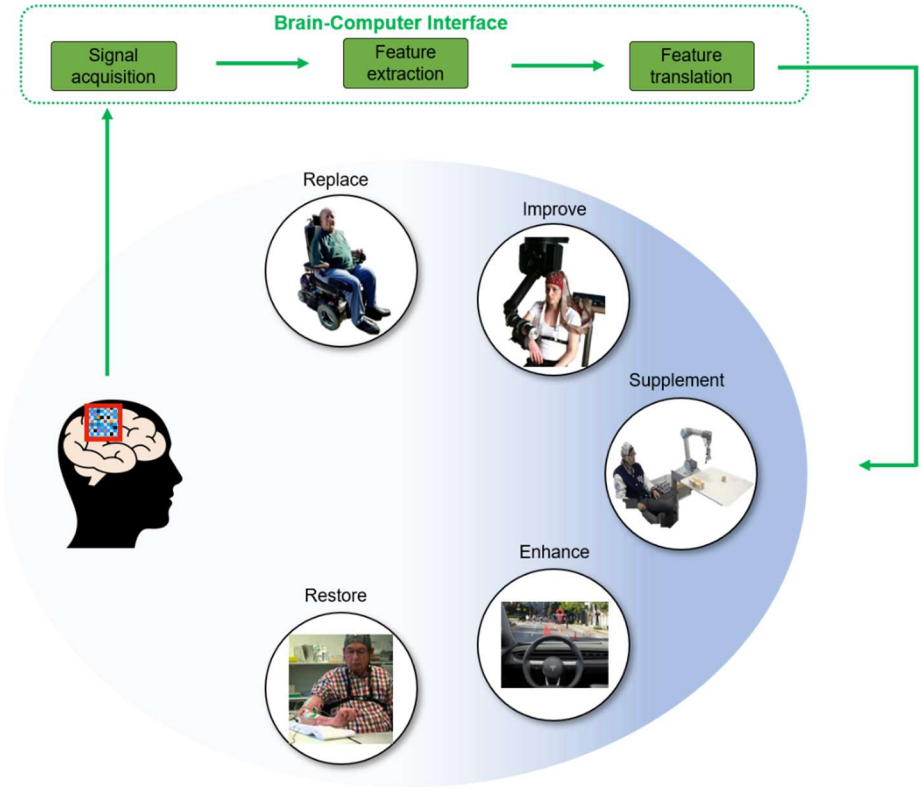


Figure 2.2. A schematic of design and operation of brain-computer interface. modified from Wolpaw et al. [27].

User's stroke affected hand is placed behind the mirror and the stroke nonaffected hand in front of the mirror. They are asked to perform wrist and finger flexion and extension movements on the nonparetic side, while they are asked to look into the mirror, watching the movement of their nonaffected hand, thus seeing the reflection of the hand movement projected over the affected hand. It is suggested that congruent visual feedback from moving nonparetic hand, provided by a mirror would restore function of the affected hand [25]. The congruent visual feedback can also be provided with BCI using a virtual avatar. Instead of giving the movement visual feedback with a mirror, an avatar with moving hands can be even a better visual feedback. The movement intention determined by BCI can control the virtual body parts of the avatar. The advantageous point is that the virtual environment can be adjusted or augmented for the sake of visual feedback.

BCI output can also help to enhance the CNS output. We might make mistakes even in routine and trivial tasks. It can be due to tiredness, confusion, or being inattentive. There might be other causes involved such as being under influence of alcohol or drug, brain or body injuries, and environmental distractions. BCI can be beneficial to determine tiredness or lapse of attention and help to reduce the corresponding human error. For instance, alertness in activities such as driving a car or monitoring radar screen to locate adversaries is of high importance. Lapse of attention even for a second may cause irreparable damage. Also, the most alert people can make mistakes if they cannot manage the burden of mental tasks. The underlying confusion is typically caused by lack of understanding and cognition, and people are usually not willing to express it. There are other situations that require detecting certain objects as targets and avoid responding to non-targets. Finding a specific picture among thousands of pictures is an example of such task. BCI can help to enhance the users' performance with providing additional information channel about their momentary attentional state. Reading brainwaves may allow us to shed light on ephemeral alertness, and to determine the present selective attention towards target and non-target object stimuli. Further, exposing users with sensory feedback on the decoded attentional state may enhance the level of attention, if applied through time in multiple sessions.

BCI output may be used as a supplement to the CNS system. We are limited by our two arms and two legs. Even, when we perform a task with one hand, still the other hand might not be able to perform another task, simultaneously. With BCI, it is possible to for instance type with two hands while also using a cell phone to dial a number or switch on the light. In addition to perform multiple concurrent things, BCI may provide capabilities that is beyond one-person stamina. For example, moving a bulky object. Supervisory control using BCI falls into this category. We can pre-define the sequence of actions of robotic arm and instead of continuously control the movement of the robotic arm, the user can initiate the actions only. The scheme makes a supplementary BCI so that users won't need to devote their entire attention to the task.

2.2 Brain Imaging Techniques for BCI Systems

Brain activity is manifested in three types of electrical, chemical, and metabolic phenomena. These phenomena are significantly different in nature. Neurons' action potentials are the result of chemical reactions in and around the neurons. We can capture the activities with through various electrical, magnetic, or metabolic modalities. They may have different spatial, temporal, and spectral resolution which impose different technical requirements. Due to its fast response, the current focus of the BCI designs are based on the electrical or magnetic signals generated by brain activity. According to the spatial resolution, we can categorize the current brain electrical activity recording methods into three categories: LFP, ECoG, and EEG. The difference between these methods lies in their spatial scale and the location of the electrode. Figure 2.3 shows the location of recording sites of different electrophysiological signals.

Local Field Potential (LFP). Placed inside the brain in the cortical tissue and records electrical activities in response to synaptic activities within 0.1 mm of the electrode. It can typically collect activities from the brain tissue volumes in the order of 10^{-3} to 1 mm^3 range. LFP captures activities in synaptic knobs in microscale spatial resolution, translate to 10^2 neurons.

Electrocorticogram (ECoG). Placed on the surface of the cortex and captures synaptic activity of 2-5 mm depth of cortex. It can record activities from the brain volume of 1-20 mm^3. ECoG captures activities mostly in microcolumn pyramidal neurons, with 10^4 to 10^6 neurons' resolution.

Electroencephalogram (EEG). Placed on the surface of scalp and each electrode can record synaptic activity from a large portion of the brain (10-40 cm^2) which corresponds to a volume of 10^3 – 10^4 mm^3. Recording of the brain activity with each EEG electrode is the average of synaptic activity over 100 million to 1 billion neurons. The spatial and temporal resolution of different brain imaging techniques are illustrated in Figure 2.4. BCIs based on electric recordings are typically easier to deploy and widely used in the literature. There is also magnetoencephalogram (MEG) that is a technology to record brain's small magnetic fields. The technology has been available since 1980s and compared to EEG, it has much higher spatial resolution so that we can better investigate sources of brain functions. This brain imaging technique has several advantages over EEG. First, the skull bones and tissues are transparent to the brain's magnetic field. This characteristic is particularly helpful because the recorded signal would be less distorted and there would be less ambiguity on the constructed related current sources. Most of this uncertainty in the EEG recording caused by heterogeneous spherical shape of the skull and discrepancy of conductivities in different regions of scalp which is not existed in MEG recording. However, this advantage is offset by the fact that with today's technology, MEG coils must be placed a few centimeters above the scalp. So, in reality, EEG electrodes are much closer to the brain cortical sources compared to MEG. Figure 2.5 shows an MEG scanner with a patient.

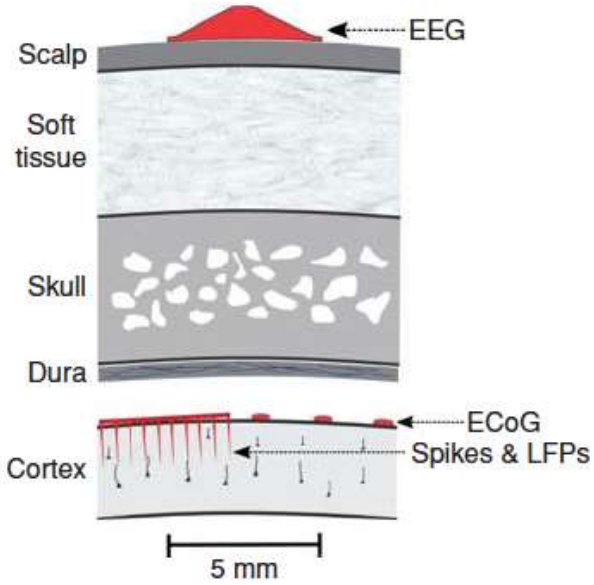


Figure 2.3. The location of different electrophysiological systems. Borrowed from [28].

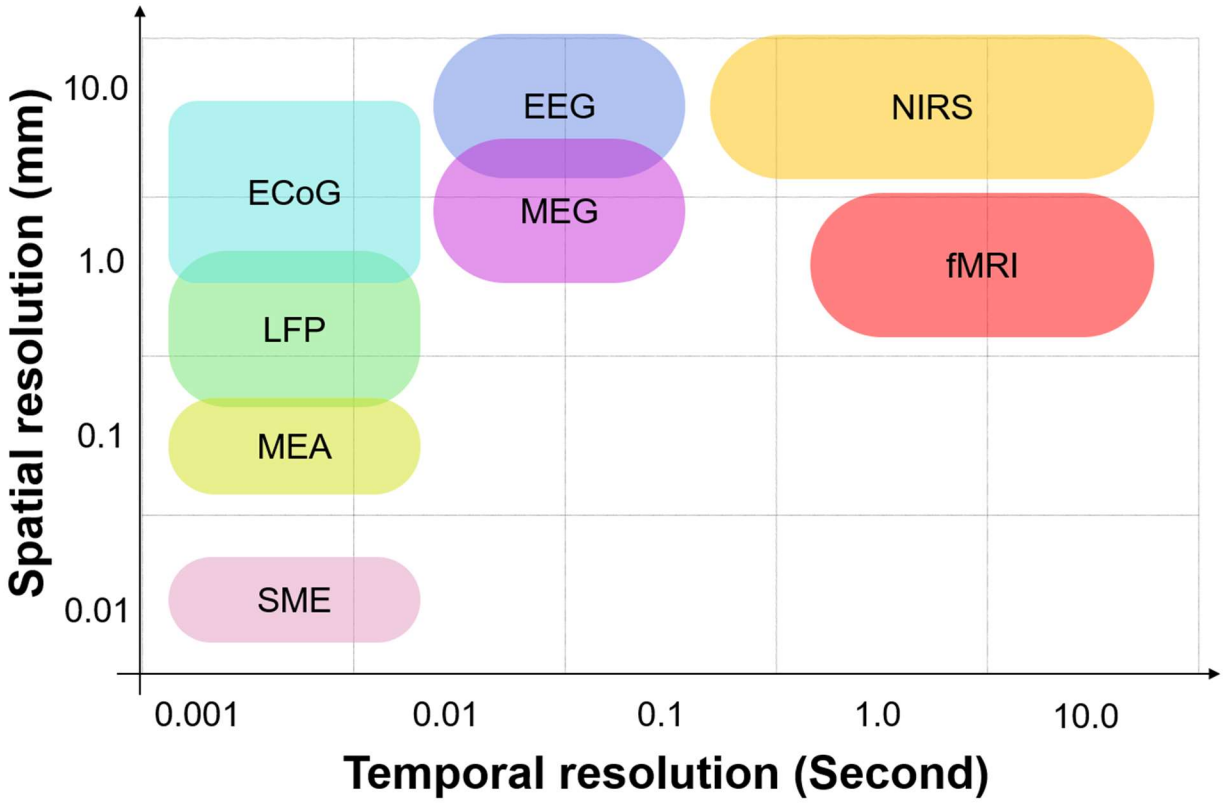


Figure 2.4. Comparison of spatial and temporal resolution of different brain imaging techniques.



Figure 2.5. MEG scanner with a patient. Borrowed from [29].

MEG technology is still expensive and not always practical to use. The technology needs shielded chamber and supercooling technology is necessary to cool down the coils. The discussed disadvantages may be a barrier to employing this brain imaging technique to be a primary method for BCI deployment.
All body organs absorb oxygen and release carbon dioxide to support the metabolic processes. Blood is pumped through veins and arteries from the heart and pass through organs and muscles. It transports oxygen and absorb carbon dioxide produced by metabolisms. The blood circulated through lungs to release the absorbed carbon dioxide and absorb fresh oxygen. The oxygenated blood pass through the heart and the cycle starts again. Hemoglobin (Hb) is an iron-containing protein in the red blood cells that carries oxygen and carbon dioxide in the blood. It is called Oxyhemoglobin (Oxy-Hb) when hemoglobin contains oxygen and deoxy-hemoglobin (deoxy-Hb) when it releases oxygen. Upon increasing metabolic activities of different brain regions, the associated neurons begin oxygen absorption from oxy-Hb. So, the consumption of hemoglobin that carries oxygen increases in the corresponding brain region. There is a delay about a few seconds between when neurons need oxygen and when oxygen absorption begins.

2.3 Closed-Loop BCI

BCI systems designed to operate in real-time. The BCI user and the BCI system interacts to accomplish a task based on the user's intent. The BCI interpret the engendered brain signals and translate these signals into outputs; i.e. outputs that different from the natural output of the CNS. The users have to be primed into those outputs in a timely manner. The timely harmonization between user intent and the corresponding BCI outputs helps users to continue generating the desired intent so as to the desired brain signals. The ultimate assessment of a BCI system is evaluating the performance of the system in real-time operation. In control system taxonomy, this is called a closed-loop system. In the closed-loop BCI, the user is repeatedly and persistently exposed to the effect of the real-time projection of his/her intention on the brain signals. It is the real-time operation of closed-loop BCI that ensures the independence of training and testing environment and is a viable testbed to evaluate BCI feature translation algorithms. Although the common practice is to infer knowledge from offline processing of the recorded signals, and to develop targeted translational algorithms, closed loop BCI is always the gold standard operation. The adaptation between the user and the closed-loop BCI may take place gradually after multiple sessions and over a prolonged experimentation. There is a great deal of individual differences that may result in differences in the adaptation process between users. Also, due to the complex effect of closed-loop experience over multiple sessions, it is very arduous to directly compare the influence of different feature selection and/or translational algorithms, even on a single user. As a result, given a BCI application, the

evaluation of different BCI setups with different feature selection and feature translation algorithms normally originates with simpler offline paradigms rather than a closed-loop online BCI. Thus, instead of evaluating the consequence of different BCI regiments and/or providing different artificial output engendered by BCI in real-time, we typically begin with exposing users with an open loop task and apply offline analysis on the recorded neural signals. A schematic of closed loop BCI is depicted in Figure 2.6.

2.4 Noninvasive EEG-based BCI paradigms

The convenience of recent technical improvements in portable wireless neurophysiological recording and the upsurge of machine learning analysis, in addition to the inherent high temporal resolution, have made EEG signals the choice of interest for clinical BCI applications [30]. EEG measures mostly the synchronized synaptic excitations of neuronal dendrites in the cortex. EEG may also include the synaptic activity in the deep brain structures. EEG-based BCIs have been used to control devices such as wheelchairs [31] and communication aid systems [32]. During the past decade, EEG methods have also become a promising approach in controlling assistive and rehabilitation devices [33]. To implement an EEG-based BCI system for a particular application, a specific protocol and paradigm has to be chosen for the experiment of interest. First, the user performs a particular task (e.g., imagery task, visual task) to familiarize with the task and to know how to modulate the brain activity while EEG signals are recorded. Using the recorded EEG as training data, a neural decoder for the paradigm is generated. Afterward, the user performs the task again and the neural decoder is used for BCI control.

2.4.1 Endogenous Paradigms Based on Motor Imagery Paradigms

Motor imagery is described as imagining a movement rather than executing a real movement (for more detail on motor imagery see [34]). Previous studies have shown that imagery movement corresponds to premotor, motor, and supplementary motor areas of the brain. These areas in the cortex are responsible for motor-related brain activities [35]. The most common motor imagery paradigms are sensorimotor rhythms (SMR) and imagined body kinematics (IBK).

2.4.1.1 Sensorimotor Rhythms (SMR) Paradigms

SMR is defined as the continuous imagination/execution of movement of large body parts such as hands, feet, and tongue, which could result in modulations of brain activity [36-38]. The imagery body movement associated with the paradigm causes event-related (de)synchronization (ERD) in mu (8-12 Hz) and beta rhythms (18-26 Hz). In contrast, relaxation results in event-related synchronization (ERS), (for an in-depth review see [39]).

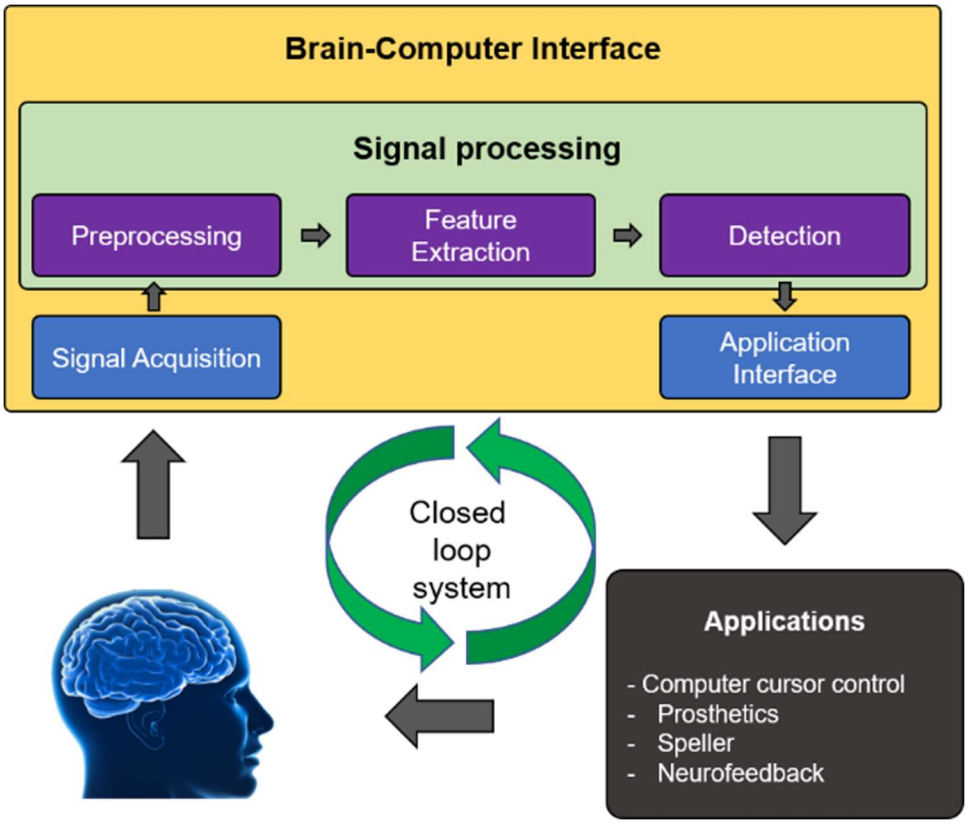


Figure 2.6. A schematic of closed-loop BCI.

The brain signal modulation caused by ERD and ERS are mostly projected in EEG signals over Cz, C3, and C4 (10/20 international system) which are locations above motor cortex. The modulated brain activity can be utilized as an additional output of CNS system to drive different applications. Wolpaw et al. [40] used the paradigm to control a computer cursor in one-dimension by mapping the relative mu power to the cursor velocity. Figure 2.7 shows examples of change in frequency spectra of SMR during imagination of hands. SMR has been one of the most promising paradigms used by patients with tetraplegia, spinal cord injury, and Amyotrophic Lateral Sclerosis (ALS) to repair or restore natural motor function. The paradigm was employed in a one-dimensional computer cursor control task by Wolpaw et al. [40]. Wolpaw and McFarland [41] used mu rhythms from four channels across left and right central sulci to move a cursor in 2D space to targets located in the four corners of a computer monitor. Subsequently, they used the same paradigm with people who had spinal cord injuries to guide the cursor to eight different targets on the sides of a monitor by imagining right and left-hand movement [42].They expanded the work into a 3D cursor control [43]. Guger et al. [44] used the paradigm on a prosthetic hand flexion to open and close artificial hand palm. Pfurtscheller et al. [45] used imagery of foot movement to restore hand grasp in a patient with tetraplegia.

Muller-Putz et al. [46] developed an EEG-based BCI system based on SMR using imagined foot and hand movements to help a paralyzed patient do simple tasks such as grasping a cylinder-like mold and moving an object using a functional electrical stimulation (FES) device.

2.4.1.2 Imagined Body Kinematics Paradigms

Imagined body kinematics (IBK) is a motor imagery paradigm that has been borrowed from invasive BCI technology [47, 48]. In IBK, the subject is asked to imagine a continuous natural movement of one body part in multi-dimensional space. The recorded signals are then decoded in the time domain using slow-wave low-frequency EEG signals. This paradigm is sometimes referred to as a natural imagery movement. In noninvasive devices, Bradberry et al. [49] investigated 2D cursor control with a natural imaginary movement paradigm and analyzed the data in time-domain frequencies of less than 1 Hz. In addition to Bradberry et al.'s work, Ofner et al. [50] studied the continuous and natural imagery movements of the right hand in a 2D plane. They estimated the imagined continuous velocities from EEG signals. Kim et al. [51] decoded the three-dimensional trajectory of imagined right-hand movement in space and also studied the influence of eye movements on linear and nonlinear decoding models in this paradigm. IBK paradigm is still an unexcavated method to noninvasive devices. Thus far, it has been applied to a limited number of applications. The reason for this is most likely due to the poor decoding of EEG signals [52]. Abiri et al. employed natural imagery movements of one hand to control different gestures of a social robot [53, 54] and to manipulate a robotic arm [55].

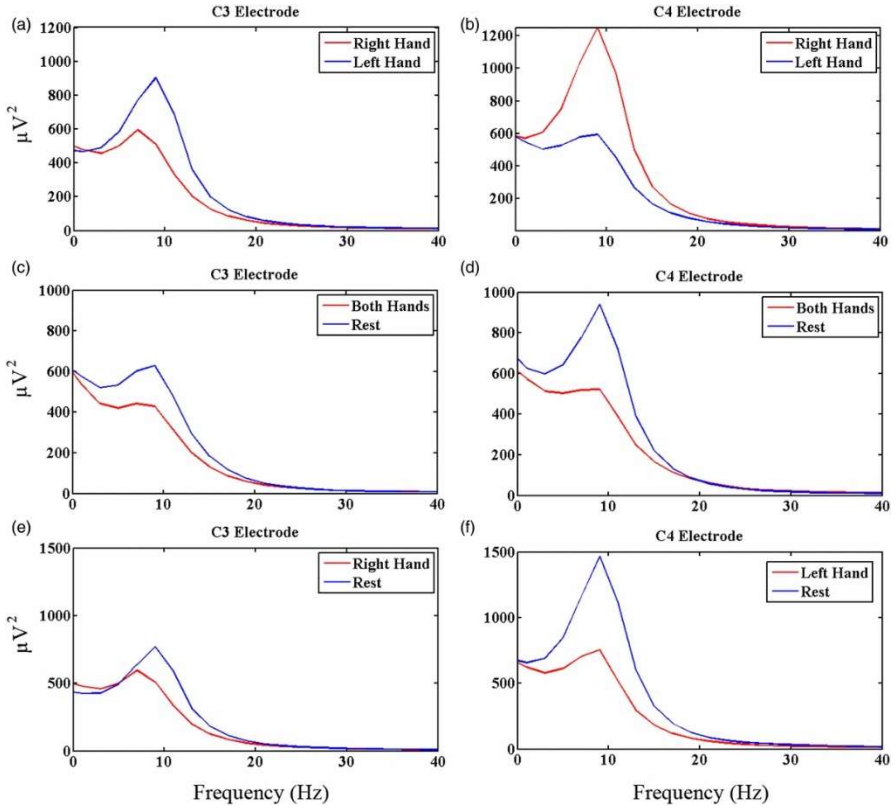


Figure 2.7. An example of a change in frequency spectra for EEG recorded from C3 and C4. The top row (a, b) shows spectral power changes in C3 and C4 electrodes while performing imagined movement of right hand versus left hand. The middle row (c, d) shows spectral power change in C3 and C4 electrodes while performing imagined movement of both hands versus rest. The bottom row (e, f) shows spectral power change in C3 and C4 electrodes for imagined movement of right hand versus rest and left hand versus rest, respectively (Figure copied from [56] with permission of a Creative Commons Attribution (CC BY) license).

Gu et al. [57] employed the imagined speed of wrist movements in paralyzed ALS patients. It was shown that employing natural IBK paradigms can potentially reduce the associated training time and may accelerate user adaptation.

2.4.2 Exogenous Paradigms Based on External Stimulation Paradigms

Brain activity can be affected by external stimulations such as visual, auditory, and/or somatosensory inputs. The altered EEG activity can be collected and decoded to control real or virtual objects or external prosthetics. The following sections discuss the most common external stimulation paradigms employed by BCI researchers.

2.4.2.1 Visual P300 Paradigms

Introduced first by Farwell and Donchin in 1988 [58], visual P300 is one of the most popular paradigms which has been known for the P300 speller. P300 is a brain signal signature elicited in response to infrequently presented phenomena (here visual stimuli) using what is known as an “oddball paradigm”. It is the largest positive peak in the event-related potential (ERP) ranging from 5 to 10 microvolts in size and a latency between 220 to 500ms posterior to the event onset (see Figure 2.8). ERP is defined as an average increase in the amplitude of time series of brain signals which is most significant at midline locations (Pz, Cz, and Fz in the 10/20 international system). This exogenous (stimulus-driven) paradigm has the advantage of eliciting almost a robust EEG signals among most people. Thus, it is expected to use P300 with less calibration time and high accuracy. Disadvantages of the paradigm include fatigue caused by the high level of attention and visual focus required to use the system [59], and the incapability to use for people with visual impairments [60].

Visual P300 has been embedded in prosthetic keyboards to provide an additional communication pathway for disabled patients. Usually, spellers consist of a matrix of alphanumeric characters [61]. Rows and columns of this matrix are flashed in (random) sequence, and the user has to focus attention to the character of interest. The BCI uses a statistical model to identify the character. People with ALS [62-64] and brainstem stroke [65] can type and communicate with P300 spellers. The paradigm has also been investigated as a mean for robotic BCI [66] for different applications such as control a humanoid robot [67], to navigate a wheelchair [68, 69]. and to control a computer cursor in 2D space [70].

2.4.2.2 Steady State Visual Evoked Potential Paradigms

In SSVEP paradigm, a constant frequency flickering stimulus on the central retina results in an EEG pattern consistent with the flickering rate. The frequencies of stimulation can be varied from low (1~3.5 Hz) to high frequency (75~100 Hz) [71]. The stimulus can be produced using a light-emitting diode (LED) or a cathode ray tube (CRT).

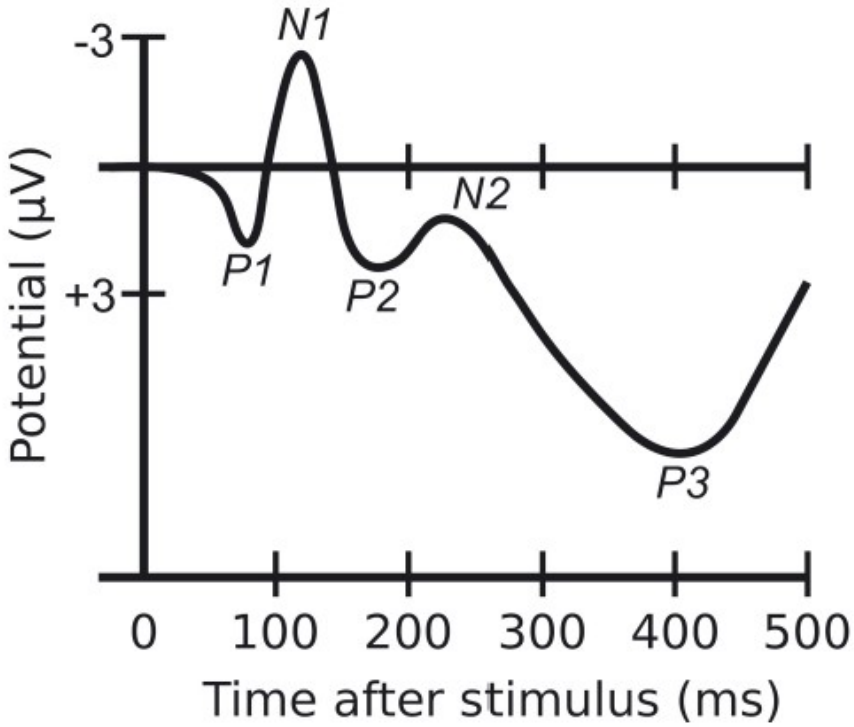


Figure 2.8. ERP components after the onset of a visual stimulus (figure copied from [62] with permission).

Multiple flickering targets with distinct flickering frequencies are typically presented to the user. There is a strong correlation between flicker frequency plus its harmonics and the observed frequency of the EEG. The user's intended target is determined by matching the pattern of EEG activity to the command associated with the particular frequency.
There are advantages associated with SSVEP paradigm. Because the stimuli are exogenous, it is a no-training paradigm that can be used by many subjects. The stimuli flash at many different frequencies, thereby resulting in many commands and more degrees of freedom to control prosthetic devices. In addition, the SSVEP frequencies can be more reliably classified than event-related potentials. However, the use of flickering stimuli could lead to fatigue for the subject, mainly when using low flickering frequency [72-75]. This paradigm is also not well suited for people with visual impairments due to the required gaze shifts during use. However, Min et al. [76] have recently proposed a new SSVEP paradigm that uses a grid-shaped line array. They suggested that this novel presentation is gaze independent. There are also steady-state somatosensory evoked potentials (SSSEP) [77] and hybrid SSSEP and P300 applications [78].

2.4.2.3 Error-Related Potential

Error-related potential (ErrP) recently is an ERP response occurs when there is a mismatch between a user's intention to perform a given task and the response provided by the BCI [79]. For instance, assume a user intend to move a cursor from the middle of a monitor to the left side of the monitor. If the cursor erroneously moves to the right, an error-related potential is engendered. ErrP is mostly pronounced at frontal and central lobes and has a latency of 200-700ms. The paradigm no longer relies on an average number of trials like in P300, but it uses a short window in a single trial basis. Ferrez and Millan [80] decoded errors followed the occurrence of miss recognition of user intent by the BCI system. Subsequently, Chavarriaga and Millan [81] utilized ErrP to control an external autonomous device using the concept of shared autonomy. The shared autonomy describes the situation where the user has only a supervisory control over the action of a system upon which he/she has no continuous control. They could extract ERP response located over the medial-frontal cortex with a negative amplitude around 260ms after an error was detected by the user. Moreover, it has been shown that the amplitude of the ERP is inversely [81] modulated by the frequency of the autonomous system error. A real-time and closed-loop BCI system can be regarded as a control problem. The ErrP can be used to adjust the input control signals to the device. While in a traditional control system, the adjustment is performed by the using linear or nonlinear controllers, in a BCI system where the brain plays the role of controller, the adjustment can be automatically performed by the power of brain signals (for more information see review [82]). Finding a suitable controller in a traditional

control system has become a solvable problem; however, understanding brain-controlled signals and translating them into logical and stable commands for usage in an external device remains challenging. This investigation is further discussed in a study by Artusi et al. [83]. The process of using ErrP in a closed-loop BCI system could be considered as analogous to “learn from your mistake”. In contrast to a traditional control system, in which error signal can be sensed in milliseconds, the brain does not produce an ErrP until 200ms-700ms after the subject receives feedback [80, 83]. The feedback is the relevant event whose onset engages the brain circuits to process error-related information. The delay and non-stationarity of the signal slows the system and makes real-time implementation difficult. Additionally, since the ErrP does not contain any information about direction or magnitude, there is still the challenge of how to adjust command signals based on detected ErrP in a multi-degree-of-freedom control system. Thus, most BCI systems are designed using pre-learned algorithms to perform a task in a closed-loop BCI [81, 84]. Recently, Iturrate et al. [85] developed a BCI system using the ErrP to autonomously complete a task after a training time of several minutes. In their task, a brain-controlled robotic arm learned how to reach a specific target based on a pre-learned algorithm using ErrP paradigm.
The use of ErrP in BCI systems was initially investigated by Ferrez and Millan [80]. Chavarriaga and Millan [81] employed the ErrP to allow a user to control and correct the behavior of an external autonomous system. In their approach, the user watched and maintained supervisory control over the autonomous system in order to correct behavior of a system without any direct or continuous control. ErrP has been employed for robot reinforcement learning [86], 1D cursor control, [80, 81, 87-91] and 2D cursor control [85, 92]. Iturrate et al. [84] used ErrP with shared control for a 2D reaching task. ErrP has also been used in BMI systems to control artificial [93] and robotic arms, [90, 94], and it has been used to teach a robotic BMI system how to reach a particular target in a 2D plane [85]. The ErrP can provide additional information to improve closed-loop BCI systems. It is likely that, in the future, the ErrP will allow a user to observe and spontaneously make the desired change in a BCI system without the need for directly performing a control task [95, 96].

2.4.3 Hybrid Paradigms

A hybrid paradigm refers to a combination of two or more physiological measures in which at least one is EEG (for review see [97-99]). The other physiological measures could be other bio-signals such as heart rate (ECG), eye movements (EOG) or hemodynamic signal recorded by fNIRS [100]. In hybrid paradigms, sequential or simultaneous processing structures can be used to output control commands to the BCI system [98]. Visual P300, SSVEP, and SMR paradigms are the most prevalent paradigms in the development of hybrid BCI systems [101, 102].

In recent BCI studies, combining various mentioned paradigms or combining a BCI paradigm with another interface has shown to enhanced BCI performance. For example, Luth et al. [103] paired P300 and SSVEP in controlling an assistive robotic arm. In a 2D cursor task, Li et al. [104] used Mu and Beta rhythms for controlling horizontal movement and P300 for vertical movement. Bi et al. [105] also used a combination of SSVEP and P300. The SSVEP paradigm was used to extract directional information (clockwise/counterclockwise), and the P300 was used to decode the speed of the cursor. To minimize false positive rates of the user's resting state, Pfurtscheller et al. [106] introduced a hybrid BCI that combined of event-related synchronization (ERS) and SSVEP collected from an EEG channel located above motor cortex and another electrode located above visual cortex. Allison et al. [107] developed a 2D cursor control BCI incorporating SSVEP for decoding horizontal and event-related desynchronization (ERD) for vertical movements.

Hybrid paradigms have been developed and applied to many BCI applications. Some studies have used a combination of two EEG signals to control virtual objects and prosthetic devices. For example, Bi et al. [105] used P300 and SSVEP paradigms to control a 2D computer cursor. Allison et al. [107] used SMR and SSVEP paradigms to control a computer cursor in 2D space. Li et al. [104] used SMR and P300 paradigms to control a 2D computer cursor. Horik et al. [108] combined SMR and SSVEP to control a 2-DOF artificial upper limb. Also using SMR and SSVEP, Duan et al. [109] controlled a humanoid robot to perform simple tasks. Pfurtscheller et al. [106] evaluated the feasibility of orthosis control using a combination of SSVEP and motor imagery paradigms. Yu et al. [110] also used a combination of SSEVP and motor imagery to enhance training performance for a motor imagery paradigm. Luth et al. [103] employed a hybrid P300 and SSVEP for a low-level application of a semi-autonomous robotic rehabilitation system.

In other hybrid BCI systems, EEG is combined with other bio-signals such as EOG. For example, Kim et al. [111] and Malechka et al. [112] developed wearable hybrid BCI systems using EEG and an eye-tracking device. Kim et al. [113] employed their system with a motor imagery paradigm to control a quadcopter in three-dimensional space. Ma et al. [114] developed a novel hybrid BCI using eye movements and the P300 ERP to control devices such as mobile robots and humanoid robots. Other studies have combined EEG paradigms with other neuroimaging techniques (e.g., fNIRS) for communication purposes in ALS and monitoring of patients vigilance state [100] and to control external devices such as quadcopters [115]. Figure 2.9 demonstrates the taxonomy for BCI systems.

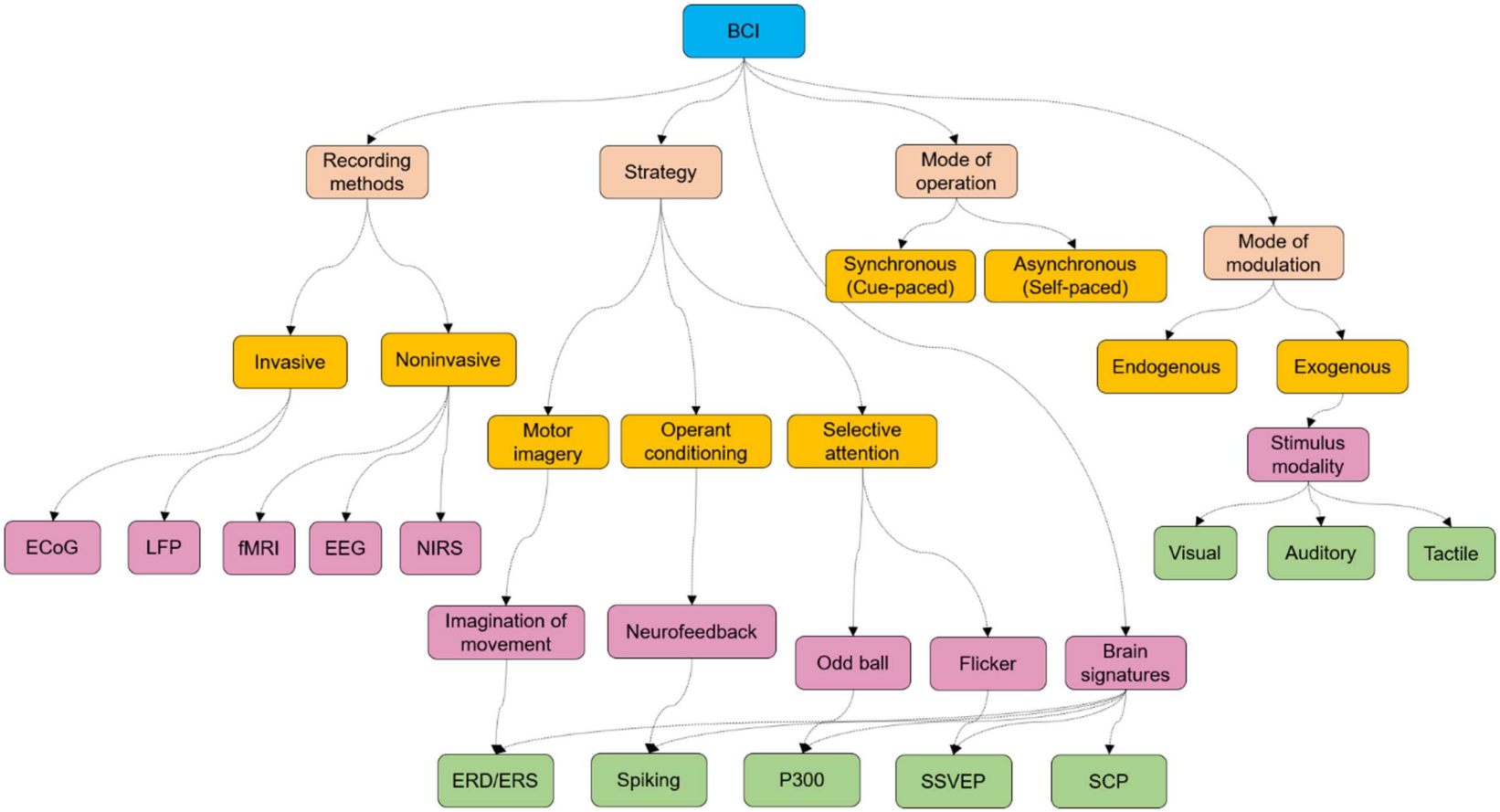


Figure 2.9. Flow diagram of taxonomy for BCIs.

3 Chapter Three: Modeling the Imagined Body Kinematics and Optimizing Model Prediction

3.1 Introduction

The interest in Brain Computer Interface (BCI) applications has grown and advanced since its initial establishment in the 1960s [30]. A brain-controlled computer cursor is commonly investigated as one of the primary testbeds for BCI applications. The cursor control platform can be used to control external devices, which may be used to help individuals who are suffering from the most severe motor disabilities, including people with amyotrophic lateral sclerosis (ALS), spinal cord injury, stroke, and other serious neuromuscular diseases or injuries. The activities of the brain during control of the computer cursor are recorded by either invasive or noninvasive means [30]. In the invasive domain, many systems have been developed using electrocorticography (ECoG), single units, and local field potentials on humans and primates [47, 48, 116]. While these systems have achieved impressive results, there are potential risks from surgeries and implantations associated with invasive BCIs. To combat some of these issues, noninvasive methods such as electroencephalography (EEG) has been investigated as a more attractive option due to its low-cost, portability, and less associated risks [30]. Using these techniques, several paradigms have been developed for EEG [117], including sensorimotor rhythms (SMR) [40, 42, 43, 118], external stimulation [119], and imagined body kinematics (IBK) [38, 49, 120].

SMR has been one of the most prevalent paradigms in BCI applications that involves extracting the mental states from imagined movements of large body parts such as the hands, legs, or tongue [38]. This approach is based on the variations in the Mu and Beta rhythms from the sensorimotor cortex [36, 37]. Using SMR, various researchers have mapped these signals to the kinematic parameters of a computer cursor in one dimension (1D) [40], two dimensions (2D) [41, 42, 121], and three dimensions (3D) [43]. Other studies have explored using a hybrid EEG paradigm between SMR and other methods [98]. For example, SMR has been merged with Steady State Visual Evoked Potential (SSVEP) [119] and P300 potential [104] to attempt 1D and 2D cursor control. The issue with SMR-based approaches is a lengthy training time (often several days or weeks) for subjects to learn how to modulate the specific frequency bands necessary to manipulate the cursor in the desired manner [40-43].

Recently, IBK has been proposed as a novel approach for noninvasive computer cursor control [49, 120] and real-time robotic manipulation [122]. In IBK, the subject is asked to imagine the continuous movement of one body part in multi-dimensional space. The recorded signals are then decoded in the time domain. Bradberry et al. [49] investigated the 2D cursor control problem with this EEG-based BCI paradigm. They instructed their subjects to use the natural imaginary movement of the right-hand index finger to track a computer-controlled cursor. The approach has been previously investigated in the invasive BCI domain, where subjects with implanted electrodes could achieve target

acquisition using imagined kinematics of one body part [48, 123]. Also, Ofner et al. [50] studied the underlying neural patterns in continuous and natural imaginary movements of the right hand in a 2D plane. They used continuous EEG signals to estimate the imagined velocities. Andres et al. [124] investigated the influence of eye movements on both linear and nonlinear EEG decoding models on a two-dimensional trajectory of imagined right-hand movements. Kim et al. [51] conducted a similar study in 3D space using linear models. Gu et al. [125] decoded the imaginary movements of the right wrist at two different speeds and in another study [57] utilized the imagined speed of wrist movements in paralyzed ALS patients. There are other studies on the imaginary movements of the shoulder, elbow, wrist, and finger [126-128]. It is believed that the IBK paradigm is a more natural cursor control method compared to SMR and SSVEP since the IBK decoder directly maps the user's intention to the cursor kinematics [129, 130]. In contrast, the SMR paradigm requires the user to imagine activating a body part, which is associated with a predefined cursor movement [121]. On the other hand, the SSVEP paradigm utilizes shifting gaze between lights flickering at different frequencies [107]. IBK also provides the benefit of a significantly reduced training time compared to these other approaches [129]. Using IBK, Bradberry et al. controlled a cursor in a 2D space with just 40 minutes of training and calibration [49]. This suggests that using the more natural paradigm of imagined body kinematics can significantly reduce training time. The paradigm of IBK utilizes the low-frequency components of EEG (less than 1 Hz) to extract the kinematic information necessary for control of external devices [49, 52]. In the previous study, a decoder model of multiple linear regression was used to predict the velocity of a computer cursor from EEG [120]. This model allowed for fast processing times and decent accuracy during online trials. In this work, we aim to explore optimal channels and algorithms to decode cursor kinematics from IBK data.

3.2 Methods

3.2.1 Data

Data used in this work was collected in [120]. A total of 32 healthy subjects with no prior experience in participating in any BCI studies were fully informed about experimental procedures, potential risks, and benefits. All experimental procedures were approved by the Institutional Review Board at the University of Tennessee. The subjects were recruited from the University of Tennessee. The study included 32 healthy subjects (7 females and 25 males; with age of 22.7 ± 3.5) with no prior experience of using BCI. No subjects reported any neurophysiological problems. Twenty-nine participants were right-handed, two were left-handed, and one was ambidextrous. Subjects participated in the tests after signing informed consent. For the experiments, a dual-monitor PC was provided; one monitor for the experimenter and another one for the subjects. Participants were asked to sit comfortably in a fixed chair and at arm's length in front of their monitor, with their hands resting in their lap. An Emotiv EPOC headset with 14

channels was chosen to collect EEG signals wirelessly [131]. The electrodes were hydrated and placed on the subjects' heads in a way to make correct contact with the scalp (scalp-electrode resistance < 10KΩ). The quality of electrodes' contact with the scalp skin was monitored via the TestBench software from Emotiv during recordings. Both EEG data and cursor kinematics were collected and stored by the BCI2000 software system at 128 Hz during the experiments. Meanwhile, a band-pass filter with cutoff frequencies at 0.2 Hz and 30 Hz was applied to the collected EEG signals [132]. Figure 3.1 shows a schematic of the BCI platform and the task.

3.2.2 Training Protocols

During the training phase, the participants were shown a computer cursor whose movements started from the center of the workspace and advanced with an automated trajectory in one dimension; refer to Figure 3.2. The subjects were instructed to track the cursor while imagining moving a computer mouse with their dominant hand at the same speed and direction. They were asked to maintain normal eye movement while keeping their focus on the cursor. Meanwhile, they were asked to avoid blinking or moving their own body parts to prevent any further artifacts while the test was active. The dimension of the workspace was a 33 cm × 33 cm square on the monitor. The diameter of the cursor was selected to be 1.5cm (0.20% of the workspace) and targets were 2.4% of workspace with width 8% and length 30% of screen width. The training phase consisted of 5 runs of cursor horizontal movement and 5 runs of cursor vertical movement. The duration of each run was 60 seconds. The cursor movement in each run was a replay from a record, where the cursor was manually moved. The 5 horizontal runs and 5 vertical runs were recorded beforehand, and the sequence of the runs was kept the same for all participants. Figure 3.3 shows the cursor trajectory in runs 1 and 2 in horizontal and vertical directions, respectively.

3.2.3 Multivariate Regression of Cursor Velocity

It has been identified in multiple studies that among various kinematic parameters (position, velocity, and acceleration), decoding velocity of body parts has shown higher predictive capabilities in both offline analysis and real-time implementation [49, 133-135]. To correlate the brain's activities and the movement of body parts, many decoding algorithms for EEG data have been investigated by researchers in both frequency and time domains. Most of the studies based on the sensorimotor-rhythms paradigm were developed in the frequency domain for cursor control and external devices control [33, 40, 42, 43, 56, 121, 136-139]. In time domain, various linear and nonlinear decoding methods have been developed to directly present a prediction model for the body kinematics parameters based on EEG signals. For example, Kalman filter [140], particle filter model [141], and kernel ridge [51] were applied in decoding EEG signals for offline analysis and prediction of body velocity parameters.

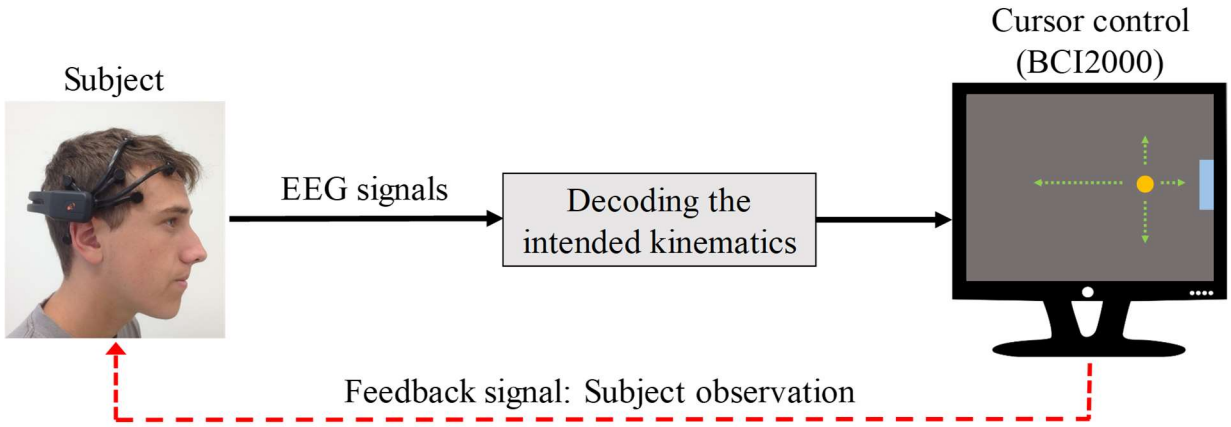


Figure 3.1. Schematic of the EEG-based BCI platform in cursor control task.

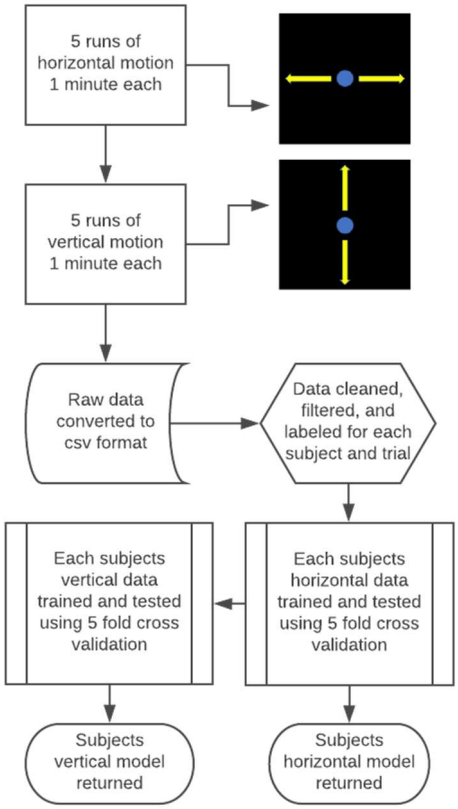


Figure 3.2. Training protocol and model generation for horizontal and vertical trials.

Ordinary least square (OLS) as a multiple linear regression has been the most common method for decoding EEG data in offline modes [51, 133-135, 142, 143] and in real-time implementation [49]. It is a generalized multiple linear regression model to estimate a single response variable by multiple explanatory variables (features). It uses the least square error as an objective function. The OLS minimizes the sum of the squared error (L2 norm); see Equation 3.1

Equation 3.1
$$\beta_{OLS} = argmin \sum_{i=1}^{n} (y_i - X\beta)^2$$

where y_i represents the response (dependent variable), X represents the independent variables, and β is the model coefficient. The technique is unbiased since the expected values of the model coefficients (β) over multiple sets of data samples is very close to each other. This analysis can be represented by the following equations. Equation 3.1 and Equation 3.2 map the acquired EEG data to the observed cursor velocities in the horizontal (x) and vertical (y) directions from the training data. In other words, the aim is to reconstruct the cursor trajectories off-line from EEG data and obtain a calibrated decoder for real-time implementation for each subject, individually. Output velocities at time sample t in the x (horizontal) direction is $u[t]$ and in the y (vertical) direction is $v[t]$. In these equations, $e_n[t-k]$ is the measured voltage of EEG electrode n at time lag k where the total number of EEG sensors is $N = 14$ and the total lag number is $K = 12$. These numbers were determined during previously published works by the authors [120]. The variables a and b are the weights that could be obtained through multiple linear regression. To assess whether this method is the optimal model for velocity prediction, a standard least squares model was tested against several other regression techniques. The OLS allows more than one explanatory feature to be employed in the model, which may raise concern when there is correlation (multicollinearity) between the explanatory variables. Two other models selected for comparison were ridge regression and Theil-Sen regression [144]. Ridge regression is a multiple regression method, which tries to address the multicollinearity problem in the data feature. OLS regression although unbiased, can suffer a high variance if data features are highly correlated. This causes dramatically large regressor coefficients. Ridge regression minimize the squared residuals in addition to a regularization term to reduce unregularized errors; see Equation 3.2.

Equation 3.2
$$\beta_{Ridge} = argmin \sum_{i=1}^{n} (y_i - X\beta)^2 + \lambda \sum_{j=1}^{p} \beta_j^2$$

where λ is a regularization term to avoid large regressor coefficient. We also used a nonlinear estimator named Theil-Sen regressor. It is less sensitive to outliers and

potentially can achieve more robust and accurate results compared to OLS linear regression. The regressor looks at all possible pairs of the data points and computes a list of slopes. Then, the regressor considers median for the estimation. Since the median does not care about a single value but it cares about the data rank, the Theil-Sen regression can be robust to the outliers. These models were chosen to assess the inclusion of L2 regularization on velocity prediction as well as to better deal with outlier data.

For training of the multiple linear regression model, 12 previous points of EEG data from each channel in memory along with the current sample were used as features. The model was then cross-validated against the other four trials of the same dimension (leave-one-trial-out cross-validation). This cross-validation was repeated for all five combinations of models to ensure the most accurate prediction. The models were evaluated using a developed correlation score called Goodness-of-Fit (GoF). This scoring technique separated the trial into segments of 5 seconds and averaged the Pearson correlation scores between the predicted and actual cursor velocities. Then, the averaged value of the Pearson correlation scores over each trial was defined as the GoF. Pearson correlation coefficient indicates how far away the predicted velocity is to the scaled cursor velocity [144]. Although we asked participants to minimize their body movement, noise caused by eye blinks is non-separable part of EEG response. Despite the very short period of spikes caused by the eye blinks, it usually affects the Pearson correlation to a great extent. Instead, our proposed definition of Goodness-of-fit takes the average Pearson correlation among segments of the 5-second period into the account. The 5-second period is roughly the period of pre-recorded cursor movement. The new definition of Goodness-of-fit is more robust to abrupt changes and occurring artifacts in one segment may not exceedingly affect the GoF of the whole trial. Thus, the method provided a better representation of fit by not allowing one improperly fit window to reduce the overall model's score.

Channel-wise prediction accuracy was investigated to identify patterns in predictive capability for both horizontal and vertical trials. The channels with the higher prediction accuracy could then be weighted more heavily during online testing while the channels with lower prediction can be eliminated. To perform the channel-wise identification, only the data from one channel was analyzed using the optimal regression model. The filtered data from each sample along with the 12 previous samples in memory were used as features. The model was then validated using leave-one-trial-out cross-validation. The prediction accuracy for the channel was scored using the Goodness-of-Fit metric.

3.2.4 Classification of Cursor Movement Direction

It was hypothesized that a classifier for horizontal and vertical motion could be employed as a method to improve the accuracy of the prediction model. This classifier

could be used as a gate to generate predictions on a model tailored for horizontal or vertical data. The foundation of the hypothesis is based on the assumption that imagined hand movements in the horizontal and vertical directions correspond to different brainwave patterns in EEG. Our assumption is indirectly motivated and supported by previous studies that successfully decode individual finger movement using EEG [145]. To classify cursor movement direction, EEG data in each trial were divided into 60 non-overlapping segments, each of which is 1-second duration. Features for each segment were collected by taking the Fourier Transform of the EEG data from each channel. Specifically, the mean, median, maximum, and minimum values of the power spectral density across the Theta (4-7 Hz), Alpha (8-15 Hz), Beta (16-32 Hz), and Gamma (32-40 Hz) bands were used to train a Classifier to discriminate between horizontal and vertical movements.

We chose to use the random forest for classification. The method uses a multitude of decision trees trained at training time to model the data [144]. Decision tree tends to overfit the data. However, by using an ensemble model like a random forest that utilizes underlying decision trees, we can reduce the variance. The method aims to reduce the correlation between decision trees using the pruning technique. It is robust to scaling and inclusion of sometimes irrelevant features. The classifier was cross-validated by splitting 70% of the randomized samples for training data and 30% for testing. Results were quantified using accuracy as the metric.

3.3 Results

3.3.1 Multiple Linear Regression

The multiple linear regression model was used as a predictor for cursor velocity from the filtered EEG signals. Goodness-of-Fit scoring was used to calculate the prediction accuracy. Each trial was cross-validated by training the linear regression model on the other four trials and testing on the current trials. For comparison, we evaluated the decoding algorithm using randomly generated signals and ran the simulations for 1000 times, which indicates the outcome at chance level [146]. The mean [standard deviation] from the chance level simulations is 12.9% [5.5]. Figure 3.3 shows a sample of two horizontal and vertical trials for illustration. Ten trials for all 32 subjects were analyzed, and their prediction scores were averaged for vertical and horizontal trials. The mean [standard deviation] of GoF for horizontal accuracy using least squares regression across all subjects was 70.79% [29.14] and the mean [standard deviation] of GoF for vertical accuracy was 38.33% [30.14], both of which are significantly higher than the chance level.

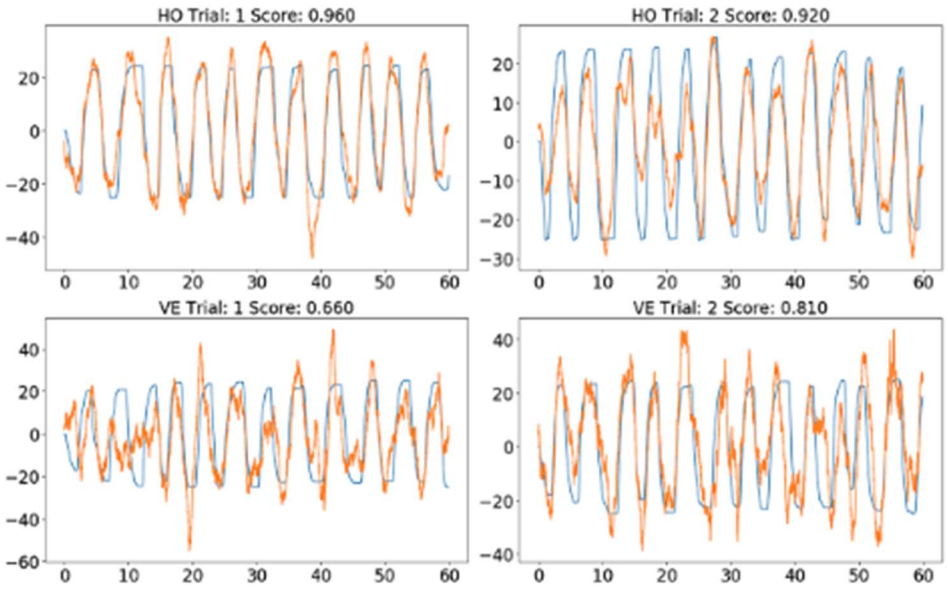


Figure 3.3. Regression results of one subject across two horizontal (top) and vertical (bottom) trials. Predicted velocity (orange) and target velocity (blue) with goodness of fit score above plot.

Aside from least squares, the model was trained using several other variations of the least-square algorithm such as ridge regression and Theil-Sen regression. Ridge regression was trained using a regularization alpha of 1.0. The higher regularization of the data leads to less accurate results across all subjects. Theil-Sen regression was trained with a subpopulation of 10,000 and showed slight improvements in most subjects. Table 3.1 and Figure 3.4 shows a comparison between the three models to illustrate the similarities in prediction capabilities. From our analysis of the performance of these models, linear regression demonstrated one of the best results for both horizontal and vertical predictions across all subjects. Theil-Sen regression preformed close to and in some places better than linear regression; however, this was often at the cost of a higher time complexity leading to longer training times. For this reason, the least squares model was identified as the optimal model out of the three evaluated techniques when taking into account time and GoF performance. Figure 3.5 shows the average GoF of individual EEG channels for horizontal and vertical trials.

We observed higher accuracy in participants' kinematics prediction from the horizontal compared to the vertical direction (Figure 3.5) during the training phase. One possible reason for this phenomenon may be explained by the fact that eye blink as a vertical eye movement may interfere with the model and interpreted as the actual cursor kinematics during the training of vertical cursor movement while the same is not true for the horizontal movement. Kinematics direction of eye blink is almost orthogonal to the horizontal eye movement, and it may not interfere easily with the actual cursor movement in the linear model [124]. The inherent difference of the requested task and the associated visual stimulation between the training and the target acquisition phases can be a consequential factor. The participants were trained to imagine moving the cursor in horizontal and vertical directions separately, but they were asked to imagine moving the cursor in two dimensions, concurrently in the target acquisition phase. The distinction in the training and testing phases may spell out the uncorrelated outcome measure in both phases. Also, it has been suggested that training is a reciprocal and bidirectional process [147]. Although having a personalized model is pivotal for a BCI platform, users adaptation and motor learning usually take place over multiple sessions of experiment [147]. Finally, using target hit rate as a measure of controllability for testing mind-controlled cursor control may be debatable, since it is possible to attain certain target hit rate without necessarily enough controllability over the cursor. We tried to address the issue by having a questionnaire to specifically collect the information. It is crucial to resolve the issue in the future works.

3.3.2 Channel-Wise Regression

Figure 3.6 shows a heat map of the average GoF scores across all subjects using each individual channel.

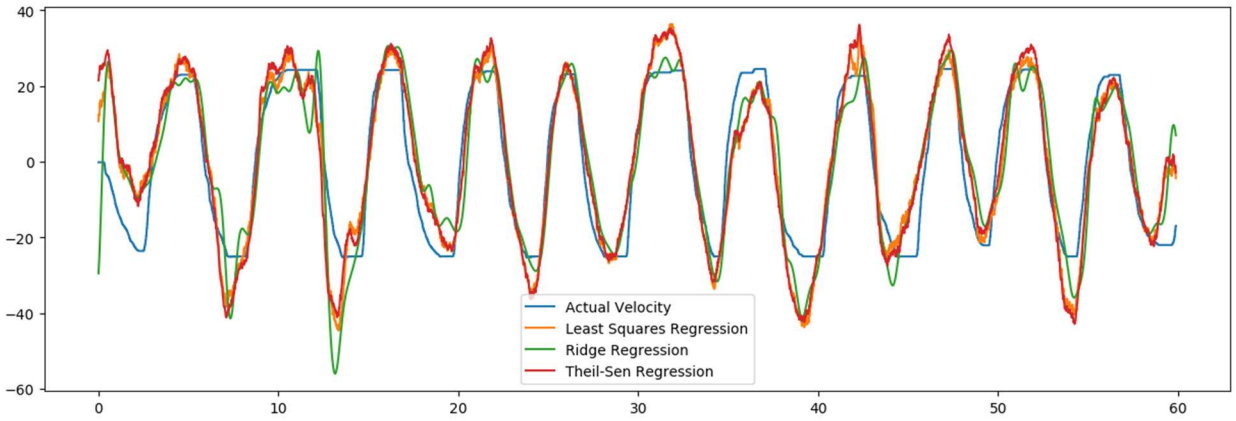
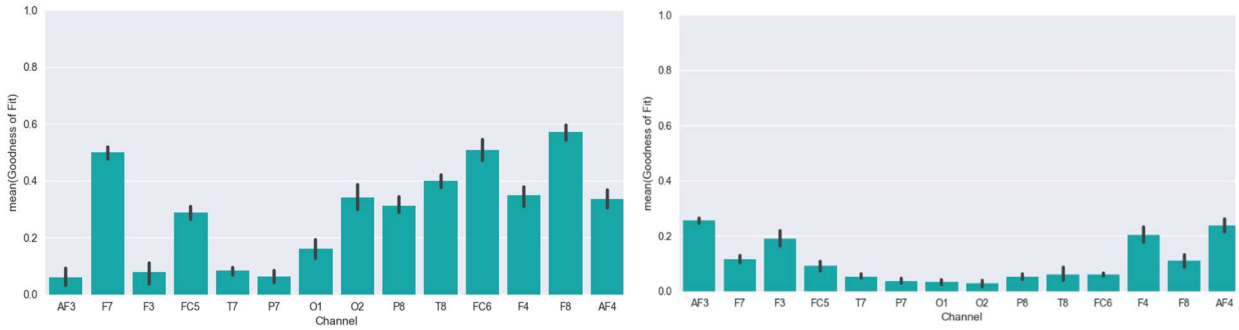


Figure 3.4. Predicted velocities plotted over the target for least squares, Ridge, and Theil-Sen regression for one sample subject and one sample horizontal trial.



a) Horizontal trials b) Vertical trials

Figure 3.5. Average goodness of fit of each channel for a) horizontal trials and b) vertical trials (bottom).

Table 3.1. Model comparisons for horizontal and vertical trials

Model	Avg. Horizontal GoF	Horizontal STD	Avg. Vertical GoF	Vertical STD
Multiple Linear Regression	70.79	29.14	38.33	30.14
Ridge Regression	68.18	28.30	35.40	28.23
Theil-Sen Regression	71.04	29.69	40.28	30.21

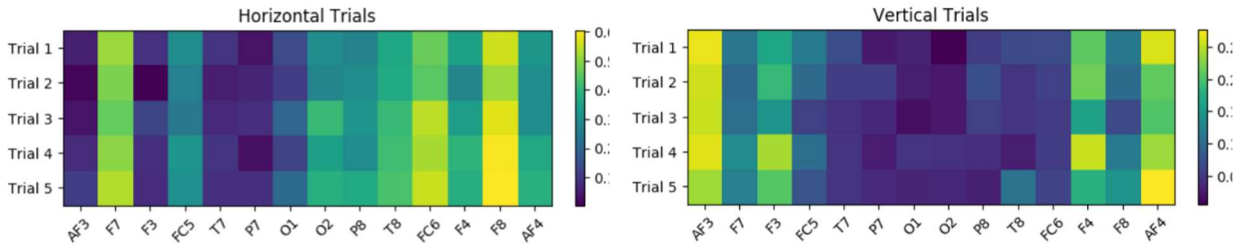
Here, the channel-wise analysis was based on the optimal regression model to determine which channels contributed the most to the overall prediction.
The results are based on leave-one-trial-out cross-validation. For reference, the 14-channel layout for the Emotiv Epoc headset used in this study is presented in Figure 3.5. The horizontal data showed that the F7 and F8 channels contributed the most toward velocity prediction. It is also noteworthy to mention that the right hemisphere demonstrates much higher prediction accuracy than the left hemisphere for horizontal trials. The vertical data indicates that the AF3, F3, F4, and AF4 channels contribute the most.
Using this information, different combinations of these relevant channels can be used in our prediction model in an attempt to improve the overall accuracy. The combinations were selected based on the prediction capability represented by the heat map in Figure 3.6. Table 3.2 shows the results of channel analysis for horizontal and vertical accuracy. Our results showed that horizontal accuracy could be improved most by using the channel combination of F7, FC5, T8, FC6, F4, and F8. For vertical accuracy, it was found that all channels are necessary for the highest prediction accuracy. However, it is interesting to note that the six frontal channels (AF3, AF4, F3, F4, F7, and F8) demonstrated accuracy comparable to all 14 channels (see Figure 3.7).

3.3.3 Classification

We also conducted numerical experiments to determine the movement direction from a segment of EEG signals. A Random Forest Classifier was used to discriminate between horizontal or vertical movement. Figure 3.8 presents the classification accuracies for four different features sets. The average classification accuracy was 79% for all channels and all features of mean, median, maximum and minimum of the four frequency bands of Theta, Alpha, Beta, and Gamma. Using only the mean values from the four frequency bands yielded an average classification accuracy of 80%. The same methods of all features and only means were repeated on the six frontal EEG channels of AF3, AF4, F3, F4, F7, and F8. These provided an average classification accuracy of 68% and 69%, respectively.

3.4 Discussion

Several models were used to test the prediction accuracy of the BCI platform. From a cursory analysis of various models and previous literature [51, 133-135, 142, 143], we choose to focus on variations of the least squares algorithm as they have typically shown the best performance. Ridge regression was chosen to test how the inclusion of L2 regularization affected the predicted velocity.



a) Horizontal trials b) Vertical trials

Figure 3.6. Heat map for channel-wise prediction in a) horizontal and b) vertical trials.

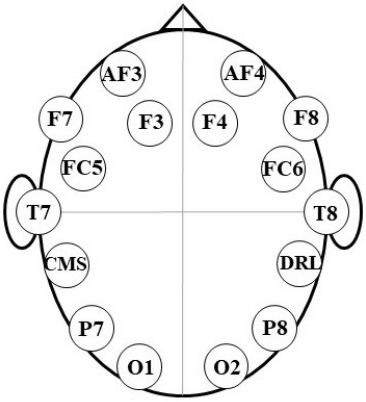


Figure 3.7. Emotiv EPOC channel locations.

Table 3.2. Prediction accuracy for various channel combinations

Channels	Horizontal Accuracy	Vertical Accuracy
F7, F8	69.96%	15.27%
F7, F8 + FC5, FC6, F4, T8	72.41%	31.78%
F7, F8 + O2, P8, T8, FC6, F4, AF4	71.03%	33.67%
AF3, AF4	41.89%	27.55%
AF3, AF4 + F3, F4	49.21%	28.35%
AF3, AF4 + F3, F4, F7, F8	70.02%	34.32%
All Channels	70.79%	38.33%

Ridge regression saw the lowest GoF scores even when the regularization parameter was set to near zero (zero regularization simply being least squares).
Theil-Sen regression was chosen for its advantages in dealing with outlier data and general robustness to corrupted data [148]. Theil-Sen reported slightly better GoF for most subjects which suggests that some noise, artifacts, or outliers are still present even after filtering. This shows the potential usefulness of robust least square estimators for BCI implementations. Models such as Theil-Sen regression and ridge regression often provided comparable accuracy to our multiple linear regression model based on least squares regression but at a much longer processing time. For this reason, the least squares model was chosen for the remaining tests. As demonstrated in the literature [12, 39, 41], the contribution of (electrooculogram) EOG to the decoding accuracy is insignificant. Bradberry et al. [12] also showed that the influence of muscle activity on the cursor movement is low. Since the EEG signal is subjected to a band-pass filter [0.2, 1] Hz, artifacts out of this range are removed from the regression.
During the evaluation of individual channels, it is interesting to note that there is a distinct pattern between the most predictive channels for horizontal and vertical trials. The F7 and F8 channels showed the highest standalone prediction for horizontal trials while the AF3, AF4, F3, and F4 channels were the highest for vertical. Using just the F7 and F8 channels as features for the linear regression model provided a GoF score that was less than 1% lower than using all channels for horizontal trials. This suggests that a headset with two sensors can be used with great effectiveness in horizontal tasks compared to 14 channels.
Vertical channels were unable to be improved by using different channel combinations. The combination of AF3 and AF4 channels gives the worst score among the tested combinations in Table II. Since AF3 and AF4 are influenced the most by eye movement, this indicates that eye movement may play an insignificant role in velocity prediction. It is worthy of pointing out that using EEG headsets with 32 or 62 electrodes may improve the decoding accuracies.
It can be seen from the results that horizontal prediction accuracy is much higher than vertical prediction accuracy. Further research is needed to determine the cause of this difference. It is also interesting to note that Figure 3.6 shows the channels located on the right hemisphere of the brain as more relevant to velocity prediction. The results of the classification approach show a very promising method of distinguishing between the intended horizontal and vertical movement. By achieving an average accuracy of 80%, this classifier can potentially be used in front of the regression model to improve performance. It is also noteworthy to mention that subjects with high Goodness-of-Fit scores did not always achieve high classification accuracies. In some cases, subjects with low-velocity prediction scores have much higher classification scores. Unlike previous work in the literature [49, 124], this research separated the training for two-dimensional cursor control into two simple one-dimensional training in horizontal and

vertical directions, respectively. The results here suggest a novel approach to expand the cursor control experiment from one direction to higher dimensions. Since the horizontal and vertical training are conducted separately, it allows us to distinguish between horizontal and vertical trials. The classification results suggest that patterns of the brain activities are different during horizontal and vertical cursor movements. The classification models developed here may be used to inform better decoding mechanisms.

Eye movement and muscle activity. One of the main questions in the BCI is to what extent different independent components, including neural activity, eye movement, and muscle activities may contribute to the experiment outcome. Eye movement artifacts can be removed using approaches such as Independent Component Analysis (ICA) [149] and Artifact Subspace Reconstruction (ASR) [150]; however, applying these approaches for real-time cursor control may be impractical because the methods require multiple iterations to converge which is not feasible in real-time. In the present study, we asked the participants to prevent overt body movement during the training and the target acquisition phases to reduce the impact of non-neural activities. However, there is an undeniable contribution of different neural and non-neural components. Brain activity measured over each EEG channel is a linear mixture of distinct cortical and non-cortical sources of activities. We utilized EEGLAB [151] for channel and source space processing. A high-pass filter with cut-off frequency of 0.3Hz was applied to remove the baseline drift and to reduce the ICA bias towards high amplitudes. We applied the Infomax ICA method [152] to extract independent contributing sources of signals. Then, we applied ICLabel plug-in [153] to classify the derived sources into neural activity, EOG, and others, including muscle activity, heartbeat, line noise, channel noise classes. Figure 3.9 shows the estimated heatmap of estimated components for neural activity, vertical, and horizontal eye movement. Afterward, we evaluated the predictability of 1) EEG with removed EOG components, 2) neural plus EOG components and 3) EEG signals. Figure 3.10, and Figure 3.11 shows the predictability of the MLR model with different signal sources, for horizontal and vertical cursor movements, respectively. As demonstrated in the literature [38, 49, 154, 155], although eye movement has a contribution to decoding imagined body kinematics; however, the results suggest that the enhanced outcome occurs when all signal components are included. In other words, neural activity and EOG together carry more information and are better predictive signals for the cursor kinematics compared to solitary neural activity. Such a positive correlation between eye movement and kinematics of a mind-controlled computer cursor has also been reported in [51, 124]. The results further suggest that cursor kinematics (here velocity) is not only encoded in neural and EOG components, but other signal components may carry the information.

Table 3.3 summarized previous BCI studies on EEG-based object control. For a thorough review of conventional EEG paradigms and associated decoding approaches, we refer the readers to our recent review article [117]. The main difference between our work and other relevant works in terms of efficiency may be related to the EEG headset. Unlike previous BCI studies with EEG headsets with typically many sensors (32 or 64 electrodes) and a higher sampling rate, we were interested to use a wireless and easily portable headset with only 14 electrodes.

Comparison of the usability with previous BCI studies: Usability of a BCI setup can be measured with a different objective and subjective measures. Task accuracy and information transfer rate are the most common objective measures while satisfaction, cognitive workload, and ease of use are the most common subjective measures [156]. There are a few usability studies on BCI-controlled applications. Using an SMR-based MI experiment, Nijboer et al. [157] investigated the effect of motivational factors such as confidence and fear of incompetence on the performance of BCI among individuals with amyotrophic lateral sclerosis (ALS). Although they could not show that motivational factors are always correlated with the BCI performance, they found that the higher training duration and lower information transfer rate on SMR-based MI compared to P300-based BCI may adversely impact the user's motivation. With a user-centered perspective, Kubler et al. [158] conducted a comprehensive usability evaluation on various communication and assistive BCI applications. The work also includes suggestions on the type of questionnaire and the associated BCI applications. They queried user's satisfaction on a Likert-type scale. The results showed that the users favored P300-based BCI over SMR-based MI BCI due to the learnability.

However, the users reported equal satisfaction on those paradigms when using BCI for entertainment despite the lower effectiveness (accuracy) and efficiency (information transfer rate) in SMR-based BCI. An inherent limitation of using a questionnaire is the susceptibility to self-perception, interviewer/observer, and recall biases. Although we attempted to minimize the impact of the biases, having a case-control design may help to address the limitation further. We may conduct a case-control design in the future study using random kinematics for the computer cursor in the control group to better examine the exposure to different confounding variables in tandem with the experiment outcome (controllability over the cursor).

3.5 Conclusion

In this work, an EEG-based Brain-Computer Interface platform was optimized through the evaluation of machine learning techniques, channel selection, and classification of cursor movement direction. Offline analysis of 32 healthy subjects' training data from a two-dimensional cursor control task was analyzed. A multiple linear regression decoder model derived from least squares was compared to models of ridge regression and Theil-Sen regression.

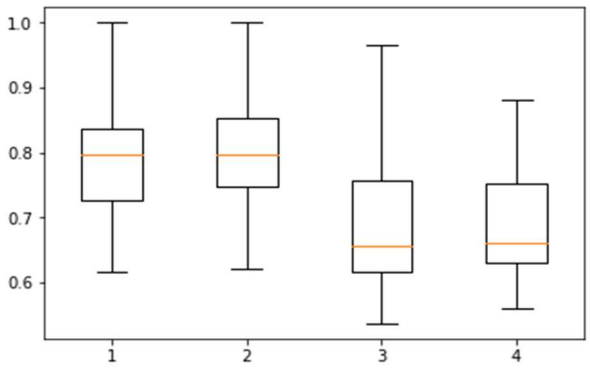
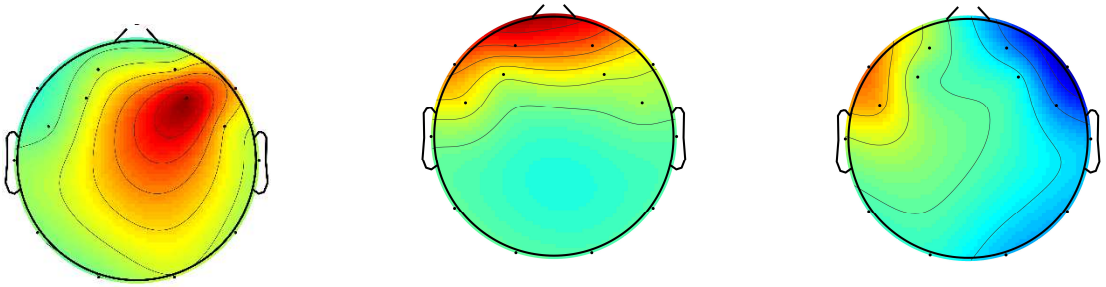


Figure 3.8. Boxplots of the classification accuracies using four different feature sets. (1) All channels and all features; (2) all channels and mean of the 4 frequency bands independently; (3) six channels (AF3, AF4, F3, F4, F7, and F8) and all features; (4) six channels (AF3, AF4, F3, F4, F7, and F8) and all features; (4) six channels (AF3, AF4, F3, F4, F7, and F8) and mean of the 4 frequency bands independently.



(a) (b) (c)

Figure 3.9. Estimated independent components of a) neural activity, b) vertical eye movement, and c) horizontal eye movement from a sample participant

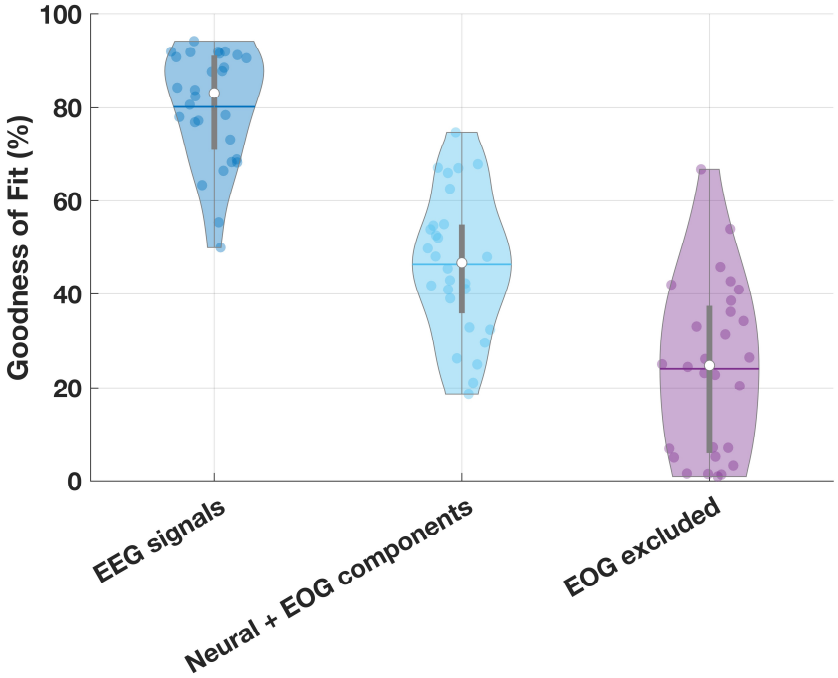


Figure 3.10. Violin plot of Goodness of Fit (%) for horizontal cursor velocity showing the contribution of different components

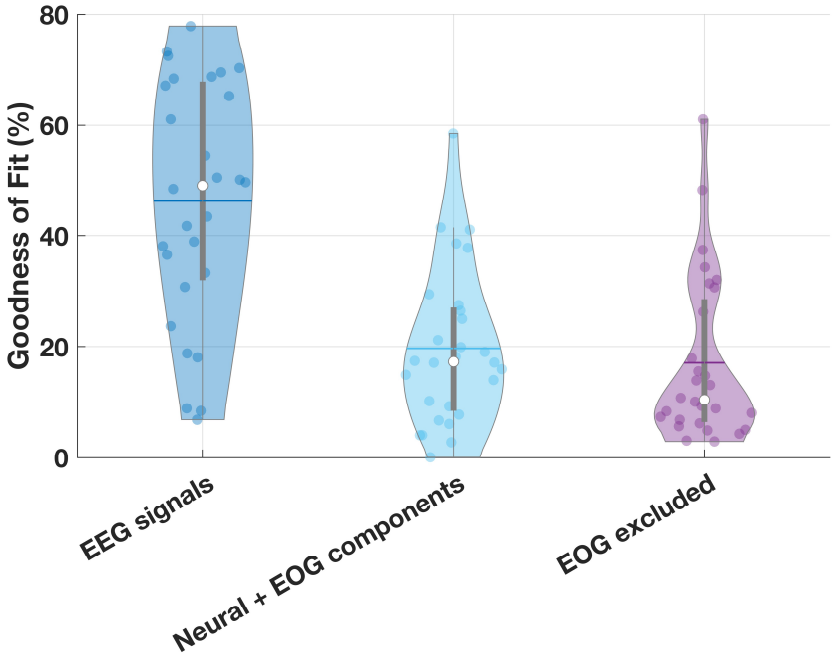


Figure 3.11. Violin plot of Goodness of Fit (%) for vertical cursor velocity showing the contribution of different components

Table 3.3. Previous BCI studies on EEG-based object control. ERS/ERD: event-related synchronization/desynchronization. LMS: least square method. SVM: support vector machine. PSD: power spectral density. LDA: linear discriminant analysis. KPLS: kernel partial least squares classification. MLD: Mahalanobis linear distance. RBF: radial basis function. GA: genetic algorithm.

EEG paradigms	References	No. of subjects	Control paradigm	Analysis	Mean success rate
SMR	Wolpaw et al. [40]	5	1D: hit 2 targets	Frequency analysis	76.0%
SMR	Wolpaw et al. [41]	5	2D: hit 4 targets on a screen	FFT	60.4 %
SMR	Wolpaw et al. [42]	4	2D: hit 8 targets on a screen	Linear regression + LMS	82.2%
SMR	McFarland et al. [43]	4	3D: hit an arbitrary target	FFT	75.8%
IBK	Bradberry et al. [49]	5	2D: 4 targets on a screen	Linear Regression on time-shifted EEG samples	73%
IBK	Current Study	28	2D: 4 targets on a screen	Linear Regression on time-shifted EEG samples	66.5%
1D: SMR 2D: SSVEP	Trejo et al. [119]	6	1D & 2D: hit a target	1D (KPLS) 2D (KPLS)	1D: 88% 2D: 80-100%
SMR+SSVEP	Allison et al. [107]	10	2D: hit 8 targets	LDA on both EEG paradigms	60%
SMR+P300	Li et al. [104]	6	2D: hit an arbitrary target	SVM classification	90.3%
SMR+P300	Long et al. [159]	11	2D: hit an arbitrary target	SVM classification	93.99%
Real hand movement or SMR	Kayagil et al. [160]	4	2D: hit an arbitrary target through obstacles	Bhattacharyya distance of PSD	86%
Motor execution	Huang et al. [161]	5	2D: hit an arbitrary target among obstacles	GA-based MLD classifier on the ERD/ERS features	85%
SSVEP+P300	Bi et al. [105]	8	2D: hit 8 targets	RBF SVM for SSVEP + LDA for P300	85%

While our results showed that the Theil-Sen model demonstrated the highest accuracy, the model generated from least squares regression provided comparable accuracy at a lower processing time which is necessary for online trials. Therefore, it was determined that the least squares method is the optimal model of the three regression techniques. The platform can also see minor improvement through channel selection during dimensional tasks. For instance, tasks involving primarily horizontal movement can place a higher weight on channels F7 and F8 along with channels located on the right hemisphere of the brain. However, for vertical trials, there was no combination of channels that provided improved results found in this study. A classifier for horizontal and vertical direction can also be implemented as a gate to generate predictions on a model tailored for the intended dimension. The approach can be used to improve the accuracy of the model beyond regression alone. Our results showed a classification accuracy of 80% for mean values of power spectral density across the Theta, Alpha, Beta, and Gamma frequency bands for all channels.

It is interesting to note that prefrontal electrodes produce the best decoding results. This probably indicates that the IBK paradigm relies on higher cognitive functions compared to sensorimotor and externally triggered sensory paradigms. As pointed out in Min et al. [162], paradigms based on prefrontal cognitive functions are natural candidates for efficient and intuitive applications in goal-directed BCIs, which have great potential for applications in improving the quality of life of individuals with sensorimotor or cognitive impairments [163, 164]. While linear regression has given the best results so far, there remains the question of whether it is optimal. Further research needs to be done to explore other models and parameters (such as a Long Short-Term Memory network and variations of support vector machines) as well as methods to transfer knowledge from other subjects' data [165]. Future work will also include implementing what we have learned from channel selection and classification in real-time testing.

4 Chapter Four: Brain Connectivity Evaluation during Selective Attention Using EEG-based Brain-Computer Interface

4.1 Introduction

Many assistive and rehabilitative BCI systems have been designed using noninvasive brain imaging techniques [166]. Brain, as a complex system contains nonlinear dynamics and nonstationary behavior, which makes it difficult to describe. Making assumptions could simplify the understanding of the brain. Recently, model-based approaches offer a systematic modeling of complex systems such as the brain. The approach mitigates the curse of dimensionality by making some assumptions about the structure, dynamics, or statistics of the system under observation. By modeling, we can make some assumptions to tractably understand the system. Here, the complex system (e.g., brain model with millions of neurons) is estimated with linear dynamics and far fewer variables.

We exposed a number of healthy human participants to 1) a sequence of images of faces and scenes, and 2) a sequence of superimposed face and scene images while priming them to maintain focus and distinguish between the image categories. EEG time series were collected during the tasks using a 14-channel EEG headset. A preliminary analysis was conducted in [163]. We applied the concept of Granger causality [167] between selected sources of brain activities to reveal the interdependence between different brain regions using the EEG time-series. According to the Granger causality scheme, a time-series x(n) can be granger cause of another time-series y(n) if information about x(n)'s past improves the prediction of the variable y(n), above and beyond the information contained in past of y(n) (and other measured variables) [168, 169]. We focused on the metric of Granger-Geweke Causality (GGC) as a measure of directed connectivity [170-172].

4.2 Materials and methods

4.2.1 Participants

Thirty-eight college students (11 females: 21.3±1.9 years and 27 males: 23.1±5.2 years) participated in the experiment. There were 33 right-handed and five left-handed participants. There are studies in the literature that support the potential impact of hand preference on cognition [173, 174]. Due to low number of left-handed participants, we may not be able to carry out a statistically significant analysis considering the handedness as a variable. Thus, we decided to exclude the left-handed responses to control for potential variability in the results. The participants all had normal or corrected to normal vision. They had no known history of neurological or psychological disorder. The experimental protocol was approved by the Institutional Review Board at the University of Tennessee, Knoxville. All participants were asked to read and sign a consent form prior to participating in the study. The experiment consisted of two phases, which are described in Sections II.C and II.D.

4.2.2 EEG recording

EEG Data was acquired using a water-hydrated 14-channel Emotiv EPOC wireless EEG headset over AF3, F7, F3, FC5, T7, P7, O1, O2, P8, T8, FC6, F4, F8, AF4 according to 10-20 standard with a sampling rate of 128Hz. We ensured to maintain low impedance (<10KΩ) for all EEG electrodes during the experiments. The EPOC TestBench software was used to monitor the quality of EEG signals. The received signals were referenced with respect to P3/P4 electrodes over left and right mastoids.

4.2.3 Phase 1: Image recognition

4.2.3.1 Experimental protocol

Each participant was conditioned to recognize 200 “Face” and 200 “Scene” individual images as trials by keypresses. The conditioned trials were divided into eight blocks, in which the two image categories were equally distributed. There was a short pause between blocks. The participants were exposed to male and female faces in four blocks and indoor and outdoor scenes in the other four blocks. To ensure high attention to the image category throughout the experiment, we instructed the participants to distinguish between the subcategory images. An illustration of this phase is shown in Figure 4.1. The sequence of images was displayed on a 33cm×33cm LCD monitor with a 60 Hz refresh rate and 1920×1200 resolution. Participants were asked to look at the center of the monitor and keep their distance at 60 cm. Each trial was a single greyscale image followed by a black screen. Each block started with a 1000ms cue texture that guided participants on the attended images and the expected behavioral response. Then, it continued by showing single images randomly selected from scene subcategories (Indoor scene and outdoor scene) or face subcategories (male face & female face) with a black screen between images. Each image was shown for 1000ms and the inter-trial duration was a random variable between 1000ms and 1500ms. Overall, 50 images were shown to each participant during each block.

A computer keyboard was used to collect behavioral responses of participants. Pressing Back quote button on the top left corner collected left-hand responses and hyphen button on the top right corner collected right-hand responses. Table I shows the expected behavioral responses for corresponding subcategories of images for eight blocks. Keyboard button assignments were counterbalanced across all blocks to minimize the projection of motor-related activities over EEG signals. A one-minute practice block was designed to familiarize the participants with the task. The participants were asked to minimize eye blinks and body movements during the experiment. This phase took approximately 20 minutes.

4.2.3.2 Input and ground truth

We aimed to analyze and generate an individual model of visual attention. Since there were 33 participants in this study, the data have been utilized to analyze and generate

33 individual models. We chose a trial-wise training scheme, which considers EEG data of a whole trial as an input to the model. We primed participants to discriminate between male and female subcategories in four blocks and between indoor and outdoor subcategories in the other four blocks by key presses. Using this strategy, we assumed that the participants have relatively high attention towards face and scene categories in the corresponding blocks. Consistently, the shown image category (regardless of the subcategories) during each trial has been chosen as the ground truth.

4.2.4 Phase 2: Attention evaluation

4.2.4.1 Experimental protocol

Each participant was conditioned to recognize 200 “Face” and 200 “Scene” superimposed images as trials by keypresses. During each trial, the participants were exposed to a male or a female face that was superimposed by an indoor or an outdoor scene image. The conditioned image trials were evenly divided into eight blocks. The participants were instructed to discriminate between male and female subcategories in the sequence of superimposed images in four blocks, and to discriminate between indoor and outdoor subcategories in the sequence of superimposed images in the other four blocks by key presses. The two conditioned image subcategories were equally distributed to cancel out the associated motor-related response on the EEG signals. There was a short pause between blocks. Figure 4.2 illustrates a schematic of the phase. A pilot study was conducted using the same experimental protocol [175]. The same keyboard buttons as phase 1 were assigned for collecting participants’ behavioral response. The conditioned visual stimuli were displayed on the same screen as phase 1. We ensured that images used to construct the superimposed images had the same opacity, contrast, and luminance level. This phase took approximately 10 minutes.

4.2.4.2 Input and ground truth

In phase 2, participants were conditioned to discriminate between male and female subcategories in four blocks and between indoor and outdoor subcategories in other four blocks by key presses when exposed with the sequence of composite images. Compared to the phase 1, phase 2 did not have a black screen between trials.

4.2.5 Statistical analysis of the behavioral responses

After collecting the behavioral response, we examined the ability of participants to accurately distinguish between faces and scenes in both “image recognition” and “attention evaluation” phases. Specifically, we examined the difficulty of the task by evaluating the mean RT for the attended face and scene stimuli. We only included key presses during the trial and excluded all other key presses after the one-second trial.

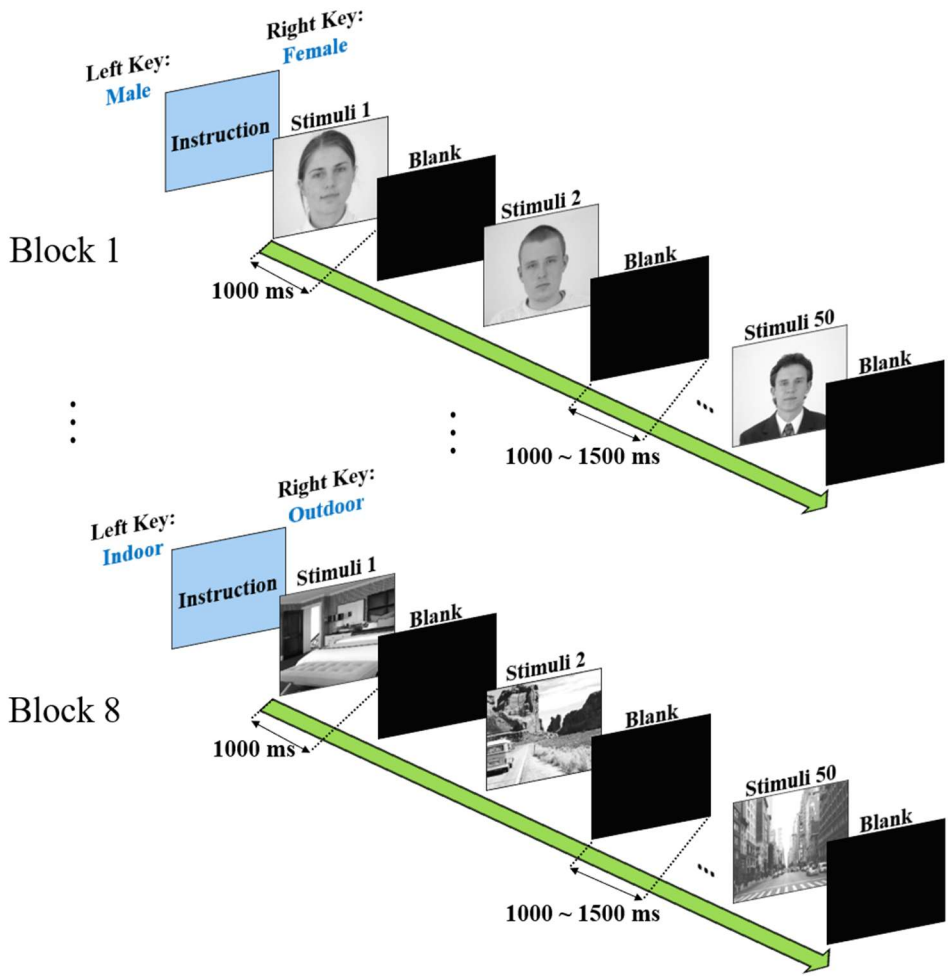


Figure 4.1. A schematic of sample blocks of trials of phase 1: image recognition phase.

Table 4.1. The subcategories of images to which a participant should pay attention during each block and the expected behavioral responses from the participant.

Block No. and stimuli (attended) category	**Left-Hand Response**	**Right-Hand Response**
1: Face category	Male face	Female face
2: Scene category	Indoor scene	Outdoor scence
3: Scene category	Outdoor scence	Indoor scene
4: Face category	Female face	Male face
5: Scene category	Indoor scence	Outdoor scence
6: Face category	Male face	Female face
7: Face category	Female face	Male face
8: Scene category	Outdoor scene	Indoor scence

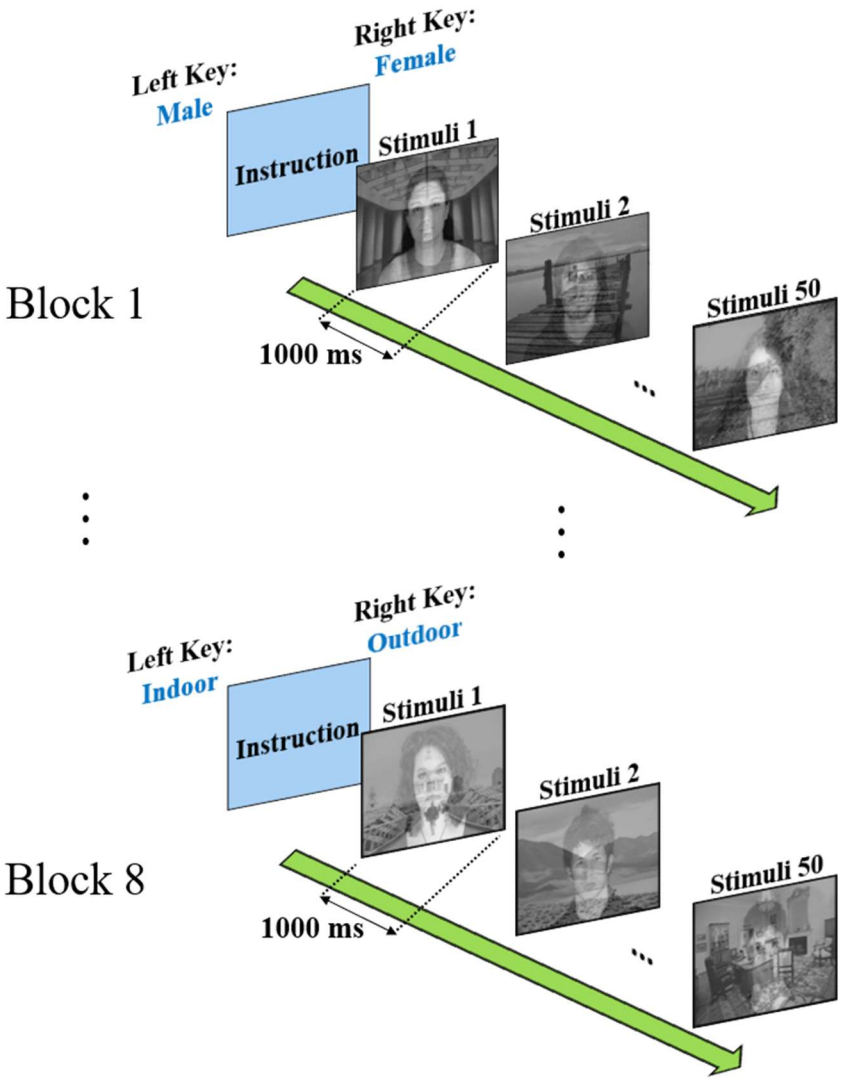


Figure 4.2. A schematic of sample phase 2: attention evaluation phase using superimposed images.

We applied a paired two-tailed t-test on the correct responses between the average RT to attended faces and scenes to determine the difficulty of focusing attention towards face versus scene for both clear and ambiguous stimuli.

4.2.6 Signal preprocessing

The experimental setup was designed using MATLAB and Simulink software. While participants were performing the experiment, the continuous EEG signals, as well as the key presses (behavioral responses), were recorded. Psychophysics Toolbox extensions were incorporated to calculate response time (RT) and account for the synchronous collection of behavioral response [176-178]. The EEG signals were filtered out using an intrinsic [0.16-46] Hz band-pass filter and stored on the computer. We utilized EEGLAB for EEG channels and source space processing using a pipeline outlined in Figure 4.3 [151]. The EEG signals collected during each block of stimuli for each participant were merged to yield a solitary set of independent component weights common to all conditions. The continuous data were first filtered with a 1 Hz high-pass Finite-Impulse Response (FIR) filter. The filter removed the signal drift, cope with the non-stationarity of EEG signals caused by sweating and stabilize the subsequent Independent Component Analysis (ICA). Then, bad channels and large amplitude noise caused by muscle artifacts were identified and rejected using Artifact Subspace Reconstruction (ASR) [179]. Since the EEG signals are generated with no external source, the potentials over all EEG channels are summed up to zero at every moment. So, we re-referenced the EEG signals to the average channel values. Re-referencing is also helpful to reject external noise. To minimize the risk of bias in the referencing, the previously rejected channels were interpolated using sphering transformation [180]. To avoid confusion caused by the channel interpolation, we applied Principal Component Analysis (PCA) to keep the data full-rank.

4.2.7 Independent component analysis

Brain activity measured over each EEG channel is a linear mixture of different cortical and different non-cortical sources of activities. There are methods proposed to estimate sources of activity. ICA was applied to extract maximally independent sources of information. The EEG signals recorded during all eight blocks of selective attention task during the associated phase for each participant were combined. Then, the ICA method was applied to continuous data to extract independent sources. The scheme yielded a single set of ICA weights common to “Faces” and “Scenes” stimuli on each phase. The scheme manifests a valid approach since the EEG headset was constantly turned on, and the headset placement was not altered during each phase of the experiment. This allows for comparisons of neural activity conditioned by the various visual selective attention within independent components common to the different stimuli. We used the AMICA algorithm to decompose the EEG signals [180]. The algorithm pulled out the

contributing source of EEG signals that helped later for signal source and causality analysis. Using Emotiv EEG headset, at most, we could have extracted 14 independent sources for EEG signals collected during each selective attention task. Each component was then projected on to the scalp map using the inverse weight matrix. We evaluated each component to discriminate between neural and non-neural signal sources using different methods.

Comparing the components' activity spectrum gave a good illustration for determining the non-neural sources. With a semi-automated procedure, we included mutually inclusive neural sources identified by two EEGLAB libraries named ADJUST [181] and ICLabel [153]. This allows for accurate rejection of non-neural sources. The ICA over the datasets yielded 472 ICs. We found a high commonality of more than 99% between 41 ICs of 36 participants within the right fusiform gyrus which is associated with the face fusiform form area (FFA). We focused on the participants' contributing ICs for all event-related spectral perturbation (ERSP) analysis in the result section. The data were segmented into 1200 ms epochs, starting 200 ms prior to and 1000ms after the stimulus onset. The baseline was considered the neural activity during -200 ms to 0 ms relative to stimulus onset.

4.2.8 Equivalent current dipole extraction

Following to the ICA decomposition, equivalent current dipole models were fitted for each component by using the DIPFIT2 EEGLAB extension [182]. The spherical head model was co-registered to Montreal Neurological Institute (MNI) head model to better localize the estimated current dipoles. The default parameters were applied to transform between ICA and the estimated current dipole [183]. Then, K-means clustering was applied, and the estimated current dipoles were clustered into 10 different clusters. Due to the difference among participants' scalp sizes, we excluded estimated outlier current dipoles.

4.2.9 Calculation of ERSP

We focused on the estimated current dipole cluster over the FFA area (Figure 4.4). Time-frequency analysis was performed using EEGLAB toolbox on all participants' ICA components on this cluster. We calculated ERSP over the epoched data to measure power fluctuations on the independent component in the frequency range of [3-40] Hz. A tapered moving Hanning window with a Morlet wavelet transforms extracted the time-frequency event-related perturbation over all trials of each participant [184]. We applied a linearly increasing cycle of 1 at 3Hz and 7 at 40Hz for the wavelet transform. To obtain ERSP, we averaged the spectral power across all trials of "Faces" and "Scenes" stimuli, separately. Then, the calculated spectral power converted to log power for better illustration.

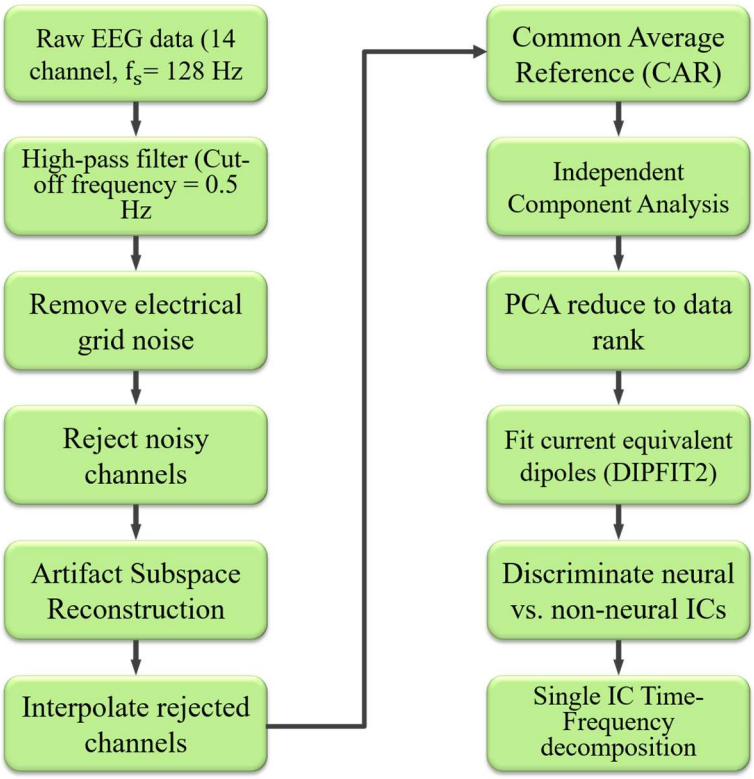


Figure 4.3. Data processing pipeline using EEGLAB.

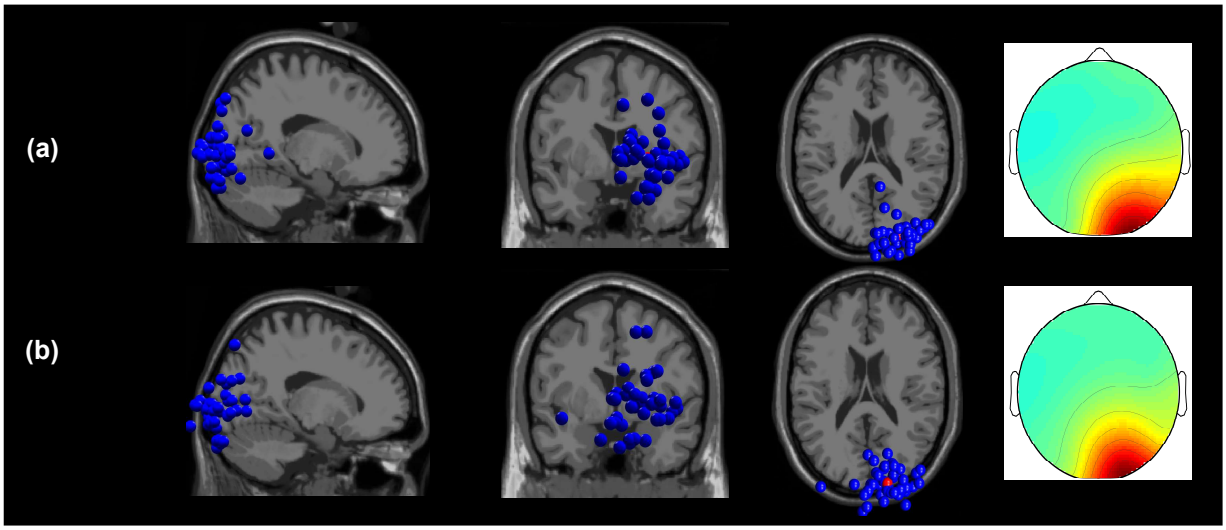


Figure 4.4. Estimated current dipoles of each participant's independent component in the FFA cluster for the trials during a) "image recognition" and b) "attention evaluation" phases. The picture from left to right constitutes sagittal, coronal, and axial slices

Baseline correction was applied by subtracting mean signal power at 100ms prior to the onset of each image category. The event-related synchronization (ERS) for both phase 1 and phase 2 has been calculated as follows:

Equation 4.1
$$ERS(freq, time) = \frac{1}{N}\sum_{i=1}^{N}|W(freq, time)|^2$$

where N is the number of trials associated with a condition and W is the Morelet wavelet transform over each epoch of data. The ERSP is computed separately across trials of "Faces" and "Scenes" for each individual participant.

Equation 4.2
$$ERSP(freq, time) = 10\, log_{10}\left(\frac{ERS(freq, time)}{\Gamma}\right)$$

where Γ is the mean spectral power at the defined baseline.

4.2.10 Group level analysis

By collecting components associated with neural patterns conditioned by faces and scenes stimuli for each individual, we conducted a group analysis using EEGLAB STUDY module. The group study allows for comparison between associated components across participants. To determine ICs with a non-neural source of activities among the participants' batch datasets, we clustered all the ICs using estimated current dipoles as the feature with K-means clustering method into 10 clusters. Then, the time-frequency representations of neural sources in the cluster over the right occipital cortex (over the FFA) has been extracted.

4.2.11 Causal connectivity analysis

According to Bullmore and Sporns [185], there are three types of brain connectivity:
Structural (anatomical) connectivity. This type of connectivity describes how different areas of the brain are anatomically wired together [186]. It shows how different parts of the brain can communicate with each other. The axial dendritic connections in the brain depict the possibility of exchanging information and not the actual connection in every moment. Methods such as Diffusion Tensor Imaging (DTI) can visualize this kind of connectivity. This type of connectivity is state invariant; the dynamics of this connectivity at the level of networks of the brain evolves very slowly over the course of days and years [187].
Functional connectivity. Taking the assumption that different areas of the brain can communicate with each other, functional connectivity studies correlation patterns and spectral coherence between different areas [188]. Although this type of connectivity is dynamic, state-dependent, and can evolve in the order of milliseconds and seconds, it does not necessarily imply a causal link [189].

Effective connectivity. The method suggests that different areas of the brain may have not only correlative activities but also causal relationships. One area can exchange information and drive another area. The connectivity is dynamic, state-dependent, and can evolve in the order of milliseconds and seconds. While the functional connectivity can reveal mutual synchronization between different brain regions, the effective connectivity aims to uncover causal interaction and connectivity among sources of brain activities.

Effective connectivity has been mostly explored in functional MRI (fMRI) studies, multivariate analysis in milliseconds of EEG signals has been lacking. Here, we explored effective connectivity in a selective attention task using EEG signals.

There are various post-hoc analysis applied to neural activity to estimate effective connectivity, such as Dynamic Causal Modeling (DCM) [190] and structural equation modeling [191]. The methods are confirmatory in the sense that these connectivity tests can reveal connectivity by imposing different hypothesis. By conducting statistical tests, the models can confirm if the hypothesis is significant. Other exploratory approaches assume a model for neural activity and test the different hypothesis under the data-driven model. We applied Granger causality as an exploratory method since it is data-driven, scalable to many variables, extendable to nonlinear [192] nonstationary [193, 194] and/or nonparametric [195] systems. These characteristics make it a good fit for EEG neural responses. The method is also capable of evaluating the hypothesis of a system being affected by an unobserved exogenous cause [196, 197]. The framework allows us to explore time and frequency varying multivariate causal relationships in the EEG data. We identified three cortical sources of interest over left occipital cortex (OccL), right occipital cortex (OccR), left supplementary motor area (SmaL), right supplementary motor area (SmaR). We assume a linear multivariate autoregressive (MVAR) dynamic system for the brain. The model describes EEG data as a linear combination of k data samples into the past. The model can represent as:

Equation 4.3

$$X_k(t) = \sum_{k=1}^{p} A_N^k(t)\, X_N(t-k) + E(t)$$

where X_N is N channel EEG signals, p is the model order defined the number of data points in the past to look for a causal relationship, A is the model coefficients, and E is random Gaussian noise. We assume stationarity of the data within a short time window and stability of the model. The stability corresponds to all eigenvalues of matrix A being less than one. Practically, it means that the amplitude of the EEG as a time series is always bounded.

The important parameter to choose is the order of the MVAR model. There are different methods to determine the optimal number of data points in the past to include in the model. We can use data itself to calculate the model order. Data-driven criterion such as Akaike Information Criteria (AIC) [198], Schwarz-Bayes, and Hannan-Quinn can be

utilized to calculate model order. Basically, all of these methods may suggest a different model order based on penalizing a different criterion. However, the simpler model (model with smaller p) is always preferred over other higher order models. Also, the model order depends on the EEG sampling rate. The higher the sampling rate, the higher the model order should be. Because the information above 64 Hz on the collected EEG signals may be insignificant, down-sampling of the EEG signals to somewhat 100 to 120 Hz for linear modeling is preferred. Since the original sampling rate of the EEG signals (128Hz) was about the preferred sampling rate, we decided to keep the original data sampling rate. We chose the window size of 0.3 s with 90% overlap on windows to ensure the conformity with the AIC criterion [199, 200]. A range of possible model order between 1 to 40 was computed for Face and Scene trials in image recognition and attention evaluation phase for each participants' data, independently. The optimal model order for each criterion was automatically determined by choosing the minimum order that meets the constraints.

4.2.12 Connectivity model validation

In order to evaluate the accuracy of the model to capture the sources of interested dynamics, we conducted various tests. We ran whiteness test to make sure that the information left on the residuals is insignificant, consistency test with a random signal as an input to the model to see if the model can generate data with the same correlation structure as the real data, and stability test to assess the stability and stationarity of the model. On average, the model order for all the participants' EEG data was 16.

4.3 Results

4.3.1 Behavioral response

Figure 4.5 shows the violin plot [201] of the mean correct RT for attended faces and scenes in the "image recognition" and "attention evaluation" phases. The analysis revealed a significantly lower average RT for face versus scene in the "image recognition" phase (*p_value* < 0.05). This supports the assumption that, compared to scenes, it is easier to distinguish faces since faces are the most distinctive visual stimuli [202]. The question is how adding ambiguity to the visual stimuli by superimposing images with another image may affect the attention demand and cognitive-motor responses. Although the t-test still shows a significantly lower average RT for attended faces versus scenes (*p_value* < 0.05) on noisy images on the "attention evaluation" phase, the mean value for the two categories are very close. We also expected that adding ambiguity would increase the average RT for each attended category. The t-test also revealed a significant difference between the average RT to the attended categories between phase 1 and the ambiguous categories in phase 2 (*p*_value < 0.05). Figure 4.6 shows the percentage of correct responses in both phase 1 and phase 2. As

expected, adding ambiguity to the stimuli and eliminating the inter-trial blank screen result in lower correct responses in the “attention evaluation” phase.

4.3.2 Time-Frequency EEG response

Phase 1: Image recognition task. We inspected the corresponding time-frequency plots to identify the components of interests. Figure 4.7 shows the spectral perturbation associated with face and scene stimuli conditions in one sample participant during image recognition task. Using 10% bootstrap significance level (α) on 200 trials collected under each condition for each participant’s data, we filtered out the non-significant perturbations which are showed by green areas. A stronger activation pattern in frequencies (25 – 40 Hz) across scene condition compared to face condition for the image recognition phase is identified. The pattern is more pronounced within the time window between 50 and 350 ms after stimulus presentation.

Phase 2: Attention evaluation task. We also inspected the corresponding time-frequency plots to identify the components of interests. Figure 4.8 depicts the calculated ERSP on a representative participant over faces and scenes conditioned trials during attention evaluation task. The same significance level of $\alpha = 10\%$ was applied to filter out non-significant perturbations. The overlapped image of face and scene seems to shift the pattern to the face conditioned stimuli. As Figure 4.8 shows, a stronger activation pattern on the frequencies (15-25 Hz) for the face conditioned stimuli is depicted during the attention evaluation phase. Also, scene-conditioned stimuli exhibit higher gamma within the time window between 100 and 500 ms after stimulus presentation.

4.3.3 Connectivity Analysis using time-frequency distribution

We investigated causal relationships between OccL, OccR, SmaL, and SmaR brain regions for face and scene conditions. We assumed that left and right occipital areas might represent participants’ perception towards attended image category while brain activities over supplementary motor area represent category selection for the behavioral task. We extracted time-frequency illustrations of Granger causality between the regions of interest (ROI) considering the statistical significance of *p_value* < 0.05 for the conditioned stimuli for both “image recognition” (Figure 4.9) and “attention evaluation” (Figure 4.10) phases. The figures show the changes in Granger causality over the time course of selective attention towards different image categories between ROIs on a sample participant’s data. The blue regions indicate non-significant connectivity, and the warmer regions (yellow to red) indicates stronger connectivity. During the beginning of face trials, the information outflow between the independent neural components over OccL area and SmaR area becomes hyper-coupled. The occipital region over FFA drives the neural activity in the supplementary motor area across both Theta and Beta

waves (Figure 4.9.a). In contrast, the connectivity between OccL area and SmaR is more pronounced over the Alpha wave (Figure 4.9.b).

4.4 Discussion

In this work, we developed an EEG-based BCI platform using a portable, water-hydrated, and wireless EEG headset. We conducted two human experiments to evaluate brain connectivity patterns during selective visual attention to the face and to scene images by discriminating image categories using key presses.

In the first experiment, participants conducted visual perceptual discrimination with low attention demand. In the second experiment, a sequence of noisy, superimposed images was displayed while there was no pause between trials. Thus, high attention demands were required mentally. We analyzed stable time-frequency representations of selective visual attention towards face and scene images both in a pure and in a noisy environment. Comparing visual perceptual discrimination in low and high demand tasks shows a reduced performance in participants. Thus, a lowered accuracy and prolonged reaction times were found in visual discrimination of superimposed images. The mean response time was 547 ms vs. 633 ms for faces vs. scenes in low attention demand task (phase 1) while the mean response time was increased to 667 ms vs. 706 ms for faces vs. scenes in high attention demand task (phase 2). The accuracy of behavioral response showed a decrease from 95.7 % in low attention demand to 88.1 % in high attention demand task. Face or scene image discrimination under superimposed images takes longer than visual object discrimination without visual distraction. According to Yantis [203], selective attention is an example of contextual neural modulation. Selective modulation of neural activity is made necessary by the hierarchical organization of the primate visual system. Higher level neurons with larger receptive field respond to multiple visual objects in their receptive fields, some of which would effectively drive the neurons if they were presented in isolation (as our Phase I) and others that would not. Not all these stimuli can be represented simultaneously. It takes longer to process visual object in the cluttered visual scenes.

We also investigated causal connectivity between brain regions associated with category identification and selection. Our analysis focused on the Granger causality underlying selective attention towards face and scene images in as a pure or a noisy image. Connectivity models of selective attention can provide us with a better understanding of the neural processes for object recognition and category selection, which is pivotal for the potential next step, which is the online brain modulation or biofeedback of brain activity. The models have been recognized and received support in the literature. Friston et al. [204] reviewed different approaches to dynamic causal modeling.

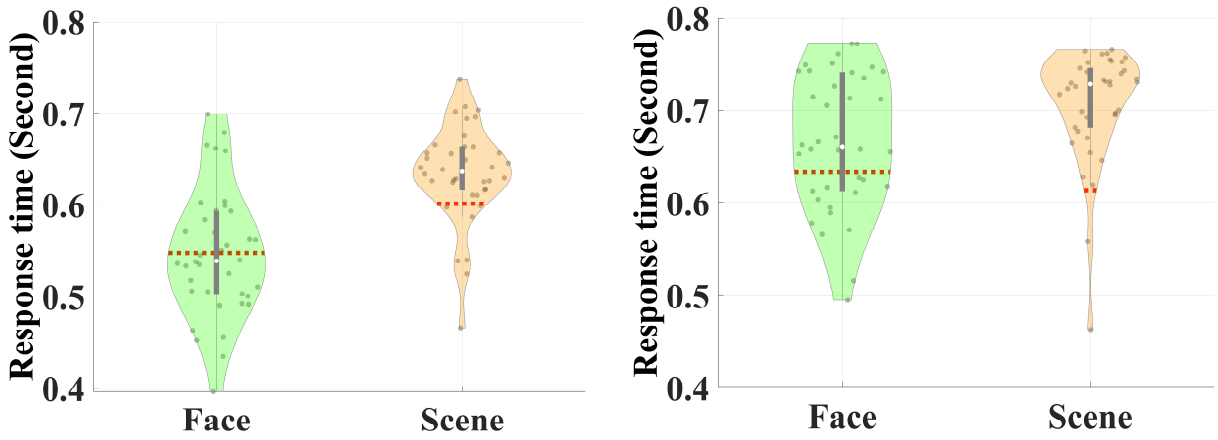


Figure 4.5. Violin plot of the mean RT in the a) "Image recognition" and b) "Attention evaluation" phases. The red dotted line shows the mean correct response time (RT) over all participants.

a) Mean[std] RT was 547[69] ms for faces and 633 [53] for scenes

b) Mean[std] RT was 667[73] ms for faces and 706 [62] for scenes

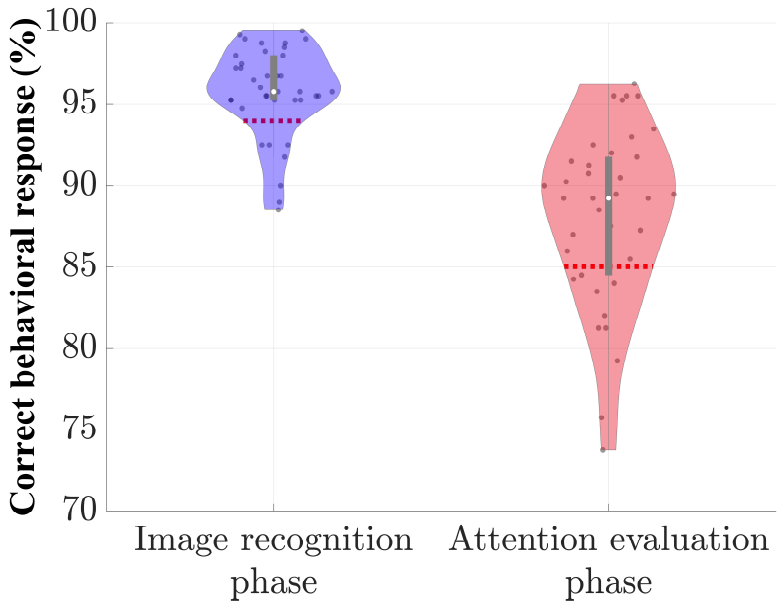


Figure 4.6. Violin plot of mean correct responses in both "Image recognition" and "Attention evaluation" phases. The red dotted line shows the average over all participants. The mean[std] behavioral performance was 95.7 [2.7] % for "Image recognition" and 88.1 [5. 4] % for "Attention evaluation" phases.

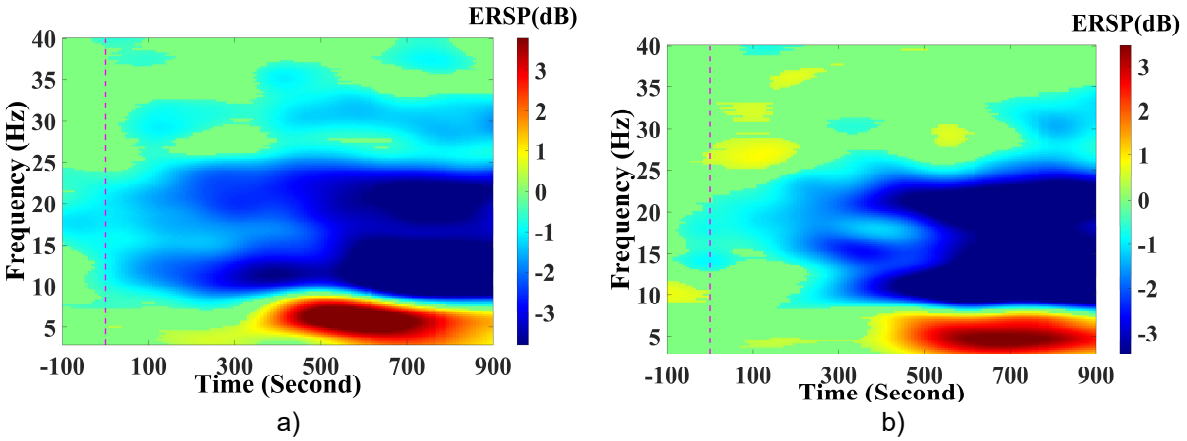


Figure 4.7. ERSP response for a representative participant over all a) face and b) scene stimuli in image recognition phase. An enhanced response was found in [25-40] Hz in scenes vs. faces

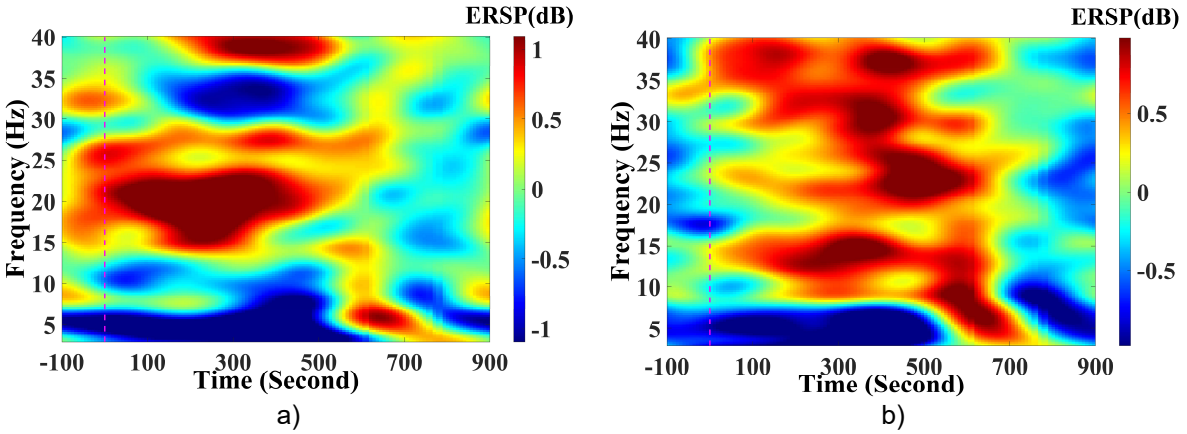


Figure 4.8. ERSP response for a representative participant over all a) face and b) scene stimuli in attention evaluation phase. Stronger early response was found during high attention demand, in faces vs. scenes in [15-30] Hz.

There are studies that have included measures of fMRI connectivity to predict selective attention in people with different clinical conditions including TBI [205] and ADHD [206]. The measure has shown a potential to predict abnormalities in selective attention [207] with resting state blood oxygen-level dependent (BOLD) signals. The information flow during object-based attention has been studied with fMRI [208]. Baldauf and Desimone [208] investigated the neural connectivity during streams of overlapping objects of faces and houses. They identified the causality network between attention-related and object recognition-related ROIs. The measure of EEG signals connectivity has also been investigated with resting state and task-related activities. For instance, channel-space functional connectivity using EEG signals collected in a continuous attention task were used to discriminate target and non-target visual stimuli [209]. The directionality of brain oscillations extracted with Granger causality on a visual object recognition task showed different patterns with familiar versus unfamiliar objects [210].
We also conducted a nonlinear modeling using convolutional neural networks (CNN) to evaluate how automatically generated features of selective attention may help to discriminate between visual objects [211]. An interesting study for future work can be utilizing connectivity-related features in a real-time brain-computer interface discrimination task [212]. We will also conduct a group-level analysis to mathematically model the selective attention using both neural and behavioral response to construct the model. The linear model built upon both measures may enhance our understandings of the neural structure for visual object discrimination. Moreover, future studies shall address the significance of phase-related connectivity.

4.5 An Application of Selective Attention Combined with Motor Imagery: A BCI Car Racing Game

Employing concurrent visual selective attention and motor imagery, I designed and developed of a BCI car racing game. Motor imagery (MI) and steady-state visually evoked potentials (SSVEP) are used in real-time to steer a virtual racing car in a simulated environment. The game uses selective attention to flashing objects to determine direction and intention of pushing and being still to determine moving the car forward or being still, respectively.

4.6 Significance

Supervised and unsupervised alternatives for machine learning models have their own advantages and disadvantages. While supervised learning may bring about better accuracy of detecting user’s intention and decoding brainwaves, unsupervised learning may ease data collection and promotes a practical plug-and-play alternative. However, we know that tuning a brainwave classifier or decoder to detect user’s intention in a reliable and robust way is a fundamental challenge in BCI systems.

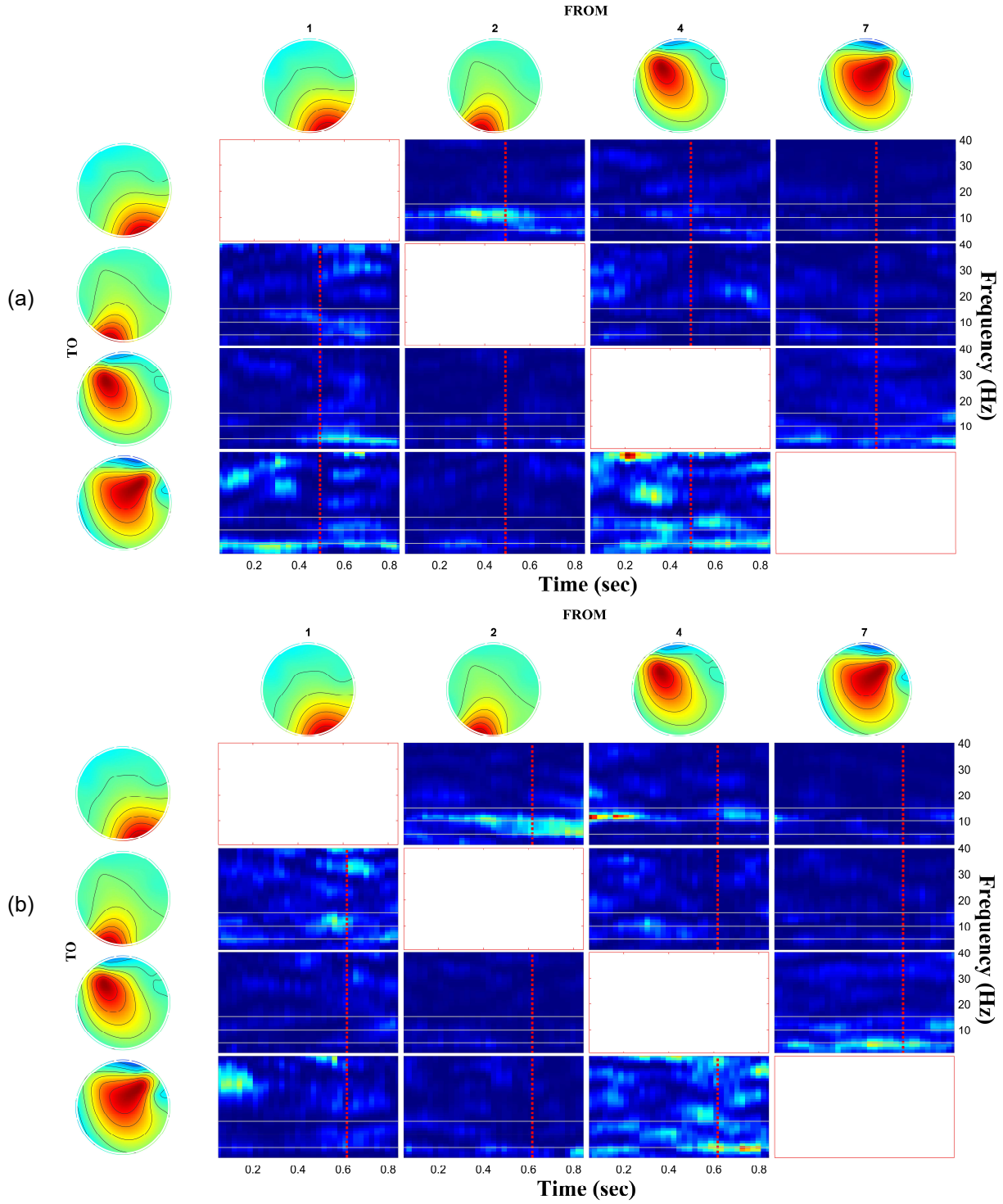


Figure 4.9. Time-frequency distribution of Granger causality from left occipital (OccL), right occipital (OccR), left supplementary motor area (SmaL), and right supplementary motor area (SmaR) as source on the columns to the same areas on the rows as sink for (a) Face trials and (b) Scene trials in the image recognition phase. The red dotted lines show the average behavioral response time for each condition. Non-zero connectivity with the significance level of *p_value* < 0.05 is illustrated with warm regions (Red).

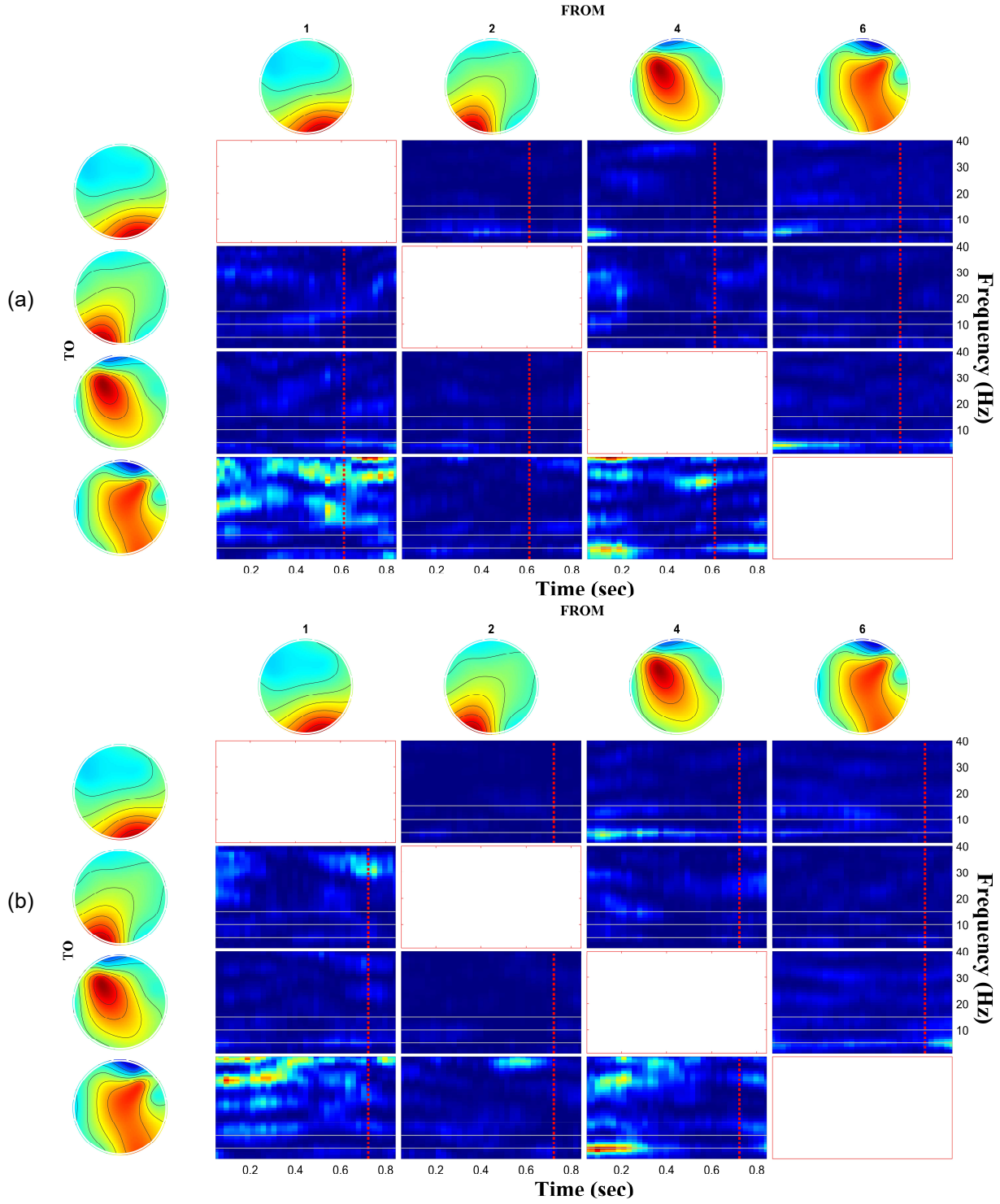


Figure 4.10. Time-frequency distribution of Granger causality from left occipital (OccL), right occipital (OccR), left supplementary motor area (SmaL), and right supplementary motor area (SmaR) as source on the columns to the same areas on the rows as sink for (a) Face trials and (b) Scene trials in the attention evaluation phase. The red dotted lines show the average behavioral response time for each condition. Non-zero connectivity with the significance level of *p_value* = 0.05 is illustrated with warmer regions (Red).

Although information can be transferred between different subjects and different sessions of a single subject, difference in brainwave pattern demands training and calibrating the decoder prior to each BCI session. In calibration phase, the user is required to perform tasks in order to collect sample data, for which the user's intentions are known. The recorded labeled data samples are used to tune the trained machine learning models towards the extraction of subject-specific brainwave features and determine user's intention on new data samples, in real-time. Predicting user's intention can be used as an engine in control scenarios to an extent that can enable moving physical objects. The paradigm brings a potential to replace some of the lost functions among people with motor disabilities. In this extension and application of previous study of the selective attention and motor imagery, I have designed and developed a BCI car racing game in a three-dimensional (3D) virtual environment using MATLAB and Unity software. The 3D virtual environment consists of two racing cars, tracks, as well as surrounding terrain that includes trees, grass, buildings, mountains, and the sky. Three cameras have been set up to show a driver's view, a bird's-eye view, and a following camera's view. Kinetic parameters of the cars are chosen to simulate physical movements of the car. The two racing cars are separately controlled by two individual drivers' brainwaves. Players' selective attention to flashing flickers, intention of pushing, and relaxation is determined by brainwave signals collected by mobile EEG. EEG brainwaves are monitored in real time using a g.tec Nautilus 32-channels gel-based system through MATLAB/Simulink. The collected brainwave signals are analyzed online in MATLAB using machine learning algorithms to decode the intended kinematics.

The machine learning algorithms have been trained to classify the driver's instantaneous intention into different categories: moving forward, moving backward, turning left, turning right, and maintaining rest. A control signal is then calculated based on the decoded kinematics and sent through the TCP/IP protocol to Unity to steer the car (see Figure 4.12).

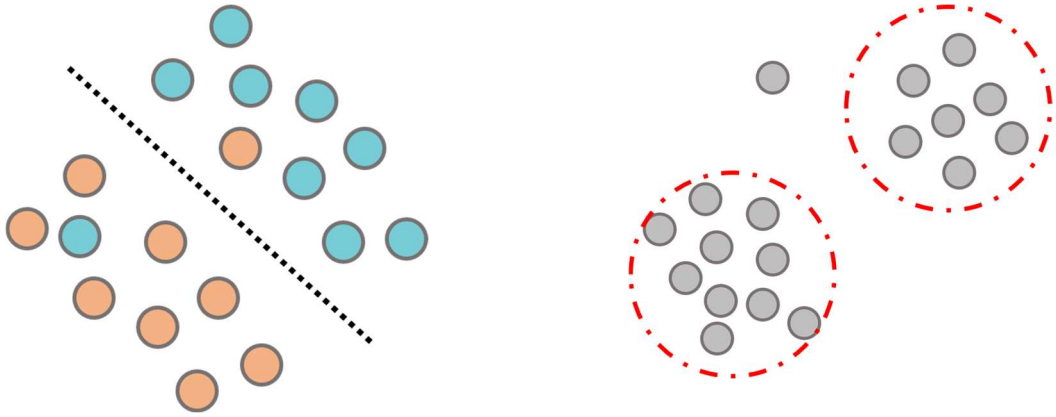
4.7 Training paradigm

In order to evaluate the feasibility of the idea, I designed a training protocol. The protocol includes exposing a number of participants to three different stimuli while asking them to do a task. On the first stimuli, the user expose to four different flashing square on the four corners of the screen. The flashing squares flickers consistently with 7.5 Hz, 10 Hz, 12 Hz, and 15 Hz. The choice of flashing frequency depends on the refresh rate of the screen. The flashing frequency can be an integer divider of the screen's refresh rate. I chose a computer monitor with a 60 Hz refresh rate.
The second stimuli include flashing squares, with incongruent frequencies, i.e., the squares on the four corners of the screen flickers with random frequencies. I included

the stimuli to evaluate the robustness and accuracy of the real-time decoding of visual attention to the flickers.
The third stimuli include a fixed diamond-like object, which supposed to induce minimum visual interference. The is employed as a cue to ask users to modulate motor imagery into resting and pushing objects. Figure 4.13 shows a schematic of the experimental training phase.

4.8 Results

I recruited twenty-eight young adults to participate in the training protocol. They were exposed to all three stimuli while their brainwave signals collected with a wireless gel-based EEG headset with 32-electrodes named gtec Nautilus SCARABEO. The headset covers FP1, FP2, AF#, AF4, F7, F3, Fz, F4, F8, FC5, FC1, FC2, FC6, T7, C3, Cz, C4, T8, CP5, CP1, CP2, CP6, P7, P3, Pz, P4, P8, PO7, PO3, PO4, PO8, and Oz. The headset can collect EEG signals with 250 Hz and 500 Hz. I collected EEG signals with a 250 Hz sampling rate. After a high-pass filter at the cut-off frequency of 0.5 Hz to remove signal drift caused by noise and sweat, I removed the electrical grid noise with a notch filter at 60 Hz. Because in this study my goal was to assess the feasibility and the precision of a plug-and-play, unsupervised hybrid BCI, I did not apply any extreme EEG preprocessing. I applied as much as preprocessing pipeline on the offline analysis that I could employ on the real-time data. Then, I extracted independent components from EEG signals using Infomax algorithm.
Using motor imagery paradigm, I extracted even-related spectral perturbation (ERSP) from EEG electrodes over central and parietal lobes (See Figure 4.14). Using event-related synchronization/desynchronization over Alpha and Beta rhythms, the motor imagery intention of relaxation and pushing objects are modulated and depicted.
From the previous study on the visual selective attention, I practically recognized the significance of the brainwaves recorded over the occipital area for visual attention. Likewise, in this work I focused on the neural sources over the occipital area. See Figure 4.15 for all the independent neural sources on the population's EEG data.
Figure 4.16 shows the power spectral density when the participants were exposed to a) 7.5 Hz, b) 10 Hz, c) 12 Hz, and d) 15 Hz flashing squares over multiple trials. The power spectral density shows that EEG brainwaves over occipital area peaks at the exact flashing frequency and its harmonics. The peaks are prominent signature of the SSVEP paradigm and there are ways to identify the existence of the peaks.
I employed an algorithms named canonical correlation analysis (CCA) [213], which has been proved to be an efficacious and enhanced method, especially when identifying target with a low signal-to-noise ratio carrier such as EEG. CCA is a statistical method to maximize underlying correlation between two given multivariate signals.



a) b)

Figure 4.11. A schematic of a) supervised and b) unsupervised learning

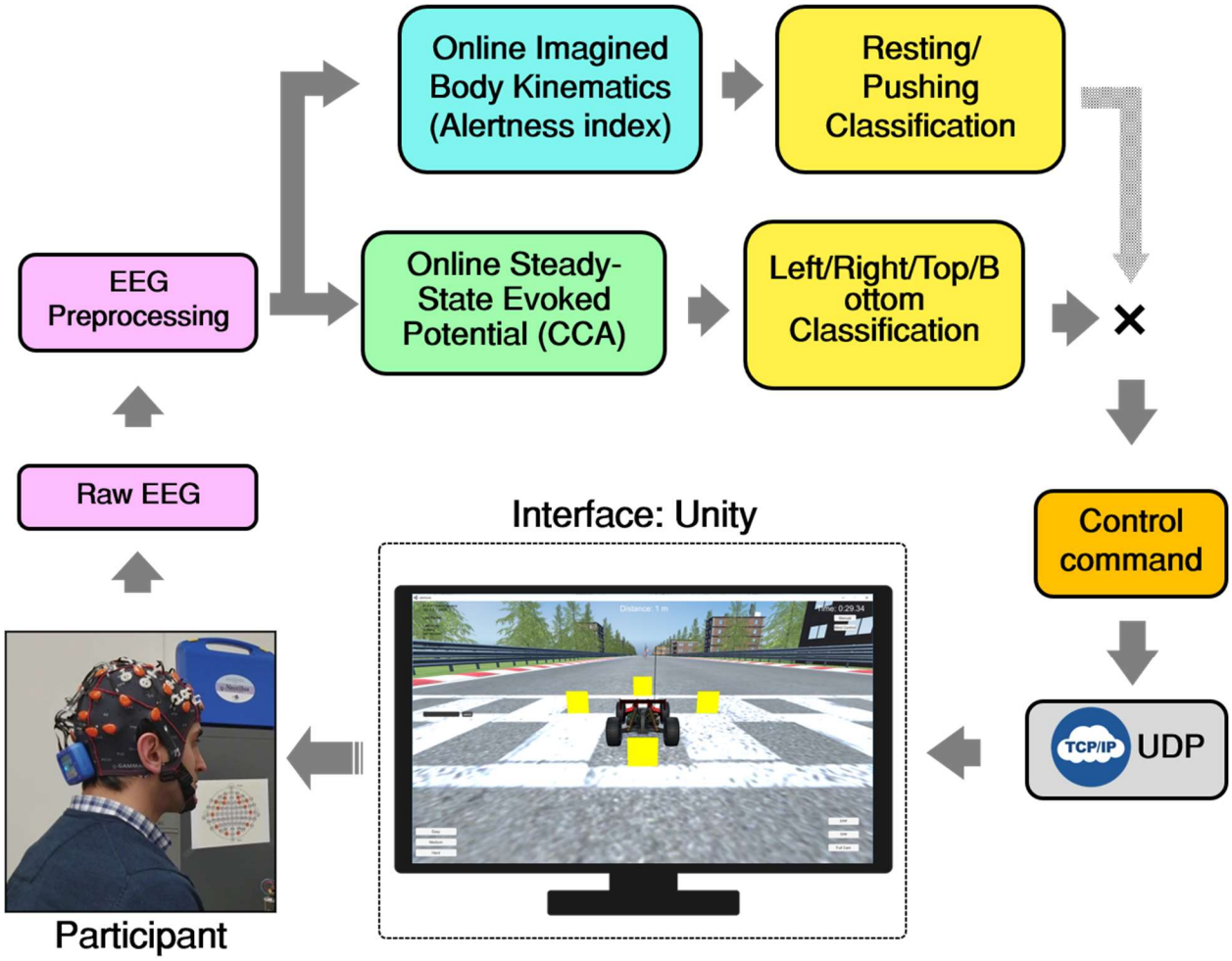


Figure 4.12. A schematic of the hybrid BCI game and the data decoding pipeline

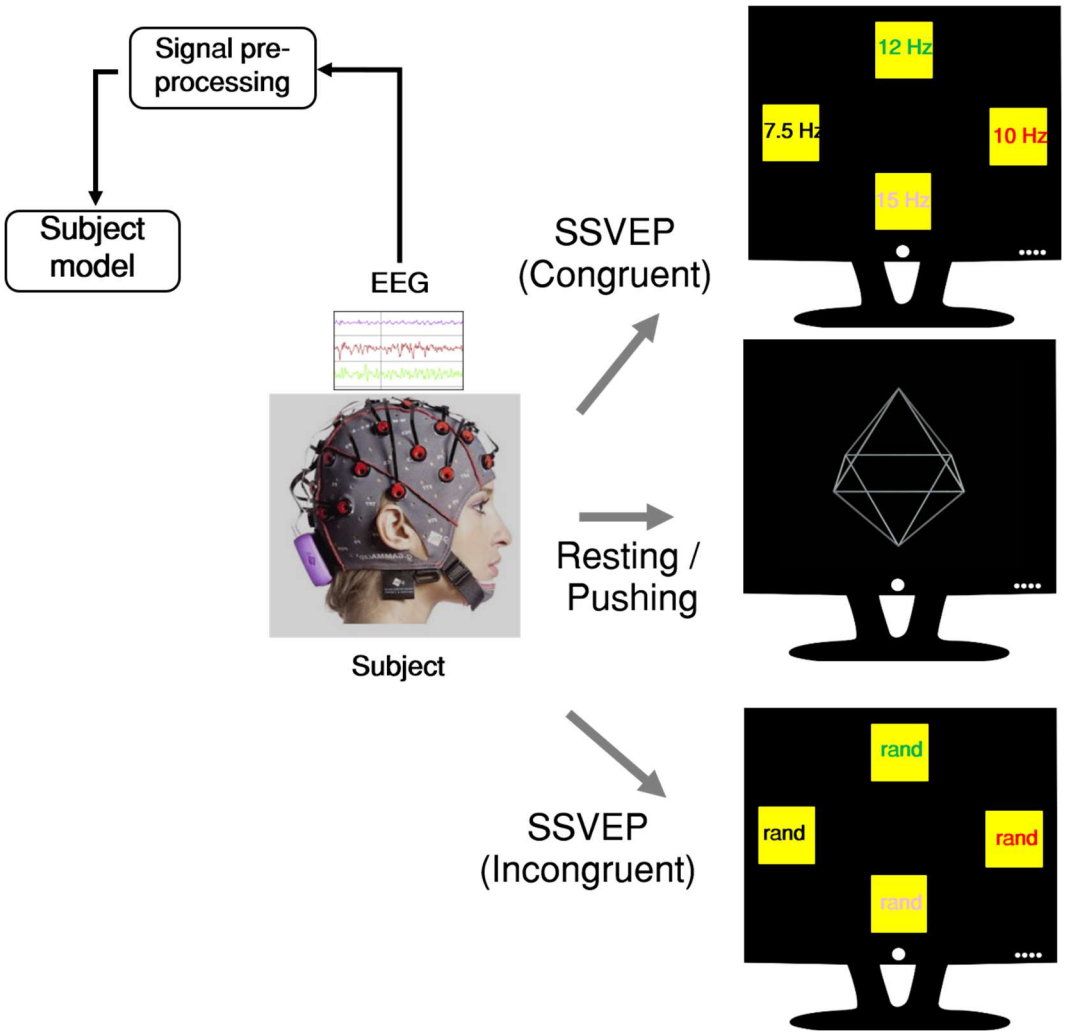
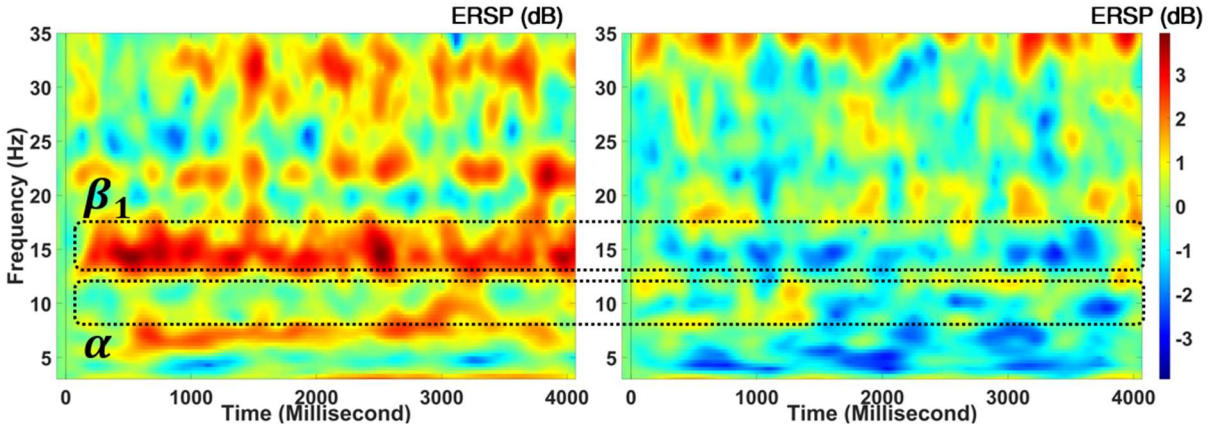


Figure 4.13. A schematic of the hybrid MI/SSVEP training experimental setup



a) b)

Figure 4.14. Event-related spectral perturbation (ERSP) averaged over EEG signals of central lobe over all subjects for a) Resting and b) Pushing states

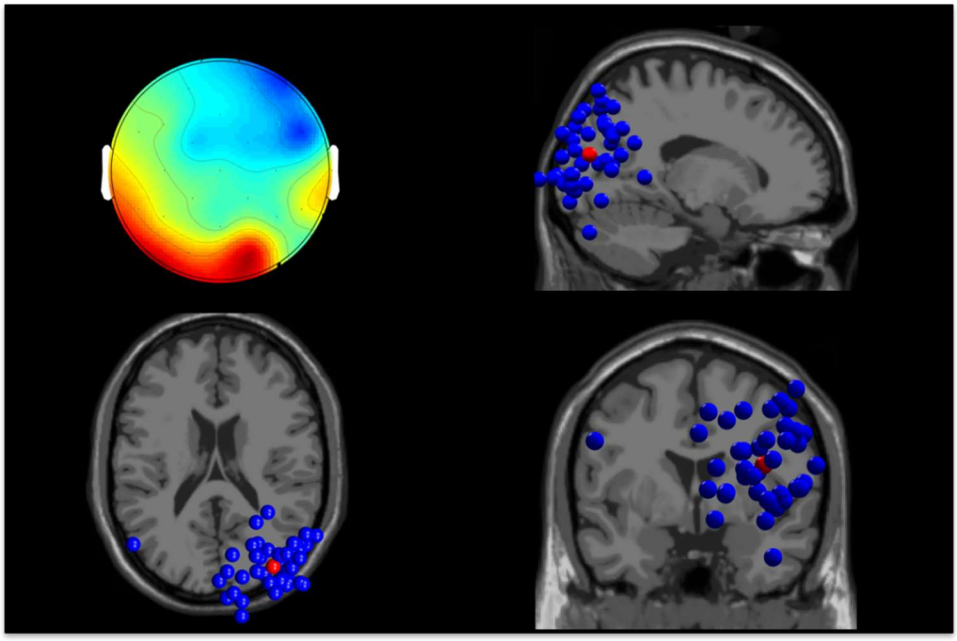


Figure 4.15. Estimated current dipoles from each participating independent component (blue) and their centroid (red). The rendered maps are coronal (bottom right), sagittal (top right), and axial (bottom left) slices of the Montreal Neurological Institute (MNI) template.

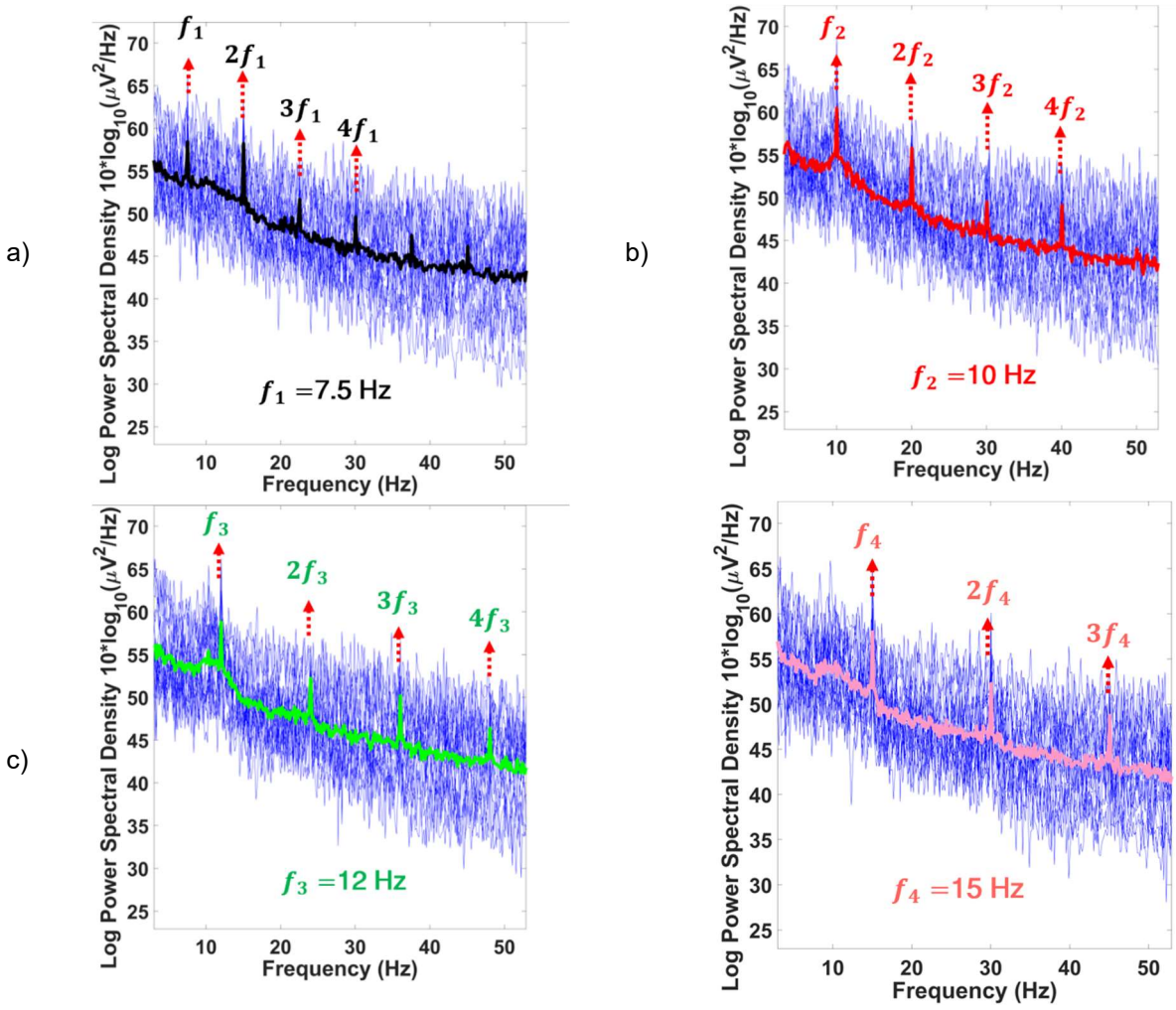


Figure 4.16. Power spectral density (PSD) averaged over EEG signals of occipital cortex over all subjects for a) Left flicker, b) Right flicker, c) Top flicker, and d) Bottom flicker

CCA finds weights of W_x and W_y by projecting signal x to signal y under a condition to maximize the canonical correlation ρ where ρ is:

$$\rho(x, y) = \frac{E(W_x^T\, x\, y^T\, W_y)}{\sqrt{E(W_x^T\, x\, x^T\, W_x) E(W_y^T\, y\, y^T\, W_y)}}$$

Where x is epochs of EEG signals and y refers to a set of reference signals generated as follows:

$$y = \begin{bmatrix} sin(2\pi f_n t) \\ cos(2\pi f_n t) \\ \vdots \\ sin(2\pi N_h f_n t) \\ cos(2\pi N_h f_n t) \end{bmatrix}, \qquad n = \frac{1}{f_s}, \frac{2}{f_s}, \ldots, \frac{N}{f_s}$$

Where f_s is the sampling frequency of EEG signals, f_n is the frequency of flashing square, and N_h is the number of harmonics to include. CCA calculates $\rho(x, y)$, resulting in the canonical correlation between the reference and the EEG epochs. The maximum correlation between the EEG epoch and the reference sets of signals attains the frequency of flashing object, i.e., the one on the user is focused on at the time. To test the robustness and the accuracy of the decoding algorithm, I compared the accuracy of decoding the real-time selective attention to the congruent flashing squares with the incongruent ones. Figure 4.17 shows the decoding accuracy of the SSVEP paradigm using CCA on all participants' EEG data over a varied range of real-time epoch time window length. The graph shows that on average, with around 80% accuracy, we could tell apart the selective attention to focused flashing square, considering 2 seconds time window size. It means having 2 seconds of EEG data is sufficient to classify visual selective attention to flashing objects. The game provides closed-loop system, with a potential to experience BCI in an immersive environment.

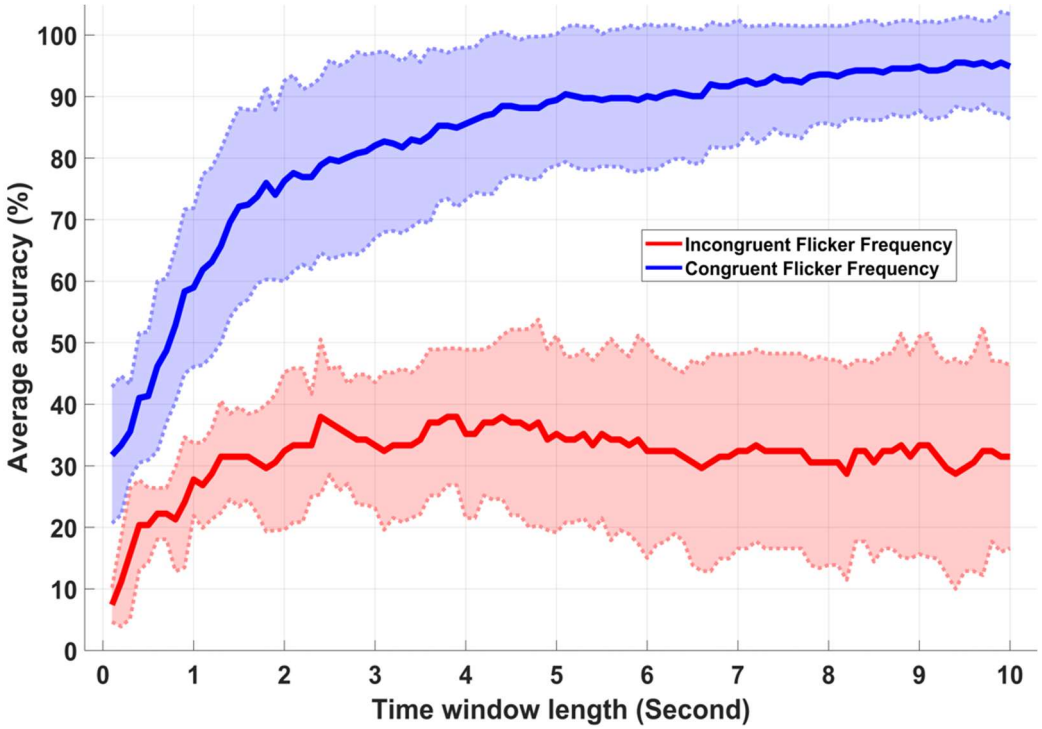


Figure 4.17. An evaluation of CCA decoding accuracy on the Congruent vs. Incongruent flicker frequency with respect to varied sliding window size

5 Chapter Five: Gauging Working Memory Using Resting-State and Task-Related Brainwaves in Healthy Older Adults

This chapter covers the analysis of neural correlates of visual working memory during task non-specific resting-state and task specific short-term memory. An overview of the significance of working memory as a pivotal brain mechanism is explained. Then, a conducted experiment, the results, and the findings are discussed.

5.1 Memory and different models of short-term and long-term memory

We can define memory as the retention of information over time. However, most researchers could subdivide memory into three memory systems: sensory memory, short-term memory, and long-term memory. Figure 5.1 demonstrates the information flows in three subdivisions of memory based on Atkinson and Shiffrin model [214]. These memory subdivisions vary at least along two aspects; 1) the amount of information each subsystem can retain and 2) the duration of information retention. Although, the difference between these subsystems are not always crystal-clear.

Sensory memory. Watching television is a good example of sensory memory. When we watch a program, we experience a steady stream of visual information. However, in reality, it is a series of disconnected frames, each divided by an extremely brief interval of darkness normal eyes cannot perceive. Our brain sees a seamless blended series of frames as a whole. This is because our brain retains each frame in our sensory memory and sensory memory briefly maintains our perceptions in a buffer before passing them into the next memory subsystem. Sensory memory buys out our brain a little time to process incoming sensational information while allow us to perceive our world as an uninterrupted and continuous stream. Each sensory input including vision, auditory, somatosensory, gustatory (taste), and olfactory (smell) have its dedicated sensory memory. The type of sensory memory that applies to vision is also called iconic or eidetic memory and the one that applies to hearing is called echoic memory.
Short-term memory. Once the sensory information passes our sensory buffer, it enters short-term memory for brief period of time. It is closely related to another system that is called working memory which refers to our capability to focus on the real-time information we are thinking to or we are attending to [215]. Psychologists have conducted different experiments to estimate the duration of short-term memory. The observation from recalling strings of letter and backward counting shows that after about 10 to 15 seconds, most of participants' information retrieval is not better than the chance level. So, they believe that the duration of short-term memory is less than ten seconds [216]. Short-term memory fade away over time. The longer we wait, the less information is left. Short-term memory is also limited by capacity. In normal subjects, it can store approximately four to seven items at a time.

Long-term memory. It is human relatively enduring storage of information. The long-term memory includes the life experiences, skill sets, and the evidences we all have attained during our lifetimes. In contrast to short-term memory that can usually hold at most four to nine stimuli in hand at a single time, the capacity of long-term memory is enormous. No one knows what size our long-term memory is, but scientists have estimated as much information as more than a couple of hundreds of Encyclopedia Britannica. Also, information in short-term memory usually vanishes after about 15 seconds but information in long-term memory can reside for decades, or even stays there permanently. Furthermore, types of mistakes in memory retention is different between short-term and long-term memory. Errors in long-term memory tend to be semantic, errors on the meaning of the information. However, errors in short-term memory is usually acoustic, errors on the sound of information. For instance, we might misremember seeing a “cat” as a “dog” in a semantic error case or misremember the word “tall” as the word “ball” in an acoustic error case. The model considers separate mechanisms, information buffers, and information storage based on the type of information for different memory types.

Another theory for memory lies on the basis of unitary storage of memory. In that sense, short-term and long-term memory have not separable architectures. Instead, short-term memory is temporary activations of long-term representations in memory. The theory almost presented in parallel with the Baddeley and Hitch model but it has been recently received attention again [217-219]. According to unitary model of memory, there is only single representations of items in memory i.e., the one in long-term memory which can alter in strength as a function of frequency of occurrence and recency. During cognitive tasks, the stored representations are made available for retrieval, staged to short-term memory. Being within the focus of attention also makes the representation available. Further, Baddeley and Hitch [220] claimed that the Atkinson and Shiffrin model cannot explain the role of attention and consciousness. They developed a model of working memory which is defined the part of memory needed to organize and execute an action. So, working memory is intertwined by sensory feedback and attention and a central executive is responsible for gauging and controlling attention to focus the memory on the current task. Figure 5.2 illustrates the flow of information according to unitary architecture of memory.

5.2 Brain areas associated with short-term memory

Investigating neural activities during short-term memory tasks indicated a highly overlapped activity in the frontal and temporal brain areas for the short-term and long-term memory [221]. Although literature may have demonstrated varied neuroimaging results, studies on patients with lesioned brain have shown that damage on parietal and temporal lobe have significantly correlated with impaired short-term memory [222].

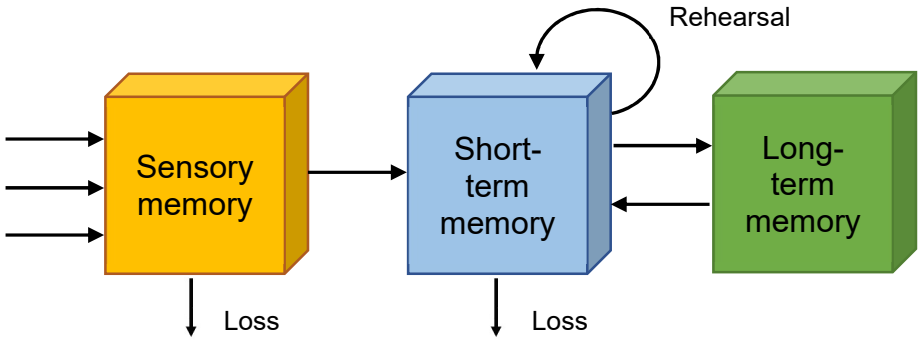


Figure 5.1. Three subdivisions of the memory system. The figure shows information flows for both information retention and information retrieval according to Atkinson and Shiffrin model [214].

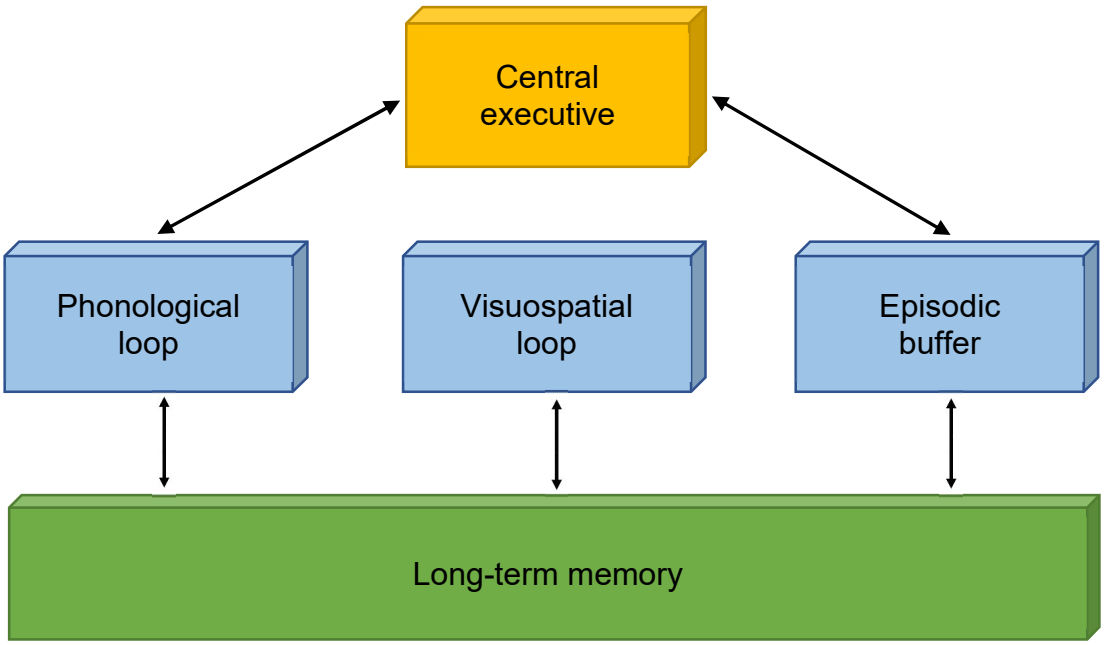


Figure 5.2. A schematic of information flow according to Baddeley and Hitch model [220].

The same studies have demonstrated that short-term memory and long-term memory involve different brain areas, mostly medial temporal lobe (MTL) for long-term memory. The advancement in neuroimaging techniques, especially with fMRI, have shown information-specific areas for memory. It has shown that right posterior dorsal frontal and right parietal areas are associated with spatial short-term memory and left inferior frontal, left parietal areas are associated with verbal short-term memory, and left parietal, left inferior temporal, and left inferior frontal are associated with visual short-term memory [223].

The Baddeley and Hitch model [220] considers a central executive role for attention as a separate process from memory. Studies from different neuroimaging signals on the difference in low and high distraction tasks, tasks that required involving executive processes, have shown that frontal lobe is associated with executive processing. Investigation on patients with brain lesion have confirmed the findings [223]. The study shows that processes involved in memory primarily involve posterior areas while executive processes to govern the task during high interference involve mainly involve dorsolateral frontal and posterior parietal areas.

5.3 Processes associated with short-term memory

We can understand the short-term memory mechanism by stratifying it into three processes: encoding, maintenance, and retrieval.

Encoding. Encoding is a process that allows the perceived representations to be converted into cognitive focus. It is assumed that cognitive focus has instantaneous access to sensory input as the perceived representation. This includes the instantaneous access to the immediate present and immediate past [224]. There are two theories regarding the encoding of perceived representations. One theory stated that the incoming input item completely replaces the previous item. Another theory posited that the new entering item into the cognitive focus may compete with the old item as a function of similarity or partly overwrite the old item representation. The observations from discontinuity in behavioral response suggest that the first theory may apply. Another observation suggest that attention works as a faucet that can control and modulate the amount and direction of cognitive focus to perceptual inputs.

Maintenance. Maintenance is a process of consolidating the cognitive representation and maintain it from decay or interference. Studies on fMRI and EEG signals have shown that maintenance occurs in neurons of prefrontal and posterior areas. Maintenance can modulate cognitive focus to prevent incoming stimuli interfere with the currently focused representation.

Retrieval. Retrieval refers to the process of re-accessing of information from the past and put them into cognitive focus. By switching the attentional focus, it is possible to retrieve information either from highly activated parts of long-term memory or even from a dormant portion of long-term memory. Except for the most recent item which can be

accessed and retrieved more instantly, the short-term memory retrieval is believed to be a parallel process. The consistency in the reaction time for all items is an evidence for that.

5.4 Significance of the resting-state brainwaves

Working memory is a core cognitive function and its deficit is one of the most common cognitive impairments. Reduced working memory capacity manifests in reduced accuracy in memory recall and prolonged speed of memory retrieval in older adults. Currently, the relations between healthy older individuals' age-related changes of resting brain oscillations and their working memory capacity is not clear. Eyes-closed resting-state EEG (rEEG) is gaining momentum as a potential neuromarker of mild cognitive impairments. We used a wearable and wireless headset measuring key electrophysiological brain signals during rest and a working memory task. We test the hypothesis that resting-state electroencephalogram (EEG; e.g. eyes close for 90 seconds) features are surrogate markers for working memory capacity in heathy older adults. Forty- three older adults' memory performance and brain oscillations and inter-channel magnitude-squared coherence during rest were measured. We report several new findings that support the hypothesis including (1) Individuals with a higher memory retrieval accuracy are significantly correlated with a lower Alpha and Beta oscillations over the right parietal site; and Lower Gamma oscillations over the right frontal sites correlates to better memory accuracy; (2) Slowed memory retrieval is significantly correlated with increased Delta and Theta band powers over the left parietal sites. (3) Increased coherence between the right parietal site and the left frontal area is correlated with slowed speed in memory retrieval. Our results suggest that resting EEG brain oscillations at local and distant neural circuits are surrogates of working memory retrievals accuracy and reaction times. Our findings indicate that rEEG frequency and coherence features recorded by wearable headsets are potential neuromarkers for working memory capacity, which is useful for fast screening of cognitive impairments.

5.5 Significance of task-related brainwaves

Decline in working memory retrieval has been suggested as one of the hallmarks of cognitive deficits. Behavioral response gauged by performance score (correct percentage) and reaction time has been the prominent indicators of individuals' working memory performance. In spite of the correlation of performance score and reaction time with cognitive states, they may not always reveal the complete picture. In this study, we aimed to understand neural correlates of memory retrieval in which the participants were accurate and fast and compare it with the associated memory retrieval neural pattern that they were slow and inefficient. This work is a preliminary analysis to comprehend the neural surrogates of "fast and efficient" versus "slow and inefficient" memory retrieval for a comprehensive neurofeedback study with wearable EEG

headset. We found that fast and correct retrieval is significantly correlated with the neural activities over the left frontal sites.

5.6 Identification of task-related EEG surrogates for “efficient” short-term memory using machine learning

From previous studies we know that behavioral response is not always provide us with a discriminative outcome measure to diagnose lapse of attention or short-term memory [225]. Li et al. [225] investigated behavioral and neural data collected in a delayed match-to-sample task among control healthy people, people with amnestic mild cognitive impairment, and people with Alzheimer’s disease to find a biomarker. The amount of difficulty in the design of the task allowed all participants from different groups, even the impaired groups not only complete the task, but also projected similar behavioral response. The measured reaction time showed comparable behavioral outcome. However, the ERP response calculated during the neural data collection of the short-term memory task revealed a distinctive pattern among three different cohorts. Figure 5.3 shows the grand average ERP response of normal healthy control group, the amnestic mild cognitive impairment group, and the Alzheimer’s disease group.

We can observe almost identical average EEG deflection over central and posterior areas among three cohort groups. However, the ERP response over frontal area demonstrate the difference between three groups. Figure 5.4 demonstrates the spatial distribution of the neural activity by subtracting the ERP response of target match and target non-match visual stimuli for normal healthy control group, the amnestic mild cognitive impairment group, and the Alzheimer’s disease group in the same study. The figure shows how three cohorts have distinctive spatial distribution of ERP response over the scalp.

Collecting neural and behavioral response during a short-term memory task can provide us with an effective methodology for studying neural dynamics of human cognition. Specifically, EEG signals, which has a high temporal resolution can potentially shed light on the neural patterns of memory encoding and memory maintenance. Within just 15 minutes of EEG recording we have tens of thousands of data samples acquired from each EEG electrode. Considering the vast amount of information embedded in spatial, temporal, and spectral characteristics of EEG signals, the data recorded during a short-term memory task may further advance our understanding of the neural processes involved in short-term memory. Analyzing event-related potentials (ERPs) to determine neural patterns for memory encoding and memory maintenance has been a common practice among investigators [226, 227]. ERPs are defined as an average EEG pattern time-locked to a stimulus onset, an event which is enumerated by peak amplitudes [58].

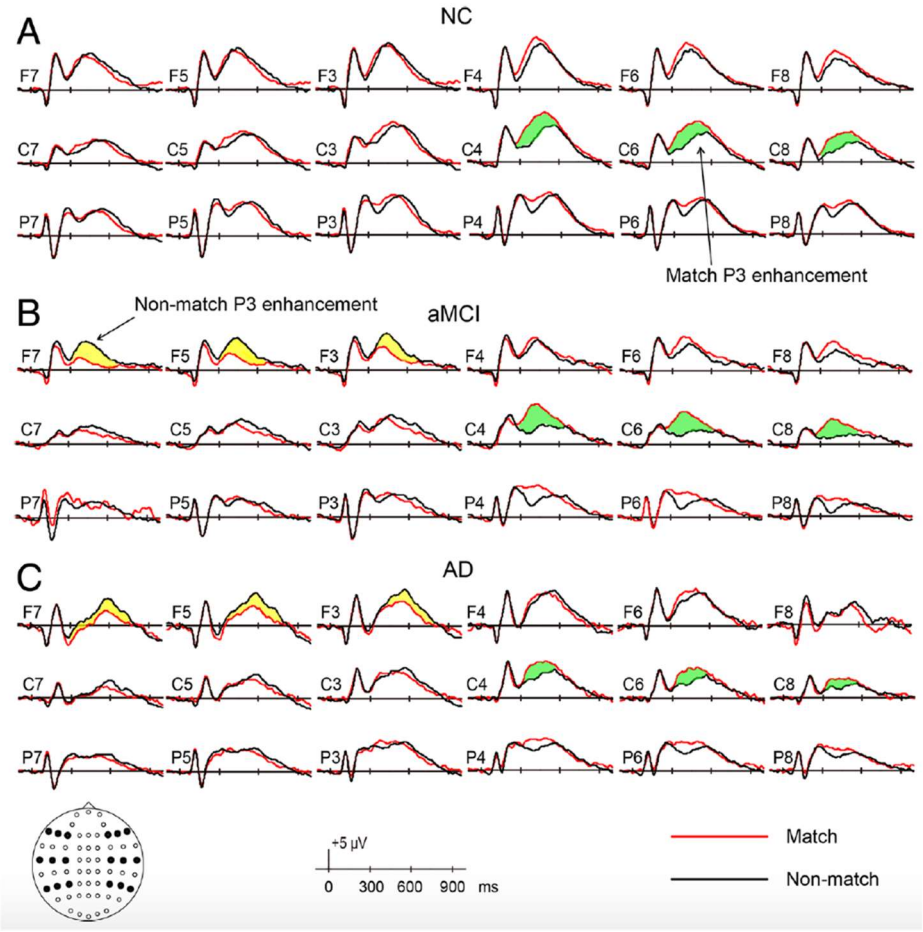


Figure 5.3. The ERP response generated as the grand average EEG waveform deflection over all participants of A) Normal healthy control group, B) the amnestic mild cognitive impairment group, and C) the Alzheimer's disease group over the correct behavioral response for target match and target non-match visual stimuli, borrowed from [225].

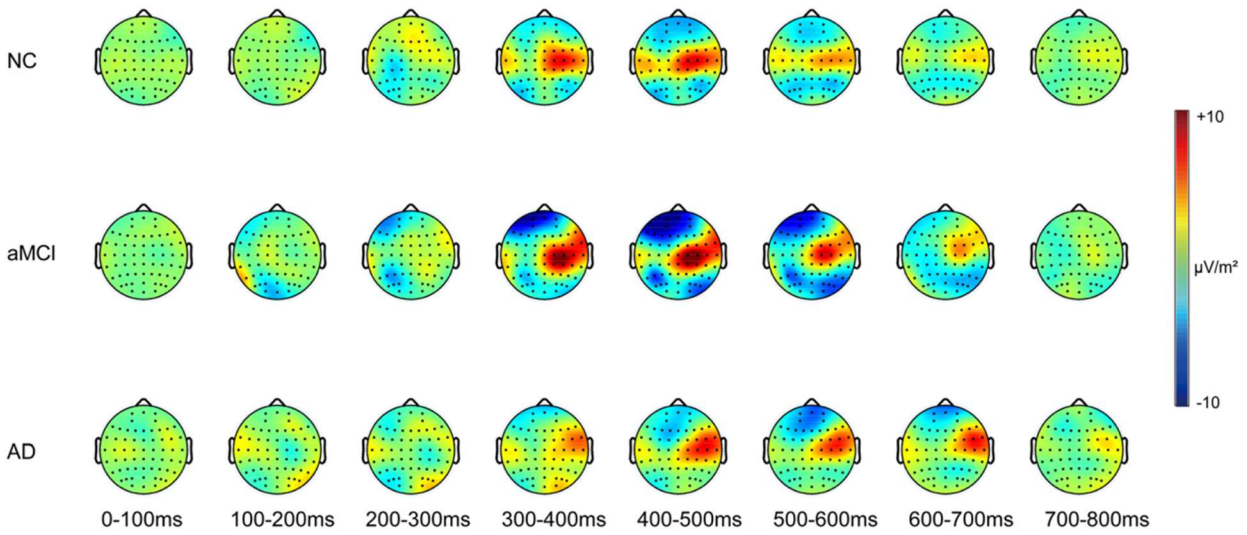


Figure 5.4. The spatial distribution of the neural activity by subtracting the ERP response of target match and target non-match visual stimuli for normal healthy control group, the amnestic mild cognitive impairment group, and the Alzheimer's disease group, borrowed from [225].

ERPs' focus is mostly on the temporal characteristics of EEG signals which is engendered exogenously because of the stimuli while discarding the other valuable endogenous information from neural activities, i.e., the buried information during the intervals of the associated memory processes. Information extracted from neural oscillations collected prior, during, and following a task may improve our understanding or neuromodulation. Thus, analyzing of ERP may provide us with a replicated method to compare the results with the prior studies. However, we are interested to look for significant features of short-term memory that might be overlooked or have not been discovered yet.

Also, applying signal processing approaches on multi-channel EEG signals spawns even more features which may call for a need in machine learning approaches capable of identifying significant and informative features that best fit to our question. These approaches include probabilistic modeling and discriminative analysis to uncover knowledge from neural signals. The methods are especially getting momentum in medical and psychological sciences because not only they may outperform the conventional approaches in terms of predictive analysis, but they can potentially provide us with expressive analysis of the recorded neurophysiological signals, and more knowledge on our neural substrate. This could be used in diagnosis of neurophysiological and cognitive deficits, discovery of disease biomarkers, and more conveniently track the treatment adaptation by the users. Moreover, the approach can be embedded in a computerized neurofeedback therapy for short-term memory.

In visual short-term memory tasks, participants maintain items in memory for a brief time (usually less than 15 seconds) while the performance is translated into the short-term memory capacity. The variability of performance in trial to trial basis may explain the variations in the short-term memory capacity and the fluctuation in the response time may reveal the momentary attention. However, a quick response time (faster than usual) or prolonged response time (slower than usual) may reveal lapse of attention. We hypothesize that variations in the attention may predict the performance of the short-term memory task, though the variations in the short-term memory capacity. This is based on the observations that shows lower capacity of short-term memory is correlated with worse performance in sustained attention tasks [228]. By tapping into behavioral response, considering response time and performance as proxies for sustained attention and short-term memory, here the goal is to identify a continuous individualized neural measure of "efficient" short-term memory using signal processing and machine learning. Extracting such a continuous, trial-by-trial measure may provide us with a predictive biomarker of task performance, even before the actual motor selection. The measure may allow to investigate spatial, temporal, and spectral dynamics of memory encoding and memory retrieval. Furthermore, the knowledge may contribute to a range of BCI applications in cognitive control for cognitive state monitoring and neurofeedback purposes.

Highlights of findings:

- Accuracy of working memory retrievals is correlated with higher frequency brain oscillations (Gamma, Beta and Alpha) at local and distant neural circuits in the right hemisphere support.
- Slowed memory retrieval is significantly correlated with increased Delta and Theta band powers over the left parietal sites.
- Increased coherence between the right parietal site and the left frontal area is correlated with slowed speed in memory retrieval.
- Using wearable and wireless headset, eyes-closed resting EEG under 3 minutes, index working memory retrieval speed and accuracy, which is a noninvasive, quick, and affordable pre-screening tool of cognitive decline in clinical application.

5.7 Findings on the resting-state brainwaves correlates of cognitive control

Visual working memory plays pivotal roles in daily goal directed activities such as searching for a car in a parking lot and driving. To find the right car, one must keep task-relevant information (e.g. color of the car) in mind as memory target, while rejecting non-target information. While driving, one needs to survey the mirror and putting the in-motion surroundings and cars into working memory and retrieve related information fast. Retrieval accuracy and speed are important memory performance measures that reflect the capacity of working memory as temporary storage of information and its later manipulation [229]. Changes in working memory occur during cognitive aging [230] presented by slowed neural processing speed or reaction times [231].
Synchronized neural activity in local or distant circuits can be measured at milliseconds scale using electroencephalography (EEG). Although EEG technologies have been around for many decades, recent advances in machine learning algorithms and wireless technology makes wearable EEG gaining new tractions as a convenient method to measure brain activity [232]. Despite low spatial resolution, EEG signals are capable of providing information about the oscillatory activity and the brain functional connectivity across long-range brain networks [232]. We rely on the high temporal resolution (< 1 ms) of EEG signals to investigate cortical rhythms during wakeful resting and cognitive tasks. Investigation of resting-state and task-induced non-random intrinsic patterns of brain activities brings about major advantages of being noninvasive, lower-cost, and portable [233-237]. For instance, analyzing event-related potentials (ERPs), which is the average EEG brain response onset to a series of stimuli, offers a brain imaging technique to gauge lapse of cognition [238-241]. On the one hand, excessive body movement causes channel noise and artifacts in the recorded EEG signals that negatively impact the quality of the task-induced EEG signals. On the other hand, recording brainwaves during rest does not require additional instruments to induce a

series of stimuli, i.e., the one similar to ERP-like experiments. It has also the benefit of inducing less fatigue and anxiety to the participants. Here we investigated the extent of which individual working memory performance indicators are correlated with neural oscillations at rest measured by EEG signals.

The dominant brain oscillation in awake resting-state is low alpha oscillation (8-10 Hz) showing global vigilance and attention. An overall increase in low alpha in the eyes-closed compared to the eyes-opened resting would be easily depictable [242], and the increase is manifested over parietal and occipital areas [242]. Increased alpha power in the resting-state has been associated with higher accuracy and faster reaction times during verbal recognition tasks [243]. An age-related decline in the posterior low alpha and delta oscillations in resting-state was discovered among a large sample study of 215 healthy subjects [244] while the high alpha (10-13 Hz) is mostly correlated with brain activities associated with sensorimotor and semantic processing [245]. People with dementia showed higher delta (1-4 Hz) and theta (4-8 Hz) and lower beta (13-28 Hz) power oscillations compared to normal aging adults [246]. In contrast, people with cerebrovascular dementia can be identified by an overall higher theta oscillation compared to people diagnosed with AD [247]. Resting-state measurements obtained during participants' wakeful eyes-open suggest that delta power from the left frontal and temporal regions correlates well with faster reaction time and even less variability in reaction times among adult healthy participants [248]. Additionally, higher frontal and parietal alpha correspond to lower measures of accuracy and higher inter-trial variability of reaction time [248]. Patients with a lower capacity of working memory have been shown to exhibit larger changes between delta/theta ratios in resting-state with eyes open and eyes closed in specifically the right posterior frontal and parietal cortices [249]. Increased beta and gamma power over the right temporal and parietal areas during eyes-closed resting-state were positively correlated with second language acquisition [250], which is an indicator of working memory capacity. Many studies have examined the characteristics of resting-state measures to explain the neurophysiology of various diseases, including migraine and AD – further highlighting the utility and quality of information obtained from resting-state EEG measurements [251, 252].

Older adults with Cognitive impairment and preclinical AD pathologies also show changes in network connectivity subserving working memory functions [253]. High temporal resolution of EEG signals allows the evaluation of functional connectivity through the estimation of coupling between different pairs of independent signal sources or different electrodes across frequency bands. The connectivity can capture relationships between different brain areas, providing valuable information to discover novel neuromarkers. Magnitude-squared coherence is a normalized measure of co-activation and temporal synchronization in the spectral domain between pairs of

sources or electrodes which represents functional coupling. The measure calculated by Fast Fourier Transform (FFT), illustrate information processing during motor and cognitive processing between the involved regions.

There is a network of brain regions subserving working memory functions. Thus, coherence during resting-state is a potential neuromarker of different neurodegenerative diseases. Babiloni et al. [254] investigated the coherence network during resting-state between normal aging, MCI, and AD cohorts. The study revealed that AD cohorts have higher coherence over delta band and lower coherence over alpha oscillations compared to MCI and normal aging cohorts. Using MEG brain imaging, Stam and van Dijk showed that a decrease in total brain synchronization in the beta and gamma bands among AD cohorts is significant compared to normal aging people [255]. Bosboom et al. showed that dementia in people with Parkinson's disease is highly correlated with the decease of alpha frontotemporal coherence and loss of local gamma oscillation during resting-state [256]. Decrease of frontoparietal and interhemispheric coherence in the delta and alpha bands during rest in people with AD has also been depicted [257]. Overall, a decrease in the measure of coherence in people with AD is often associated with damage in the cholinergic system and its interactions with the intrinsic neurotransmitters' excitation and inhibitions along pathways that connecting the frontal area to other brain regions including temporal, occipital, and parietal areas [258]. The increase of coherence between the temporal region and other brain regions is considered a compensatory mechanism to tackle decline in the coherence between other regions [259].
In this study, we explored the correlations between rhythms of EEG signals during resting-state and performance measures of working memory. We correlated mean reaction time and mean accuracy score of target matching memory task and the corresponding EEG rhythms during eyes-closed resting-state EEG among a normal aging cohort. Also, we explored connectivity between all pairs of EEG electrodes in all oscillation bands. We utilized magnitude-squared coherence between two EEG sites as the connectivity estimation metric. We identified the neural correlates of resting-state EEG that correspond to task-dependent behavioral scores in a population of elderly adults with normal cognition. We aimed to discover a neuromarker for the utilization of resting-state EEG recordings to identify age-related subclinical changes in task-dependent behavioral measures. The identification of these correlates is the first step towards early identification of subclinical changes in working memory that may allow for early intervention and prolongation of the maximal functioning of older adults. We hypothesize that resting-state EEG (rEEG) features (brain oscillations and inter-channel magnitude-squared coherence) are correlated with individuals' memory accuracy and reaction times. We predict that individuals with a higher memory retrieval accuracy are significantly correlated with certain brain oscillations at local and distant neural circuits.

Additionally, different neural circuits or global oscillatory activity supports the speed of working memory retrievals.

5.8 Findings on the task-related brainwaves correlates of working memory

In a dynamic and ever-changing visual environment, successful navigation requires attending to task-relevant information while ignoring task-irrelevant information. This goal-directed behavior is believed to be facilitated by task-relevant information template representations that help direct attention to matching visual input and are activated in visual working memory [229]. Working memory encompasses temporary storage of information and its later manipulation.

Changes in working memory retrieval occur during cognitive aging. Slowed cognitive processing speed and reaction time occur in the general aging population and, depending on the degree of change, may provide evidence of pathologic cognitive changes beyond age related decline. The rate of decline in accuracy and reaction time are closely associated with working memory retrieval, which has been shown to provide a reliable measure of cognitive decline. Evidence suggests that perception-motor coordination portrayed in processing speed is an indicator of age-related working memory decline [260]. Currently, clinicians rely on behavioral and cognitive testing and various imaging modalities to identify changes in memory in the aging population. Cognitive testing is less sensitive for the small changes in memory that accumulate overtime but can identify the summation of the changes when the effect is significant. Imaging modalities are utilized, but can be expensive, logistically challenging and time consuming and may also be less sensitive to subclinical changes.

Neuroimaging technologies has provided neurophysiological explanations for the decline in working memory in the aging population. fMRI has been employed to investigate the brain substrates associated with the impairment of working memory in older adults [261-266]. Todd et al. [263] investigated the brain areas activated during encoding and retrieval given face and color stimuli and found an area of activation in the lateral prefrontal cortex. Suzuki et al. [267] probed differences in brain patterns between young and elderly adults during memory maintenance in an n-back memory task. Higher activity in the right caudal dorsolateral prefrontal cortex (DLPFC) was found with fMRI during active memory maintenance. Rypma and D'esposito [261] studied activities in the prefrontal cortex (PFC) during a delayed-response WM task and found that fast older subjects showed greater dorsolateral PFC (DLPFC) activation during memory retrieval than slow older subjects. Later, D'Ardenne et al. [264] identified that the DLPFC plays a critical role in WM updating. Evidently, fMRI has provided crucial insights into the involvement of the DLPFC in working memory retrieval and suggest that changes in this area may be involved in working memory decline.

Electroencephalogram (EEG) signals as an alternative to fMRI brain imaging offers a convenient brain imaging modality to investigate WM-related neurophysiologic activity, with major advantages of being non-invasive, lower-cost and portable [233-237]. EEGs measure cortical activity, with increasing signals suggesting synchronized neuronal firing and therefore connectivity [268]. Information regarding neuronal connectivity can be obtained at rest (resting-state) while participants remain seated with eyes open or closed, and while participants perform varieties of tasks (task-dependent).
EEG analysis has also provided insights into neural activity during tasks. EEG analysis has widely shown alpha and theta powers to be associated with processes of working memory. During memory encoding, different neural signatures have been identified in older adults compared to younger adults [269]. This validates EEG measurements as being sensitive to alterations in neuronal activity between different age populations. Evidently, much research has highlighted the applicability and validity of EEG measurements towards discovery of underlying neurophysiology from both resting-states and various task induced states. Getzmann et al. [270] identified the event-related potentials (ERPs) associated with inhibition for working memory processes in memory storage and retrieval tasks. It was found that task-relevant stimuli are associated with more pronounced P2 and P3b amplitudes than task-irrelevant stimuli. Similarly, with the measurements of ERPs via EEG, Simard and Cadoret [271] studied the difference in neural correlates of active-controlled retrieval between children and adults, showing that there are differences in brain activity in the window of 300ms to 500 ms interval onset to the stimulus presentation corresponding to the memory retrieval. In a study of the retrieval practice effect, Guran et. al [235] found that the difference in the power of alpha and beta bands between retrieval and encoding is more remarkable in the elderly than in the young.
In this study, we seek to determine neural correlates of “fast and efficient” memory retrieval that correspond with task-dependent behavioral scores among a population of elderly adults with normal cognition. We intend this analysis to provide a framework to quantify age-related subclinical changes in task-dependent behavioral and neural measures. The identification of wearable EEG correlates of “fast and efficient” compared to “slow and inefficient” memory retrieval is essential to establish mobile EEG for early identification of subclinical changes in working memory that may allow for early intervention and prolongation of maximal functioning of elderly adults.

5.9 Materials and methods

5.9.1 Human Participants

Using identical Bluegrass memory protocol, 43 community dwelling older adults (Age >= 60) including 20 male (median= 68, interquartile range (IQR)=5.5), and 23 female (median= 72, IQR=10) were recruited and tested at the University of Kentucky (UK) Alzheimer’s Disease Center (UK-ADC), or tested in Aging, Brain and Cognition

Laboratory, at the Department of Behavioral Science, College of Medicine. The average age of the older adults was 71.6±7.0 (min: 60, max: 91), had a normal or corrected-to-normal vision, and were not under the influence of any drowsiness-inducing or cognitive enhancing medication. Participants were all native English speakers, and mostly right-handed (6 were left-handed). The experimental protocol was approved by the Institutional Review Board (IRB) of the University of Kentucky, Lexington, KY. All participants provided signed informed consent in accordance with UK IRB.

5.9.2 Wireless EEG signal acquisition and the experimental procedure

Neural data collection was performed in a quiet and dimly lit room. A water-hydrated, portable, and wireless EEG headset, Emotiv EPOC+, was used for recording EEG signals. The headset has 14 channels over AF3, F7, F3, FC5, T7, P7, O1, O2, P8, T8, FC6, F4, F8, AF4 according to 10-20 International Electrode Placement System, and collect brain electrical activities with a sampling rate of 128Hz with 14 bits resolution. We maintained low impedance (<10KΩ) for all EEG electrodes during the experiments. EEG signals were electrically referenced using CMS/DRL references at the left/right mastoid (P3/P4). Participants were seated comfortably on a chair 50 cm from a 24-inch LCD monitor. Participants completed a 60-second resting session with eyes open, followed by a 60-second resting session with eyes closed. The experimental interface provided the participants with instruction and primed them with a count-down to initiate resting sessions. By finishing the resting-state sessions, participants were instructed to prepare for a memory task. We adopted a delayed-match-to-sample (DMS) task to assess simultaneous visual matching ability and short-term visual recognition memory. This short-term memory task, which is a variant of the Sternberg memory-scanning task [272] has been well-studied and can modulate various cognitive processes including encoding, decision making, visuomotor selection, rehearsal, and retrieval. In our version of the task, we instructed the participants to memorize two sample images in five seconds. Two target images with a green border were initially presented for 5 seconds (initial memory encoding). After a jittered delay (1.6~1.8 seconds), a sequence of 12 test images, including target and distractor images, were serially presented. The participants responded to 12 consecutive test images, whether each matched or did not match any of the sample target images by pressing keys on the keyboard. The number of target and distractor images were fairly distributed in each trial. Each trial lasted around 40 seconds, which includes a 3 – second encoding period, 1-second presentation of test images and a fixation jittered inter-trial of (1.6~1.8 seconds); See Figure 5.5. Stimuli included two-dimensional black and white images of familiar objects taken from Snodgrass and Vanderwart [273]. Each picture was presented with a black background and within an area of 8.3 cm × 5.8cm. All stimuli were presented on a high-resolution color monitor.

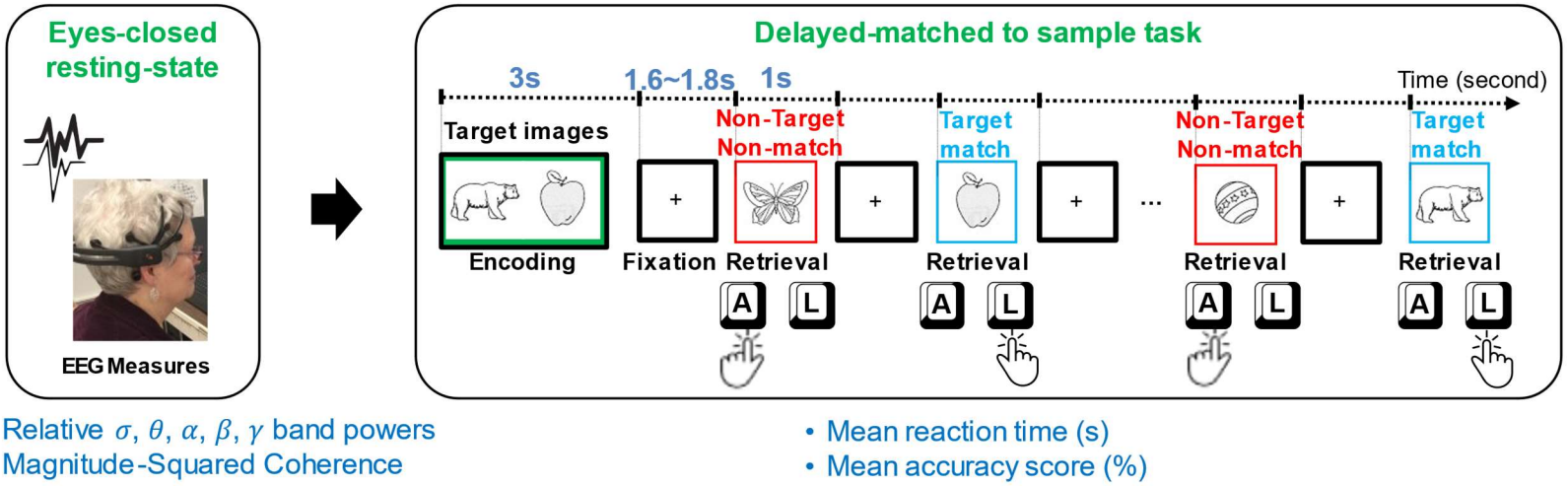


Figure 5.5. A schematic of the resting EEG (rEEG) and Bluegrass short-term memory in a right-hand dominate human participant. The participants' (age 60 and over) eyes-opened resting-state, followed by eyes-closed resting-state EEG followed by a memory task (a modified delayed match-to-sample paradigm) where a subject encoded two targets in mind, then responded with the right index to indicate the memory target match (pressing L key on the key board) and left index finger for non-target in a 5-min task; During the second 5-min testing block, the participant was asked to indicate memory target match by using the left index finger (pressing A key on the key board).

Stimuli were presented at a 65-cm visual distance and a visual angle of approximately 7 degrees. Test images were normalized across retrieval status (i.e., matching or non-matching) for image familiarity and image complexity. The participants practiced two sample trials before starting the memory task. The task was performed in two blocks of 8 trials each. During the first block, the participants responded to target images with their dominant hand (right hand) and in the second block, they responded with their non-dominant hand to the target stimuli. Overall, the short-term memory task lasted approximately 15 minutes.

5.9.3 Experimental design

We utilized PsychoPy3 builder and coder [274, 275] to design and present the visual stimuli in a timely synchronous manner. The software suite is a new version of the Psychopy python library used for the development, measurement, and the delivery of different behavioral experiments. Behavioral responses in terms of key presses along with the continuous EEG signals were recorded during the experiment. We utilized Lab Streaming Layer (LSL) [276] to synchronize behavioral and neural responses and record them into a single file. We also developed and publicly shared a low-latency pipeline in Java programming language to parse in the real-time measured EEG data from the Emotiv EPOC+ application development interface (API) and parse out in LSL [277]. LabRecorder software [278] was utilized as a unified recorder to collect and save behavioral and neural time series in a single file with the .xdf file extension. XDF is an open-source and general-purpose file format designed in tandem with LSL and supports all features of LSL protocol. The file extension is compatible with MATLAB and Python and provides a convenient data structure container to record various data modality streams in LSL, concurrently. We have publicly shared the experimental setup under open-source terms and conditions for other researchers [279]. The developed platform with all its software dependencies was installed on a workstation in UK-ADC.

5.9.4 Data analysis

5.9.4.1 Resting-state EEG preprocessing and frequency analysis

During the eyes open condition, participants were requested to stay relaxed and look straight at a fixed-in-time and pleasant scenery of the blue ocean and avoid mind wandering. During eyes closed condition, participants were requested to stay relaxed and avoid falling asleep. The impedance between each electrode and scalp were kept below 10KΩ. EEGLAB software library [151] was employed for preprocessing and noise removal. EEG signals were re-referenced to the average and online band-pass filtered between 0.5 and 46 Hz. EEG recordings were analyzed for eye blinks and muscle artifacts. We used artifact subspace reconstruction (ASR) algorithm [280, 281] implemented in the EEGLAB software to cope with channel noise and artifacts. ASR algorithms is an advanced method that allows the detection and the reconstruction of

noisy and artifactual chunks of EEG signals. We followed the Makoto's EEG preprocessing pipeline [282] to setup the parameters of the ASR algorithm. We detected and removed channels being more than 5 seconds flat, channels with abnormal high or low peaks. ASR finds the cleanest part of data as the calibration data. Then, it applies 0.5-second sliding window principal component analysis (PCA) on the continuous EEG data to classify principal components into high variance (20 x standard deviation of the calibration data) or normal variance. By detecting high variance chunks of signals, ASR reconstructs the high variance subspace using the normal calibration chunks. A minimum of 60 seconds from each participant's data after channel noise and artifact removal was kept for analysis. A FFT on 4-second epochs of EEG yield a 0.25 Hz frequency resolution over the frequency span of [1-46] Hz. A sliding window of 4-second window length with a 2-second overlap was used to minimize the effect of the windowing of FFT procedure. We computed band power in Delta (δ:1-4 Hz), Theta (θ: 4-8 Hz), Alpha (α: 8-13 Hz), Beta (β: 13-28 Hz), and Gamma (γ: 28-46 Hz) frequency bands from all 14 EEG electrodes. The absolute band power in each frequency band as well as magnitude-squared inter-channel coherence are computed for the eyes-closed resting-state session.

5.9.4.2 Task-dependent EEG preprocessing

As we would like to generalize our results to a broad range of experimental recordings, no participants were excluded during the data preprocessing. EEGLAB functions and extensions [151] combined with MATLAB software [283] were used for data preprocessing and generating the figures. First, the EEG signal was high-pass filtered to 0.4 Hz to remove baseline drift and then low-pass filtered to 40 Hz to cut-off before the frequency line and for anti-aliasing. Artifact subspace reconstruction (ASR) [284] was applied to reject bad channels and deal with channel noise and artifacts in the signal. We interpolated the channels that were removed by artifact rejection from the remaining channels. Subsequently, the neural time-series were re-referenced to an average reference. Afterward, EEG data were epoched, 200 ms before, and 900 ms after target and non-target stimuli onset. Epochs in which the participants responded correctly were included for the analysis. Incorrect and too fast (<300 ms) responses were excluded (see Figure 5.6).

5.9.4.3 Resting-state EEG coherence analysis

We conducted an electrode-by-electrode analysis to correlate rEEG band powers and magnitude-squared coherence with the performance measures of the memory task. The approach helped to identify correlations between band-delimited power in all electrodes and the memory task performance. Pearson correlations between EEG band power and task performance presented the relationship and significant correlations depicted the dominant pattern among the participants.

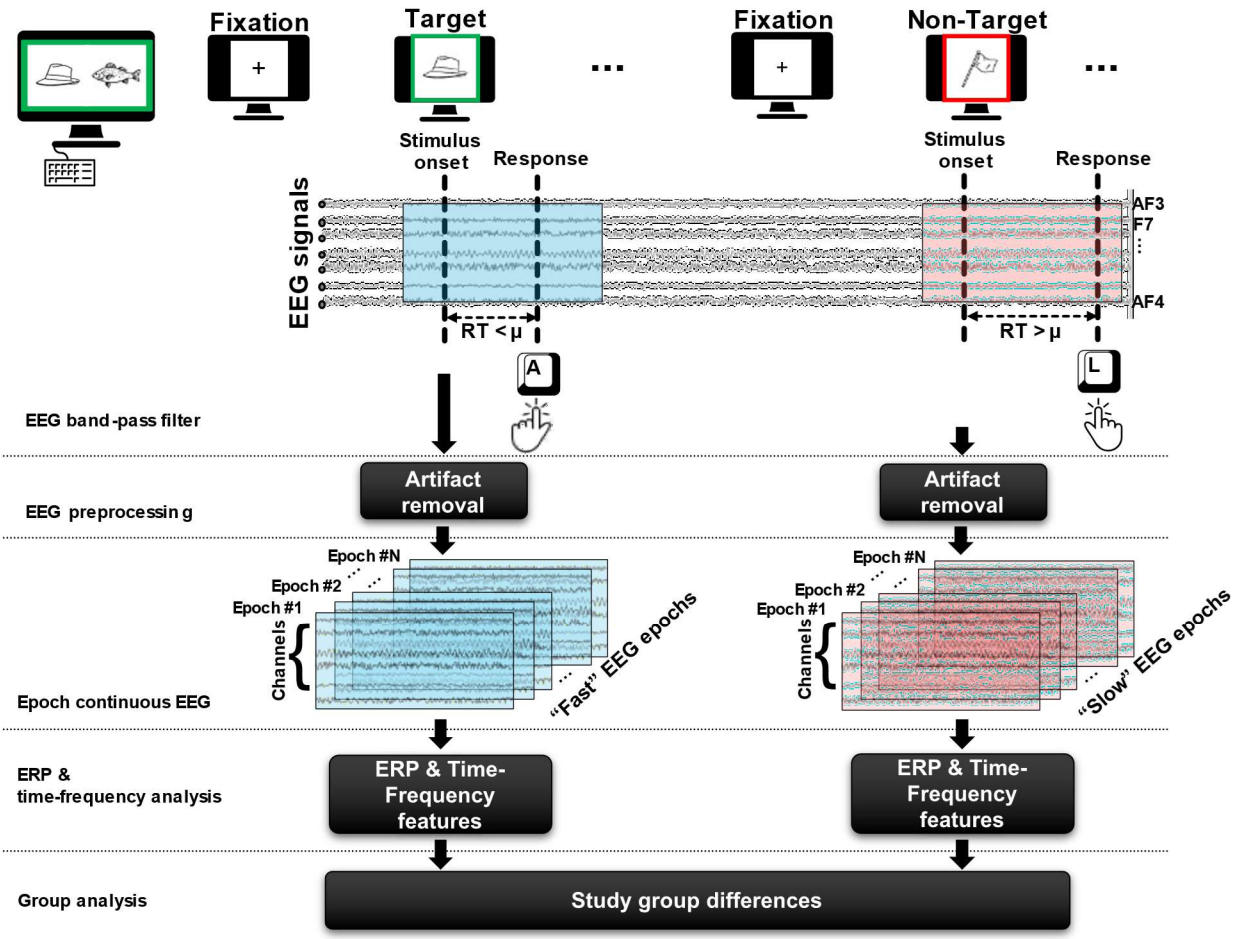


Figure 5.6. Schematic representation of task-related EEG data epoching and analysis.

We analyzed the recorded EEG data using custom scripts in the MATLAB language (Mathworks Inc., Natick, Massachusetts) [285]. For each electrode, the correlation between the participants' behavioral measures of the memory task (mean reaction time and mean accuracy score) and mean power bands in the Delta (δ:1-4 Hz), Theta (θ: 4-8 Hz), Alpha (α: 8-13 Hz), Beta (β: 13-28 Hz), and Gamma (γ: 28-46 Hz) frequency bands were calculated using Pearson correlation. Also, we analyzed the coherence of all EEG electrode pairs during resting-state and investigated the correlation between coherence graph network and memory task performance measures. We used MATLAB connected topoplot toolbox [286] to illustrate pairs of inter-channel coherence showing with significant correlation between resting-state and task performance measures.
To explore connectivity between all pairs of EEG electrodes in all oscillation bands, we utilized magnitude-squared coherence as the connectivity estimation metric obtained by:

$$Coh_{xy}(f) = \frac{\left|G_{xy}(f)\right|^2}{G_{xx}(f).G_{yy}(f)} \qquad (1)$$

Where G_{xx} and G_{yy} are autospecral density of channels x and y and G_{xy} is the cross-spectral density between EEG signals on channel x and channel y. The autospectral and cross-spectral density are functions of frequency and the magnitude coherence between two channels, an estimate showing the predictability of information from one channel using the information of the other channel. We identified the neural correlates of resting-state EEG that correspond to task-dependent behavioral scores in a population of elderly adults with normal cognition.

5.10 Results

A visual working memory task is used to investigate the resting-state EEG surrogates of behavioral performance using a portable setup that potentially can be incorporated in both laboratory and home settings. Participants' performance, including mean reaction-time (seconds) and mean accuracy score (correct percentage), was recorded during the working memory task and significant correlations between the behavioral measures have been correlated with brainwave signals during individual's conscious and resting-state. To determine whether the correlation between task performance and the resting-state neural measure is significant, we compared the $p - value$ to the significance level ($p = 0.05$).

5.10.1 Memory performance

5.10.1.1 Accuracy of target non-target short-term memory retrieval.

Figure 5.7 shows the group mean and standard deviation of the accuracy of the participants in correctly identifying target and non-target stimuli. The mean [std]

accuracy of correct response to target and non-target stimuli are 91.56 [5.02] % and 91.93 [5.84]%, respectively.

5.10.1.2 Reaction times to target and non-target stimuli.

Figure 5.8 shows the group mean and standard deviation of the mean reaction time to target and non-target stimuli. Mean [std] of mean correct reaction time to target and non-target images are 673 [51] ms and 698 [48] ms, respectively. Non-parametric Kruskal-Wallis significance test revealed a significantly faster correct reaction to target images compared to non-target images ($p = 0.034$). Also, we extracted the mean incorrect reaction time to target and non-target (false alarm) stimuli. Mean [std] of mean incorrect reaction time to target and non-target images are 649 [85] ms and 715 [118] ms, respectively. Non-parametric Kruskal-Wallis significance test revealed a significantly slower reaction to non-target non-matched (false alarm) images compared to target images ($p < 0.05$).

The male group (n=20, median= 68, IQR=5.5) were relatively younger than the female group (n=23, median= 72, IQR=10). Unsurprisingly, males showed a relatively higher accuracy (mean=92.34%, SD=4.32%) and lower latency (mean=677ms, SD=51) (see Figure 5.9) compared to females (accuracy: mean=91.28%, SD=4.97%, RT: mean=693ms, SD=43).

5.10.1.3 "Fast" and "Slow reaction times to target and non-target stimuli.

Figure 5.10 shows a flattened histogram of sorted participants' reaction time during the memory task. The histogram of each participants' reaction time corresponds to each row in Figure 5.10. As you can see in the figure, each participants' reaction time follows a single modal gaussian distribution, with a mean shown by red color and a range of standard deviation shown by cooler colors (yellow and green). As we can see, the mean reaction time over the population in this memory task spans between ~650 ms to ~750 ms.

We investigated the behavioral response in which the individuals were faster and slower than their own average reaction time in the visual working memory task (see Figure 5.11). The behavioral data showed significant differences in the mean reaction time to fast target and fast non-target stimuli. A Wilcoxon signed-rank test showed that stimuli (target matched, non-target non-matched) had a statistically significant ($p < 10^{-6}$) effect on the reaction times in all trials. Mean[std] fast reaction time to target was 591[49] ms while the mean[std] for fast non-target stimuli was 614[47] ms.

Eyes-closed alpha band is gaining tractions as potential risk marker for cognitive impairments. We examined the group average and the group standard deviation of the Alpha band power over the parietal and occipital sites (O1, O2) during resting-state eyes open and eyes close (see Figure 5.12).

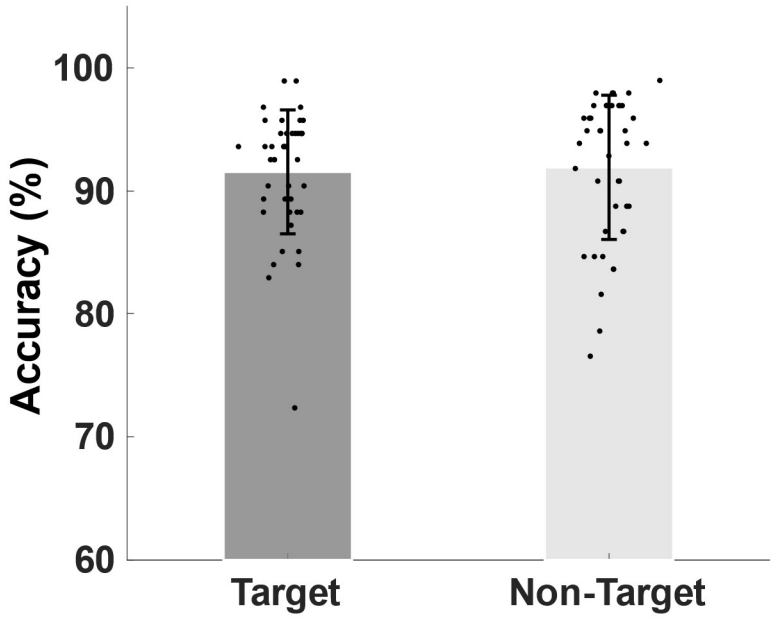


Figure 5.7. Bar plot showing group mean and standard deviation of the mean accuracy of retrieval of target and non-target stimuli.

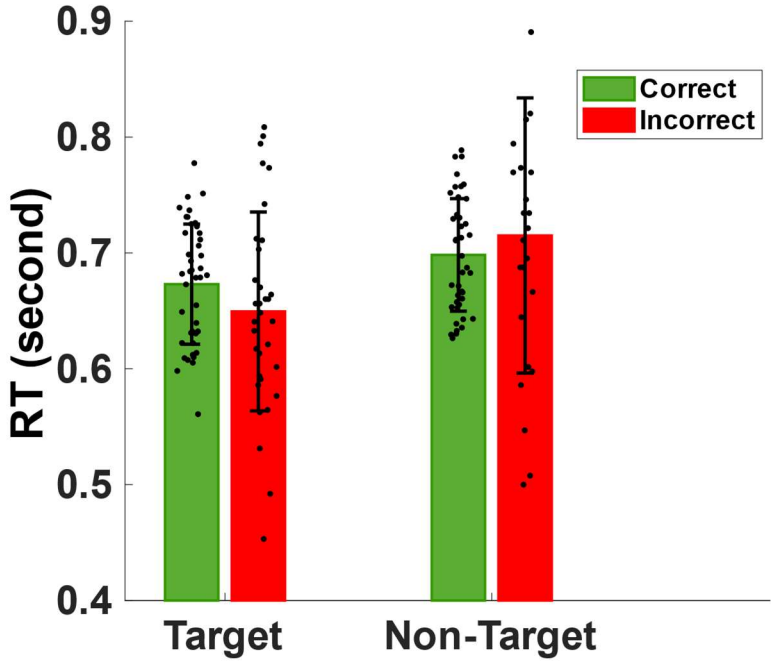


Figure 5.8. Bar plot showing the group mean and standard deviation of the reaction time to target and non-target stimuli.

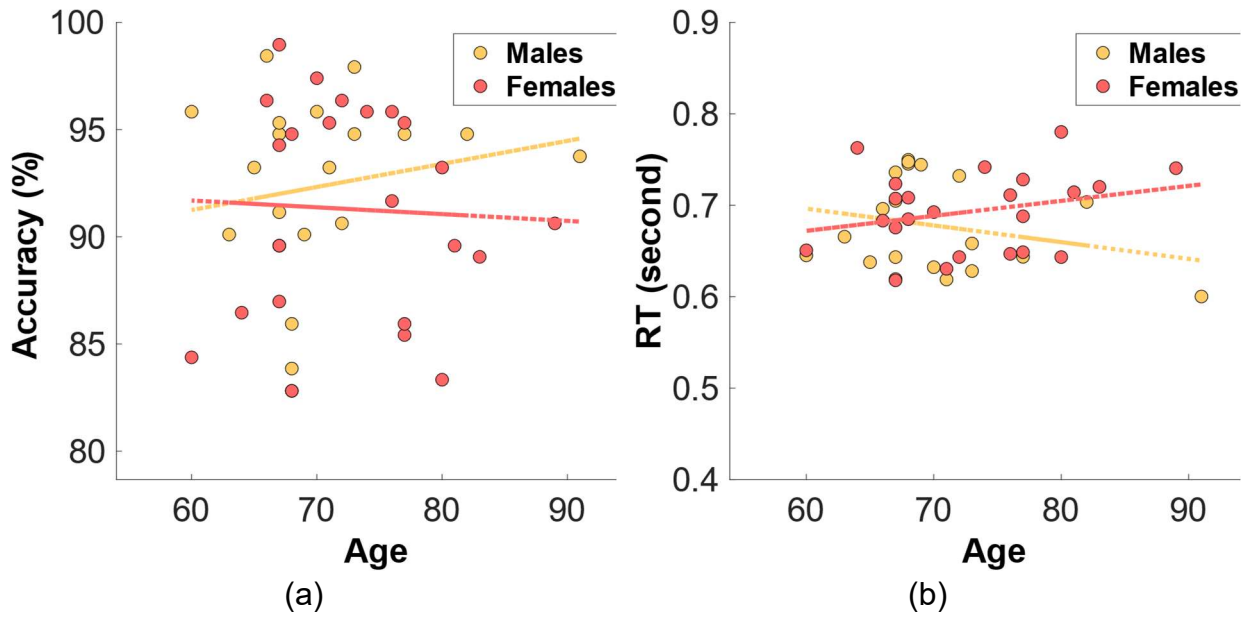


Figure 5.9. The distribution of a) mean accuracy score and b) mean reaction time (RT) across age for both male and female groups.

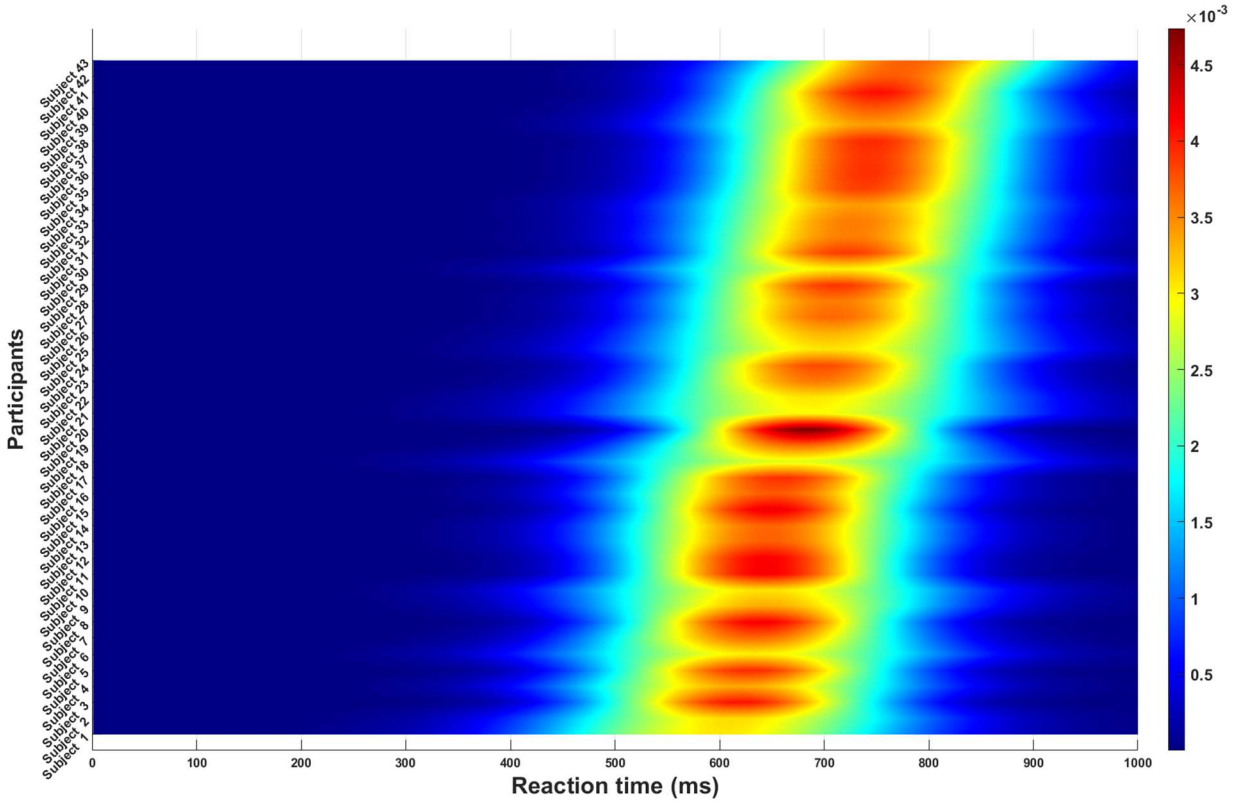


Figure 5.10. A flattened histogram distribution of all participants' reaction time. Warmer colors show a higher concentration of reaction time.

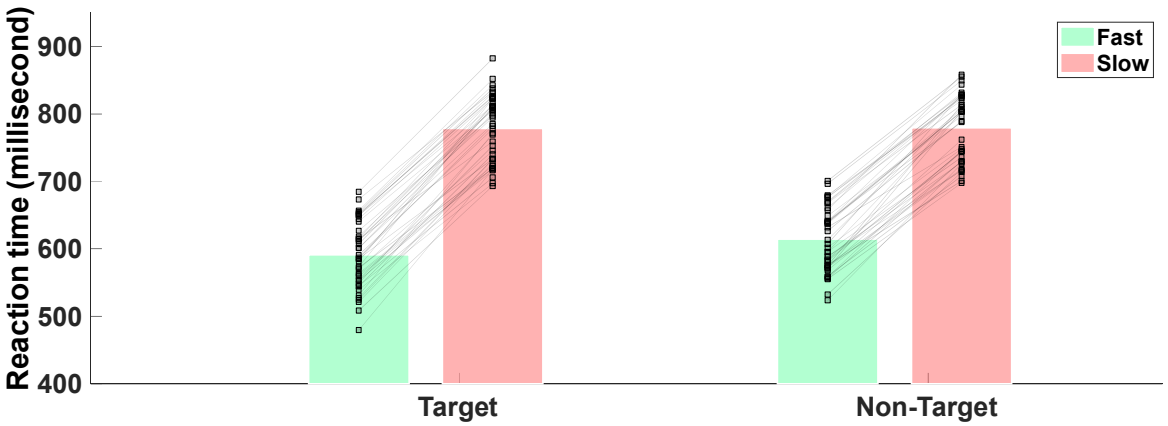


Figure 5.11. Bar plot showing the distribution of individualized “fast” and “slow” correct reaction to target and non-target stimuli during the memory task

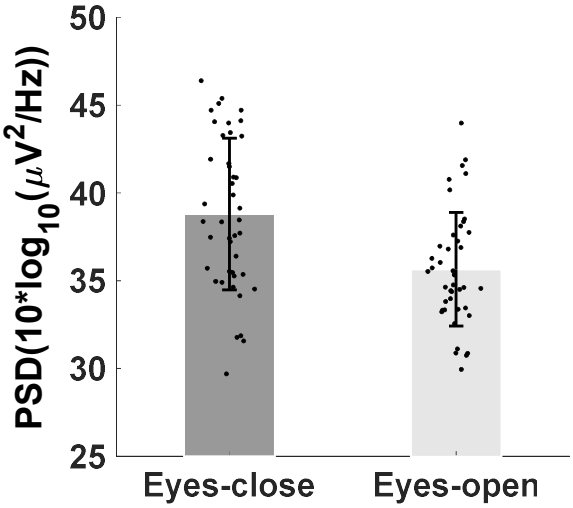


Figure 5.12. Bar plot showing the group average and standard deviation of the the Alpha band power occipital and parietal sites (O1 and O2 electrodes) during eyes-open and eyes-closed.

The group mean $\pm$ std during the resting-state eyes-close is 38.80 $\pm$ 4.32 and during resting-state eyes-open is 35.65 $\pm$ 3.23. Using nonparametric Kruskal-Wallis significance test, the average parietal and occipital Alpha during the resting-state eyes close is significantly larger than the eyes-open ($p = 3.6 \times 10^{-4}$).
Figure 5.13 illustrates average power spectral density during resting-state eyes opened and eyes closed and the corresponding topographic distribution of the alpha frequency spectrum (8–13 Hz), showing the increased occipital alpha during eyes-closed compared to eyes-open resting-state EEG.

5.10.1.4 Eyes-closed resting-state EEG and task-related behavior

We investigated the topographical distribution of Pearson correlations between rEEG relative frequency band power recorded during the resting-state eyes-closed session before the memory task and mean reaction time (seconds) during the working memory task. Figure 5.14-a. shows the Pearson correlations between EEG relative frequency band power recorded during the resting-state eyes-closed session and Figure 5.14-b show the significance level of the Pearson correlations in all electrode sites and frequency bands. We investigated the significant correlations between resting-state EEG power spectral density in each frequency band on all EEG electrodes and the individuals' performance in the working memory task.
We aim to find resting-state brainwave biomarkers of behavioral outcome. We found a significant negative correlation between individuals' mean reaction time during the working memory task and the Delta band power $(\rho(43) = -0.31, \mathrm{p} < 0.05)$. The correlation is mostly focused over the left parietal site over the P7 EEG electrode. With a slightly lower correlation, lower activities in the Theta band over the left parietal correlates with faster reaction time $(\rho(43) = -0.28, \mathrm{p} = 0.07)$. Brainwave EEG during resting-state did not correlate with mean reaction time in the other frequency bands. We did not find any significant correlation between individuals' mean reaction time and their EEG frequency band power during eyes-closed resting-state in Alpha, Beta, and Gamma bands. Increased mean reaction times correspond to the higher activity in the higher frequency bands (Beta and Gamma) and decreased mean reaction time corresponds to the higher activity in the lower frequency bands (Delta and Theta).
Then, we explored a potential neuromarker using resting-state eyes-closed EEG signals to evaluate individuals' mean accuracy scores (percentage of correct responses) during a short-term memory task. Figure 5.15-a shows the topographical distribution of Pearson correlations between EEG band powers recorded during resting-state eyes-closed and the mean accuracy score (% correct response) during the memory task and Figure 5.15-b shows the significance level of all EEG electrode sites in all frequency bands. We found a significant negative correlation $(\rho(43) = -0.42, \mathrm{p} < 0.01)$ between individuals' EEG frequency band power in the Beta band over the right parietal area (P8).

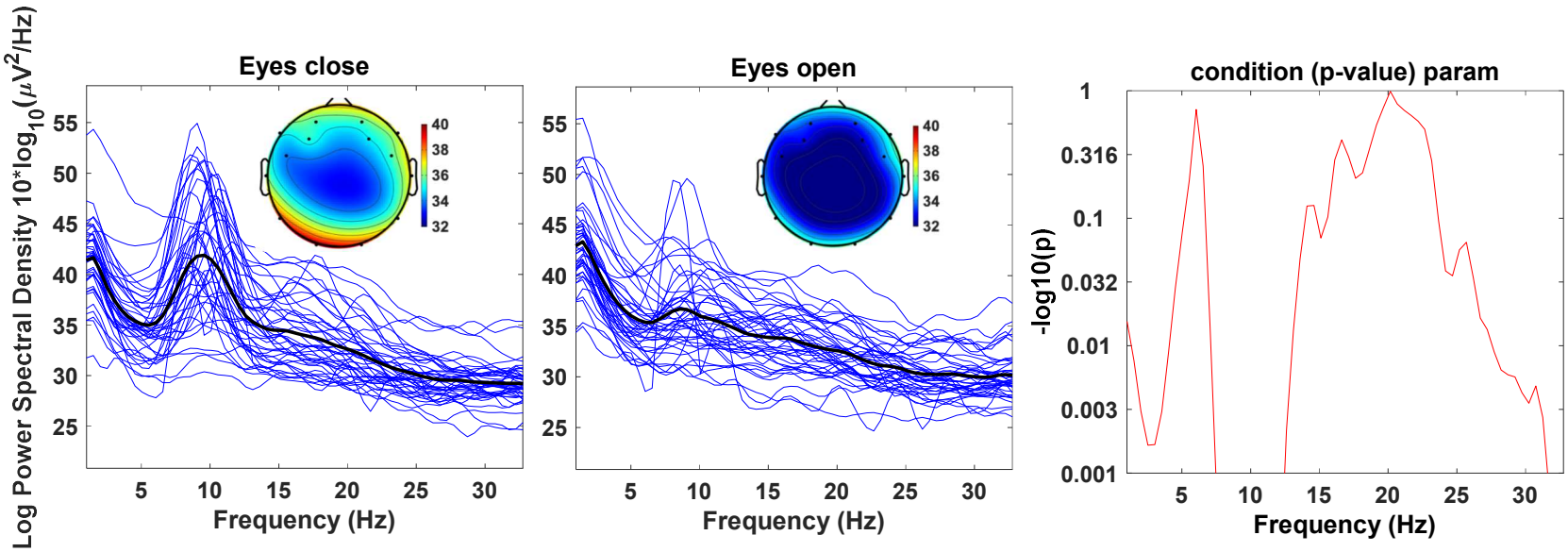


Figure 5.13. Average power spectral density over occipital sites (O1, O2), the corresponding dorsal view topographic distribution of the alpha wave (8–13 Hz), and the point by point confidence level shown by p-value during resting state eyes-close and eyes-open over all participants. The black color curves show the average over all participants and the blue curves show individuals' power spectral density.

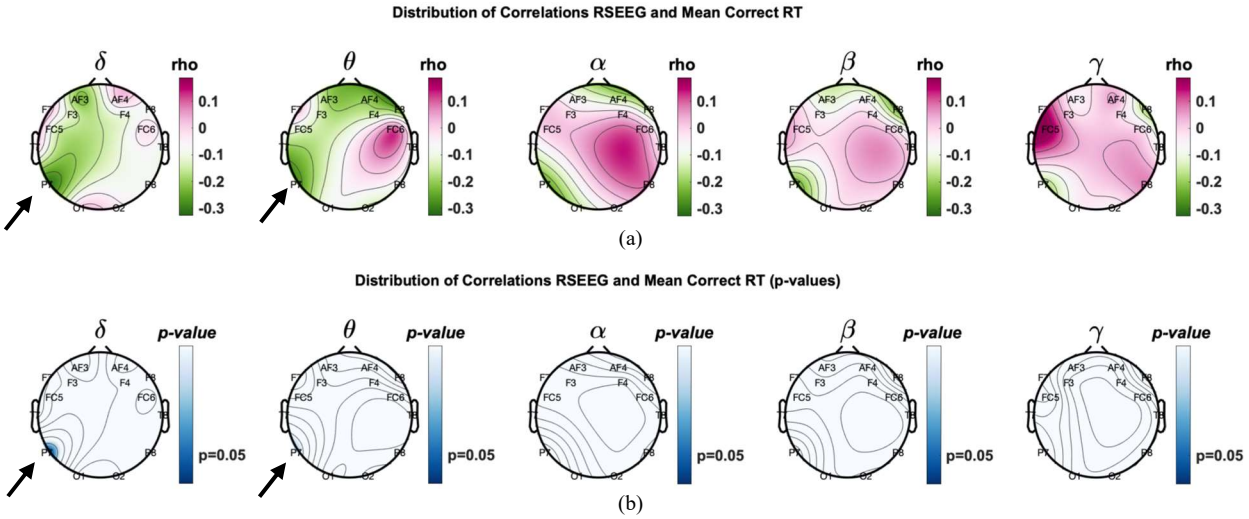


Figure 5.14. Topographical plot of Pearson correlations between EEG relative frequency band power recorded during resting-state eyes-closed before the task and mean reaction time during the working memory task. The distribution of the correlation between rEEG and mean reaction time follows a trend, meaning that increased mean reaction time corresponds to the higher activity in higher frequency bands (Beta and Gamma) over frontal sites and decreased mean reaction time corresponds to the higher activity in the lower frequency bands (Delta and Theta) over left temporal and left frontocentral

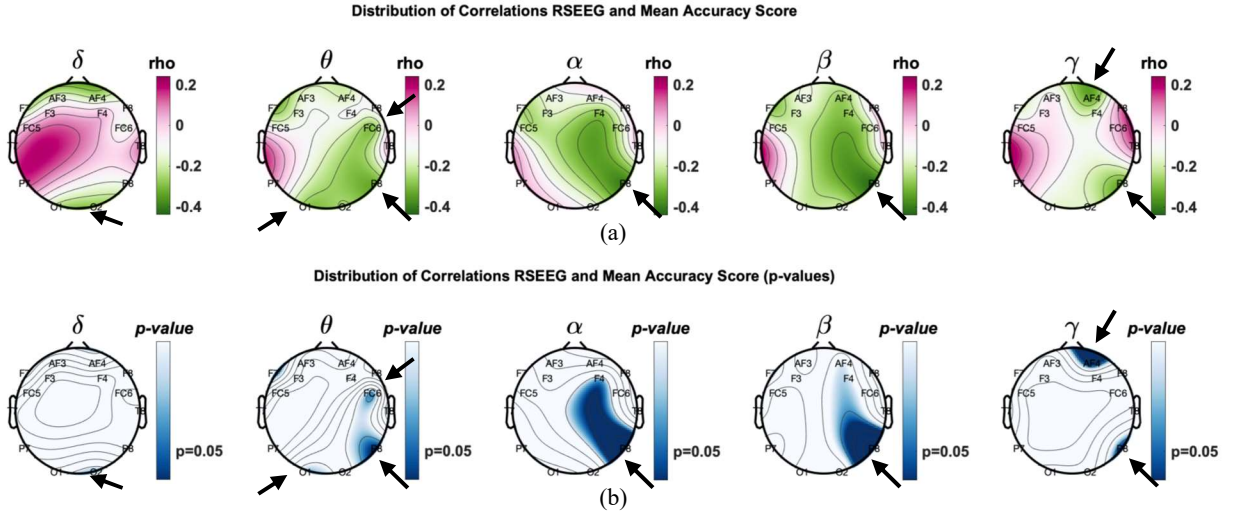


Figure 5.15. Topographical plot of Pearson correlations between EEG relative frequency band power recorded during resting-state eyes-closed before the task and accuracy score (% correct response) during working memory task.

Table 5.1 shows Pearson correlations and the significance level in terms of $p - value$ for the EEG frequency bands and EEG electrodes in which the significance level of correlations between eyes-closed resting-state and mean accuracy score during the memory task were lower than 0.07. The overall distribution of the Pearson correlations in all frequency bands and all EEG electrode sites suggests that lower brain activity over the right parietal site in Alpha and Beta bands and right frontal site in Gamma bands during eyes-closed resting-state correlates with higher ability to correctly distinguish between target and distractor images in a short-term memory task. *We found that lower Alpha and Beta activities of rEEG over right parietal areas during eyes-closed are indicators of higher accuracy score.*

Magnitude-squared coherence of the fronto-parietal sites subserving reaction times.

We explored the coupling between brain sites within Delta, Theta, Alpha, Beta, and Gamma frequency bands based on the magnitude-squared coherence algorithm. As demonstrated in Figure 5.16, significant correlations $(p < 0.05)$ between all paired EEG-electrode magnitude-squared coherence in all EEG frequency band oscillations during the eyes-closed resting-state and mean reaction time were extracted. We found significant differences mostly in the Alpha band in the EEG inter-channel coherence network. *Increased coherence between the right parietal site and the left frontal area is correlated with increased speed in memory retrieval.*

Magnitude-squared coherence of the centro-parietal sites in the Delta and Theta bands identify mean accuracy score.

As demonstrated in Figure 5.17, significant correlations $(p < 0.05)$ between all paired EEG-electrode magnitude-squared coherence in all EEG frequency band oscillations during the eyes-closed resting-state and mean accuracy score were extracted. We found significant correlations mostly in the Theta and Delta bands in the EEG inter-channel coherence network. Increased frontal contralateral coherence between frontal and temporal sites is highly correlated with increased mean accuracy scores during memory retrieval. We could not find significant correlations in the inter-channel coherence network in the Beta band and mean accuracy score.

5.10.1.5 Task-related neural measure

I stratified event-related potentials (ERPs) during the memory task into two groups: 1) ERPs that the participants responded faster than their own average and 2) ERPs that the participants responded slower than their own average. I included two standard deviation faster than individual mean reaction time and referred to them as “fast”, two standard deviation slower than individual mean reaction time and referred to them as “slow”.

Figure 5.18 shows ERP responses for both “fast” and “slow” reactions over all 14 EEG electrodes. To better illustrate the distinctive patterns of evoked brain response during “fast” and “slow” trials, we extracted dorsal view topographical illustrations of evoked brain reponses in the segmented duration of ERP after correct target/non-target memory retrieval responses in Figure 5.19.

Table 5.1. Correlations between eyes-closed resting-state EEG and mean accuracy score.

Frequency band (Hz)	***Electrode (Location)***	***Pearson correlation (ρ)***	***p***
Delta (1-4 Hz)	*O2 (right occipital)*	*-0.29*	*0.058*
Theta (4-8 Hz)	*F7 (left frontal)*	*-0.31*	*0.043**
	O1 (right occipital)	*-0.28*	*0.064**
	P8 (right parietal)	*-0.31*	*0.041**
	FC6 (right frontocentral)	*-0.29*	*0.059*
Alpha (8-13 Hz)	*P8 (right parietal)*	*-0.39*	*0.0095***
	F4 (right frontal)	*-0.28*	*0.068*
Beta (13-28 Hz)	*P8 (right parietal)*	*-0.42*	*0.0054***
Gamma (28-46 Hz)	*P8 (right parietal)*	*-0.32*	*0.0327*
	AF4(right frontal)	*-0.33*	*0.032*

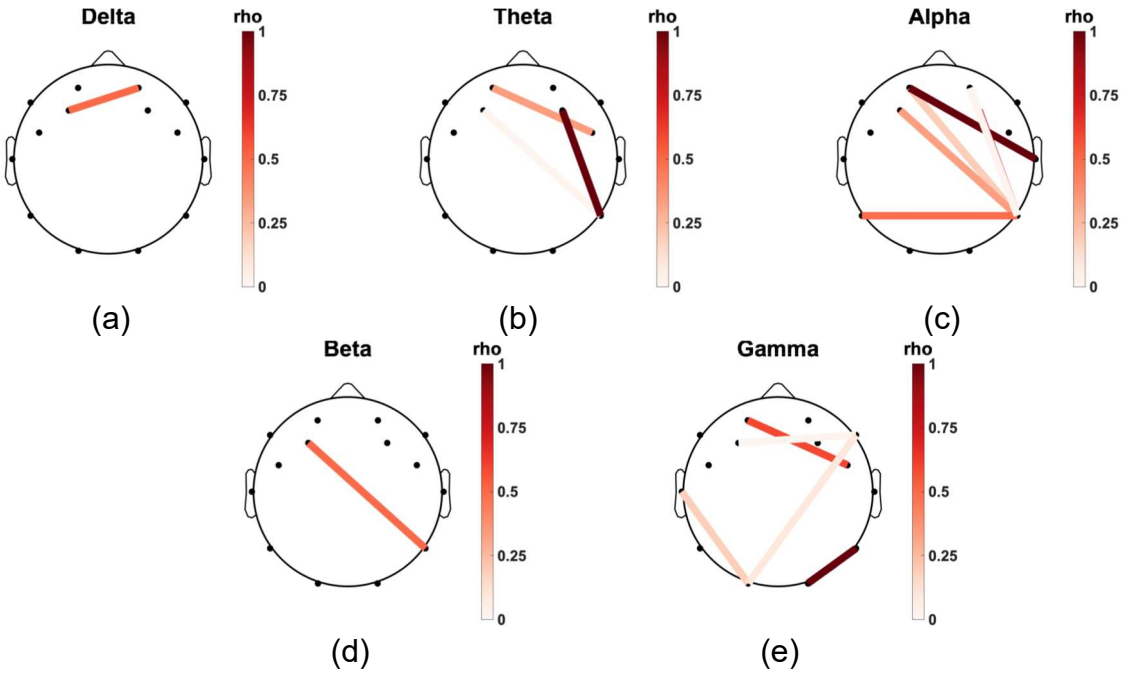


Figure 5.16. Brain connectivity graphs showing the significant correlations between paired EEG channels' magnitude-squared coherence during the eye-closed resting-state and mean reaction time in a) Delta, b) Theta, c) Alpha, d) Beta, and e) Gamma bands. The color designates the level of correlation between all paired coherence and the corresponding measure where the observed correlation was significant ($p < 0.05$).

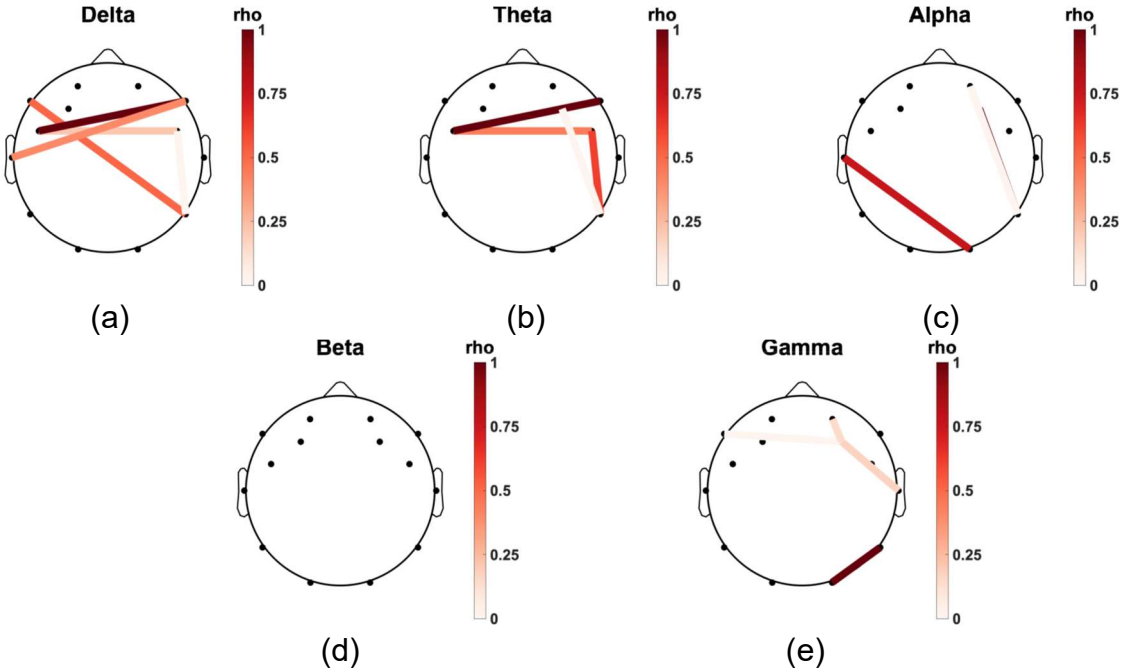


Figure 5.17. Brain connectivity graphs showing the significant correlations between paired EEG channels' magnitude-squared coherence during the eye-closed resting-state and mean accuracy score in a) Delta, b) Theta, c) Alpha, d) Beta, and e) Gamma bands. The color designates the level of correlation between all paired coherence and the corresponding measure where the observed correlation was significant ($p < 0.05$).

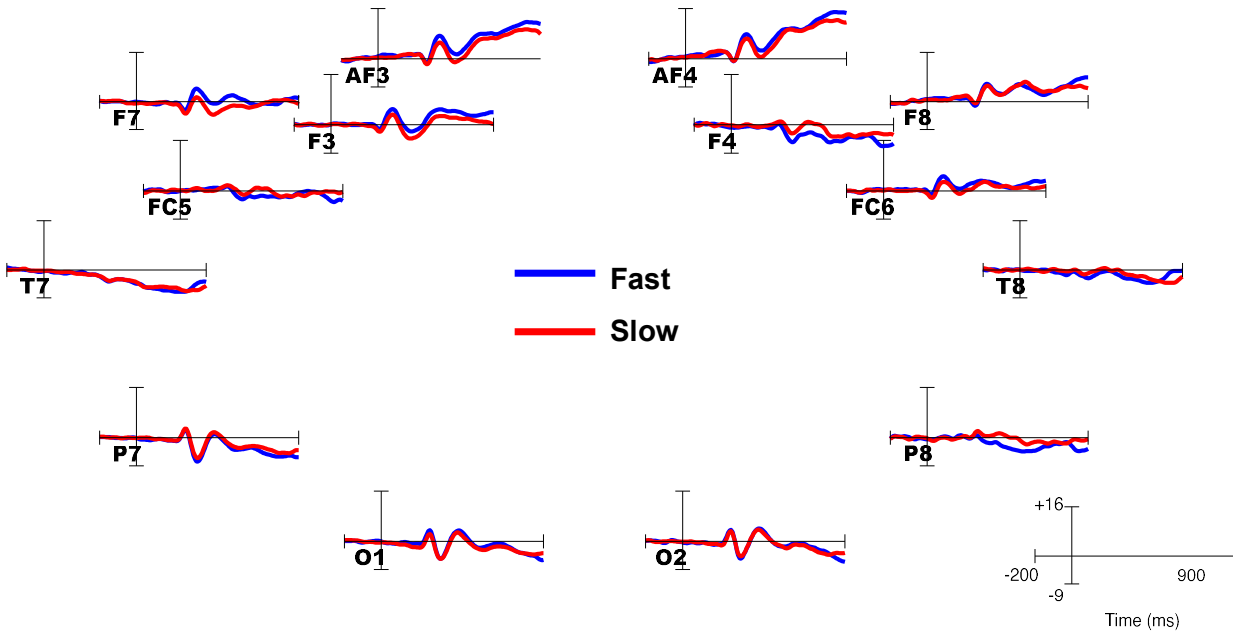


Figure 5.18. Event-related potentials of the average individualized “fast” and “slow” correct memory retrieval in all EEG electrodes

In order to find the significant differences between all EEG electrode sites in all points of time, a Wilcoxon rank sum test was performed on all EEG sites for all points of time 200 ms prior and up to 900 ms after all correct response EEG epochs. Figure 5.20-a shows the point-by-point confidence level of the Wilcoxon rank sum test on all EEG electrodes and Figure 5.20-b shows the dorsal view topographical distribution of the confidence level of the Wilcoxon rank sum test.

ERP responses showed higher late activity in Individualized stimuli for the “fast” compared to the “slow” memory retrieval. The analysis of the ERP responses showed a significant effect of retrieval speed in the P300 depicted from left frontal site, mostly from F3 EEG electrode site (see Figure 5.21). For each time point, In the early components, there was a significant main effect of retrieval speed in the P300.

Event-related spectral perturbation (ERSP) varied in the Alpha band. Figure 5.22 shows ERSP evoked responses over F3 EEG electrode site for “fast” and “slow” reactions. A significant difference in Alpha (7–13 Hz) band power was found in the early ERSP responses between “fast” and “slow” memory retrieval. A paired-bootstrap, with the False Discovery Rate (FDR) correction and a significance level of 0.02, showed a significant difference for the ERSP evoked responses of “fast” and “slow” memory retrieval between 10–15 Hz from 0 to 300 ms. A lower activity in Alpha band prior and during the early evoked response over left frontal site marked the difference in the “fast” participants’ reaction.

Also, the late evoked brain response, between 500 ms to 800 ms suggests that “fast” reactions to the target matching memory retrieval evoked higher activity in Beta band compared to “slow” reactions in the left frontal site.

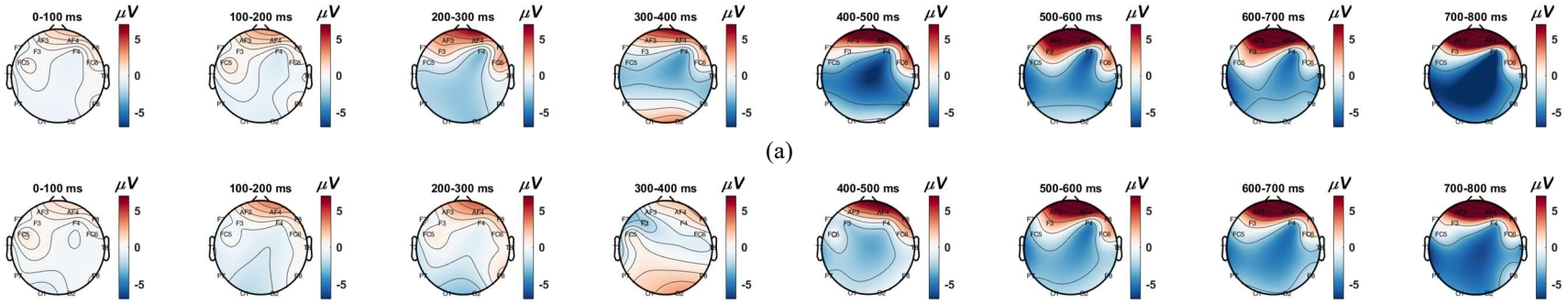
5.11 Discussions

5.11.1 Summary of the findings

To explore the clinically friendly eyes-closed rEEG and healthy older individuals’ working memory capacity, we report several new findings. First, accuracy of working memory retrievals is correlated with higher frequency brain oscillations (Gamma, Beta and Alpha) at local and distant neural circuits in the right hemisphere support. Second, slowed memory retrieval is significantly correlated with increased Delta and Theta band powers over the left parietal sites. Also, increased coherence between the right parietal site and the left frontal area is correlated with slowed speed in memory retrieval.

5.11.2 Reaction times and Delta / Theta band powers

Interestingly, we found that non-targets are always took longer time than target held in working memory (both correct and incorrect trials). We analyzed the Pearson correlation between neural oscillations in different frequency bands recorded with a wearable EEG headset during eyes-closed resting-state and the participants’ mean reaction time and mean accuracy score during a delayed visual target matching task.



(a)

(b)

Figure 5.19. Dorsal view topographical illustration of a) “fast” and b) “slow ERP responses

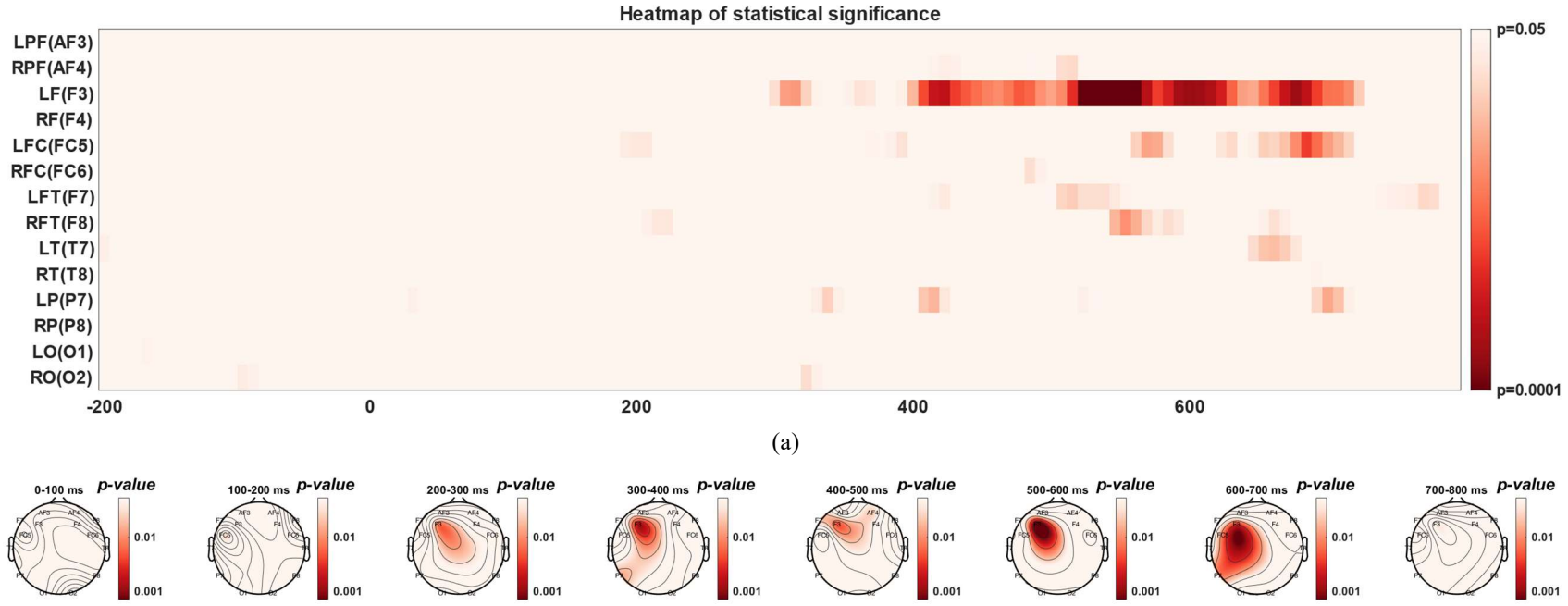


Figure 5.20. a) A point-by-point confidence level of Wilcoxon rank sum test and b) the dorsal view topographical distribution of the confidence level of Wilcoxon rank sum test

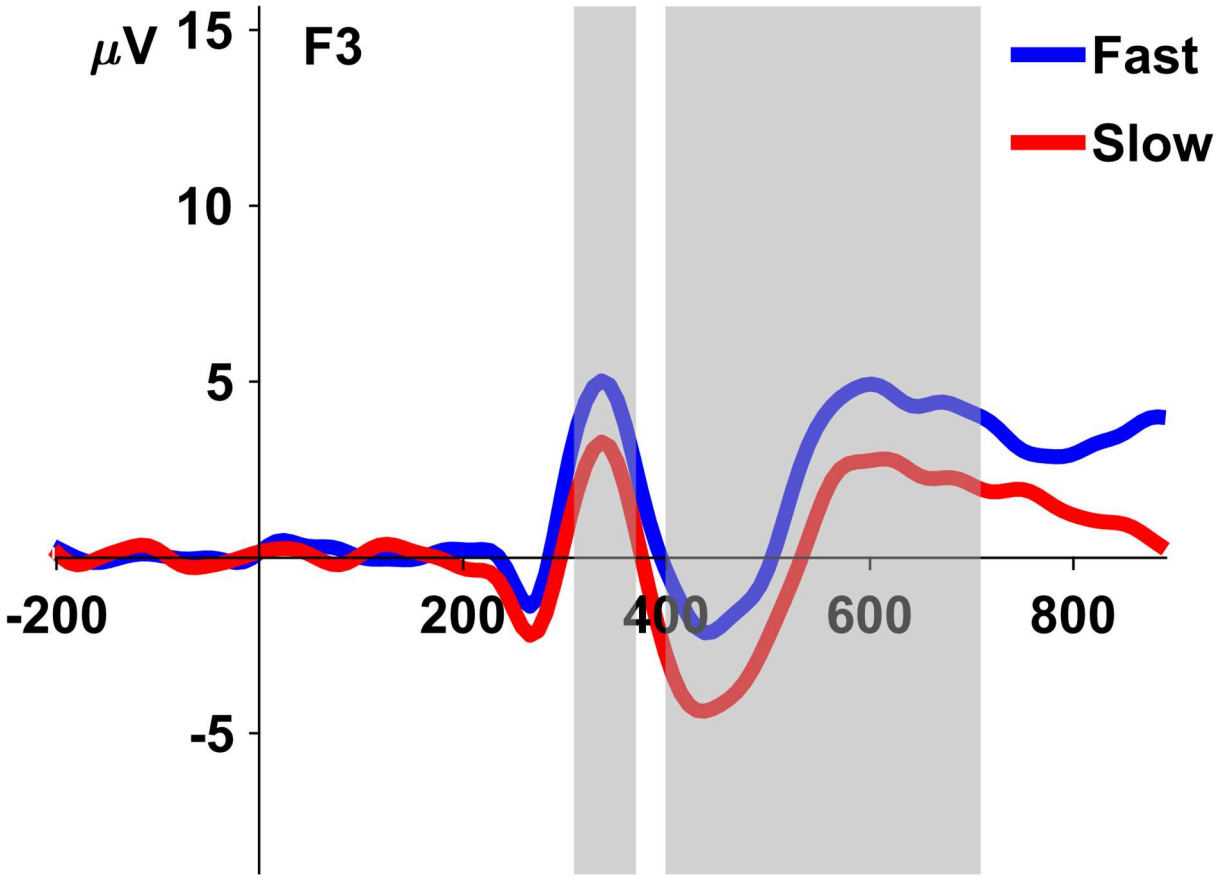
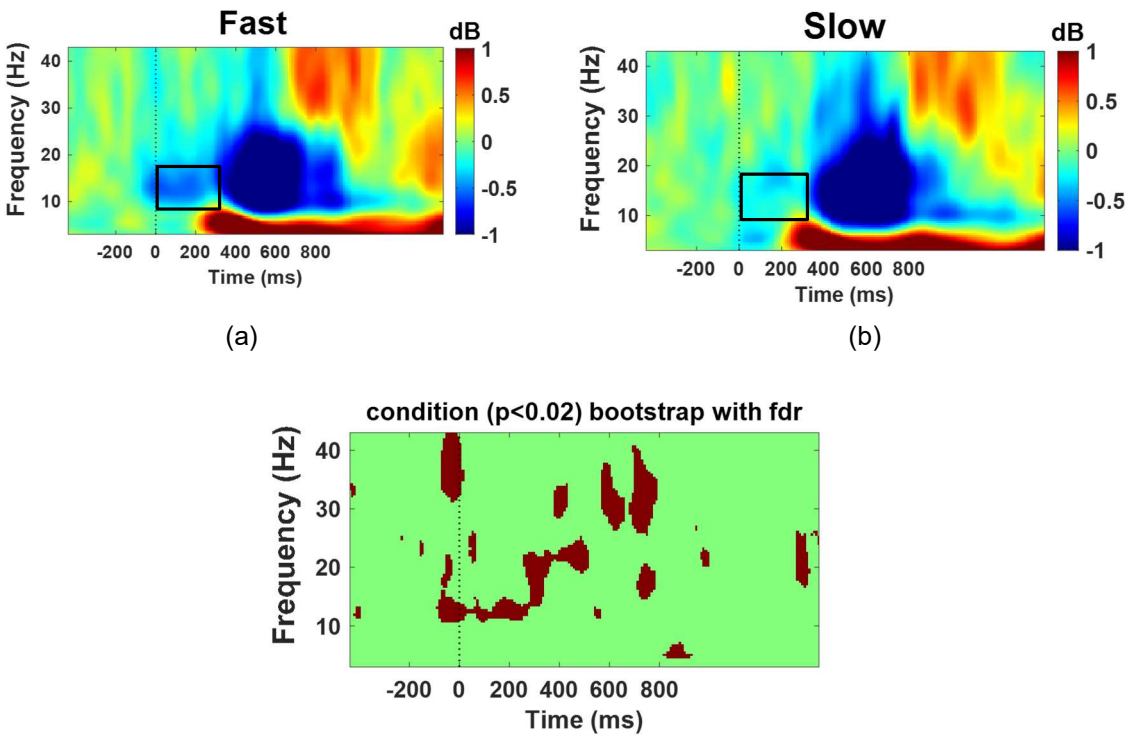


Figure 5.21. ERP response of “fast” versus “slow” in F3 EEG electrode.



(a) (b)

(c)

Figure 5.22. Event-related spectral perturbation (ERSP) response of a) “fast”, b) “slow” brain responses, and c) point-by-point time-frequency statistical significance between ERSP responses of “fast” and “slow” evoked responses with bootstrap and adjusted p-value using false discovery rate (FDR)

The results suggest that resting-state EEG in specific brain sites and specific rhythms are significantly correlated with short-term memory performance measures. We discovered that the analysis of EEG signals during resting and conscious state of mind carries a predictive utility to tell apart behavioral performance associated with short-term memory performance.
Correlative analysis between the captured EEG band powers and individuals' mean reaction time showed that a faster reaction in target matching memory task to identify among target and non-target images significantly correlates with higher Delta and Theta rhythms over left parietal sites.
We also discovered that resting-state EEG over right parietal, right frontal, and fronto-central sites carries valuable information about the mean accuracy of target recognition in the memory task. Lower brain activities in Alpha, Beta, and Gamma bands over the right parietal region correlates well with a higher accuracy score. The results suggest that resting-state EEG over the parietal can be a potential biomarker, reflecting the accuracy of memory retrieval among normal aging adults.
Our observation is consistent with the literature that higher Theta and lower Beta, which results in higher Theta/Beta ratio is an indicator of memory capacity. Heister et al. [249] studied neural associates of working memory during resting-state captured by MEG signals. They found that right frontal and parietal cortex delta/theta power were inversely correlated with three-back working memory performance. The results demonstrated that individuals with poor accuracy in three-back working memory showed larger increases in right posterior frontal and parietal delta/theta in resting-state condition. Working memory also involves attention. A new study highlighted the predictive utility of resting-state EEG and investigated neural correlates of vigilance score and response time during varying-duration sessions of sustained attention to response task (SART) [248]. The results showed that an increase in the left central and temporal gamma and upper beta during rest predicts slower reaction time.

5.11.3 Selective neural communications within working memory network via frequency oscillations and coherence

Although the nature of neural coding in mammalian brains that may support selective communication are not fully understood, it has been postulated that the structure of oscillations varies in time and space according to behavioral state. Multiplexing implemented through periodic modulation of firing-rate population codes enables flexible reconfiguration of effective connectivity [287]. Memory retrieval is a dynamic process continuously regulated by both synaptic and intrinsic neural mechanisms, e.g. intrinsic excitability, synaptic plasticity, and interactions among brain areas [288]. The results provide an understanding of selective memory performance, i.e., neural dynamics underlying accuracy are different from those underserving memory retrieval speed.

By analyzing spectral coherence between all paired EEG electrodes, we found that increased coherence in the Beta band between frontal and occipitoparietal regions is highly correlated with the participants' mean reaction time. Also, the Theta coherence between frontal and temporal regions is significantly correlated with the mean accuracy score in the target matching memory task. Literature has suggested the significance of coherence between frontal and posterior brain areas as an indicator of brain overall cognitive function. Changes in the connectivity network between different brain areas, including the frontal and parietal areas have been observed among people with MCI and AD. Babiloni et al. collected a comprehensive review of the literature [289]. It has been shown that the coherence between frontoparietal regions in the Theta band would correlate with the working memory performance-related measures on the Digit Span [290]. Fleck et al. studied resting-state EEG in search of a neuromarker of cognitive decline and they observed a positive correlation between the Delta and the Beta coherence within the frontal and posterior regions and performance on measures of memory and executive function in older adults [291].

5.11.4 Significance, limitation, and future potential

Deficits in working memory is often seen in amnestic mild cognitive impairment, an early stage of Alzheimer's disease and related dementia (ADRD). Currently, the AD biomarkers for early diagnosis of mild cognitive impairment (MCI) are expensive to measure, and demands invasive neuroimaging, laboratory examinations, and long hours of cognitive tests. Depending on the degree of change, the quantitative analysis of changes in cognitive processing may provide evidence of pathologic cognitive changes beyond age-related decline, MCI and ADRD. AD is characterized by a development of the pathological accumulation of amyloid-beta (Aβ) and hyperphosphorylated tau peptides, affecting long-range neurotransmission of the brain interconnected networks [292]. The onset of the progression can be traced back to a few years in the past. Evidence suggests that at least six years before the diagnosis of AD, memory-related pathologic changes can be identified [293]. Changes in the Aβ aggregation can be monitored with positron emission tomography with fluorodeoxyglucose and structural magnetic resonance imaging (MRI). The techniques are relatively expensive and invasive. The compromise in the synaptic neurotransmission can be spotted by loss of episodic and semantic memory [294] while impacting visuospatial attention [295] and motor reaction [296], affecting the medial temporal lobe, posterior cingulate, frontal and temporal cortex, and parietal lobe. There are pros and cons for the present rEEG approaches for gauging working memory capacity. Currently, clinicians rely on well-established but time-consuming neuropsychological testing as a proxy to identify changes in brain networks in the aging population. Different cognitive tasks such as working memory and selective attention have been used to enumerate the rate of cognitive decline measured by accuracy and

reaction time, which has been shown to provide a reliable measure of cognitive decline. Cognitive testing is less sensitive for the small changes in memory that accumulate overtime but can identify the summation of the changes when the effect is significant. However, cognitive deficiency may not be appeared and diagnosed at the onset of AD, motivating the discovery of noninvasive and inexpensive-to-collect neuromarker, i.e., a neuromarker showing altered brain connectivity across interconnected networks of the brain. The limitation of the present study is that the sample size of 43 is small, and underlying neural mechanisms need further research. Longitudinal followup of a larger healthy normal cohort are needed. Additionally, our work will need to be extended by evaluating these EEG neuromarkers in patients with amnestic MCI, or those in various dementia. Analyzing the interaction effects of age and task performance can provide a more comprehensive image of neural signatures of task performance during awake and resting condition.

Overall, using wearable and wireless EEG headset, the key resting EEG oscillations under 3 minutes indexing working memory capacity, are noninvasive, easy-to-use, and affordable pre-screening tool at doctor’s office before sophisticated biomarkers tests in various clinical populations.

6 Chapter Six: Portable Neurofeedback Intervention for Cognitive Control

This chapter covers the development of a novel EEG neurofeedback for enhancing cognitive control. An overview of the operant conditioning is described. Then, an EEG-based BCI for training short-term memory is discussed. Thereafter, the novel developed platform is explained in detail. Because of the COVID-19 pandemic, I was not able to test the efficacy of the platform with human subjects. However, the platform has been developed and will be shared to public for scientific use.

6.1 Operant conditioning

The interaction between an organism's behavior and its surrounding environment (learning) significantly changes the brain which contributes to the brain plasticity [297]. Classical Conditioning (CC) is a type of associative learning that happens as a result of making associations between two stimuli to elicit a response.

A series of experimentation in relation to the presentation of food to dogs and the amount of salivation in dogs conducted in 1927 [298] established the concept as a learning mechanism which categorized under Pavlovian learning as opposed to unconditioned responses called inborn reflexes. The behavioral model of Pavlovian learning is depicted in Figure 6.1.

Operant Conditioning (OC), also a type of associative learning, causes increasing a behavior that is reinforced and/or decreasing a behavior that is penalized. Both reinforcement and penalty events can be positive (i.e., arrival of a pleasant or unpleasant consequence) or negative (removal of something unpleasant or pleasant). The evidence of the phenomenon has been observed in human and nonhumans. For instance, the behavior of a rat pressing a lever or a pigeon pressing a key to obtain a food pellet in Skinner box are examples of operant conditioning [299]. In an study on monkeys, it has been shown that with an OC paradigm, they are able to self-regulate prefrontal cortex neurons [300].

6.2 Neurofeedback

Neurofeedback is a type of operant conditioning scheme that exploits real-time neural states of the user as input and the feedback allows "rewarding" or "penalizing" particular pattern of interest with some sort of sensory stimulation including, visual, auditory, and/or haptic feedback to modulate brain's activity [301]. The instantaneous feedback mechanism facilitates a voluntary and self-learning process for the brain pattern to change towards the pattern of interest. This adjustment includes alteration in the frequency, amplitude, or other neurophysiological signals of the participant. Although the participant may perceive the changes after a couple of neurofeedback sessions, it is suggested that the process at least to be single-blinded for the participants.

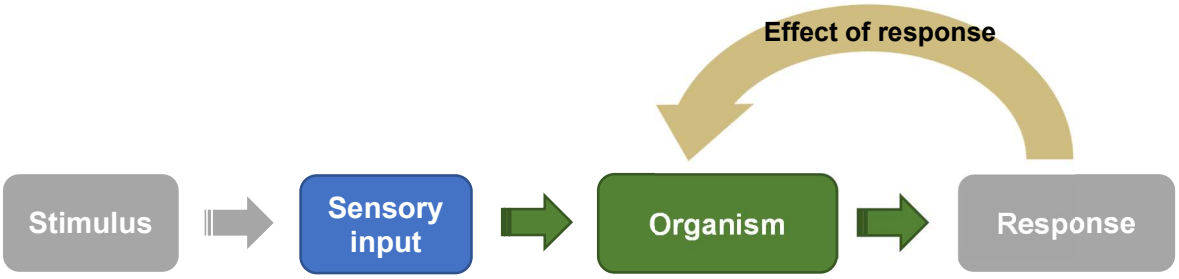


Figure 6.1. The behavioral model of learning based on operant conditioning.

6.3 How BCI can help Neurofeedback

While there is fundamental disparity between neurofeedback and BCI, combining both approaches can potentially help to expand achievements of each individual approach. For instance, the goal in motor-imagery BCIs is to control an external object by inducing and modulating the brainwaves of interest during the training session so that the BCI system can determine user's intention in real-time in testing sessions. Users need to learn how to regulate their brainwaves and it makes the BCI analogous to neurofeedback. In both, users need to learn modulating their brain activity to acquire a certain feedback, specific output, or more reward. The similarity may result in triggering similar cognitive and neural processes. In that sense, the training process of BCI may expand our knowledge in neurofeedback.

Most of the neurofeedback studies have utilized a few channels of EEG signals or a fixed and narrow range of frequencies [302, 303] while most of the BCI systems, such as motor-imagery BCIs have incorporated multiple EEG channels and individualized and adaptable range of frequencies determined by signal processing, machine learning, or deep learning approaches. Embracing those approaches in neurofeedback regiments may help to distinguish and extract individualized features from EEG signals with which we may obtain higher efficacy compared to having a fixed channels and fixed frequency approach [304].

There is also research about task-unspecific internal and external confounding variables characterized and studied in the BCI literature. For instance, the attentional state of the user has been quantified with the level of mu and gamma bands in different brain areas. The measure has helped to enumerate the level of attention and motivation in a motor-imagery BCI task [305]. Having those measures alongside the neurofeedback therapy can be beneficial to assess how likely a user is motivated to participate in a neurofeedback therapy and how one neurofeedback regiment may be adapted and accepted by the users over another one.

Type and form of feedback signal is another instrumental element in neurofeedback. We have five sense including vision, auditory, somatosensory, olfactory, and gustatory. Although vision is the most prominent sensory feedback in human compared to other primates, other sensory feedbacks may play a significant role in learning and modulating our brainwaves in response to different phenomena.

There are challenges to apply neurofeedback. One challenge is how to define the reinforcement signal. It might be easier and ethically more appropriate to define the reinforcement signal in non-human experiments. For example, withholding food from a rat and providing it later as a reward when the animal successfully modulates a neurophysiological signal may not be an ethical concern (at least now), but it would be more challenging and clearly unethical to deprive human subjects of food. Another challenge is that there is no guarantee if a human subject would interpret the feedback

as a reward. So, the motivational state of the subject results in different interpretation of the feedback signal.

Neurofeedback works with involvement of executive functions. Executive functions encompass the mental processes that allow individuals to take control over automatic responses of the brain in order to produce goal-oriented behaviors [306]. The goal-directed behaviors are strongly associated with the brain activity in prefrontal cortex [307]. The functions enable individuals complex and/or suboptimal situations. The functions comprise of planning, goal setting, decision making, voluntary attention, task switching, set shifting, behavioral and perceptual inhibitions, voluntary regulation, and error correction. In therapeutical neurofeedback, especially the ones that target cognitive control, some of the aforementioned functions seem to be fundamental to set up intrinsic reward, to integrate feedback information, and to self-regulate behavior. Most of those functions interact with attention, a broad concept that can be defined as the set of processes dealing with the allocation of working memory to the different neural representations available in the brain [308]. There are studies indicating a shared neural mechanisms that support both attention and working memory [309, 310]. The shared neural mechanisms support the theory that there is also a mutual connection between the two brain functions. Attention plays a critical role to allocate the brain resources to working memory while high-level cognition relies on working memory to learn tasks [311].

Clinical neurofeedback training have been shown to be an effective treatments for people with a wide range of deficits, including: epilepsy [312, 313], attention deficit hyperactivity disorder (ADHD) [314, 315], stroke [316], autistic spectrum disorder (ASD) [317], emotional disorders [318], and tinnitus [319]. Furthermore, neurofeedback has been evaluated as a means to enhance the cognitive control in healthy people [302, 303, 320, 321]. The quality and quantity of changes (effect size) due to the neurofeedback regiment can be enumerated with behavioral response, measured by cognitive scoring questionnaires, or demonstrated by neural measures of cognition.

6.4 Neurofeedback training for improving memory performance

Early deficits in memory related processes are the most common and earliest symptoms of Alzheimer’s disease and related dementia (ADRD). Given that there are few effective drug treatment options that may ameliorate cognitive decline, noninvasive brain training to boost memory functions in older adults is an increasingly attractive therapeutic option for the treatment of preclinical Alzheimer’s disease (AD). The proposed neurofeedback training is poised to investigate novel, state-of-art, neurofeedback methods for augmenting short-term memory function in the aging population at risk for AD. The method seeks to refine our understanding at developing specialized neurofeedback systems in memory training, and further investigate how to train the brain during memory retrieval by providing real-time, subliminal feedback on

brainwave patterns that are associated and reinforced the efficient memory retrieval. The central hypothesis is that optimal memory-related brainwave patterns can be entrained, and real-time feedback can allow maximization of brainwave patterns associated with enhanced cognitive states and improved short-term memory performance. The experiment represents the earliest attempt to develop closed loop, neural modulation of neurophysiological signals associated with short-term working memory.

Spectral correlates of short-term memory. Exciting progress has been made to improve short-term working memory using neurofeedback. EEG signals in alpha frequency band (8-12 Hz) is conventionally considered an indicator of relaxation and the de-synchronization is correlated with excitation. Feedback based on the upper alpha (10-12 Hz) frequency showed efficacy to improve short-term memory among healthy individuals [322] which make sense since lower alpha band is associated with attentional demands and upper alpha is generally associated with semantic memory. We know that upper has a crucial role in executive function processes. We also identify the role of upper alpha on inhibition, when withholding response in a motor task is required [323]. The task shows de-synchronization during the motor activity and synchronization after that. The pattern is mostly recognized in central and parietal areas [302]. Feedback on upper alpha also shows efficacy in short-term memory capacity [324]. Neurofeedback causes increase of power in upper alpha. Clark et al. [325] have identified that the frequency of the peak alpha is negatively correlated with cognitive aging, and the pattern is more discernable in frontal rather than posterior location. Figure 6.2 demonstrates the difference in neural and behavioral response in cognitively old and young adults.

Theta frequency band (4-7 Hz) is conventionally associated with arousal and drowsiness. Posterior theta is negatively correlated with low arousal and tiredness while it has also been found a close correlation between theta activity, memory encoding, memory load, and memory retrieval [326]. Frontal theta activity has also a significant role in memory consolidation during sleep [327], and synchronizes with attention demanding tasks [328]. Frontal theta has been identified as a marker of executive function and cognitive control [329, 330], and been used from training aging population [321]. It is interesting to know that the results supports the efficacy of theta training on the improvement in the speed performance in the target selection task but not necessarily on the accuracy of the selection [331].

From the conventional perspective to EEG signals we know that cognitive engagement has correlation with beta band (13-30 Hz) and the beta over theta ratio is one of the well-established neurofeedback regiments for ADHD. However, it has been few research studies investigating the significance of beta feedback training. There are few studies highlight the significance of beta training for enhanced arousal [332], recognition

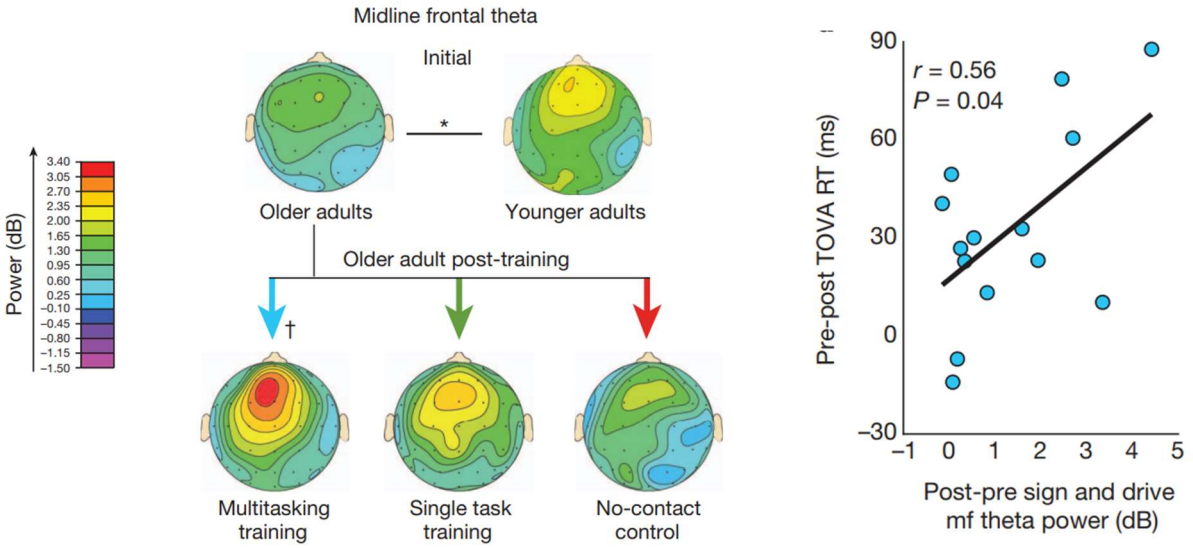
(episodic) memory [333], problem solving in a novel situation [334].

New neurofeedback Method. Traditional brain training typically applied frequency-based EEG features. Applying EEG-based neurofeedback for improving cognitive performance (see a review by [335-337]. The brain dynamics (EEG long-range temporal correlations) can be modulated with stimulation in an involuntary manner, which is an excitation-inhibition balance change achieved by the closed loop neuro-regulation [338-340]. The feedback signal is a variable delayed stimulus.

The variation of the delay is computed based on the personalized cognitive model of short-term memory extracted from the offline short-term memory evaluation, described in the previous chapter. The neurofeedback setup includes the last three consecutive response (neural plus behavioral) to determine the variation of the delay for the next stimulus which comes after that. The process is repeatedly applied on the entire series of stimuli in a neurofeedback trial. Figure 6.3 shows schematic of a sample neurofeedback trial. Previous study highlights the observation that neural response along with behavioral response carries valuable information about cognitive state, incorporating it in the closed-loop neurofeedback system may portray a more comprehensive image of a cognitive deficit. Thus, in this novel neurofeedback scheme, we try to address this insufficiency with including both neural and behavioral measures of cognitive states to improve the precision, accuracy, and efficacy of the constructed feedback signal. Since the setup is designed to be universal to the operating system, neurophysiological signals modality, and neurophysiological device manufacturer, it may also offer a potential testbed for researchers to test different other hypothesis with the cognitive control assessment.

Unfortunately, due to the COVID-19 pandemic, I was unable to collect data and evaluate the platform. However, here I provide the system architecture, and components. Further the software is open-source and will be available to the public for further research. The platform is going to be used by VA Health Care System in Lexington, Kentucky.

The online neurofeedback system provides a positive reward onto enhanced working memory-related neuromarker (e.g. rewarding higher left frontal Alpha power, and boosting frontal responses to memory targets), and provide a negative reward to the diminished neuromarker. The system incorporates the individualized analysis of “fast” and “slow” reactions, explained in the previous chapter, to promote and reinforce “desired” evoked response of the brain, associated with top memory retrieval performance (high accuracy and fast reaction times).



(a) (b)

Figure 6.2. a) The intensity of Midline Frontal Theta of cognitively young and old adults and b) the correlation between the Theta power intensity and the reaction time in short term memory task, borrowed from [341].

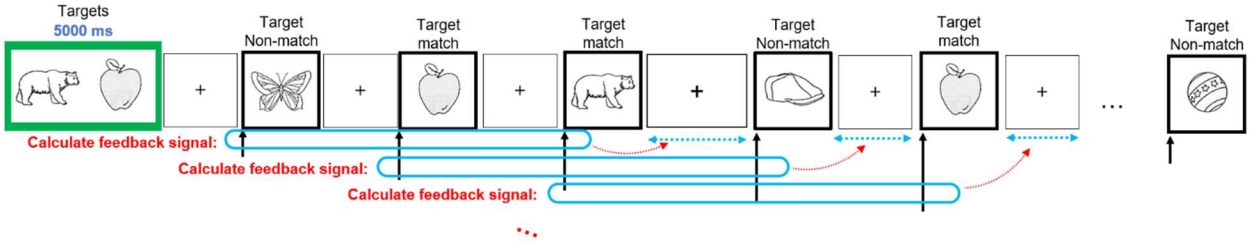


Figure 6.3. A sample short-term memory neurofeedback trial. The feedback signal will be designed based on the average neural response of the last 3 consecutive responses.

6.5 Neurofeedback software architecture

The designed neurofeedback setup is developed using Python scripting language. The setup has included several modules necessary to conduct the experiment while brings a great deal of modularity and expandability to further types of BCI experiments. Figure 6.4 shows a schematic of the neurofeedback experimental setup.
The current setup customized to handle synchronous event-driven experiments, however with little changes experimenters can run asynchronous nonevent-driven experiments as well. Figure 6.5 shows a high-level diagram of the designed neurofeedback software.

6.5.1 GUI

A simple graphical user interface (GUI) is designed to give convenience to experimenter in running the experiment. Using the GUI, experimenter can collect participant's related metadata and parameters including participant ID, age, sex, handedness, as well as the intended phase of the experiment. Experimenter can choose between practice, training, and neurofeedback experiment modes. See Figure 6.6 for details. GUI encapsulate the selected parameters in Javascript Object Notation (JSON) format to interact with the experimental designed task. See 7.5 in Appendix.

6.5.2 Signal acquisition module

Having a hardware-agnostic approach towards the neurofeedback software design, the implementation of LSL as the data communication protocol potentially allows using data acquisition from LSL-compatible devices. However, I specifically customize the setup to be compatible with Emotiv EPOC, Emotiv EPOC +, gtec Unicorn, gtec Nautilus dry and gel-based electrodes. Users can choose the EEG headset of choice from a combo box on GUI. See 7.7 in Appendix.

6.5.3 Visualizer module

An independent multithreaded software is designed and implemented in python to provide users with real-time visualization of 1) time-series 2) power spectral density (PSD), 3) time-frequency moving window of signal streams. The visualizer software allows real-time visualization of one, group of, or all EEG channels as a time-series. Also, the software can visualize PSD for a selected channel. Moreover, the visualizer can provide a real-time moving window time-frequency visualization of the selected EEG channel. The visualizer module provides a simple-to-use interface to low-pass, high-pass, or band-pass the data stream at a user-defined frequency. Once the user set the cut-off frequency of the choice, the visualizer adapts the real-time plots, accordingly. The visualizer has been uploaded and been shared for public use under GNU license. It is accessible through this link:
https://github.com/soheilbr82/lslbuffer/tree/dev

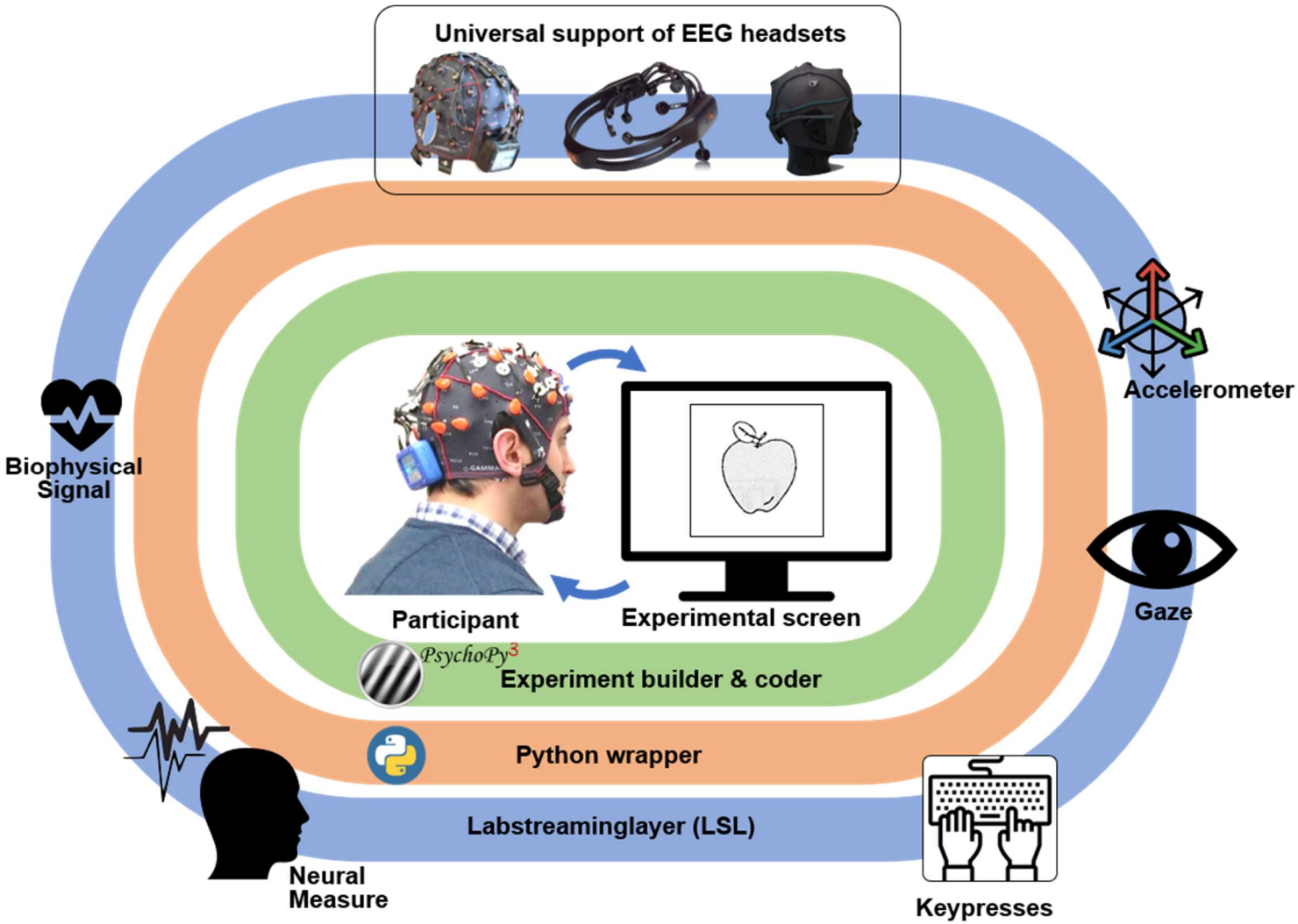


Figure 6.4. A schematic of the experimental setup.

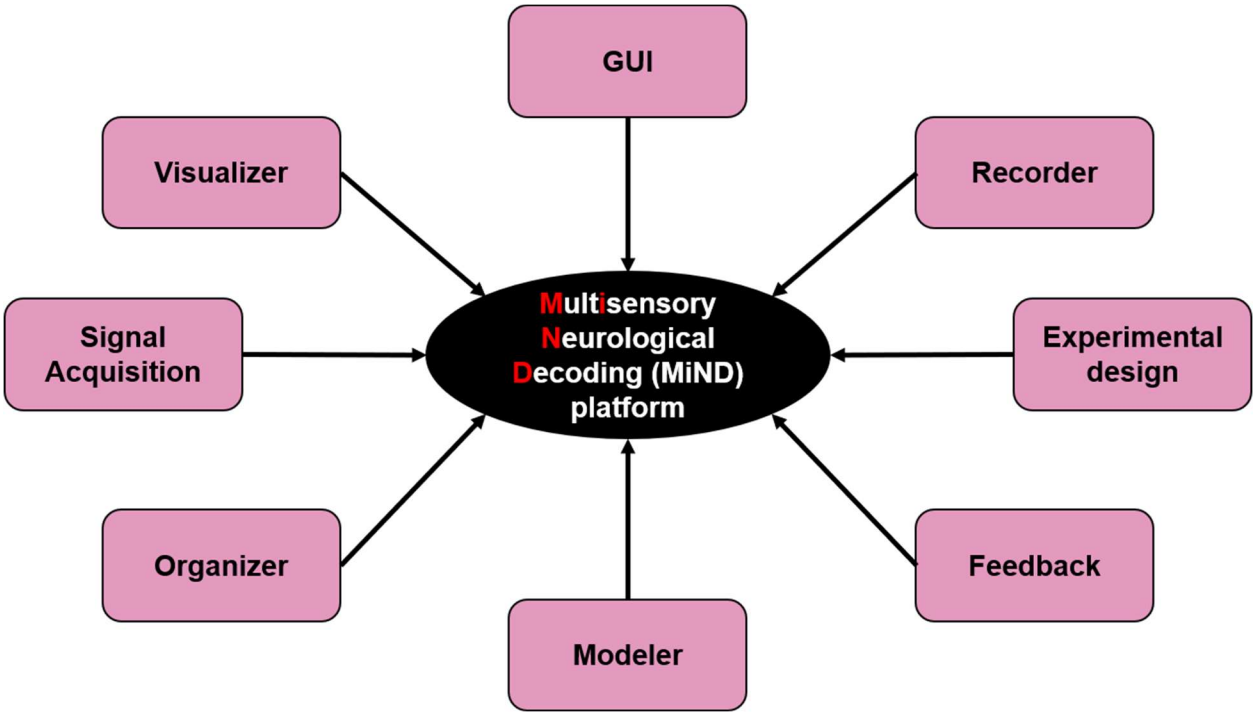


Figure 6.5. A high-level diagram of the designed neurofeedback software and the associated modules.

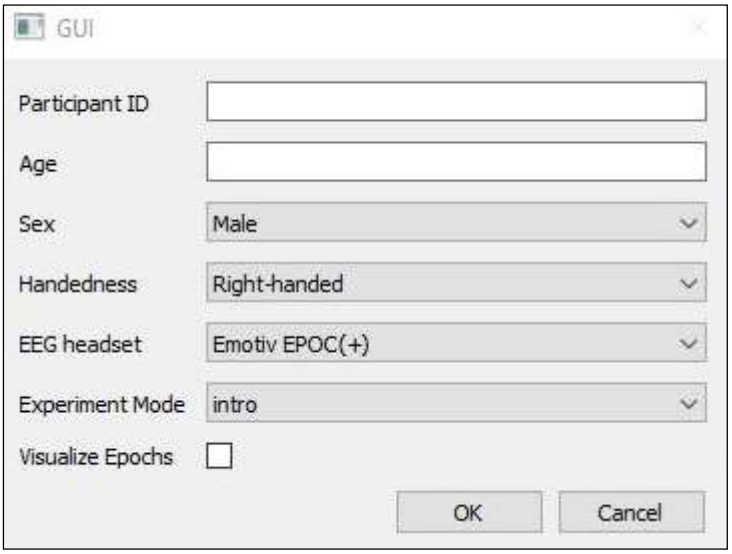


Figure 6.6. A snapshot of the designed GUI

6.5.3.1 Epoch visualizer

An epoch visualizer module is designed with PyQt and PyQtgraph python libraries. The module accepts encapsulated epochs data streams in two data classes via LSL and visualize them in a separate QtGui Window in an uninterrupted model. The current settings allow concurrent illustration of the currently received data epoch as well as past four more data epochs with varied plot transparency and line width for each target and non-target classes of data. This way, experimenter can track real-time changes in brainwaves during the experiment. See 7.6 in Appendix.

6.5.4 Recorder module

LabRecorder is used to record brainwaves EEG signals along with time-synchronized stimulus event markers generated in from the experiment script across a local wired network connection. LabRecorder saves all available data streams in a single file with .XDF file format. I automate calling the software in the background so that execution of the recorder module will not interrupt the experiment procedure. See 7.8 in Appendix.

6.5.5 Experimental design

In general, current setup of MiND platform can handle event-driven experiments. A new modified version of delayed-matched to sample task with familiar objects is designed to training and modulate working memory network of the brain in three modes:

1) “Practice” mode: It allows familiarization to the task without including the collected data into consideration. Using GUI, experimenter can navigate the experiment into the practice mode to let participants familiarize with the task. Familiarization is instrumental to the brain-computer interfaces and neurofeedback experiments. It helps to have a stable EEG recording, allows better electrode-skin conductivity, and participants become accustomed to the task.
2) “Training” mode: Once experimenter run the platform in training mode, the setup calls the experimental design script. Concurrently, the setup calls recorder module to save the neural and behavioral (key presses) data into XDF file format for further offline analysis. The experimental script displays target and non-tagret stimuli in a pseudo-random timely sequence with a fixation blank screen as inter-stimulus. The duration and clarity of the sequence of stimuli are fixed.
3) “Neurofeedback” mode: By collecting the “Training” mode data, the platform generates an individualized machine learning model of “fast” memory retrieval. The machine learning model, which is built upon Scipy/Sklearn Python library consumes epochs of real-time EEG signals as input and identify the patterns of brainwaves associated with the target individualized “fast” memory retrieval.

7 Chapter Seven: Conclusions and future works

7.1 Noninvasive assistive BCI

We implemented and assessed the user experience on a common assistive BCI, imagined body kinematics using computer cursor control. We could identify a motor learning pattern, even with a wearable EEG headset. The pattern shows a higher activity on the early trials in the lower frequency bands mostly Delta and Theta. The activity faded away in the next trials on the Delta and Theta band and brainwave activity shifted towards Alpha band. This shift in the brainwave pattern can be explained by a motor learning effect, reported previously in the literature. Recently, a study in invasive domain using electrocorticogram (ECoG) signals presented a plug-and-play approach to minimize the training protocol using an adaptive closed-loop decoder. Some of these approaches can be borrowed and be repurposed for noninvasive domain. The relatively lower risk on the potential users of the technology plus the advent of the internet of things (IoT) technology are some of the near future driver technologies for embracing noninvasive neurotechnologies for daily use. At that time, providing a plug-and-play noninvasive assistive BCI would be necessary. Thus, the improvement of the neural decoder to enhance the user experience would be essential.

7.2 Investigating brainwave biomarkers for cognitive decline

In this dissertation, I investigated potential biomarker of visual selective attention to faces and scenes in occlusion free and occluded conditions. Also, in another study of short-term memory, I explored for noninvasive surrogates of working memory performance including accuracy score and reaction time. Stratification of the EEG response and analyzing temporal and spectral features of EEG over the entire scalp showed a distinctive early evoked response for “fast” versus “slow” reactions in a target matching memory task. The study has potential to expand for different age groups including young normal adults, old normal adults, people with mild cognitive impairment, and people with Alzheimer’s disease. The quantification, enumeration, and stratification of brain response in a more comprehensive clinical trial while correlating them with other brain imaging data and cognitive assessment questionnaires, though expensive to run, can give the scientific community a more comprehensive clue to recognize novel biomarkers to diagnose different cognitive disease at early stage.

7.3 Closed-loop neurotechnologies for targeted treatments

I studied visual selective attention and working memory using EEG-based noninvasive BCI. The works analyzed and extracted EEG correlates of the behavioral responses in various conditions. Also, I tracked the correlations between task non-specific resting-state and the performance indicators of the participants in a short-term memory task. The analysis reveals a significant brainwave pattern among the population, showing the predictive utility of the resting-state captured by EEG signals. I expanded the work to

propose the utility of a real-time closed loop noninvasive neuromodulation technique, known as neurofeedback to alter the brain mechanisms associated with short-term memory retrieval. I designed a novel noninvasive closed-loop neurofeedback paradigm for evaluation and enhancement of working memory. Having implemented a vendor-agnostic and open-source design, the software embeds Lab Streaming Layer (LSL) to access real-time biosignals and Python Tensorflow/Sklearn libraries to model, analyze, and encode the feedback response to target working memory. The work has potential to expand in different perspectives. First, including multimodal neurophysiological signals besides EEG signals likely to provide more comprehensive information about our brain and the behavior. So far, hybrid BCI systems such as EEG-NIRS have shown more efficiency in understanding our brain mechanisms. The work can be expanded by including galvanic skin response (GSR), eye-tracking, heart rate, and NIRS. Each signal modality may provide information that other modalities may not be able to attain. Also, the feedback mechanism can be enhanced and amplified to give a more immersive experience and potentially faster treatment. Instead of using varied visual elements as the feedback of the current state of the brain, a curated, trimmed, timely synchronous audiovisual and vibrotactile feedback, if mounted in a virtual reality headset has potential to target and manipulate different neural circuits, and treat the corresponding neural circuit dysfunctions. Furthermore, the concurrent application of noninvasive brain imaging (EEG/NIRS) and brain stimulation (tDCS/tES) is an active research field. On the one hand, the advances in the computational power and machine learning, and on the other hand, the progress on making the neurotechnologies more portable and wearable brings about a promising future to implement and study concurrent brain imaging and stimulation with a higher temporal and spatial resolution.

7.4 Embodied cognition: Applying multisensory BCI to human-robot interaction

Embodied cognition entails the connection of the mind and the body to an extent that the mind is not only connected to the body, but the body influences the mind. It means that our perception and cognition is not confined to our central nervous system or peripheral nervous system, but our perception and cognition is also influenced by our experiences. This is a relatively new approach in cognitive science. Recent developments in BCI have made the connection between human and machine possible. While BCI translates human intention and the associated brain activity into control commands. This translation of human intention would not necessarily involve neuromuscular system, a natural output of the central nervous system. As machines and robots are moving from fiction to our reality of life, the sophisticated and unorthodox human-robot interaction would be an inseparable part of our lives. Social robots are becoming new norm, and human’s perception, cognition, and communication with the artificial agents in the form of robots are being concerned. So far, video, audio, speech,

and tactile have been the common interfaces between human and artificial agents. However, the potential of using BCI as an emerging communication and information pathway between humans and robots has been studied. BCIs can provide an alternative communication channel, with direct access to physiological changes in the brain. The use of BCI in the human-robot interaction as an alternative medium provide an opportunity to research embodied cognition by manipulating the behavior of the artificial agent. Also, BCI specifies a communication channel for people with different disabilities, made them benefit from human-robot interaction through the BCI channel. Furthermore, the conventional BCI designed to be state and context specific. For instance, an assistive BCI for moving a wheelchair is designed to map user's intention of movement to different directions into the movement of the wheelchair. If user intend to switch to another task, e.g. typing a sentence, the current BCI system is not intelligent enough to determine automatically switch to a new task. Putting the artificial intelligent system in the loop of BCI allows a mutual learning between two systems help in both ways. It makes the BCI system robust and flexible while making the artificial intelligent agent being cognizant and aware of human cognitive state through this very alternative communication channel. The situational awareness achieved through concurrent human-robot interaction and brain-computer interface can reinforce and complement each other and promotes human-robot teaming.

Bibliography

[1] M. Fotuhi, D. Do, and C. Jack, "Modifiable factors that alter the size of the hippocampus with ageing," *Nature Reviews Neurology,* vol. 8, no. 4, p. 189, 2012.

[2] S. C. Cramer *et al.*, "Harnessing neuroplasticity for clinical applications," vol. 134, no. 6, pp. 1591-1609, 2011.

[3] J. Wolpaw and E. W. Wolpaw, *Brain-computer interfaces: principles and practice*. OUP USA, 2012.

[4] J. R. Wolpaw *et al.*, "Brain-computer interface technology: a review of the first international meeting," *IEEE transactions on rehabilitation engineering,* vol. 8, no. 2, pp. 164-173, 2000.

[5] M. A. Lebedev *et al.*, "Future developments in brain-machine interface research," vol. 66, pp. 25-32, 2011.

[6] United Nations. "Ageing." http://www.un.org/en/sections/issues-depth/ageing/ (accessed 4 Mar, 2019).

[7] J. C. McVay, M. E. Meier, D. R. Touron, and M. J. J. A. p. Kane, "Aging ebbs the flow of thought: Adult age differences in mind wandering, executive control, and self-evaluation," vol. 142, no. 1, pp. 136-147, 2013.

[8] J. D. Jackson, D. A. J. P. Balota, and aging, "Mind-wandering in younger and older adults: Converging evidence from the sustained attention to response task and reading for comprehension," vol. 27, no. 1, p. 106, 2012.

[9] D. A. Ziegler, O. Piguet, D. H. Salat, K. Prince, E. Connally, and S. J. N. o. a. Corkin, "Cognition in healthy aging is related to regional white matter integrity, but not cortical thickness," vol. 31, no. 11, pp. 1912-1926, 2010.

[10] A. Gazzaley and M. D'esposito, "Top-down modulation and normal aging," *Annals of the New York Academy of Sciences,* vol. 1097, no. 1, pp. 67-83, 2007.

[11] T. S. Braver and D. M. Barch, "A theory of cognitive control, aging cognition, and neuromodulation," *Neuroscience Biobehavioral Reviews,* vol. 26, no. 7, pp. 809-817, 2002.

[12] K. M. Langa and D. A. Levine, "The diagnosis and management of mild cognitive impairment: a clinical review," *Jama,* vol. 312, no. 23, pp. 2551-2561, 2014.

[13] R. F. Zec and N. R. Burkett, "Non-pharmacological and pharmacological treatment of the cognitive and behavioral symptoms of Alzheimer disease," *NeuroRehabilitation,* vol. 23, no. 5, pp. 425-438, 2008.

[14] P. B. Behere, A. Das, and A. P. Behere, "Drugs Used in Dementia," in *Clinical Psychopharmacology*: Springer, 2019, pp. 141-150.

[15] S. M. Dyer, S. L. Harrison, K. Laver, C. Whitehead, and M. J. I. p. Crotty, "An overview of systematic reviews of pharmacological and non-pharmacological interventions for the treatment of behavioral and psychological symptoms of dementia," vol. 30, no. 3, pp. 295-309, 2018.

[16] J. L. Cummings, T. Morstorf, and K. Zhong, "Alzheimer's disease drug-development pipeline: few candidates, frequent failures," *Alzheimer's research & therapy,* vol. 6, no. 4, p. 37, 2014.

[17] C. T. Liverman, K. Yaffe, and D. G. Blazer, *Cognitive aging: Progress in understanding and opportunities for action*. National Academies Press, 2015.

[18] S. Musallam, R. A. Andersen, B. D. Corneil, B. Greger, and H. Scherberger, "Cognitive control signals for neural prosthetics," ed: Google Patents, 2010.
[19] K. Jerbi, S. Freyermuth, L. Minotti, P. Kahane, A. Berthoz, and J. P. Lachaux, "Watching brain TV and playing brain ball: Exploring novel BCI strategies using real-time analysis of human intracranial data," *International review of neurobiology,* vol. 86, pp. 159-168, 2009.
[20] M. Van Gerven and O. Jensen, "Attention modulations of posterior alpha as a control signal for two-dimensional brain–computer interfaces," *Journal of neuroscience methods,* vol. 179, no. 1, pp. 78-84, 2009.
[21] M. S. Treder, A. Bahramisharif, N. M. Schmidt, M. A. Van Gerven, and B. Blankertz, "Brain-computer interfacing using modulations of alpha activity induced by covert shifts of attention," *Journal of neuroengineering Rehabilitation Engineering, IEEE Transactions on,* vol. 8, no. 1, p. 24, 2011.
[22] H. Morioka *et al.*, "Decoding spatial attention by using cortical currents estimated from electroencephalography with near-infrared spectroscopy prior information," *Neuroimage,* vol. 90, pp. 128-139, 2014.
[23] P. Andersson, N. F. Ramsey, M. Raemaekers, M. A. Viergever, and J. P. Pluim, "Real-time decoding of the direction of covert visuospatial attention," *Journal of neural engineering,* vol. 9, no. 4, p. 045004, 2012.
[24] E. L. Altschuler *et al.*, "Rehabilitation of hemiparesis after stroke with a mirror," *The Lancet,* vol. 353, no. 9169, pp. 2035-2036, 1999.
[25] G. Yavuzer *et al.*, "Mirror therapy improves hand function in subacute stroke: a randomized controlled trial," *Archives of physical medicine Rehabilitation Engineering, IEEE Transactions on,* vol. 89, no. 3, pp. 393-398, 2008.
[26] J. R. Wolpaw, "Brain–computer interfaces as new brain output pathways," *The Journal of physiology,* vol. 579, no. 3, pp. 613-619, 2007.
[27] J. R. Wolpaw, N. Birbaumer, D. J. McFarland, G. Pfurtscheller, and T. M. Vaughan, "Brain–computer interfaces for communication and control," *Clinical neurophysiology,* vol. 113, no. 6, pp. 767-791, 2002.
[28] J. R. Wolpaw, N. Birbaumer, D. J. McFarland, G. Pfurtscheller, and T. M. Vaughan, "Brain-computer interfaces for communication and control," (in eng), *Clinical neurophysiology,* vol. 113, no. 6, pp. 767-91, Jun 2002.
[29] National Institute of Mental Health. "MEG scanner with patient." https://images.nimh.nih.gov/public_il/image_details.cfm?id=80 (accessed.
[30] L. F. Nicolas-Alonso and J. Gomez-Gil, "Brain computer interfaces, a review," *Sensors,* vol. 12, no. 2, pp. 1211-1279, 2012.
[31] L. Bi, X.-A. Fan, and Y. Liu, "EEG-based brain-controlled mobile robots: a survey," *Human-Machine Systems, IEEE Transactions on,* vol. 43, no. 2, pp. 161-176, 2013.
[32] N. Birbaumer *et al.*, "A spelling device for the paralysed," *Nature,* vol. 398, no. 6725, pp. 297-298, 1999.
[33] J. Meng, S. Zhang, A. Bekyo, J. Olsoe, B. Baxter, and B. He, "Noninvasive electroencephalogram based control of a robotic arm for reach and grasp tasks," *Scientific Reports,* vol. 6, p. 38565, 2016.

[34] T. Mulder, "Motor imagery and action observation: cognitive tools for rehabilitation," *Journal of neural transmission,* vol. 114, no. 10, pp. 1265-1278, 2007.
[35] G. Pfurtscheller and C. Neuper, "Motor imagery activates primary sensorimotor area in humans," *Neuroscience letters,* vol. 239, no. 2, pp. 65-68, 1997.
[36] H. Yuan and B. He, "Brain-Computer Interfaces Using Sensorimotor Rhythms: Current State and Future Perspectives," 2014.
[37] B. He, B. Baxter, B. J. Edelman, C. C. Cline, and W. Y. Wenjing, "Noninvasive brain-computer interfaces based on sensorimotor rhythms," *Proceedings of the IEEE,* vol. 103, no. 6, pp. 907-925, 2015.
[38] V. Morash, O. Bai, S. Furlani, P. Lin, and M. Hallett, "Classifying EEG signals preceding right hand, left hand, tongue, and right foot movements and motor imageries," *Clinical neurophysiology,* vol. 119, no. 11, pp. 2570-2578, 2008.
[39] G. Pfurtscheller and F. L. Da Silva, "Event-related EEG/MEG synchronization and desynchronization: basic principles," *Clinical neurophysiology,* vol. 110, no. 11, pp. 1842-1857, 1999.
[40] J. R. Wolpaw, D. J. McFarland, G. W. Neat, and C. A. Forneris, "An EEG-based brain-computer interface for cursor control," *Electroencephalography and Clinical Neurophysiology,* vol. 78, no. 3, pp. 252-259, 3// 1991, doi: http://dx.doi.org/10.1016/0013-4694(91)90040-B.
[41] J. R. Wolpaw and D. J. McFarland, "Multichannel EEG-based brain-computer communication," *Electroencephalography and Clinical Neurophysiology,* vol. 90, no. 6, pp. 444-449, 6// 1994, doi: http://dx.doi.org/10.1016/0013-4694(94)90135-X.
[42] J. R. Wolpaw and D. J. McFarland, "Control of a two-dimensional movement signal by a noninvasive brain-computer interface in humans," *Proceedings of the National Academy of Sciences of the United States of America,* vol. 101, no. 51, pp. 17849-17854, 2004.
[43] D. J. McFarland, W. A. Sarnacki, and J. R. Wolpaw, "Electroencephalographic (EEG) control of three-dimensional movement," (in eng), *Journal of neural engineering,* vol. 7, no. 3, p. 036007, Jun 2010, doi: 10.1088/1741-2560/7/3/036007.
[44] C. Guger, W. Harkam, C. Hertnaes, and G. Pfurtscheller, "Prosthetic control by an EEG-based brain-computer interface (BCI)," in *Proc. aaate 5th european conference for the advancement of assistive technology*, 1999, pp. 3-6.
[45] G. Pfurtscheller, G. R. Müller, J. Pfurtscheller, H. J. Gerner, and R. Rupp, "'Thought' – control of functional electrical stimulation to restore hand grasp in a patient with tetraplegia," *Neuroscience letters,* vol. 351, no. 1, pp. 33-36, 11/6/ 2003, doi: http://dx.doi.org/10.1016/S0304-3940(03)00947-9.
[46] G. R. Muller-Putz, R. Scherer, G. Pfurtscheller, and R. Rupp, "EEG-based neuroprosthesis control: a step towards clinical practice," (in eng), *Neuroscience letters,* vol. 382, no. 1-2, pp. 169-74, Jul 1-8 2005, doi: 10.1016/j.neulet.2005.03.021.
[47] L. R. Hochberg *et al.*, "Neuronal ensemble control of prosthetic devices by a human with tetraplegia," *Nature,* vol. 442, no. 7099, pp. 164-171, 2006.

[48] S.-P. Kim, J. D. Simeral, L. R. Hochberg, J. P. Donoghue, and M. J. Black, "Neural control of computer cursor velocity by decoding motor cortical spiking activity in humans with tetraplegia," *Journal of neural engineering,* vol. 5, no. 4, p. 455, 2008.
[49] T. J. Bradberry, R. J. Gentili, and J. L. Contreras-Vidal, "Fast attainment of computer cursor control with noninvasively acquired brain signals," *Journal of neural engineering,* vol. 8, no. 3, p. 036010, 2011.
[50] P. Ofner and G. R. Müller-Putz, "EEG-Based Classification of Imagined Arm Trajectories," in *Replace, Repair, Restore, Relieve–Bridging Clinical and Engineering Solutions in Neurorehabilitation*: Springer, 2014, pp. 611-620.
[51] J.-H. Kim, F. Biessmann, and S.-W. Lee, "Decoding Three-Dimensional Trajectory of Executed and Imagined Arm Movements from Electroencephalogram Signals," 2014.
[52] R. Abiri, G. Heise, F. Schwartz, and X. Zhao, "EEG-based control of a unidimensional computer cursor using imagined body kinematics," in *Biomedical Engineering Society Annual Meeting (BMES 2015)*, 2015.
[53] R. Abiri, X. Zhao, G. Heise, Y. Jiang, and F. Abiri, "Brain computer interface for gesture control of a social robot: An offline study," in *Electrical Engineering (ICEE), 2017 Iranian Conference on*, 2017: IEEE, pp. 113-117.
[54] R. Abiri, S. Borhani, X. Zhao, and Y. Jiang, "Real-time brain machine interaction via social robot gesture control," in *ASME 2017 Dynamic Systems and Control Conference*, 2017: American Society of Mechanical Engineers, pp. V001T37A002-V001T37A002.
[55] R. Abiri, j. Kilmarx, S. Borhani, X. Zhao, and Y. Jiang, "A Brain-Machine Interface for a Sequence Movement Control of a Robotic Arm," in *Society for Neuroscience (SfN 2017)*, 2017.
[56] K. LaFleur, K. Cassady, A. Doud, K. Shades, E. Rogin, and B. He, "Quadcopter control in three-dimensional space using a noninvasive motor imagery-based brain–computer interface," *Journal of neural engineering,* vol. 10, no. 4, p. 046003, 2013.
[57] Y. Gu, D. Farina, A. R. Murguialday, K. Dremstrup, P. Montoya, and N. Birbaumer, "Offline identification of imagined speed of wrist movements in paralyzed ALS patients from single-trial EEG," (in English), *Frontiers in Neuroscience,* Original Research vol. 3, 2009-August-10 2009, doi: 10.3389/neuro.20.003.2009.
[58] L. A. Farwell and E. Donchin, "Talking off the top of your head: toward a mental prosthesis utilizing event-related brain potentials," *Electroencephalography and clinical Neurophysiology,* vol. 70, no. 6, pp. 510-523, 1988.
[59] R. Fazel-Rezai, B. Z. Allison, C. Guger, E. W. Sellers, S. C. Kleih, and A. Kübler, "P300 brain computer interface: current challenges and emerging trends," *Frontiers in neuroengineering,* vol. 5, 2012.
[60] L. M. McCane *et al.*, "Brain-computer interface (BCI) evaluation in people with amyotrophic lateral sclerosis," *Amyotrophic Lateral Sclerosis and Frontotemporal Degeneration,* vol. 15, no. 3-4, pp. 207-215, 2014.

[61] E. Donchin, K. M. Spencer, and R. Wijesinghe, "The mental prosthesis: assessing the speed of a P300-based brain-computer interface," *Rehabilitation Engineering, IEEE Transactions on,* vol. 8, no. 2, pp. 174-179, 2000.
[62] P. Cipresso *et al.*, "The use of P300-based BCIs in amyotrophic lateral sclerosis: from augmentative and alternative communication to cognitive assessment," *Brain and behavior,* vol. 2, no. 4, pp. 479-498, 2012.
[63] F. Nijboer *et al.*, "A P300-based brain–computer interface for people with amyotrophic lateral sclerosis," *Clinical neurophysiology,* vol. 119, no. 8, pp. 1909-1916, 2008.
[64] E. W. Sellers, T. M. Vaughan, and J. R. Wolpaw, "A brain-computer interface for long-term independent home use," *Amyotrophic lateral sclerosis,* vol. 11, no. 5, pp. 449-455, 2010.
[65] E. W. Sellers, D. B. Ryan, and C. K. Hauser, "Noninvasive brain-computer interface enables communication after brainstem stroke," *Science translational medicine,* vol. 6, no. 257, pp. 257re7-257re7, 2014.
[66] E. A. Aydın, Ö. F. Bay, and İ. Güler, "Implementation of an Embedded Web Server Application for Wireless Control of Brain Computer Interface Based Home Environments," *Journal of medical systems,* vol. 40, no. 1, pp. 1-10, 2016.
[67] C. J. Bell, P. Shenoy, R. Chalodhorn, and R. P. Rao, "Control of a humanoid robot by a noninvasive brain–computer interface in humans," *Journal of neural engineering,* vol. 5, no. 2, p. 214, 2008.
[68] I. Iturrate, J. M. Antelis, A. Kubler, and J. Minguez, "A noninvasive brain-actuated wheelchair based on a P300 neurophysiological protocol and automated navigation," *IEEE Transactions on Robotics,* vol. 25, no. 3, pp. 614-627, 2009.
[69] S. He *et al.*, "A P300-Based Threshold-Free Brain Switch and Its Application in Wheelchair Control," *IEEE Transactions on Neural Systems and Rehabilitation Engineering,* vol. 25, no. 6, pp. 715-725, 2017.
[70] L. Citi, R. Poli, C. Cinel, and F. Sepulveda, "P300-based BCI mouse with genetically-optimized analogue control," *IEEE transactions on neural systems and rehabilitation engineering,* vol. 16, no. 1, pp. 51-61, 2008.
[71] C. S. Herrmann, "Human EEG responses to 1–100 Hz flicker: resonance phenomena in visual cortex and their potential correlation to cognitive phenomena," *Experimental brain research,* vol. 137, no. 3-4, pp. 346-353, 2001.
[72] M. H. Chang, H. J. Baek, S. M. Lee, and K. S. Park, "An amplitude-modulated visual stimulation for reducing eye fatigue in SSVEP-based brain–computer interfaces," *Clinical Neurophysiology,* vol. 125, no. 7, pp. 1380-1391, 2014.
[73] G. G. Molina and V. Mihajlovic, "Spatial filters to detect steady-state visual evoked potentials elicited by high frequency stimulation: BCI application," *Biomedizinische Technik/Biomedical Engineering,* vol. 55, no. 3, pp. 173-182, 2010.
[74] S. M. T. Müller, P. F. Diez, T. F. Bastos-Filho, M. Sarcinelli-Filho, V. Mut, and E. Laciar, "SSVEP-BCI implementation for 37–40 Hz frequency range," in *Engineering in Medicine and Biology Society, EMBC, 2011 Annual International Conference of the IEEE*, 2011: IEEE, pp. 6352-6355.
[75] I. Volosyak, D. Valbuena, T. Luth, T. Malechka, and A. Graser, "BCI demographics II: How many (and what kinds of) people can use a high-frequency

SSVEP BCI?," *IEEE Transactions on Neural Systems and Rehabilitation Engineering,* vol. 19, no. 3, pp. 232-239, 2011.
[76] B.-K. Min, S. Dähne, M.-H. Ahn, Y.-K. Noh, and K.-R. Müller, "Decoding of top-down cognitive processing for SSVEP-controlled BMI," *Scientific Reports,* vol. 6, 2016.
[77] G. R. Muller-Putz, R. Scherer, C. Neuper, and G. Pfurtscheller, "Steady-state somatosensory evoked potentials: suitable brain signals for brain-computer interfaces?," *IEEE transactions on neural systems and rehabilitation engineering,* vol. 14, no. 1, pp. 30-37, 2006.
[78] C. Pokorny, C. Breitwieser, and G. R. Müller-Putz, "The role of transient target stimuli in a steady-state somatosensory evoked potential-based brain–computer interface setup," *Frontiers in neuroscience,* vol. 10, p. 152, 2016.
[79] R. Chavarriaga, A. Sobolewski, and J. d. R. Millán, "Errare machinale est: the use of error-related potentials in brain-machine interfaces," *Using Neurophysiological Signals that Reflect Cognitive or Affective State,* p. 53, 2015.
[80] P. W. Ferrez and J. d. R. Millán, "Error-related EEG potentials generated during simulated brain–computer interaction," *IEEE transactions on biomedical engineering,* vol. 55, no. 3, pp. 923-929, 2008.
[81] R. Chavarriaga and J. d. R. Millán, "Learning from EEG error-related potentials in noninvasive brain-computer interfaces," *IEEE transactions on neural systems and rehabilitation engineering,* vol. 18, no. 4, pp. 381-388, 2010.
[82] J. Wright, V. G. Macefield, A. van Schaik, and J. C. Tapson, "A Review of Control Strategies in Closed-Loop Neuroprosthetic Systems," *Frontiers in Neuroscience,* vol. 10, 2016.
[83] X. Artusi, I. K. Niazi, M.-F. Lucas, and D. Farina, "Performance of a simulated adaptive BCI based on experimental classification of movement-related and error potentials," *IEEE Journal on Emerging and Selected Topics in Circuits and Systems,* vol. 1, no. 4, pp. 480-488, 2011.
[84] I. Iturrate, L. Montesano, and J. Minguez, "Shared-control brain-computer interface for a two dimensional reaching task using EEG error-related potentials," in *2013 35th Annual International Conference of the IEEE Engineering in Medicine and Biology Society (EMBC)*, 2013: IEEE, pp. 5258-5262.
[85] I. Iturrate, R. Chavarriaga, L. Montesano, J. Minguez, and J. d. R. Millán, "Teaching brain-machine interfaces as an alternative paradigm to neuroprosthetics control," *Scientific reports,* vol. 5, 2015.
[86] I. Iturrate, L. Montesano, and J. Minguez, "Robot Reinforcement Learning using EEG-based reward signals," in *Robotics and Automation (ICRA), 2010 IEEE International Conference on*, 2010: IEEE, pp. 4822-4829.
[87] T. Tsoneva, J. Bieger, and G. Garcia-Molina, "Towards error-free interaction," in *2010 Annual International Conference of the IEEE Engineering in Medicine and Biology*, 2010: IEEE, pp. 5799-5802.
[88] M. K. Goel, R. Chavarriaga, and J. d. R. Millán, "Cortical current density vs. surface EEG for event-related potential-based Brain-Computer interface," in *Neural Engineering (NER), 2011 5th International IEEE/EMBS Conference on*, 2011: IEEE, pp. 430-433.

[89] H. Zhang, R. Chavarriaga, M. K. Goel, L. Gheorghe, and J. d. R. Millán, "Improved recognition of error related potentials through the use of brain connectivity features," in *2012 Annual International Conference of the IEEE Engineering in Medicine and Biology Society*, 2012: Ieee, pp. 6740-6743.
[90] I. Iturrate, R. Chavarriaga, L. Montesano, J. Minguez, and J. d. R. Millán, "Latency correction of error potentials between different experiments reduces calibration time for single-trial classification," in *2012 Annual International Conference of the IEEE Engineering in Medicine and Biology Society*, 2012: IEEE, pp. 3288-3291.
[91] I. Iturrate, L. Montesano, and J. Minguez, "Task-dependent signal variations in EEG error-related potentials for brain–computer interfaces," *Journal of neural engineering,* vol. 10, no. 2, p. 026024, 2013.
[92] J. Omedes, I. Iturrate, R. Chavarriaga, and L. Montesano, "Asynchronous Decoding of Error Potentials During the Monitoring of a Reaching Task," in *Systems, Man, and Cybernetics (SMC), 2015 IEEE International Conference on*, 2015: IEEE, pp. 3116-3121.
[93] A. Kreilinger, C. Neuper, and G. R. Müller-Putz, "Error potential detection during continuous movement of an artificial arm controlled by brain–computer interface," *Medical & biological engineering & computing,* vol. 50, no. 3, pp. 223-230, 2012.
[94] J. Omedes, I. Iturrate, L. Montesano, and J. Minguez, "Using frequency-domain features for the generalization of EEG error-related potentials among different tasks," in *2013 35th Annual International Conference of the IEEE Engineering in Medicine and Biology Society (EMBC)*, 2013: IEEE, pp. 5263-5266.
[95] L. George and A. Lécuyer, "An overview of research on" passive" brain-computer interfaces for implicit human-computer interaction," in *International Conference on Applied Bionics and Biomechanics ICABB 2010-Workshop W1" Brain-Computer Interfacing and Virtual Reality"*, 2010.
[96] T. O. Zander and C. Kothe, "Towards passive brain–computer interfaces: applying brain–computer interface technology to human–machine systems in general," *Journal of neural engineering,* vol. 8, no. 2, p. 025005, 2011.
[97] S. Amiri, R. Fazel-Rezai, and V. Asadpour, "A review of hybrid brain-computer interface systems," *Advances in Human-Computer Interaction,* vol. 2013, p. 1, 2013.
[98] G. Pfurtscheller *et al.*, "The hybrid BCI," *Frontiers in neuroscience,* vol. 4, p. 3, 2010.
[99] H. Banville and T. Falk, "Recent advances and open challenges in hybrid brain-computer interfacing: a technological review of non-invasive human research," *Brain-Computer Interfaces,* vol. 3, no. 1, pp. 9-46, 2016.
[100] U. Chaudhary, B. Xia, S. Silvoni, L. G. Cohen, and N. Birbaumer, "Brain–computer interface–based communication in the completely locked-in state," *PLoS biology,* vol. 15, no. 1, p. e1002593, 2017.
[101] S. Amiri, A. Rabbi, L. Azinfar, and R. Fazel-Rezai, "A review of P300, SSVEP, and hybrid P300/SSVEP brain-computer interface systems," *Brain-Computer Interface Systems—Recent Progress and Future Prospects,* 2013.
[102] D. Kapgate and D. Kalbande, "A Review on Visual Brain Computer Interface," in *Advancements of Medical Electronics*: Springer, 2015, pp. 193-206.

[103] T. Luth, D. Ojdanic, O. Friman, O. Prenzel, and A. Graser, "Low level control in a semi-autonomous rehabilitation robotic system via a brain-computer interface," in *Rehabilitation Robotics, 2007. ICORR 2007. IEEE 10th International Conference on*, 2007: IEEE, pp. 721-728.
[104] Y. Li *et al.*, "An EEG-based BCI system for 2-D cursor control by combining Mu/Beta rhythm and P300 potential," *Biomedical Engineering, IEEE Transactions on,* vol. 57, no. 10, pp. 2495-2505, 2010.
[105] L. Bi, J. Lian, K. Jie, R. Lai, and Y. Liu, "A speed and direction-based cursor control system with P300 and SSVEP," *Biomedical Signal Processing and Control,* vol. 14, pp. 126-133, 2014.
[106] G. Pfurtscheller, T. Solis-Escalante, R. Ortner, P. Linortner, and G. R. Muller-Putz, "Self-paced operation of an SSVEP-Based orthosis with and without an imagery-based "brain switch:" a feasibility study towards a hybrid BCI," *Neural Systems and Rehabilitation Engineering, IEEE Transactions on,* vol. 18, no. 4, pp. 409-414, 2010.
[107] B. Z. Allison, C. Brunner, C. Altstätter, I. C. Wagner, S. Grissmann, and C. Neuper, "A hybrid ERD/SSVEP BCI for continuous simultaneous two dimensional cursor control," *Journal of neuroscience methods,* vol. 209, no. 2, pp. 299-307, 2012.
[108] P. Horki, T. Solis-Escalante, C. Neuper, and G. Müller-Putz, "Combined motor imagery and SSVEP based BCI control of a 2 DoF artificial upper limb," *Medical & biological engineering & computing,* vol. 49, no. 5, pp. 567-577, 2011.
[109] F. Duan, D. Lin, W. Li, and Z. Zhang, "Design of a Multimodal EEG-based Hybrid BCI System with Visual Servo Module," *IEEE Transactions on Autonomous Mental Development,* vol. 7, no. 4, pp. 332-341, 2015.
[110] T. Yu *et al.*, "Enhanced motor imagery training using a hybrid BCI with feedback," *IEEE Transactions on Biomedical Engineering,* vol. 62, no. 7, pp. 1706-1717, 2015.
[111] M. Kim, B. H. Kim, and S. Jo, "Quantitative evaluation of a low-cost noninvasive hybrid interface based on EEG and eye movement," *IEEE Transactions on Neural Systems and Rehabilitation Engineering,* vol. 23, no. 2, pp. 159-168, 2015.
[112] T. Malechka, T. Tetzel, U. Krebs, D. Feuser, and A. Graeser, "sBCI-Headset—Wearable and Modular Device for Hybrid Brain-Computer Interface," *Micromachines,* vol. 6, no. 3, pp. 291-311, 2015.
[113] B. Hyung Kim, M. Kim, and S. Joevaluated, "Quadcopter flight control using a low-cost hybrid interface with EEG-based classification and eye tracking," *Computers in biology and medicine,* 2014.
[114] J. Ma, Y. Zhang, A. Cichocki, and F. Matsuno, "A Novel EOG/EEG Hybrid Human–Machine Interface Adopting Eye Movements and ERPs: Application to Robot Control," *IEEE Transactions on Biomedical Engineering,* vol. 62, no. 3, pp. 876-889, 2015.
[115] M. J. Khan, K.-S. Hong, N. Naseer, and M. R. Bhutta, "Hybrid EEG-NIRS based BCI for quadcopter control," in *Society of Instrument and Control Engineers of Japan (SICE), 2015 54th Annual Conference of the*, 2015: IEEE, pp. 1177-1182.

[116] G. H. Mulliken, S. Musallam, and R. A. Andersen, "Decoding trajectories from posterior parietal cortex ensembles," *the Journal of Neuroscience,* vol. 28, no. 48, pp. 12913-12926, 2008.
[117] R. Abiri, S. Borhani, E. W. Sellers, Y. Jiang, and X. Zhao, "A comprehensive review of EEG-based brain-computer interface paradigms," *Journal of neural engineering,* 2018.
[118] E. Abdalsalam, M. Z. Yusoff, A. Malik, N. S. Kamel, and D. Mahmoud, "Modulation of sensorimotor rhythms for brain-computer interface using motor imagery with online feedback," *Signal, Image and Video Processing,* vol. 12, no. 3, pp. 557-564, 2018.
[119] L. J. Trejo, R. Rosipal, and B. Matthews, "Brain-computer interfaces for 1-D and 2-D cursor control: designs using volitional control of the EEG spectrum or steady-state visual evoked potentials," *Neural Systems and Rehabilitation Engineering, IEEE Transactions on,* vol. 14, no. 2, pp. 225-229, 2006.
[120] R. Abiri, S. Borhani, J. Kilmarx, C. Esterwood, Y. Jiang, and X. Zhao, "A Novel User-Centered Approach for EEG-Based Computer Cursor Control via Imagined Body Kinematics," *Manuscript submitted for publication,* 2018.
[121] B. Xia *et al.*, "A combination strategy based brain–computer interface for two-dimensional movement control," *Journal of neural engineering,* vol. 12, no. 4, p. 046021, 2015.
[122] J. Kilmarx, R. Abiri, S. Borhani, Y. Jiang, and X. Zhao, "Sequence-Based Manipulation of Robotic Arm Control in Brain Machine Interface," *International Journal of Intelligent Robotics and Applications,* 2018, doi: 10.1007/s41315-018-0049-7.
[123] D. M. Taylor, S. I. H. Tillery, and A. B. Schwartz, "Direct cortical control of 3D neuroprosthetic devices," *Science,* vol. 296, no. 5574, pp. 1829-1832, 2002.
[124] A. Úbeda, J. M. Azorín, R. Chavarriaga, and J. d. R. Millán, "Evaluating decoding performance of upper limb imagined trajectories during center-out reaching tasks," in *Systems, Man, and Cybernetics (SMC), 2016 IEEE International Conference on*, 2016: IEEE, pp. 000252-000257.
[125] Y. Gu, K. Dremstrup, and D. Farina, "Single-trial discrimination of type and speed of wrist movements from EEG recordings," *Clinical Neurophysiology,* vol. 120, no. 8, pp. 1596-1600, 8// 2009, doi: http://dx.doi.org/10.1016/j.clinph.2009.05.006.
[126] A. Vuckovic and F. Sepulveda, "Delta band contribution in cue based single trial classification of real and imaginary wrist movements," (in eng), *Medical & biological engineering & computing,* vol. 46, no. 6, pp. 529-39, Jun 2008, doi: 10.1007/s11517-008-0345-8.
[127] T. Chakraborti *et al.*, "Implementation of EEG based control of remote robotic systems," in *Recent Trends in Information Systems (ReTIS), 2011 International Conference on*, 2011: IEEE, pp. 203-208.
[128] A. K. Mohamed, T. Marwala, and L. R. John, "Single-trial EEG discrimination between wrist and finger movement imagery and execution in a sensorimotor BCI," (in eng), *Conference proceedings : ... Annual International Conference of the IEEE Engineering in Medicine and Biology Society. IEEE Engineering in*

Medicine and Biology Society. Conference, vol. 2011, pp. 6289-93, 2011, doi: 10.1109/iembs.2011.6091552.
[129] P. Ofner and G. R. Müller-Putz, "Using a noninvasive decoding method to classify rhythmic movement imaginations of the arm in two planes," *IEEE transactions on biomedical engineering,* vol. 62, no. 3, pp. 972-981, 2015.
[130] J.-H. Kim, F. Bießmann, and S.-W. Lee, "Decoding three-dimensional trajectory of executed and imagined arm movements from electroencephalogram signals," *IEEE Transactions on Neural Systems and Rehabilitation Engineering,* vol. 23, no. 5, pp. 867-876, 2015.
[131] Emotiv. http://emotiv.com/ (accessed.
[132] G. Schalk, D. J. McFarland, T. Hinterberger, N. Birbaumer, and J. R. Wolpaw, "BCI2000: a general-purpose brain-computer interface (BCI) system," *Biomedical Engineering, IEEE Transactions on,* vol. 51, no. 6, pp. 1034-1043, 2004.
[133] T. J. Bradberry, R. J. Gentili, and J. L. Contreras-Vidal, "Reconstructing Three-Dimensional Hand Movements from Noninvasive Electroencephalographic Signals," *The Journal of Neuroscience,* vol. 30, no. 9, pp. 3432-3437, March 3, 2010 2010, doi: 10.1523/jneurosci.6107-09.2010.
[134] T. J. Bradberry, R. J. Gentili, and J. L. Contreras-Vidal, "Decoding three-dimensional hand kinematics from electroencephalographic signals," (in eng), *Conference proceedings : ... Annual International Conference of the IEEE Engineering in Medicine and Biology Society. IEEE Engineering in Medicine and Biology Society. Conference,* vol. 2009, pp. 5010-3, 2009, doi: 10.1109/iembs.2009.5334606.
[135] P. Ofner and G. R. Muller-Putz, "Decoding of velocities and positions of 3D arm movement from EEG," (in eng), *Conference proceedings : ... Annual International Conference of the IEEE Engineering in Medicine and Biology Society. IEEE Engineering in Medicine and Biology Society. Conference,* vol. 2012, pp. 6406-9, 2012, doi: 10.1109/embc.2012.6347460.
[136] T. Li, J. Hong, J. Zhang, and F. Guo, "Brain–machine interface control of a manipulator using small-world neural network and shared control strategy," *Journal of neuroscience methods,* vol. 224, pp. 26-38, 2014.
[137] M. K. Hazrati and U. G. Hofmann, "Avatar navigation in Second Life using brain signals," in *Intelligent Signal Processing (WISP), 2013 IEEE 8th International Symposium on*, 2013: IEEE, pp. 1-7.
[138] B. J. Edelman, J. Meng, N. Gulachek, C. C. Cline, and B. He, "Exploring cognitive flexibility with a noninvasive BCI using simultaneous steady-state visual evoked potentials and sensorimotor rhythms," *IEEE Transactions on Neural Systems and Rehabilitation Engineering,* vol. 26, no. 5, pp. 936-947, 2018.
[139] B. S. Baxter, B. J. Edelman, N. Nesbitt, and B. He, "Sensorimotor rhythm BCI with simultaneous high definition-transcranial direct current stimulation alters task performance," *Brain stimulation,* vol. 9, no. 6, pp. 834-841, 2016.
[140] J. Lv, Y. Li, and Z. Gu, "Decoding hand movement velocity from electroencephalogram signals during a drawing task," *Biomedical engineering online,* vol. 9, no. 1, p. 64, 2010.

[141] J. Zhang, J. Wei, B. Wang, J. Hong, and J. Wang, "Nonlinear EEG Decoding Based on a Particle Filter Model," *BioMed Research International,* vol. 2014, 2014.
[142] J. M. Antelis, L. Montesano, A. Ramos-Murguialday, N. Birbaumer, and J. Minguez, "On the usage of linear regression models to reconstruct limb kinematics from low frequency EEG signals," *PloS one,* vol. 8, no. 4, p. e61976, 2013.
[143] A. Ubeda, E. Ianez, E. Hortal, and J. M. Azorin, "Linear decoding of 2D hand movements for target selection tasks using a non-invasive BCI system," in *Systems Conference (SysCon), 2013 IEEE International*, 15-18 April 2013 2013, pp. 778-782, doi: 10.1109/SysCon.2013.6549972.
[144] A. J. Izenman, "Modern multivariate statistical techniques," *Regression, classification and manifold learning,* 2008.
[145] K. Liao, R. Xiao, J. Gonzalez, and L. J. P. o. Ding, "Decoding individual finger movements from one hand using human EEG signals," vol. 9, no. 1, p. e85192, 2014.
[146] G. Müller-Putz, R. Scherer, C. Brunner, R. Leeb, and G. Pfurtscheller, "Better than random: a closer look on BCI results," *International Journal of Bioelectromagnetism,* vol. 10, no. EPFL-ARTICLE-164768, pp. 52-55, 2008.
[147] D. J. McFarland and J. R. Wolpaw, "Brain-computer interfaces for communication and control," *Commun. ACM,* vol. 54, no. 5, pp. 60-66, 2011, doi: 10.1145/1941487.1941506.
[148] X. Dang, H. Peng, X. Wang, and H. Zhang, "Theil-Sen estimators in a multiple linear regression model," *Olemiss. edu,* 2008.
[149] M. Mennes, H. Wouters, B. Vanrumste, L. Lagae, and P. J. P. Stiers, "Validation of ICA as a tool to remove eye movement artifacts from EEG/ERP," vol. 47, no. 6, pp. 1142-1150, 2010.
[150] C.-Y. Chang, S.-H. Hsu, L. Pion-Tonachini, and T.-P. Jung, "Evaluation of Artifact Subspace Reconstruction for Automatic EEG Artifact Removal," in *2018 40th Annual International Conference of the IEEE Engineering in Medicine and Biology Society (EMBC)*, 2018: IEEE, pp. 1242-1245.
[151] A. Delorme and S. Makeig, "EEGLAB: an open source toolbox for analysis of single-trial EEG dynamics including independent component analysis," *Journal of neuroscience methods,* vol. 134, no. 1, pp. 9-21, 2004.
[152] D. Langlois, S. Chartier, and D. J. T. i. Q. M. f. P. Gosselin, "An introduction to independent component analysis: InfoMax and FastICA algorithms," vol. 6, no. 1, pp. 31-38, 2010.
[153] L. Pion-Tonachini, S. Makeig, and K. Kreutz-Delgado, "Crowd labeling latent Dirichlet allocation," *J Knowledge information systems,* vol. 53, no. 3, pp. 749-765, 2017.
[154] A. S. Royer, A. J. Doud, M. L. Rose, and B. He, "EEG control of a virtual helicopter in 3-dimensional space using intelligent control strategies," *Neural Systems and Rehabilitation Engineering, IEEE Transactions on,* vol. 18, no. 6, pp. 581-589, 2010.

[155] A. J. Doud, J. P. Lucas, M. T. Pisansky, and B. He, "Continuous three-dimensional control of a virtual helicopter using a motor imagery based brain-computer interface," *PloS one,* vol. 6, no. 10, p. e26322, 2011.
[156] I. Choi, I. Rhiu, Y. Lee, M. H. Yun, and C. S. Nam, "A systematic review of hybrid brain-computer interfaces: Taxonomy and usability perspectives," *PloS one,* vol. 12, no. 4, p. e0176674, 2017.
[157] F. Nijboer, N. Birbaumer, and A. Kübler, "The influence of psychological state and motivation on brain–computer interface performance in patients with amyotrophic lateral sclerosis–a longitudinal study," *Frontiers in neuroscience,* vol. 4, 2010.
[158] A. Kübler *et al.*, "The user-centered design as novel perspective for evaluating the usability of BCI-controlled applications," *PLoS One,* vol. 9, no. 12, p. e112392, 2014.
[159] J. Long, Y. Li, T. Yu, and Z. Gu, "Target selection with hybrid feature for BCI-based 2-D cursor control," *IEEE Transactions on biomedical engineering,* vol. 59, no. 1, pp. 132-140, 2012.
[160] T. A. Kayagil *et al.*, "A binary method for simple and accurate two-dimensional cursor control from EEG with minimal subject training," *Journal of neuroengineering and rehabilitation,* vol. 6, no. 1, p. 1, 2009.
[161] D. Huang, P. Lin, D.-Y. Fei, X. Chen, and O. Bai, "Decoding human motor activity from EEG single trials for a discrete two-dimensional cursor control," *Journal of neural engineering,* vol. 6, no. 4, p. 046005, 2009.
[162] B.-K. Min, R. Chavarriaga, and J. del R. Millán, "Harnessing Prefrontal Cognitive Signals for Brain–Machine Interfaces," *Trends in Biotechnology,* vol. 35, no. 7, p. 13, 2017.
[163] S. Borhani, R. Abiri, S. Esfahani, J. Kilmarx, Y. Jiang, and X. Zhao, "Decoding Visual Attentional State using EEG-based BCI," in *2018 Annual Meeting Society for Neuroscience (SfN2018)*, 2018.
[164] S. Borhani, J. Yu, J. Cate, J. Kilmarx, R. Abiri, and X. Zhao, "Clash of Minds: A BCI Car Racing Game in Simulated Virtual Reality Environment," in *2018 Biomedical Engineering Society (BMES) Annual Meeting*, 2018.
[165] S. Borhani, R. Abiri, X. Zhao, and Y. Jiang, "A Transfer Learning Approach towards Zero-training BCI for EEG-Based Two Dimensional Cursor Control," in *Society for Neuroscience (SfN 2017)*, 2017.
[166] R. Abiri, S. Borhani, E. Sellers, Y. Jiang, and X. Zhao, "A comprehensive review of EEG-based brain-computer interface paradigms," *Journal of neural engineering,* vol. 16, no. 1, p. 011001, 2018.
[167] C. W. Granger, "Investigating causal relations by econometric models and cross-spectral methods," *Econometrica: Journal of the Econometric Society,* pp. 424-438, 1969.
[168] E. Siggiridou and D. Kugiumtzis, "Granger causality in multivariate time series using a time-ordered restricted vector autoregressive model," *IEEE Transactions on Signal Processing,* vol. 64, no. 7, pp. 1759-1773, 2016.
[169] K. So, A. C. Koralek, K. Ganguly, M. C. Gastpar, and J. M. Carmena, "Assessing functional connectivity of neural ensembles using directed information," *Journal of neural engineering,* vol. 9, no. 2, p. 026004, 2012.

[170] F. H. Lin *et al.*, "Dynamic Granger–Geweke causality modeling with application to interictal spike propagation," *Human brain mapping,* vol. 30, no. 6, pp. 1877-1886, 2009.
[171] L. Zhang, G. Zhong, Y. Wu, M. G. Vangel, B. Jiang, and J. Kong, "Using Granger-Geweke causality model to evaluate the effective connectivity of primary motor cortex (M1), supplementary motor area (SMA) and cerebellum," *Journal of biomedical science and engineering,* vol. 3, p. 848, 2010.
[172] M. Dhamala, H. Liang, S. L. Bressler, and M. Ding, "Granger-Geweke causality: Estimation and interpretation," *NeuroImage,* vol. 175, pp. 460-463, 2018.
[173] M. Somers, L. S. Shields, M. P. Boks, R. S. Kahn, and I. E. Sommer, "Cognitive benefits of right-handedness: a meta-analysis," *Neuroscience & Biobehavioral Reviews,* vol. 51, pp. 48-63, 2015.
[174] S. M. Hardie and L. Wright, "Differences between left-and right-handers in approach/avoidance motivation: influence of consistency of handedness measures," *Frontiers in Psychology,* vol. 5, p. 134, 2014.
[175] R. Abiri, S. Borhani, Y. Jiang, and X. Zhao, "Decoding Attentional State to Faces and Scenes Using EEG Brainwaves," *J Complexity,* vol. 2019, 2019.
[176] D. H. Brainard and S. Vision, "The psychophysics toolbox," *Spatial vision,* vol. 10, pp. 433-436, 1997.
[177] D. G. Pelli, "The VideoToolbox software for visual psychophysics: Transforming numbers into movies," *Spatial vision,* vol. 10, no. 4, pp. 437-442, 1997.
[178] M. Kleiner, D. Brainard, D. Pelli, A. Ingling, R. Murray, and C. Broussard, "What's new in Psychtoolbox-3," *Perception,* vol. 36, no. 14, p. 1, 2007.
[179] T. R. Mullen *et al.*, "Real-time neuroimaging and cognitive monitoring using wearable dry EEG," *IEEE Transactions on Biomedical Engineering,* vol. 62, no. 11, pp. 2553-2567, 2015.
[180] A. Delorme, J. Palmer, J. Onton, R. Oostenveld, and S. Makeig, "Independent EEG sources are dipolar," *PloS one,* vol. 7, no. 2, p. e30135, 2012.
[181] A. Mognon, J. Jovicich, L. Bruzzone, and M. Buiatti, "ADJUST: An automatic EEG artifact detector based on the joint use of spatial and temporal features," *Psychophysiology,* vol. 48, no. 2, pp. 229-240, 2011.
[182] R. Oostenveld, "Academic Software Applications for Electromagnetic Brain Mapping Using MEG and EEG."
[183] C. Piazza *et al.*, "An automated function for identifying eeg independent components representing bilateral source activity," in *XIV Mediterranean Conference on Medical and Biological Engineering and Computing 2016*, 2016: Springer, pp. 105-109.
[184] N. Naghavi and E. Wade, "Prediction of Freezing of Gait in Parkinson's Disease using Statistical Inference and Lower–Limb Acceleration Data," *IEEE transactions on neural systems and rehabilitation engineering,* 2019.
[185] E. Bullmore and O. Sporns, "Complex brain networks: graph theoretical analysis of structural and functional systems," *Nature Reviews Neuroscience,* vol. 10, no. 3, p. 186, 2009.
[186] J. P. Donoghue, "Plasticity of adult sensorimotor representations," *Current opinion in neurobiology,* vol. 5, no. 6, pp. 749-754, 1995.

[187] R. J. Nudo, E. J. Plautz, and G. W. Milliken, "Adaptive plasticity in primate motor cortex as a consequence of behavioral experience and neuronal injury," in *Seminars in Neuroscience*, 1997, vol. 9, no. 1-2: Elsevier, pp. 13-23.
[188] G. Nolte, O. Bai, L. Wheaton, Z. Mari, S. Vorbach, and M. Hallett, "Identifying true brain interaction from EEG data using the imaginary part of coherency," *Clinical neurophysiology,* vol. 115, no. 10, pp. 2292-2307, 2004.
[189] A. M. Bastos and J.-M. Schoffelen, "A tutorial review of functional connectivity analysis methods and their interpretational pitfalls," *Frontiers in systems neuroscience,* vol. 9, p. 175, 2016.
[190] K. J. Friston, L. Harrison, and W. Penny, "Dynamic causal modelling," *Neuroimage,* vol. 19, no. 4, pp. 1273-1302, 2003.
[191] J. B. Ullman and P. M. Bentler, "Structural equation modeling," *Handbook of Psychology, Second Edition,* vol. 2, 2012.
[192] W. A. Freiwald *et al.*, "Testing non-linearity and directedness of interactions between neural groups in the macaque inferotemporal cortex," *Journal of neuroscience methods,* vol. 94, no. 1, pp. 105-119, 1999.
[193] M. Kamiński, M. Ding, W. A. Truccolo, and S. L. Bressler, "Evaluating causal relations in neural systems: Granger causality, directed transfer function and statistical assessment of significance," *Biological cybernetics,* vol. 85, no. 2, pp. 145-157, 2001.
[194] Y. Chen, G. Rangarajan, J. Feng, and M. Ding, "Analyzing multiple nonlinear time series with extended Granger causality," *Physics Letters A,* vol. 324, no. 1, pp. 26-35, 2004.
[195] A. G. Nedungadi, G. Rangarajan, N. Jain, and M. Ding, "Analyzing multiple spike trains with nonparametric granger causality," *Journal of computational neuroscience,* vol. 27, no. 1, pp. 55-64, 2009.
[196] S. Guo, A. K. Seth, K. M. Kendrick, C. Zhou, and J. Feng, "Partial Granger causality—eliminating exogenous inputs and latent variables," *Journal of neuroscience methods,* vol. 172, no. 1, pp. 79-93, 2008.
[197] T. Ge, K. M. Kendrick, and J. Feng, "A novel extended Granger causal model approach demonstrates brain hemispheric differences during face recognition learning," *PLoS computational biology,* vol. 5, no. 11, p. e1000570, 2009.
[198] H. Akaike, "A new look at the statistical model identification," in *Selected Papers of Hirotugu Akaike*: Springer, 1974, pp. 215-222.
[199] H. Courellis, T. Mullen, H. Poizner, G. Cauwenberghs, and J. R. Iversen, "EEG-based quantification of cortical current density and dynamic causal connectivity generalized across subjects performing BCI-monitored cognitive tasks," *J Frontiers in neuroscience,* vol. 11, p. 180, 2017.
[200] T. R. Mullen, *The dynamic brain: Modeling neural dynamics and interactions from human electrophysiological recordings*. University of California, San Diego, 2014.
[201] J. L. Hintze and R. D. Nelson, "Violin plots: a box plot-density trace synergism," *The American Statistician,* vol. 52, no. 2, pp. 181-184, 1998.
[202] B. Kaneshiro, M. P. Guimaraes, H.-S. Kim, A. M. Norcia, and P. Suppes, "A representational similarity analysis of the dynamics of object processing using single-trial EEG classification," *PloS one,* vol. 10, no. 8, p. e0135697, 2015.

[203] S. Yantis, "The neural basis of selective attention: Cortical sources and targets of attentional modulation," *Current Directions in Psychological Science,* vol. 17, no. 2, pp. 86-90, 2008.
[204] K. Friston, R. Moran, and A. K. Seth, "Analysing connectivity with Granger causality and dynamic causal modelling," *Current opinion in neurobiology,* vol. 23, no. 2, pp. 172-178, 2013.
[205] V. Bonnelle *et al.*, "Default mode network connectivity predicts sustained attention deficits after traumatic brain injury," *Journal of Neuroscience,* vol. 31, no. 38, pp. 13442-13451, 2011.
[206] M. D. Rosenberg *et al.*, "A neuromarker of sustained attention from whole-brain functional connectivity," *Nature neuroscience,* vol. 19, no. 1, p. 165, 2016.
[207] M. Loitfelder *et al.*, "Abnormalities of resting state functional connectivity are related to sustained attention deficits in MS," *PloS one,* vol. 7, no. 8, p. e42862, 2012.
[208] D. Baldauf and R. Desimone, "Neural mechanisms of object-based attention," *Science,* vol. 344, no. 6182, pp. 424-427, 2014.
[209] R. Kus, K. J. Blinowska, M. Kamiński, and A. Basińska-Starzycka, "Transmission of information during continuous attention test," *Acta neurobiologiae experimentalis,* vol. 68, no. 1, p. 103, 2008.
[210] G. G. Supp, A. Schlögl, N. Trujillo-Barreto, M. M. Müller, and T. Gruber, "Directed cortical information flow during human object recognition: analyzing induced EEG gamma-band responses in brain's source space," *PloS one,* vol. 2, no. 8, p. e684, 2007.
[211] S. Borhani, R. Abiri, J. Muhammad, I, Y. Jiang, and X. Zhao, "EEG-based Visual Attentional State Decoding Using Convolutional Neural Network," presented at the 7th International BCI Meeting, Pacific Grove, CA, United States, 2018-05-21, 2018. [Online]. Available: https://hal.archives-ouvertes.fr/hal-01843916.
[212] Y. Jiang, R. Abiri, and X. Zhao, "Tuning Up the Old Brain with New Tricks: Attention Training via Neurofeedback," *Frontiers in aging neuroscience,* vol. 9, 2017.
[213] G. Bin, X. Gao, Z. Yan, B. Hong, and S. Gao, "An online multi-channel SSVEP-based brain–computer interface using a canonical correlation analysis method," *Journal of neural engineering,* vol. 6, no. 4, p. 046002, 2009.
[214] R. C. Atkinson and R. M. Shiffrin, "Human memory: A proposed system and its control processes," in *Psychology of learning and motivation*, vol. 2: Elsevier, 1968, pp. 89-195.
[215] N. Unsworth and R. W. Engle, "On the division of short-term and working memory: an examination of simple and complex span and their relation to higher order abilities," *Psychological bulletin,* vol. 133, no. 6, p. 1038, 2007.
[216] M. M. Sebrechts, R. L. Marsh, and J. G. Seamon, "Secondary memory and very rapid forgetting," *Memory & cognition,* vol. 17, no. 6, pp. 693-700, 1989.
[217] N. Cowan, "Evolving conceptions of memory storage, selective attention, and their mutual constraints within the human information-processing system," *Psychological bulletin,* vol. 104, no. 2, p. 163, 1988.
[218] N. Cowan, *Attention and memory: An integrated framework*. Oxford University Press, 1998.

[219] J. R. Anderson, D. Bothell, M. D. Byrne, S. Douglass, C. Lebiere, and Y. Qin, "An integrated theory of the mind," *Psychological review,* vol. 111, no. 4, p. 1036, 2004.
[220] A. D. Baddeley and G. Hitch, "Working memory," in *Psychology of learning and motivation*, vol. 8: Elsevier, 1974, pp. 47-89.
[221] R. Cabeza, F. Dolcos, R. Graham, and L. Nyberg, "Similarities and differences in the neural correlates of episodic memory retrieval and working memory," *Neuroimage,* vol. 16, no. 2, pp. 317-330, 2002.
[222] G. Vallar and T. Shallice, *Neuropsychological impairments of short-term memory*. Cambridge University Press, 2007.
[223] T. D. Wager and E. E. Smith, "Neuroimaging studies of working memory," *Cognitive, Affective, & Behavioral Neuroscience,* vol. 3, no. 4, pp. 255-274, 2003.
[224] B. McElree, "Accessing recent events," *Psychology of learning and motivation,* vol. 46, pp. 155-200, 2006.
[225] J. Li *et al.*, "A cognitive electrophysiological signature differentiates amnestic mild cognitive impairment from normal aging," *Alzheimer's research*

therapy, vol. 9, no. 1, p. 3, 2017.
[226] M. D. Rugg and T. Curran, "Event-related potentials and recognition memory," *Trends in cognitive sciences,* vol. 11, no. 6, pp. 251-257, 2007.
[227] L. S. Broster *et al.*, "Spared behavioral repetition effects in Alzheimer's disease linked to an altered neural mechanism at posterior cortex," *Journal of clinical and experimental neuropsychology,* vol. 40, no. 8, pp. 761-776, 2018.
[228] R. W. Engle, "Working memory capacity as executive attention," *Current directions in psychological science,* vol. 11, no. 1, pp. 19-23, 2002.
[229] A. Hollingworth and V. M. Beck, "Memory-based attention capture when multiple items are maintained in visual working memory," *Journal of experimental psychology: human perception and performance,* vol. 42, no. 7, p. 911, 2016.
[230] A. Gazzaley, J. W. Cooney, J. Rissman, and M. D'esposito, "Top-down suppression deficit underlies working memory impairment in normal aging," *Nature neuroscience,* vol. 8, no. 10, pp. 1298-1300, 2005.
[231] M. Wang *et al.*, "Neuronal basis of age-related working memory decline," *nature,* vol. 476, no. 7359, pp. 210-213, 2011.
[232] R. Abiri, S. Borhani, E. W. Sellers, Y. Jiang, and X. Zhao, "A comprehensive review of EEG-based brain–computer interface paradigms," *Journal of neural engineering,* vol. 16, no. 1, p. 011001, 2019.
[233] E. Noh, K. Liao, M. V. Mollison, T. Curran, and V. R. d. Sa, "Single-trial EEG analysis predicts memory retrieval and reveals source-dependent differences," *Frontiers in human neuroscience,* vol. 12, p. 258, 2018.
[234] T. V. Román-López *et al.*, "Brain electrical activity from encoding to retrieval while maintaining and manipulating information in working memory," *Memory,* vol. 27, no. 8, pp. 1063-1078, 2019.
[235] C.-N. A. Guran, N. A. Herweg, and N. Bunzeck, "Age-related decreases in the retrieval practice effect directly relate to changes in alpha-beta oscillations," *Journal of Neuroscience,* vol. 39, no. 22, pp. 4344-4352, 2019.
[236] I. Mapelli and T. E. Özkurt, "Brain Oscillatory Correlates of Visual Short-Term Memory Errors," *Frontiers in human neuroscience,* vol. 13, p. 33, 2019.

[237] E. Nyhus, W. A. Engel, T. Donatelli Pitfield, and I. Vakkur, "Increases in Theta Oscillatory Activity During Episodic Memory Retrieval Following Mindfulness Meditation Training," *Frontiers in human neuroscience,* vol. 13, p. 311, 2019.
[238] J. Li *et al.*, "A cognitive electrophysiological signature differentiates amnestic mild cognitive impairment from normal aging," *Alzheimer's research & therapy,* vol. 9, no. 1, p. 3, 2017.
[239] J. McBride *et al.*, "Scalp EEG-based discrimination of cognitive deficits after traumatic brain injury using event-related Tsallis entropy analysis," *IEEE Transactions on Biomedical Engineering,* vol. 60, no. 1, pp. 90-96, 2012.
[240] R. Abiri, S. Borhani, Y. Jiang, and X. Zhao, "Decoding attentional state to faces and scenes using EEG brainwaves," *Complexity,* vol. 2019, 2019.
[241] S. Borhani, R. Abiri, Y. Jiang, T. Berger, and X. Zhao, "Brain connectivity evaluation during selective attention using EEG-based brain-computer interface," *Brain-Computer Interfaces,* vol. 6, no. 1-2, pp. 25-35, 2019.
[242] R. J. Barry and F. M. De Blasio, "EEG differences between eyes-closed and eyes-open resting remain in healthy ageing," *Biological psychology,* vol. 129, pp. 293-304, 2017.
[243] R. A. L. Zunini, J.-P. Thivierge, S. Kousaie, C. Sheppard, and V. Taler, "Alterations in resting-state activity relate to performance in a verbal recognition task," *PloS one,* vol. 8, no. 6, p. e65608, 2013.
[244] C. Babiloni *et al.*, "Sources of cortical rhythms change as a function of cognitive impairment in pathological aging: a multicenter study," *Clinical neurophysiology,* vol. 117, no. 2, pp. 252-268, 2006.
[245] C. Babiloni *et al.*, "Resting state cortical rhythms in athletes: a high-resolution EEG study," *Brain Research Bulletin,* vol. 81, no. 1, pp. 149-156, 2010.
[246] J. Jeong, "EEG dynamics in patients with Alzheimer's disease," *Clinical neurophysiology,* vol. 115, no. 7, pp. 1490-1505, 2004.
[247] P. M. Rossini, S. Rossi, C. Babiloni, and J. Polich, "Clinical neurophysiology of aging brain: from normal aging to neurodegeneration," *Progress in neurobiology,* vol. 83, no. 6, pp. 375-400, 2007.
[248] M. Torkamani-Azar, S. D. Kanik, S. Aydin, and M. Cetin, "Prediction of reaction time and vigilance variability from spatio-spectral features of resting-state EEG in a long sustained attention task," *IEEE journal of biomedical and health informatics,* 2020.
[249] D. Heister *et al.*, "Resting-state neuronal oscillatory correlates of working memory performance," *PloS one,* vol. 8, no. 6, p. e66820, 2013.
[250] C. S. Prat, B. L. Yamasaki, R. A. Kluender, and A. Stocco, "Resting-state qEEG predicts rate of second language learning in adults," *Brain and language,* vol. 157, pp. 44-50, 2016.
[251] Z. Cao *et al.*, "Resting-state EEG power and coherence vary between migraine phases," *The journal of headache and pain,* vol. 17, no. 1, p. 102, 2016.
[252] R. Cassani, M. Estarellas, R. San-Martin, F. J. Fraga, and T. H. Falk, "Systematic review on resting-state EEG for Alzheimer's disease diagnosis and progression assessment," *Disease markers,* vol. 2018, 2018.

[253] Y. Jiang *et al.*, "Alzheimer's biomarkers are correlated with brain connectivity in older adults differentially during resting and task states," *Frontiers in aging neuroscience,* vol. 8, p. 15, 2016.
[254] C. Babiloni *et al.*, "Directionality of EEG synchronization in Alzheimer's disease subjects," *Neurobiology of aging,* vol. 30, no. 1, pp. 93-102, 2009.
[255] C. J. Stam and B. Van Dijk, "Synchronization likelihood: an unbiased measure of generalized synchronization in multivariate data sets," *Physica D: Nonlinear Phenomena,* vol. 163, no. 3-4, pp. 236-251, 2002.
[256] J. Bosboom, D. Stoffers, E. C. Wolters, C. J. Stam, and H. W. Berendse, "MEG resting state functional connectivity in Parkinson's disease related dementia," *Journal of neural transmission,* vol. 116, no. 2, p. 193, 2009.
[257] Z. Sankari, H. Adeli, and A. Adeli, "Intrahemispheric, interhemispheric, and distal EEG coherence in Alzheimer's disease," *Clinical Neurophysiology,* vol. 122, no. 5, pp. 897-906, 2011.
[258] E. Scarr, A. S. Gibbons, J. Neo, M. Udawela, and B. Dean, "Cholinergic connectivity: it's implications for psychiatric disorders," *Frontiers in cellular neuroscience,* vol. 7, p. 55, 2013.
[259] M. Demirtaş, C. Falcon, A. Tucholka, J. D. Gispert, J. L. Molinuevo, and G. Deco, "A whole-brain computational modeling approach to explain the alterations in resting-state functional connectivity during progression of Alzheimer's disease," *NeuroImage: Clinical,* vol. 16, pp. 343-354, 2017.
[260] M. D'Esposito and B. R. Postle, "The cognitive neuroscience of working memory," *Annual review of psychology,* vol. 66, pp. 115-142, 2015.
[261] B. Rypma and M. D'Esposito, "Isolating the neural mechanisms of age-related changes in human working memory," *Nature neuroscience,* vol. 3, no. 5, pp. 509-515, 2000.
[262] A. M. Morcom, J. Li, and M. D. Rugg, "Age effects on the neural correlates of episodic retrieval: increased cortical recruitment with matched performance," *Cerebral Cortex,* vol. 17, no. 11, pp. 2491-2506, 2007.
[263] J. J. Todd, S. W. Han, S. Harrison, and R. Marois, "The neural correlates of visual working memory encoding: a time-resolved fMRI study," *Neuropsychologia,* vol. 49, no. 6, pp. 1527-1536, 2011.
[264] K. D'Ardenne, N. Eshel, J. Luka, A. Lenartowicz, L. E. Nystrom, and J. D. Cohen, "Role of prefrontal cortex and the midbrain dopamine system in working memory updating," *Proceedings of the National Academy of Sciences,* vol. 109, no. 49, pp. 19900-19909, 2012.
[265] V. Siffredi, P. Barrouillet, M. Spencer-Smith, M. Vaessen, V. Anderson, and P. Vuilleumier, "Examining distinct working memory processes in children and adolescents using fMRI: Results and validation of a modified Brown-Peterson paradigm," *PloS one,* vol. 12, no. 7, 2017.
[266] F. Borgan *et al.*, "The neural and molecular basis of working memory function in psychosis: a multimodal PET-fMRI study," *Molecular Psychiatry,* pp. 1-11, 2019.
[267] M. Suzuki *et al.*, "Neural correlates of working memory maintenance in advanced aging: Evidence from fMRI," *Frontiers in aging neuroscience,* vol. 10, p. 358, 2018.

[268] D. V. Moretti *et al.*, "Individual analysis of EEG frequency and band power in mild Alzheimer's disease," *Clinical Neurophysiology,* vol. 115, no. 2, pp. 299-308, 2004.
[269] M. K. Healey and M. J. Kahana, "Age-related differences in the temporal dynamics of spectral power during memory encoding," *Plos one,* vol. 15, no. 1, p. e0227274, 2020.
[270] S. Getzmann, E. Wascher, and D. Schneider, "The role of inhibition for working memory processes: ERP evidence from a short-term storage task," *Psychophysiology,* vol. 55, no. 5, p. e13026, 2018.
[271] F. Simard and G. Cadoret, "Neural correlates of active controlled retrieval development: An exploratory ERP study," *Brain and cognition,* vol. 124, pp. 20-28, 2018.
[272] S. Sternberg, "Memory-scanning: Mental processes revealed by reaction-time experiments," *American scientist,* vol. 57, no. 4, pp. 421-457, 1969.
[273] J. G. Snodgrass and M. Vanderwart, "A standardized set of 260 pictures: norms for name agreement, image agreement, familiarity, and visual complexity," *Journal of experimental psychology: Human learning and memory,* vol. 6, no. 2, p. 174, 1980.
[274] J. Brooks, "Peirce, J., & MacAskill, M.(Eds.). Building Experiments in PsychoPy," ed: SAGE Publications Sage UK: London, England, 2019.
[275] J. Peirce *et al.*, "PsychoPy2: Experiments in behavior made easy," *Behavior research methods,* vol. 51, no. 1, pp. 195-203, 2019.
[276] C. Kothe, "Lab streaming layer (LSL)," *https://github.com/sccn/labstreaminglayer. Accessed on February 2020,* vol. 26, p. 2015, 2014.
[277] M. O'neil. "Emotiv-Headset-LSL." https://github.com/Moneil97/Emotiv-Headset-LSL (accessed 8/10/2019.
[278] "App-LabRecorder." https://github.com/labstreaminglayer/App-LabRecorder (accessed 8/10/2019.
[279] S. Borhani. "BluegrassWorkingMemory." https://github.com/soheilbr82/BluegrassWorkingMemory (accessed 8/10/2019.
[280] C. A. Kothe and S. Makeig, "BCILAB: a platform for brain–computer interface development," *Journal of neural engineering,* vol. 10, no. 5, p. 056014, 2013.
[281] L. J. Gabard-Durnam, A. S. Mendez Leal, C. L. Wilkinson, and A. R. Levin, "The Harvard Automated Processing Pipeline for Electroencephalography (HAPPE): standardized processing software for developmental and high-artifact data," *Frontiers in neuroscience,* vol. 12, p. 97, 2018.
[282] M. Makoto. "Makoto's preprocessing pipeline." https://sccn.ucsd.edu/wiki/Makoto's_preprocessing_pipeline (accessed 7/10/2020.
[283] MATLAB, "version 9.5.0 (R2018b)," *Natick, Massachusetts,* vol. The MathWorks Inc., 2018.
[284] C.-Y. Chang, S.-H. Hsu, L. Pion-Tonachini, and T.-P. Jung, "Evaluation of artifact subspace reconstruction for automatic artifact components removal in multi-channel EEG recordings," *IEEE Transactions on Biomedical Engineering,* 2019.
[285] MATLAB, "9.7.0.1296695 (R2019b)," *Natick, Massachusetts,* vol. The Mathworks Inc., 2019.

[286] P. Namburi. "Connected topoplot." https://www.mathworks.com/matlabcentral/fileexchange/32563-connected-topoplot (accessed 13/9/2020.
[287] T. Akam and D. M. Kullmann, "Oscillatory multiplexing of population codes for selective communication in the mammalian brain," *Nature Reviews Neuroscience,* vol. 15, no. 2, pp. 111-122, 2014.
[288] L. Chen *et al.*, "The role of intrinsic excitability in the evolution of memory: Significance in memory allocation, consolidation, and updating," *Neurobiology of Learning and Memory,* p. 107266, 2020.
[289] C. Babiloni *et al.*, "Brain neural synchronization and functional coupling in Alzheimer's disease as revealed by resting state EEG rhythms," *International Journal of Psychophysiology,* vol. 103, pp. 88-102, 2016.
[290] B. Tóth *et al.*, "EEG synchronization characteristics of functional connectivity and complex network properties of memory maintenance in the delta and theta frequency bands," *International Journal of Psychophysiology,* vol. 83, no. 3, pp. 399-402, 2012.
[291] J. I. Fleck, J. Kuti, J. Brown, J. R. Mahon, and C. Gayda-Chelder, "Frontal-posterior coherence and cognitive function in older adults," *International Journal of Psychophysiology,* vol. 110, pp. 217-230, 2016.
[292] M. A. Daulatzai, "Early stages of pathogenesis in memory impairment during normal senescence and Alzheimer's disease," *Journal of Alzheimer's Disease,* vol. 20, no. 2, pp. 355-367, 2010.
[293] L. Bäckman, B. J. Small, and L. Fratiglioni, "Stability of the preclinical episodic memory deficit in Alzheimer's disease," *Brain,* vol. 124, no. 1, pp. 96-102, 2001.
[294] C. Grady, "The cognitive neuroscience of ageing," *Nature Reviews Neuroscience,* vol. 13, no. 7, pp. 491-505, 2012.
[295] R. Parasuraman, P. M. Greenwood, J. V. Haxby, and C. L. Grady, "Visuospatial attention in dementia of the Alzheimer type," *Brain,* vol. 115, no. 3, pp. 711-733, 1992.
[296] J. D. Jackson, D. A. Balota, J. M. Duchek, and D. Head, "White matter integrity and reaction time intraindividual variability in healthy aging and early-stage Alzheimer disease," *Neuropsychologia,* vol. 50, no. 3, pp. 357-366, 2012.
[297] H. D. Schlinger, "Behavior analysis and behavioral neuroscience," *Frontiers in human neuroscience,* vol. 9, p. 210, 2015.
[298] R. A. Rescorla, "Behavioral studies of Pavlovian conditioning," *Annual review of neuroscience,* vol. 11, no. 1, pp. 329-352, 1988.
[299] S. McLeod, "Skinner-operant conditioning," *Retrieved from,* 2015.
[300] R. J. Schafer and T. Moore, "Selective attention from voluntary control of neurons in prefrontal cortex," *Science,* vol. 332, no. 6037, pp. 1568-1571, 2011.
[301] T. Egner and J. H. Gruzelier, "Learned self-regulation of EEG frequency components affects attention and event-related brain potentials in humans," *Neuroreport,* vol. 12, no. 18, pp. 4155-4159, 2001.
[302] J. H. Gruzelier, "EEG-neurofeedback for optimising performance. I: a review of cognitive and affective outcome in healthy participants," *Neuroscience Biobehavioral Reviews,* vol. 44, pp. 124-141, 2014.

[303] J. H. Gruzelier, "EEG-neurofeedback for optimising performance. III: a review of methodological and theoretical considerations," *Neuroscience Biobehavioral Reviews,* vol. 44, pp. 159-182, 2014.
[304] K. K. Ang, Z. Y. Chin, H. Zhang, and C. Guan, "Mutual information-based selection of optimal spatial–temporal patterns for single-trial EEG-based BCIs," *Pattern Recognition Letters,* vol. 45, no. 6, pp. 2137-2144, 2012.
[305] M. Grosse-Wentrup, B. Schölkopf, and J. Hill, "Causal influence of gamma oscillations on the sensorimotor rhythm," *NeuroImage,* vol. 56, no. 2, pp. 837-842, 2011.
[306] N. Garon, S. E. Bryson, and I. M. Smith, "Executive function in preschoolers: a review using an integrative framework," *Psychological bulletin,* vol. 134, no. 1, p. 31, 2008.
[307] E. K. Miller and J. D. Cohen, "An integrative theory of prefrontal cortex function," *Annual review of neuroscience,* vol. 24, no. 1, pp. 167-202, 2001.
[308] E. I. Knudsen, "Fundamental components of attention," *Annu. Rev. Neurosci.,* vol. 30, pp. 57-78, 2007.
[309] A. Gazzaley and A. C. Nobre, "Top-down modulation: bridging selective attention and working memory," *Trends in cognitive sciences,* vol. 16, no. 2, pp. 129-135, 2012.
[310] A. Ikkai and C. E. Curtis, "Common neural mechanisms supporting spatial working memory, attention and motor intention," *Neuropsychologia,* vol. 49, no. 6, pp. 1428-1434, 2011.
[311] N. Cowan *et al.*, "On the capacity of attention: Its estimation and its role in working memory and cognitive aptitudes," *Cognitive psychology,* vol. 51, no. 1, pp. 42-100, 2005.
[312] U. Strehl, S. M. Birkle, S. Wörz, and B. Kotchoubey, "Sustained reduction of seizures in patients with intractable epilepsy after self-regulation training of slow cortical potentials–10 years after," *Frontiers in human neuroscience,* vol. 8, p. 604, 2014.
[313] M. B. Sterman and T. Egner, "Foundation and practice of neurofeedback for the treatment of epilepsy," *Applied psychophysiology*

Biofeedback and Self-regulation, vol. 31, no. 1, p. 21, 2006.
[314] M. Arns, S. De Ridder, U. Strehl, M. Breteler, and A. Coenen, "Efficacy of neurofeedback treatment in ADHD: the effects on inattention, impulsivity and hyperactivity: a meta-analysis," *Clinical EEG*

Neuroscience & Biobehavioral Reviews, vol. 40, no. 3, pp. 180-189, 2009.
[315] E. J. Sonuga-Barke *et al.*, "Nonpharmacological interventions for ADHD: systematic review and meta-analyses of randomized controlled trials of dietary and psychological treatments," *American Journal of Psychiatry,* vol. 170, no. 3, pp. 275-289, 2013.
[316] S. Rayegani *et al.*, "Effect of neurofeedback and electromyographic-biofeedback therapy on improving hand function in stroke patients," *Topics in stroke rehabilitation,* vol. 21, no. 2, pp. 137-151, 2014.

[317] M. E. Kouijzer, J. M. de Moor, B. J. Gerrits, J. K. Buitelaar, and H. T. van Schie, "Long-term effects of neurofeedback treatment in autism," *Research in Autism Spectrum Disorders,* vol. 3, no. 2, pp. 496-501, 2009.
[318] K. Reiter, S. B. Andersen, and J. Carlsson, "Neurofeedback treatment and posttraumatic stress disorder: Effectiveness of neurofeedback on posttraumatic stress disorder and the optimal choice of protocol," *The Journal of nervous mental disease,* vol. 204, no. 2, pp. 69-77, 2016.
[319] T. Hartmann, I. Lorenz, N. Müller, B. Langguth, and N. Weisz, "The effects of neurofeedback on oscillatory processes related to tinnitus," *Brain Topography,* vol. 27, no. 1, pp. 149-157, 2014.
[320] B. Zoefel, R. J. Huster, and C. S. Herrmann, "Neurofeedback training of the upper alpha frequency band in EEG improves cognitive performance," *Neuroimage,* vol. 54, no. 2, pp. 1427-1431, 2011.
[321] J.-R. Wang and S. Hsieh, "Neurofeedback training improves attention and working memory performance," *Clinical Neurophysiology,* vol. 124, no. 12, pp. 2406-2420, 2013.
[322] C. Escolano, M. Aguilar, and J. Minguez, "EEG-based upper alpha neurofeedback training improves working memory performance," in *2011 Annual International Conference of the IEEE Engineering in Medicine and Biology Society*, 2011: IEEE, pp. 2327-2330.
[323] W. Klimesch, P. Sauseng, and S. Hanslmayr, "EEG alpha oscillations: the inhibition–timing hypothesis," *Brain research reviews,* vol. 53, no. 1, pp. 63-88, 2007.
[324] W. Nan *et al.*, "Individual alpha neurofeedback training effect on short term memory," *International journal of psychophysiology,* vol. 86, no. 1, pp. 83-87, 2012.
[325] C. R. Clark *et al.*, "Spontaneous alpha peak frequency predicts working memory performance across the age span," *International Journal of Psychophysiology,* vol. 53, no. 1, pp. 1-9, 2004.
[326] M. Grunwald *et al.*, "Theta power in the EEG of humans during ongoing processing in a haptic object recognition task," *Cognitive Brain Research,* vol. 11, no. 1, pp. 33-37, 2001.
[327] D. J. Mitchell, N. McNaughton, D. Flanagan, and I. J. Kirk, "Frontal-midline theta from the perspective of hippocampal “theta”," *Progress in neurobiology,* vol. 86, no. 3, pp. 156-185, 2008.
[328] J. Lagopoulos *et al.*, "Increased theta and alpha EEG activity during nondirective meditation," *The Journal of Alternative and Complementary Medicine,* vol. 15, no. 11, pp. 1187-1192, 2009.
[329] J. F. Cavanagh, L. Zambrano-Vazquez, and J. J. Allen, "Theta lingua franca: A common mid-frontal substrate for action monitoring processes," *Psychophysiology,* vol. 49, no. 2, pp. 220-238, 2012.
[330] J. F. Cavanagh and M. J. Frank, "Frontal theta as a mechanism for cognitive control," *Trends in cognitive sciences,* vol. 18, no. 8, pp. 414-421, 2014.
[331] M. Reiner, R. Rozengurt, and A. Barnea, "Better than sleep: theta neurofeedback training accelerates memory consolidation," *Biological psychology,* vol. 95, pp. 45-53, 2014.

[332] T. Egner and J. H. Gruzelier, "EEG biofeedback of low beta band components: frequency-specific effects on variables of attention and event-related brain potentials," *Clinical neurophysiology,* vol. 115, no. 1, pp. 131-139, 2004.
[333] A. W. Keizer, R. S. Verment, and B. Hommel, "Enhancing cognitive control through neurofeedback: A role of gamma-band activity in managing episodic retrieval," *Neuroimage,* vol. 49, no. 4, pp. 3404-3413, 2010.
[334] S. Staufenbiel, A.-M. Brouwer, A. Keizer, and N. Van Wouwe, "Effect of beta and gamma neurofeedback on memory and intelligence in the elderly," *Biological psychology,* vol. 95, pp. 74-85, 2014.
[335] J. H. Gruzelier, "EEG-neurofeedback for optimising performance. I: a review of cognitive and affective outcome in healthy participants," *J Neuroscience Biobehavioral Reviews,* vol. 44, pp. 124-141, 2014.
[336] J. H. Gruzelier, "EEG-neurofeedback for optimising performance. II: creativity, the performing arts and ecological validity," *J Neuroscience Biobehavioral Reviews,* vol. 44, pp. 142-158, 2014.
[337] J. H. Gruzelier, "EEG-neurofeedback for optimising performance. III: a review of methodological and theoretical considerations," *J Neuroscience Biobehavioral Reviews,* vol. 44, pp. 159-182, 2014.
[338] A. Zhigalov, A. Kaplan, and J. M. Palva, "Modulation of critical brain dynamics using closed-loop neurofeedback stimulation," *Clinical Neurophysiology,* 2016.
[339] J. Reis *et al.*, "An Alpha and Theta Intensive and Short Neurofeedback Protocol for Healthy Aging Working-Memory Training," *Frontiers in Aging Neuroscience,* vol. 8, 2016.
[340] T. Ros, B. J Baars, R. A. Lanius, and P. Vuilleumier, "Tuning pathological brain oscillations with neurofeedback: a systems neuroscience framework," *Frontiers in human neuroscience,* vol. 8, p. 1008, 2014.
[341] J. A. Anguera *et al.*, "Video game training enhances cognitive control in older adults," *Nature,* vol. 501, no. 7465, p. 97, 2013.

7.5 Neurofeedback GUI code

```
from psychopy import gui, core, data

"""
Step 1: Open a GUI to collect data

"""
expInfo = {'Participant ID': '', 'Age': '', 'Sex': ['Male', 'Female'],
           'Handedness': ['Right-handed', 'Left-handed', 'Ambidextrous'],
           'EEG headset': ['Emotiv EPOC(+)', 'gtec Unicorn', 'gtec Nautilus 32'],
           'Experiment Mode': ['intro', 'train', 'neurofeedback'],
           'Visualize Epochs': False}
dlg = gui.DlgFromDict(dictionary=expInfo, title='GUI', sortKeys=False)
expInfo['date'] = data.getDateStr()  # add a simple timestamp
if not dlg.OK:  # or if ok_data is not None
    core.quit()  # user pressed cancel
    print('user cancelled')
```

7.6 Neurofeedback epoch visualizer code (visualizer module)

```
import pdb
from pyqtgraph.Qt import QtGui, QtCore
from PyQt5.QtWidgets import *
from PyQt5.QtCore import *
from PyQt5.QtGui import *
import numpy as np
import pyqtgraph as pg
from pylsl import StreamInfo, StreamInlet, resolve_byprop

app = QtGui.QApplication([])

# Enable antialiasing for prettier plots
pg.setConfigOptions(antialias=True)
pg.setConfigOption('background', 'w')


class EpochViewer(pg.GraphicsWindow):
    def __init__(self, fs_new=128, channels=1):
        super(EpochViewer, self).__init__()
        self.resize(1400, 5000)
        self.fs_new = fs_new
        self.setWindowTitle('Epoch Viewer')
        self.monitor = QDesktopWidget().screenGeometry(0)
        self.move(self.monitor.left(), self.monitor.top())

        self.plots = []

        streams = resolve_byprop("type", "EPOCH", timeout=1000)  # Contains information about all
available lsl inlets
        if StreamInfo.type(streams[0]) == 'EPOCH':
            self.inlet_epoch = StreamInlet(streams[0])

        self.info = self.inlet_epoch.info()
        ch = self.info.desc().child("channels").child("channel")
        # Check if LSL contains channel labels
        if self.info.desc().child("channels").child("channel").child_value("label"):
            self.channels = []
```

```
            for k in range(channels):

                self.channels.append(ch.child_value("label"))
                ch = ch.next_sibling()
        else:
            self.channels = []
            for i in range(0, channels):
                self.channels.append("Channel " + str(i + 1))

        self.x = np.linspace(-0.2, 0.8, self.fs_new)
        self.legend = None
        self.target = True
        self.non_target = True

        self.epochOneAlphas = np.array([0.8, 1, 0.1, 0.2, 0.3])
        self.epochTwoAlphas = np.array([0.8, 1, 0.1, 0.2, 0.3])

        self.epochOneWidth = np.array([3, 5, 0.2, 0.5, 1])
        self.epochTwoWidth = np.array([3, 5, 0.2, 0.5, 1])

        self.linesPlotted = False
        self.epochOne = [[0 for i in range(5)] for c in range(len(self.channels))]
        self.epochTwo = [[0 for i in range(5)] for c in range(len(self.channels))]
        self.epochOneIndex = 0
        self.epochTwoIndex = 0

        self.ci.layout.setColumnMaximumWidth(0, 700)
        self.ci.layout.setColumnMaximumWidth(1, 700)
        for i in range(len(self.channels)):
            p = self.addPlot(title="%s" % self.channels[i], rowspan=1)
            # p.setYRange(-2, 2)
            self.plots.append(p)

            # p.addLegend()
            if i == 0:
                l = pg.LegendItem((10, 10), offset=(-10, 10))
                l.setParentItem(p.graphicsItem())
                self.legend = l

            p.enableAutoRange(axis=pg.ViewBox.YAxis, enable=True)
            # p.enableAutoRange(x=False, y=True)
            if i % 2:
                self.nextRow()
        self.createTimer()

    def createTimer(self):
        self.main_timer = QTimer()
        self.main_timer.timeout.connect(self.main_loop)
        self.main_timer.start(30)

    def main_loop(self):
        try:
            chunk, timestamp = self.inlet_epoch.pull_chunk(timeout=0.01)

        except IOError:
            pass

        if len(chunk) > 0:
            chunk = np.asarray(chunk)
            lineChange = []

            if self.epochOne[0].count(0) == 0:
```

```
                for c in range(len(self.channels)):
                    if chunk[-1][0] == 1:
                        lineOne = self.epochOne[c][self.epochOneIndex]
                        self.plots[c].removeItem(lineOne)

            if self.epochTwo[0].count(0) == 0:
                for c in range(len(self.channels)):
                    if chunk[-1][0] == -1:
                        lineTwo = self.epochTwo[c][self.epochTwoIndex]
                        self.plots[c].removeItem(lineTwo)

            for c in range(len(self.channels)):
                if chunk[-1][0] == 1:
                    p = self.plots[c].plot(x=self.x, y=chunk[c, :], clear=False,
                                           pen=pg.functions.mkPen([255, 0, 0], width=5),
name="Target")
                    self.epochOne[c][self.epochOneIndex] = p

                    if self.target:
                        self.legend.addItem(p, 'Target')
                        self.target = False

                elif chunk[-1][0] == -1:
                    p = self.plots[c].plot(x=self.x, y=chunk[c, :], clear=False,
                                           pen=pg.functions.mkPen([0, 0, 255], width=5),
name="Non-Target")
                    self.epochTwo[c][self.epochTwoIndex] = p

                    if self.non_target:
                        self.legend.addItem(p, 'Non-Target')
                        self.non_target = False

            if chunk[-1][0] == 1:
                lineChange = [x for x in range((5 - self.epochOne[0].count(0)))]
            elif chunk[-1][0] == -1:
                lineChange = [x for x in range((5 - self.epochTwo[0].count(0)))]

            if self.linesPlotted:
                for i in range(len(lineChange)):
                    for c in range(len(self.channels)):
                        if chunk[-1][0] == 1:
                            lineOne = self.epochOne[c][lineChange[i]]
                            lineOne.setAlpha(self.epochOneAlphas[i], False)
                            lineOne.setPen(pg.functions.mkPen([255, 0, 0],
width=self.epochOneWidth[i]))

                        elif chunk[-1][0] == -1:
                            lineTwo = self.epochTwo[c][lineChange[i]]
                            lineTwo.setAlpha(self.epochTwoAlphas[i], False)
                            lineTwo.setPen(pg.functions.mkPen([0, 0, 255],
width=self.epochTwoWidth[i]))

                if chunk[-1][0] == 1:
                    self.epochOneAlphas = np.roll(self.epochOneAlphas, 1)
                    self.epochOneWidth = np.roll(self.epochOneWidth, 1)
                elif chunk[-1][0] == -1:
                    self.epochTwoAlphas = np.roll(self.epochTwoAlphas, 1)
                    self.epochTwoWidth = np.roll(self.epochTwoWidth, 1)

            else:
                self.linesPlotted = True
```

```
            if chunk[-1][0] == 1:
                if self.epochOneIndex < 4:
                    self.epochOneIndex += 1
                else:
                    self.epochOneIndex = 0
            elif chunk[-1][0] == -1:
                if self.epochTwoIndex < 4:
                    self.epochTwoIndex += 1
                else:
                    self.epochTwoIndex = 0


# Start Qt event loop unless running in interactive mode or using pyside.
if __name__ == '__main__':
    import sys

    if (sys.flags.interactive != 1) or not hasattr(QtCore, 'PYQT_VERSION'):
        if len(sys.argv) > 2:
            o = EpochViewer(fs_new=int(sys.argv[1]), channels=int(sys.argv[2]))
        else:
            o = EpochViewer()
        sa = pg.QtGui.QScrollArea()
        sa.setWidget(o)
        o.show()
        sa.show()
        QtGui.QApplication.instance().exec_()
        sys.exit(1)
```

7.7 Neurofeedback signal acquisition module

```
from pylsl import StreamInlet, StreamInfo, resolve_stream, resolve_byprop
import csv
import keyboard
import time
import numpy as np
import sys

class data_init:
    def __init__(self, fs, data_type, filename=None):
        """
        # Arguments
            fs: int
                EEG sampling frequency in Hz.

            data_type: string
                'EEG' or 'marker' (trigger from experimental stimuli script,
experimentFunctions.py)

            filename: string
        """
        self.fs, self.filename, self.data_type = fs, filename, data_type

def read_EEG_stream(fs=128, max_buf=3):
    """
    Initializes the EEG stream.
    Timeout is an integer denoting the maximum number of seconds to look for whether an EEG
stream is available.

    # Arguments
        fs: int
```

```
            Sampling frequency in Hz.

        max_buf: int
            Maximum amount of data to have in the buffer (seconds).

    # Returns
        inlet_EEG: pylsl object
            The EEG recording inlet.

        store_EEG: class object
    """
    try:
        streamsEEG = resolve_byprop('type', 'EEG', timeout=3)
        inlet_EEG = StreamInlet(streamsEEG[0], max_buflen=max_buf)
        store_EEG = data_init(fs, 'EEG')  # Initialize object
        if inlet_EEG.channel_count == 8:
            store_EEG.header = ['Fz', 'C3', 'Cz', 'C4', 'Pz', 'PO7', 'Oz', 'PO8']

        elif inlet_EEG.channel_count == 18:
            store_EEG.header = ['RAW_CQ', 'AF3', 'F7', 'F3', 'FC5', 'T7', 'P7', 'O1', 'O2', 'P8',
'T8', 'FC6', 'F4',
                                'F8',
                                'AF4', 'GYROX', 'GYROY', 'TIMESTAMP']

        elif inlet_EEG.channel_count == 33:
            store_EEG.header = ['Fp1', 'Fp2', 'AF3', 'AF4', 'F7', 'F3', 'FZ', 'F4', 'F8', 'FC5',
'FC1', 'FC2', 'FC6',
                                'T7',
                                'C3', 'C4', 'Cz', 'T8', 'CP5', 'CP1', 'CP2', 'CP6', 'P7', 'P3',
'Pz', 'P4', 'P8', 'PO7',
                                'PO3', 'PO4', 'PO8', 'Oz', 'TIMESTAMP']
        print('An EEG stream is found!')
    except:
        print('No EEG stream is detected in LSL!')
        raise Exception
        sys.exit(1)
    return inlet_EEG, store_EEG


def channel_visualize(args):
    if args == 'Emotiv EPOC(+)':

        return ['AF3', 'F7', 'F3', 'FC5', 'T7', 'P7', 'O1', 'O2', 'P8', 'T8', 'FC6', 'F4', 'F8',
'AF4']

    elif args == 'gtec Nautilus 32':
        return ['Fp1', 'Fp2', 'AF3', 'AF4', 'F7', 'F3', 'FZ', 'F4', 'F8', 'FC5', 'FC1', 'FC2',
'FC6',
                'T7',
                'C3', 'C4', 'Cz', 'T8', 'CP5', 'CP1', 'CP2', 'CP6', 'P7', 'P3', 'Pz', 'P4', 'P8',
'PO7',
                'PO3', 'PO4', 'PO8', 'Oz']

    elif args == 'gtec Unicorn':
        return ['Fz', 'C3', 'Cz', 'C4', 'Pz', 'PO7', 'Oz', 'PO8']
```

7.8 Neurofeedback recorder module

```
# Open LabRecorder
import subprocess, sys, os, winpexpect, time


def run(expInfo):
    # parse in currect time and date
    currentTime = time.strftime('%m-%d-%y_%H-%M')

    # parse in participant ID
    subjectID = expInfo['Participant ID']

    # parse in experiment mode between "train" and "neurofeedback"
    expMode = expInfo['Experiment Mode']

    # path to LabRecorder
    LabrecorderPath = '..\lib\LabRecorder\LabRecorderCLI.exe'

    # path to store lsl streams
    storePath = ('..\subjectsData\%s' % subjectID)

    # run LabRecorder
    child = winpexpect.winspawn('%s %s\subject_%s_%s_%s.xdf \'name="Keyboard"\'' %
(LabrecorderPath, storePath,
                                                                                subjectID,
expMode, currentTime))

    return child


def stop(child):
    child.sendline('\r')
```

Vita

Soheil Borhani is a PhD in Biomedical Engineering at the University of Tennessee, Knoxville, USA. He received a Bachelor's degree in Electrical Engineering with a focus on Communication Systems from Isfahan University of Technology (IUT), Isfahan, Iran in 2005 and a Master's degree in Communication Systems from K.N.Toosi University of Technology (KNTU), Tehran, Iran in 2010. His research interests include rehabilitative and assistive brain-machine interfaces, signal processing, neural engineering, computational neuroscience, probabilistic modeling, machine learning, deep learning and human-AI interactions.